

VISCOUS EFFECTS IN DRIFT FORCES ON SEMI-SUBMERSIBLES

**A.K. Dev
Doctors Thesis**

Report 1059

October 14, 1996

TU Delft

Delft University of Technology

Faculty of Mechanical Engineering and Marine Technology

Ship Hydromechanics Laboratory

STELLINGEN

behorende bij het proefschrift

Viskeuze Effecten in Drift Krachten op Semi-Submersibles

van

Arun Kr. DEV

1. In een stromingsveld ten gevolge van golven alleen, is de gemiddelde horizontale viskeuze driftkracht een gevolg van de aanwezigheid van een splash (vrije oppervlak) zone van een waterdoorsnijdende cilindrische constructie terwijl het altijd ondergedompelde deel van de constructie hier geen invloed op heeft. Echter, in de aanwezigheid van stroming en golven samen worden de viskeuze driftkrachten in de splash zone versterkt en een extra bron wordt gecreëerd die een bijdrage levert aan viskeuze effecten op de continu ondergedompelde constructie.
2. Oscillerend eerste orde golfkrachten en gemiddelde driftkrachten ten gevolge van viskeuze effecten dienen bepaald te worden met behulp van de juiste waarden van respectievelijk de oscillerende weerstandscoefficiënt en de gemiddelde weerstandscoefficiënt.
3. Wanneer een frequentie domein analyse volstaat voor de bepaling van de gemiddelde viskeuze driftkracht in regelmatige golven, dan is een tijdsdomein analyse nodig voor de bepaling van de gemiddelde viskeuze en laag frequente driftkrachten in onregelmatige golven ten gevolge van de aanwezigheid van sterke niet-lineariteiten.
4. Omgevingsbelastingen ten gevolge van golven, wind en stroming, vormen tezamen een zeer complex geheel. Ze kunnen echter onafhankelijk van elkaar behandeld worden als zijnde zwak co-existerend in plaats van sterk interactief.
5. Voor een potentiaalstroming geeft een 3-D numerieke oplossings-methode vaak een voldoende nauwkeurig resultaat, terwijl in een viskeuze stroming zelfs een 2-D numerieke methode al vele onzekerheden oplevert.

6. Wetenschap is zowel constructief als destructief, maar kunst blijft altijd expressief.
7. Elk onderzoek is vol van vreugde en verdriet. Maar hoe waardeert men geluk, als men het ongeluk niet kent?
8. Hoe minder je hecht aan materialistisch gewin in de wereld, hoe meer je de vrijheid van geest waardeert.
9. Kennis stuurt aan op vriendschap en solidariteit, ongeletterdheid tot vijandigheid en diversiteit.
10. Werk (karma) en toewijding (sadhana) zouden het motto en misschien wel het succes van het leven moeten zijn.
11. Een explosieve groei van de bevolking, speciaal in de door armoede getroffen derdewereldlanden, zal het brandende vraagstuk blijven in de komende eeuw. Volksonderricht aangaande de consequenties is een mogelijke en imminente oplossing.
12. Religieuze fundamentalisten maken van iedere godsdienst een kwade filosofie.

Laboratorium voor Scheepshydronechanica
Faculteit der Werktuigbouwkunde en Maritieme Techniek
Technische Universiteit Delft

14 Oktober 1996
Delft, The Netherlands

PROPOSITIONS

belongs to the thesis

Viscous Effects in Drift Forces on Semi-Submersibles

by

Arun Kr. DEV

1. In a waves-only flow field, the horizontal viscous mean drift force is due to the presence of the splash (free surface) zone of the surface piercing cylindrical structures when the constantly submerged structures do not contribute to such forces. However, in the presence of currents with waves, the viscous drift forces due to the splash zone are enhanced and an additional source is created for further contributions of viscous effects for the constantly submerged structures.
2. Oscillatory first order forces and mean drift forces due to viscous effects are to be properly treated via the appropriate values of the oscillatory drag coefficients and the mean drag coefficients respectively.
3. When the frequency domain analysis is sufficient to deal with the viscous mean drift force in regular wave, the time domain analysis is required for the viscous mean and low frequency drift force in irregular waves due to the presence of higher nonlinearity.
4. Environmental loads like waves, winds and currents - all together are extremely complex. However, they can be treated as weakly coexisting rather than strongly interacting.
5. In the potential regime, it is possible to use a 3-D computational technique with sufficient accuracy whereas in the viscous regime even a 2-D computational method gives uncertainties.
6. Science is constructive as well as destructive but art always remains as expressive.
7. Any research is full of bliss and grief. How can one appreciate joy, if there be no sorrow ?

8. The less you become attached to the materialistic achievement in this world, the more you savor peace of mind.
9. Knowledge steers to friendship and solidarity and illiteracy to enmity and diversity.
10. Work (Karma) and devotion (sadhana) should be the motto and perhaps the succes of life.
11. Population explosion especially in the poverty stricken third world countries will be the burning issue of the next century Educating mass people about the consequences is a possible and imminent solution.
12. Religious fundamentalists make any religion an evil philosophy.

Ship Hydromechanics Laboratory
Faculty of Mechanical Engineering and Marine Technology
Delft University of Technology

14 October 1996
Delft, The Netherlands

**VISCOUS EFFECTS IN DRIFT
FORCES ON SEMI-SUBMERSIBLES**

A. K. DEV

CIP-DATA KONINKLIJKE BIBLIOTHEEK, DEN HAAG

Dev, Arun Kr.

Viscous effects in drift : forces on semi-submersibles /
Arun Kr. Dev. - Delft : Delft University of Technology,
Faculty of Mechanical Engineering and Marine Technology.
- III.

Thesis Technische Universiteit Delft. - With summary in
Dutch.

ISBN 90-370-0139-4

Subject headings: semi-submersibles / wave drift forces
/ viscous drift forces.

Opmerkingen:

Deze CIP-gegevens alleen afdrucken in de proefschrifteditie.

Technische Universiteit Delft, Fac. Werktuigbouwkunde en Maritieme Techniek,
Bibliotheek WbMT
Mekelweg 2,
2628 CD Delft

Deze CIP-gegevens ongewijzigd afdrucken op de copyrightpagina van het boek, incl. het kopje "CIP-
GEGEVENS KONINKLIJKE BIBLIOTHEEK, DEN HAAG".

Voor informatie: tel.: 070-3140414.

**Viscous Effects in Drift
Forces on Semi-Submersibles**

**Viskeuze Effecten in Drift
Krachten op Semi-Submersibles**

PROEFSCHRIFT

ter verkrijging van de graad van doctor
aan de Technische Universiteit Delft,
op gezag van de Rector Magnificus
Prof. ir. K. F. Wakker,
in het openbaar te verdedigen
ten overstaan van een commissie,
door het College van Dekanen aangewezen,
op maandag 14 oktober 1996 te 16.00 uur

door

Arun Kr. DEV

Bachelor of Science in Naval Architecture & Marine Engineering
Bangladesh University of Engineering & Technology, Dhaka

Master of Science in Marine Technology
University of Strathclyde, Glasgow

geboren te Barisal, Bangladesh

Dit proefschrift is goedgekeurd door de promotor:
Prof. dr. ir. J. A. Pinkster

Samenstelling promotiecommissie:

Rector Magnificus, voorzitter

Prof. dr. ir. J. A. Pinkster, TU Delft, Promotor

Prof. ir. B. Boon, TU Delft

Prof. dr. ir. J. A. Battjes, TU Delft

Prof. dr. ir. G. Kuiper, TU Delft

Prof. ir. W. J. Vlasblom, TU Delft

Prof. dr. ir. J. H. Vugts, TU Delft

Dr. ir. J. E. W. Wichers, MARIN

Summary

With the discovery of oil fields in deep-water offshore, semi-submersibles and tension leg platforms are nowadays often considered as strong contenders for Floating Production Systems (FPS). The hydrodynamic forces, motions and mooring forces on these platforms in exposed locations are dominated mainly by wave effects. Predictions of these quantities can be based on computational methods, model tests or a rational approach combining both.

Theoretical predictions using 3-dimensional potential theory for the mean drift forces on moored floating structures like semi-submersibles and tension leg platforms show discrepancies in both regular and irregular waves when compared with results of model tests. Such divergence is further pronounced in the low frequency range (storm condition) where diffraction effects are smaller for such structures and the divergence is thus believed to be induced by viscous effects. In this study such viscous effects have been studied in connection with moored semi-submersibles.

The viscous drag term of the Morison equation in combination with the linear (Airy) theory up to instantaneous wave elevation has been considered as the basis in order to develop the theory in a waves-only field and in a wave-current coexisting flow field. To substantiate the theory and its range of applicability and its dependency on different hydrodynamic parameters, experimental investigations were carried out with fixed vertical surface piercing model cylinders and a submerged pontoon in regular waves. Test results validate the theory with a further indication that the mean forces on completely submerged bodies are not influenced by viscous effects in a waves-only field. Model test results further reveal consistently that the viscous drift force in a waves only field cannot be obtained by subtracting the force due to currents only from that due to a wave-current coexisting flow field.

Finally, experiments were carried out for a complete semi-submersible model (ITTC Model) in regular waves (both head and beam seas) in fixed

and free floating (soft moored) conditions at zero speed and with forward velocity. The mathematical model, incorporating a relative horizontal velocity and relative surface elevation concept, enhances the theoretical predictions for the horizontal mean drift forces when experimentally obtained values of the mean drag coefficients for the cylinders and the submerged pontoon are properly applied for the complete semi-submersible in regular waves with and without currents in the frequency domain.

In order to deal with viscous effects in the low frequency behavior of a moored semi-submersible, tests were conducted in irregular waves in both head and beam seas. Results of experiments when compared to 3-dimensional (potential) predictions in time domain also show increasing divergence in the low frequency drift force. The same model for approximating viscous contributions to the mean drift forces in regular waves has now been applied in irregular waves in the time domain using the FFT for some test results. It has been shown that the correlation between measurements and predictions is improved when force coefficients obtained from regular wave tests are applied carefully in consistent with the slowly varying wave envelope and its associated frequencies.

The theory in combination with experimentally obtained force coefficients as presented and validated in this study can be used as an improved computational technique in order to calculate the viscous drift forces on a semi-submersible in a seastate.

Samenvatting

Na de ontdekking van olievelden in diepe kustwateren worden "Semi-Submersibles" (diepdrijvers) en "Tension Leg Platforms" tegenwoordig dikwijls beschouwd als goede keuzen voor Drijvende Productie Systemen (DPS). De hydrodynamische krachten, bewegingen en verankeringskrachten op deze booreilanden, in aan weer en wind onderhevige lokaties, worden voornamelijk bepaald door invloeden van golven. Voorspellingen van de omvang van deze invloeden kunnen gebaseerd worden op berekeningsmethoden, modelproeven of op een redelijke combinatie van beiden.

Theoretische voorspellingen, waarbij gebruik gemaakt wordt van de 3-dimensionale potentiaaltheorie voor de bepaling van de gemiddelde driftkrachten op verankerde drijvende constructies als "Semi-Submersibles" en "Tension Leg Platforms" in zowel regelmatige als onregelmatige golven, tonen afwijkingen ten opzichte van resultaten van modelproeven. Die afwijking is vooral duidelijk in het lage frequentie gebied (storm condities), waar de invloeden van diffractie voor zulke constructies kleiner zijn. Daarom wordt aangenomen, dat deze afwijking het gevolg is van viskeuze effecten. In deze studie zijn zulke viskeuze effecten onderzocht met betrekking tot verankerde "Semi-Submersibles".

De viskeuze weerstandsterm in de Morison vergelijking tezamen met de lineaire (Airy) theorie toegepast tot de momentane golfoppervlakte is beschouwd als de basis om een theorie te ontwikkelen voor een gebied met alleen maar golven en voor een gebied met golven in een bestaand stromingsveld. Om deze theorie en tevens het bereik van toepasbaarheid en de afhankelijkheid van verschillende hydrodynamische parameters te realiseren zijn experimentele onderzoeken uitgevoerd met vaste verticale cilindermodellen die het wateroppervlak doorsnijden en met een ondergedompelde ponton in regelmatige golven. De proefresultaten leiden wat betreft de theorie tot nog een aanwijzing, dat de gemiddelde krachten op volledig ondergedompelde lichamen in een gebied met alleen maar golven niet wor-

den beïnvloed door viskeuze effecten. Experimentele modelresultaten tonen verder consequent aan, dat de viskeuze driftkrachten in een gebied met alleen maar golven niet bepaald kunnen worden door de kracht als gevolg van alleen stroming te verminderen met de kracht die het gevolg is van golfstromen in een bestaand stromingsveld. Tenslotte zijn er proeven uitgevoerd met een volledig "Semi-Submersible"-model (ITTC Model) in regelmatige golven (zowel van voren als dwars-inkomend) bij vastgehouden en drijvende condities (licht verankerd) zonder en met voorwaartse snelheid. Het mathematisch model, dat als concept een relatieve horizontale snelheid en relatieve verhoging van het oppervlak inhoudt, maakt theoretische voorspellingen voor de gemiddelde horizontale driftkracht mogelijk, indien experimenteel verkregen waarden van de gemiddelde weerstandscoefficienten voor de cilindres en het ondergedompelde ponton op de juiste wijze toegepast worden voor de gehele "Semi-Submersible" in regelmatige golven met en zonder stromingen in het frequentie domein.

Ten einde viskeuze effecten voor het laagfrequente gedrag van een verankerde "Semi-Submersible" te kunnen introduceren, zijn proeven uitgevoerd in onregelmatige golven voor zowel van voren als dwars-inkomende zeeën. Experimentele resultaten tonen vergeleken met 3-dimensionale potentiaal voorspellingen in het tijdsdomein ook een toenemende afwijking voor de laagfrequente driftkracht. Hetzelfde model ter benadering van het viskeuze deel van de gemiddelde driftkrachten in regelmatige golven is nu toegepast voor onregelmatige golven in het tijdsdomein door gebruik te maken van de FFT voor enige proefresultaten. Aangetoond is dat de correlatie tussen metingen en voorspellingen verbeterd wordt indien kracht-coëfficiënten verkregen uit proeven in regelmatige golven zorgvuldig worden toegepast in overeenstemming met de langzaam variërende golf-omhullende en de daarbij behorende frequenties.

De theorie, gecombineerd met de experimenteel verkregen krachtcoëfficiënten, zoals gepresenteerd en vastgesteld in deze studie, kan gebruikt worden als een verbeterde berekeningstechniek om daarmee de viskeuze driftkrachten op een "Semi-Submersible" in zeegang te bepalen.

Contents

1	Introduction	1
1.1	Historical Review	3
1.2	Present State-of-the-Art	14
1.3	The Hypotheses	18
1.4	The Objectives	19
1.5	The Outlines	19
	References	21
2	Model Tests	25
2.1	The Towing Tanks	27
2.2	The Models	29
2.2.1	The Small Cylinder	29
2.2.2	The Large Cylinder	30
2.2.3	The Pontoon	31
2.2.4	The Fixed Semi-submersible	32
2.2.5	The Free Floating (Moored) Semi-submersible	33
2.3	Test Set-up and Procedure	34
2.3.1	The Small Cylinder	34
2.3.2	The Large Cylinder	37
2.3.3	The Pontoon	39
2.3.4	The Fixed Semi-submersible	41
2.3.5	The Free Floating (Moored) Semi-submersible	42
2.3.6	The Simulated Flow Fields	48
2.4	Test Equipment and Measurement	51
2.4.1	Instrumentation	51
2.4.2	Data Acquisition	51
2.5	Data Analysis of Measurements	52
	References	54

3	Viscous Mean Drift Forces on a Vertical Cylinder	55
3.1	Theoretical Evaluation	56
3.1.1	Viscous Mean Drift Forces on a Fixed Cylinder	56
3.1.2	Viscous Mean Drift Forces on a Floating Cylinder	65
3.1.3	Wave Stretching	70
3.2	Application of the Mean Drag Coefficient	75
3.3	Controlling Hydrodynamic Parameters	76
3.4	Concluding Remarks	84
3.5	Experimental Validation	86
3.5.1	Small Cylinder	87
3.5.2	Large Cylinder at DUT	94
3.5.3	Large Cylinder at MARIN	98
3.5.4	Mean Drag Coefficients	101
3.6	Concluding Remarks	112
	References	115
4	Hydrodynamic Forces on a Submerged Pontoon	117
4.1	Hydrodynamic Parameters	118
4.1.1	In Currents Only	118
4.1.2	In Waves Only	119
4.1.3	In Waves and Currents	120
4.2	Force Formulations in Head Seas	121
4.2.1	In Currents Only in Head Seas	121
4.2.2	In Waves Only in Head Seas	122
4.2.3	In Waves and Currents in Head Seas	124
4.3	Experimental Results in Head Seas	130
4.3.1	In Currents Only in Head Seas	130
4.3.2	In Waves Only in Head Seas	131
4.3.3	In Waves and Currents in Head Seas	132
4.4	Force Formulations in Beam Seas	135
4.4.1	In Currents Only in Beam Seas	135
4.4.2	In Waves Only in Beam Seas	136
4.4.3	In Waves and Currents in Beam Seas	138
4.5	Experimental Results in Beam Seas	141
4.5.1	In Currents Only in Beam Seas	141
4.5.2	In Waves Only in Beam Seas	142
4.5.3	In Waves and Currents in Beam Seas	149
4.6	Concluding Remarks	152
	References	154

5	Mathematical Model	157
5.1	Viscous Mean Drift Forces in Head Seas	159
5.1.1	Wave Kinematics	159
5.1.2	Horizontal Motions at Columns	161
5.1.3	Vertical Motions at Columns	162
5.1.4	Relative Horizontal Velocity at Columns	163
5.1.5	Relative Wave Elevation at Columns	164
5.1.6	Horizontal Motions at pontoons	164
5.1.7	Vertical Motions at pontoons	165
5.1.8	Relative Horizontal Velocity at pontoons	166
5.1.9	Viscous Mean Drift Forces on a Column	166
5.1.10	Viscous Mean Drift Forces on a Pontoon	168
5.2	Viscous Mean Drift Forces in Beam Seas	169
5.2.1	Viscous Mean Drift Forces on a Column	171
5.2.2	Viscous Mean Drift Forces on a Pontoon	173
5.2.3	Waves and Currents	173
5.3	Low Frequency Viscous Drift Forces	173
5.3.1	Hydrodynamic Parameters	175
5.4	Low Frequency Wave Drift Forces	177
5.4.1	Quadratic Transfer Functions	179
5.4.2	Drift Force in a Regular Wave Group	181
5.4.3	Symmetry of the Quadratic Transfer Functions	182
5.4.4	Evaluation of the Quadratic Transfer Functions	183
5.4.5	Time Domain Representation	183
5.5	Forces in Currents Only	185
5.5.1	Classification of Geometry	185
5.5.2	System of Axes and Definitions	188
5.5.3	Forces and Moments	188
5.5.4	Interference of Drag between Bodies	193
5.5.5	Theoretical and Experimental Results	193
5.5.6	Concluding Remarks	199
	References	201
6	Results of Computations and Measurements	203
6.1	Fixed Semi-Submersible	205
6.1.1	In Regular Waves	205
6.1.2	In Regular Waves and Currents	212
6.2	Moored Semi-Submersible	213
6.2.1	In Regular Waves	213

6.2.2	In Regular Waves and Currents	218
6.2.3	In Irregular Waves	223
References	236
7	Conclusions	237
8	Recommendations	241
	List of Symbols	245
	Acknowledgments	251
	Curriculum Vitae	253

Chapter 1

Introduction

Offshore floating structures such as semi-submersibles and tension leg platforms in recent days have had their use increased because of their recognition as floating bodies of good performance as far as small motion and stability are concerned. In recent years with the possibility and discovery of oil fields in deep-water offshore, there is a motivation for studies of deeper waters floating offshore structures. Both semi-submersibles and tension leg platforms are nowadays considered as strong contenders for Floating Production System (FPS) and such production system may be a viable economic alternative to conventional bottom standing structures. Semi-submersibles and tension leg platforms often operate under severe environmental conditions and the motions and the mooring forces are dominated by an extremely complex environmental loading particularly dominated by waves, currents, and winds. In general, the wave loading makes up the major environmental loading including its interaction with currents. The accurate estimate of the excitation forces on these floating structures is important for both economical and safe design of them. This dissertation is mainly concerned with Semi's but the general aspects of the entire research work including theory, experiment and computer coding can also be applied to tension leg platforms.

The wave excitation forces in small amplitude monochromatic long-crested waves are divided into wave frequency (first order) forces and mean and slowly varying wave (potential) drift forces in an irregular seastate. While the first order force with the wave frequency is linear with the wave height, the mean force being nonlinear is quadratic with the wave height. The slowly varying drift forces occur in irregular waves because of the ex-

istence of two waves of different frequencies (beating effect of two wave components) which always implies the existence of wave excitations at the sum and difference frequencies. The latter frequency may occur at the resonance frequency of the floating structure moored in horizontal motions. If the damping is low (as it is usually in such motions), a highly tuned resonance force is always expected although the low frequency force is generally small in amount. Accordingly, the motion of a floating structure moored in irregular waves consists of a slowly varying component and a component oscillating at wave frequencies. The spectrum of this time history (forces or motions) has thus two peaks - one occurs within the wave frequency range and the other occurs below the lowest frequency (close to resonance frequency) at which there is any significant energy in the incident waves.

These quadratic wave forces are believed to be due to potential effects and as such treated by linear potential theory like either the conservation of momentum principle (far field approach) (Maruo 1960; Newman 1967) or the pressure integration method (near field approach) (Pinkster 1980). Such methods have proved to be quite satisfactory where viscous effects are less prominent. The diffraction theory based analysis has the added advantage of allowing for diffraction forces, member interactions with incident waves and interaction between members. On the other hand, the diffraction theory neglects drag forces which ultimately influence mean and low frequency drift forces especially in large waves in extreme sea (storm) conditions and thus cannot be disregarded. For floating structures like semi-submersibles and tension leg platforms whose columns and pontoons have small ratios of cross-sectional dimension, viscous effects are equally important. Besides the mean forces, the slowly varying drift force is the most important excitation. Estimating the structure's maximum excursions caused by the resonance motion is now being considered as essential in the design of a mooring system. Apart from the contribution as a wave excitation force due to viscous effects, its presence as hydrodynamic damping is equally important with respect to the system damping towards an accurate prediction of the response. In fact, viscous damping is relatively large compared to radiation wave damping in any mode of slow drift motions. The presence of currents can further enhance such viscous effects. Currents can be expected to have an influence over the whole submerged part of the structure and also the free surface. The presence of currents has thus several effects which need to be considered in the wave excitation force calculations. The drag force on a member is proportional to the square of wave particle velocities and currents even with a low velocity may have a significant effect. This effect is very

important for slender members since the Morison equation (Morison *et al.* 1950) used to calculate the forces on such members is modified through the velocities.

The importance of viscous effects in the mean and low frequency drift forces has been in the minds of the hydrodynamicists in a parallel fashion to that of potential effects. While methods of computation concerning potential effects have been well proven, knowledge of viscous effects from the point of view of its nature and importance has not yet been fully established. In this study an attempt is made to investigate the physical phenomena of viscous effects influencing the horizontal mean and low frequency drift forces on floating structures like semi-submersibles in a waves-only flow field as well as in a wave-current coexisting flow field.

A semi-submersible consists of two major structures - the submerged underwater hull hereinafter referred to as the pontoons and the surface piercing vertical columns hereinafter referred to as the columns. Before dealing with viscous effects for a complete semi-submersible, these two structures - the vertical columns and the submerged pontoons need to be treated separately. Several authors have dealt with the mean drift force due to viscous effects concerning floating structures like semi-submersibles and tension leg platforms.

1.1 Historical Review

In this section a review is given concerning past developments in theories and experiments in connection with viscous drift forces on fixed vertical cylinders and floating structures like semi-submersibles and tension leg platforms. In the case of submerged bodies, viscous origin has been shown mainly in connection with the first order forces without mentioning the existence of the non-zero mean component due to viscous effects.

Pijfers and Brink (1977) considered the viscous drift force due to wave-current interaction in their analysis of two semi-submersibles drift forces. They tried to use the value of the mean drag coefficient (C_{Do}) as a weighted average of drag coefficient values of the Reynolds number dependent of uniform flow (the sum of current velocity and the wave (Stokes) drift velocity) and those of the Keulegan-Carpenter number dependent of harmonic horizontal water particle velocity. The authors calculated the wave drift force from viscous origin, i.e. subtracting the force due to currents alone from the force due to steady flow (current and mass transport velocities) and waves.

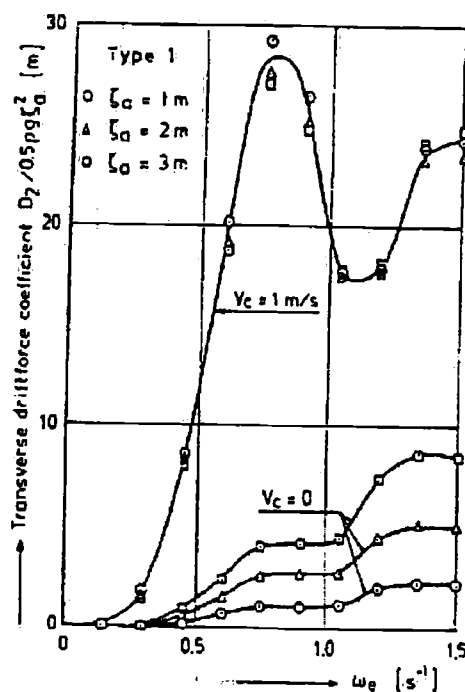


Figure 1.1: Transverse drift force coefficient [Pijfers and Brink (1977)]

Drift force coefficients were shown to be not proportional with the wave amplitude squared as shown in Figure 1.1. Denise and Heaf (1979) considered the drag force using empirical drag and friction coefficients while analyzing the response of a tension leg platform. No indication with regard to the values of the drag coefficient was given.

Huse (1976) gave an expression for the horizontal mean drift force on semi-submersibles from which a qualitative indication regarding the influence of viscous effects can be drawn. A vertical viscous drag force changes by angle of pitch motion and thus it results into a horizontal viscous force. If such factor is significant, the steady drift force contribution IV in (Pinkster 1980) must also be significant. As the first order wave force in the vertical direction includes the force component relative to the vertical velocity, the contribution IV , in natural, becomes large when the said force factor is dominant. But for a semi-submersible (Pinkster 1980), the contribution IV

is practically zero except for the very low frequency near heave and pitch resonances. Accordingly, the force factor for viscous effects is not important quantitatively. Similar conclusions were put forward by Kato and Kinoshita (1990).

Ferretti and Berta (1980) applied the Morison equation to calculate the mean drift force on a vertical cylinder due to potential effects. Damping coefficients used were obtained from 3-D potential theory. Results were compared with those by Newman (1967) for both fixed and floating conditions. The influence of wave height on the splash zone (wave stretching zone) was shown to cause the viscous mean drift force. Finally the wave-current interaction effects were explained at mean water level only showing that even a weak current leads to drift force values larger than those obtained by a simple linear superimposing of effects. All the computational results were assumed to be independent of the drag coefficient, i.e. setting its value to unity.

Lundgren *et al.* (1982) discussed the different contributions for the potential and viscous mean drift forces on a fixed cylinder in a particular sea state condition providing approximate analytical expressions. Wave-current interaction effects were also discussed. The formulation is valid when the current velocity is less than 10% of the maximum wave velocity which has been assumed to be constant over the entire draft of the cylinder. Such an approach would certainly lead to erroneous results for the viscous drift force due to wave-current interaction. The authors incorporated the values of the drag coefficient based on the oscillatory flow test results by Bearman and Graham (1979) for circular cylinders at low Keulegan-Carpenter number which does not seem appropriate for the viscous drift force due to waves only at the free surface (splash zone).

Burns (1983) developed a method to generate a "viscous drift" transfer function using the Morison formulation combining waves and currents including the motion of a TLP structure. The viscous drift force transfer function was shown to be quadratic so that a spectral analysis technique by Pinkster (1974) can be applied to calculate the viscous low frequency drift forces. The proposed governing equations are for the submerged zone of a floating structure in a wave-current coexisting flow field without taking any account of free surface effects. The drift force in waves only was obtained subtracting the force due to currents only from that due to waves and currents for quadratic RAO generation. No indication was given regarding the value of the drag coefficient. However from some results of computations which are shown here in Figure 1.2, it is worth mentioning that the surge

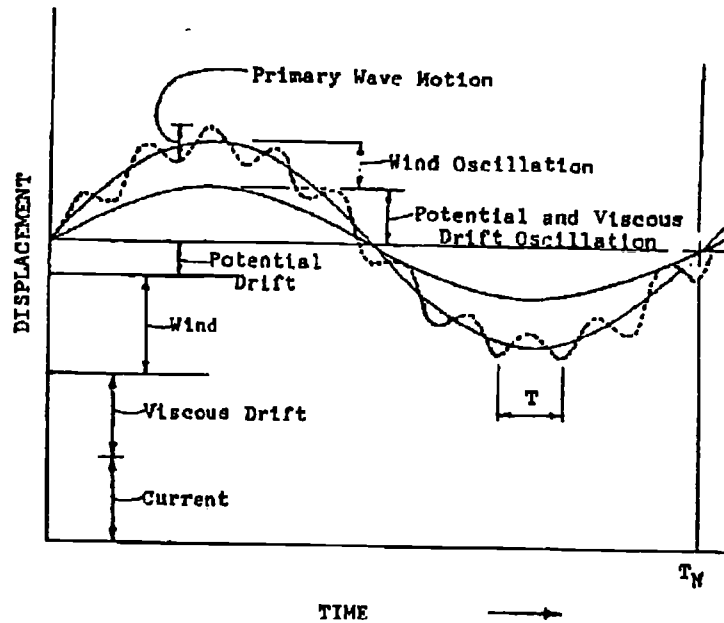


Figure 1.2: TLP displacement [Burns (1983)]

displacement due to the viscous drift is considerably larger than the offset from waves alone plus current alone.

Chakrabarti (1984) presented both potential and viscous drift forces on a fixed vertical cylinder to find their relative importance, i.e. where the viscous or potential drift force predominates. Experimental results were also presented. He discussed the viscous mean drift force both for finite water depth and deep water condition. Wave-current interaction effects were considered at mean water level. Indications were also provided for a floating cylinder. The mean drag coefficient was found to have a value of 1.10 in wave-current interaction experiments without showing any governing hydrodynamic parameter.

Kobayashi *et al.* (1985) showed that the viscous drift force is a significant component besides the wave drift force. He calculated the viscous drift force for regular wave conditions considering the fluctuation of the wetted surface area of a tension leg platform. From Figure 1.3, the difference between 3-D calculations and experiment is noticeable and should not be ignored. The

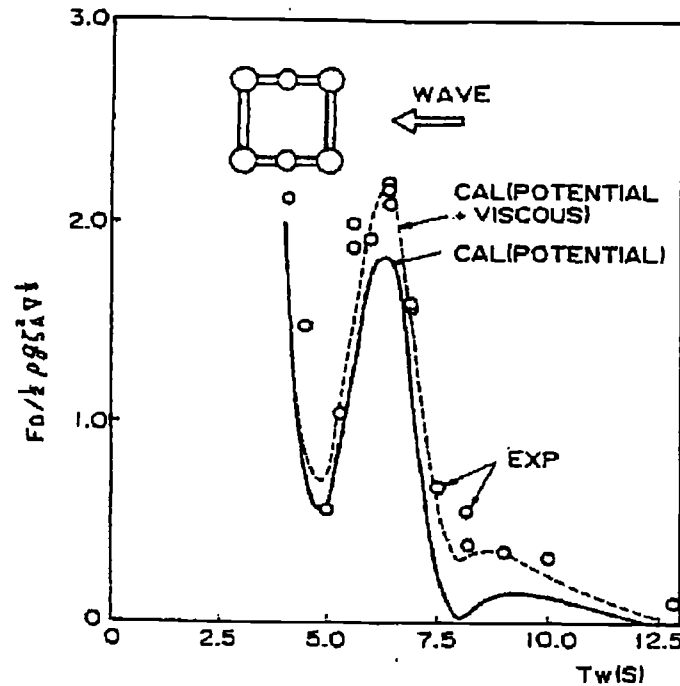


Figure 1.3: Wave drift forces in regular waves [Kobayashi, et al. (1985)]

comparison improves after the viscous contribution is added. The author does not provide any indication of the value of the drag coefficient used in the viscous drift force calculation. In a personal communication, an explanation was given which is quoted here "we sought a possibility of explaining the gap between experimental and theoretical values of wave drift forces in regular waves by introducing the nonlinear drag force. Therefore, we adopted 1.00 for the coefficient without examining its validity with great care".

Kato and Kinoshita (1990) have shown in Figure 1.4 that when $(\frac{H}{D})$ is less than 0.5, i.e. the wave height is less than half of the column diameter, the experimental results agree well with the theoretical line based on potential theory. But when $(\frac{H}{D})$ becomes larger than 0.5, both results are different considerably. The above argument is similar to diffraction effects and viscous effects respectively showing convergence and divergence with experimental results. The authors showed from experimental results for

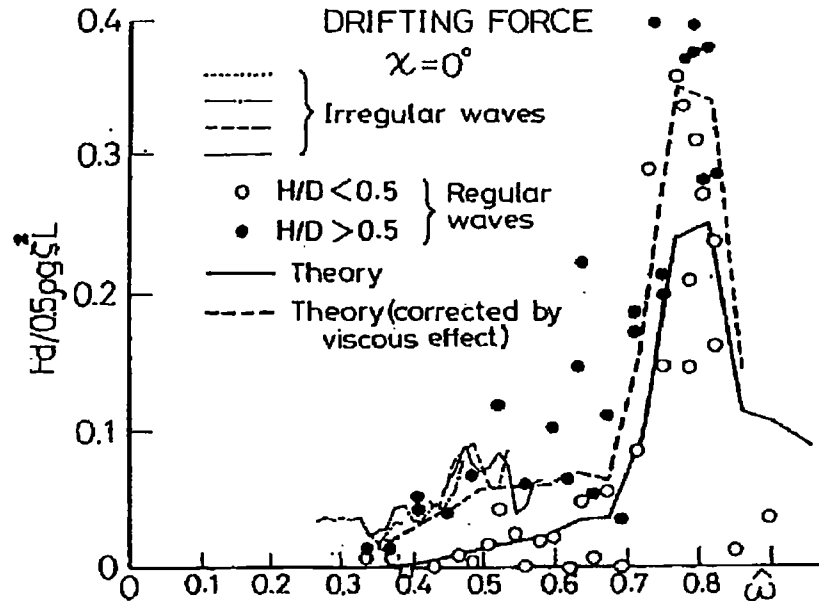


Figure 1.4: Longitudinal steady drift force [Kato and Kinoshita (1990)]

a semi-submersible that the steady drift force coefficient linearly increases with an increase of the wave height, i.e. the steady drift force is proportional to the third power of wave height. Thus the steady drift force produced by the mass transport velocity (proportional to the squared wave height) in the direction of wave propagation (Stokes 1847) may be proportional to the fourth power of wave height which is contrary to what has been found by the authors and accordingly was not considered in their work. So, the use mass transport velocity in addition to current velocity in (Pijfers and Brink 1977) is questionable.

Standing *et al.* (1991) gave an expression for the mean drag force of a single column of a semi-submersible. Both relative horizontal velocity and relative surface elevation were accounted for. Different values of the drag coefficient were used. The theoretical mean surge force was found to improve after the viscous mean drift force was added to the potential mean drift force. The authors suggested the viscous drag as one of several possibly significant factors causing the discrepancy between the predicted and the measured low-frequency motions of a semi-submersible support vessel "Uncle John".

Figure 1.5 shows the difference in horizontal drift force with and without viscous drift force. An anomaly is still the choice of the value of the drag coefficient.

Pinkster *et al.* (1993) showed the comparison of the measured and the computed mean and low frequency drift forces on two types of semi-submersibles in both regular and irregular waves showing consistent divergence between 3-D predictions and the results of experiments. Figure 1.6 and Figure 1.7 shows the discrepancy in predicting the mean drift force in regular waves for the semi-submersible I. Figure 1.8 further shows the improvement in low frequency surge force prediction when viscous contributions are added to 3-D potential computations. Constant values of the drag coefficient were used in the computations.

Chitrapu *et al.* (1993) presented a method to compute the wave and current induced viscous mean drift forces and moments on a tension leg platform in both regular and irregular waves. The basic outline of the theory is similar to what was shown in (Burns 1983), i.e. subtracting the forces due to currents alone from the viscous drift forces due to waves and currents and expressing the viscous drift force quadratic transfer functions independent of wave amplitude squared as shown in Figure 1.9. The subsequent treatment for irregular waves in both frequency and time domain is similar to Burns (1983).

A few investigations were carried out with fixed horizontal rectangular submerged cylinders in waves as well as in waves and currents.

Most of the work regarding submerged structures reported in the available literature deal with circular cylinders with a few exceptions. Koterayama (1979) investigated the wave forces on horizontal circular cylinders of different diameters in waves. The values of the drag coefficient were found satisfactory for large period parameter when compared with those in an oscillatory flow (body). Ramberg and Niedzwecki (1982) presented an investigation on a horizontal cylinder in waves where it was concluded that the values of drag coefficients approach those in steady flow at higher values of the Keulegan-Carpenter number.

Chaplin (1984) reported both horizontal and vertical mean forces for a submerged circular cylinder beneath waves. Effects of circulation were also discussed. Problems of noise in the mean force measurements were suggested as well. Forces on horizontal circular cylinders in waves and also in waves and currents were reported by (Teng and Nath 1985; Teng and Nath 1988). Values of drag coefficients in the said flow field were compared with those in planar oscillatory flow showing the effects of the vertical velocity component.

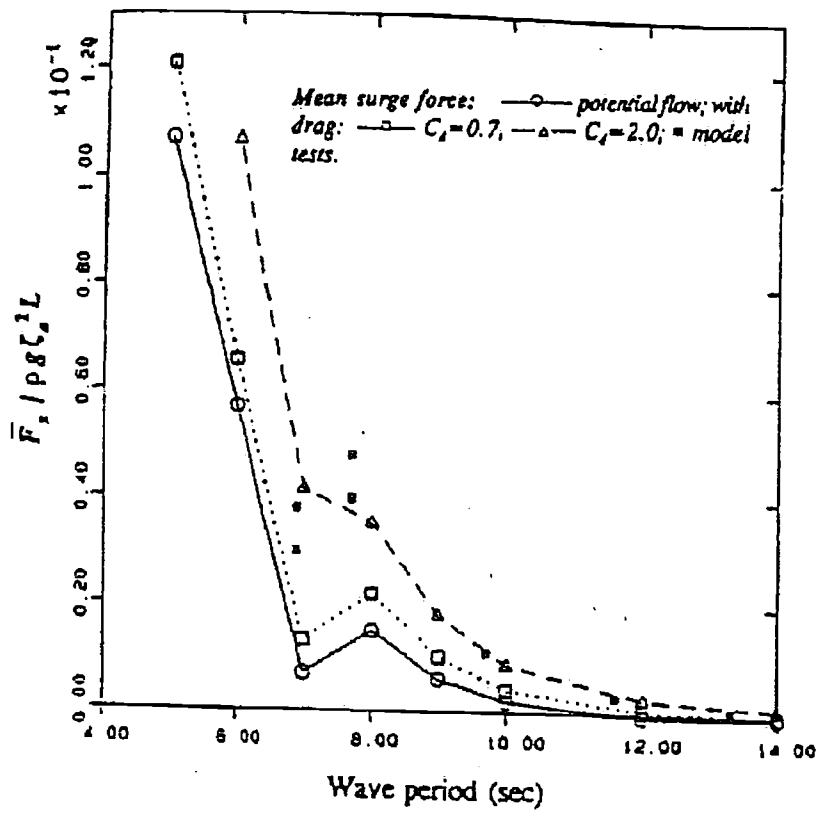


Figure 1.5: Mean surge force [Standing, et al. (1991)]

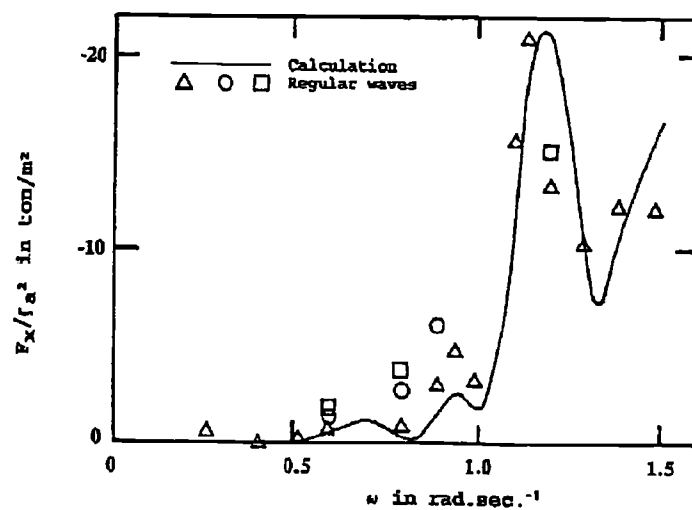


Figure 1.6: Mean surge drift force on semi-submersible I in regular head waves [Pinkster, et al. (1993)]

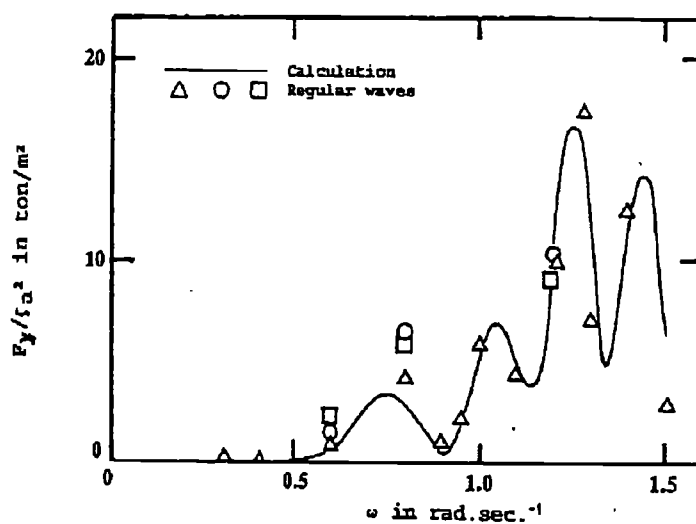


Figure 1.7: Mean sway drift force on semi-submersible I in regular beam waves [Pinkster, et al. (1993)]

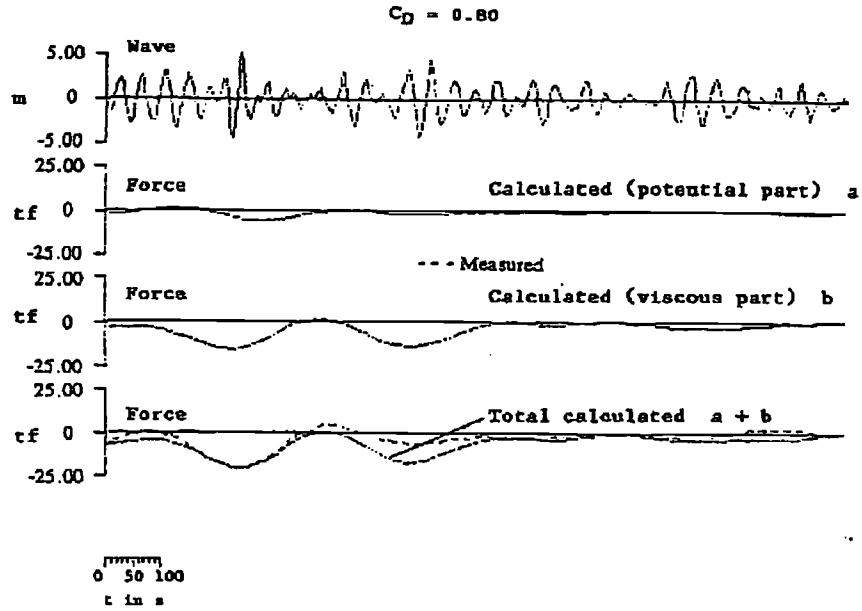


Figure 1.8: Low frequency surge drift force on semi-submersible I in irregular head seas [Pinkster, et al. (1993)]

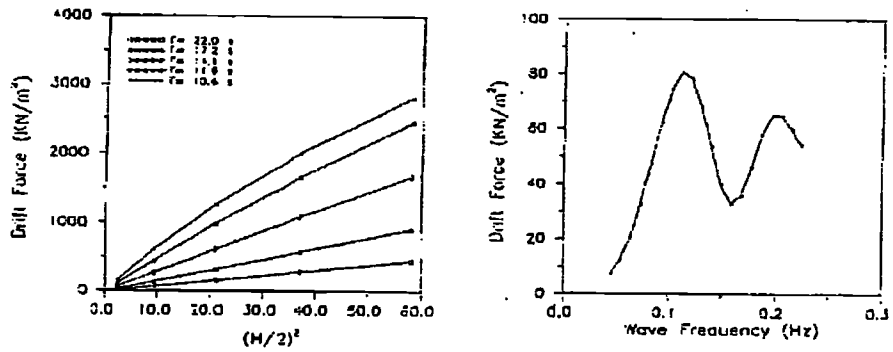


Figure 1.9: Surge drift force and transfer function in waves and currents minus currents in head waves [Chitrapu, et al. (1993)]

Values of drag coefficients were also shown as a function of the Moe-Verley number. The authors showed that the experimental technique of towing a cylinder with steady speed in waves can be used to simulate the waves and currents passing a stationary cylinder if the linear superimposition of the wave induced velocity and current velocity is assumed.

Ikeda *et al.* (1988) and Otsuka *et al.* (1993) reported the values of drag coefficients as a function of the Keulegan-Carpenter number. They were found to be higher than those in planar oscillatory flow. The presence of circulation affecting the inertia forces was shown.

Li and Xu (1989) and Li and Kang (1992) used the Morison equation to calculate the wave-current force on a vertical and a submerged horizontal cylinder in regular and irregular waves. Like previous references on both vertical and submerged horizontal cylinders, their works were also confined to the first order forces and the force coefficients mentioned were without any hint on the mean forces. However, the authors indicated the modification of the Keulegan-Carpenter number including the effects of the ratio of current velocity to fluid velocity in a wave current coexisting flow field as a better hydrodynamic parameter. The authors further revealed that force coefficients from monochromatic wave measurements can be used directly for the computation of the irregular wave-current force in time domain.

Otsuka *et al.* (1990) further discussed the presence of viscous effects when the cylinder (rectangular and circular section) and a complete semi-submersible model is subject to a low frequency motion in waves. First order viscous drag forces were shown to originate from both underwater hull and vertical columns.

Wave forces on rectangular horizontal cylinder were measured by Arai (1993) showing a reduction in the viscous drag forces with a decrease in submersion depth. The circulation phenomenon was hinted at as the cause of the reduction in the inertia forces which has been further elaborated in (Arai 1995).

A detailed experimental study was conducted by Hamel-Derouich (1993) for vertical and horizontal rectangular cylinders of different aspect ratios in a steady flow, in waves and in waves and currents. The presence of currents was shown to affect the values of the drag coefficients. The force coefficients were also shown as a function of the Keulegan-Carpenter number and the Moe-Verley number to consider the two different flow fields- waves and currents without considering the effects of interactions on the said hydrodynamic parameters.

It can be concluded from the above review that most of the approaches

share a common view of treating a single surface piercing vertical cylinder representing the columns of a semi-submersible or a tension leg platform. Furthermore, wave elevation up to the instantaneous sea level has been the cause of the viscous drift force due to waves only in most of the approaches except of a few where such viscous drift forces were obtained from waves plus currents and then minus currents leaving waves alone. Such forces were calculated by exploiting the viscous drag force term of the Morison equation in all the references. Wave-current interaction effects were shown but mainly for the mean water level only while it is expected that currents can be considered present along with waves up to the actual wave elevation. Not much or hardly any attention has so far been paid to the values of drag coefficient in an appropriate manner. Moreover, when dealing with such mean forces, should the application of the oscillating drag coefficient C_D be appropriate or the values of the mean (steady) drag coefficient C_{D0} be used? In most of the cases, only horizontal relative velocity has been considered (which is quite true for a tension leg platform) but for semi-submersibles vertical motions are significant which would create a relative wave elevation in case of a floating vertical cylinder and would also affect the exponential term in the horizontal water particle velocity in case of a floating submerged pontoon.

In almost all the work regarding completely submerged bodies, viscous forces discussed are of first order. No reference was made to viscous effects on the mean drift force although the latter has a considerable magnitude especially on a submerged structure like submerged horizontal cylinders or pontoons in the presence of even small currents.

1.2 Present State-of-the-Art

Wave forces on offshore structures are calculated mainly in two ways namely by using the Morison equation and the diffraction theory. The Morison equation is applicable when a structure is small compared to the wave length signifying the existence of the drag force. On the other hand, when the size of the structure is comparable to the wave length, the presence of the body alters the wave field in its vicinity. In such a case, the diffraction (scattering and or reflection) of the waves from the surface of the body should be considered in the computation of the wave forces. Floating offshore structures like semi-submersibles and tension leg platforms which often have slender body cylindrical structures like vertical columns, bracings, etc. are

expected to attract significant drag forces.

The principal cause of the drag force component is the presence of a wake region on the 'downstream' side of the cylinder. The wake is a region of low pressure compared to the pressure on the 'upstream' side and thus a pressure differential results at the wake between the upstream and downstream of the cylinder at a given instant of time and causes a force to be exerted in the direction of the instantaneous water particle velocity. In a steady flow as the downstream side is fixed, the drag force is proportional to the square of the water particle velocity. In an oscillatory flow (body), the absolute value of the water particle velocity is inserted to insure that the drag force is in the same direction as the velocity.

Due to the empirical nature of the Morison equation, its application in a time dependent separated flow sometimes can be questionable. But since its inception in the early 50's, there have been and still many attempts are being made to modify and or derive new formulations for better accuracy. In spite of its critical assessment (Sarpkaya 1981), the original Morison equation remains as the strong design tool and has proved quite reliable in accurately predicting the wave force on a slender body structure though it is not a good basis for interpreting the physical flow mechanisms. Anomaly present or found are not important when many other uncertainties do exist in any design of an offshore structure. In this study, the use of the Morison equation should not surprise the readers that the author is tempted to be preoccupied with such a simple analytical expression keeping aside the difficulties. Note that two decades ago with the introduction of offshore structures, a simple two-term expression based on a linear-quadratic sum of forces was rather a universal one for the determination of the wave force but nowadays another alternative, the diffraction theory, is also available for such computation. At this stage, it is of paramount importance first to understand the viscous phenomena (difficulties associated with simple flows but rather complex) in their contribution towards the mean and slowly varying forces for a slender body type floating structure. So, it is desirable rather not to get bogged down with an extremely difficult numerical simulation without complete understanding of the physics of the phenomenon before the different fundamental aspects of the problem are investigated and treated. Studies of physical mechanisms of the force coefficients from the Morison equation from small scale, idealized models to large scale structures in real seas, should not in any way hinder the importance of the fundamental studies. The attempt would certainly lead to some progress towards unraveling the complexities en route to providing again some design data for the viscous regime.

In the present study, an attempt is made to establish the physical aspects and to derive a computational technique for the calculation of the viscous drift force (mean and slowly varying) on a moored semi-submersible mainly in extreme seas, i.e. in high waves associated with low frequencies. The method originates from the viscous drag force term of the Morison equation for small bodies when applied to the wetted surface in the splash zone of a surface piercing column of a semi-submersible. Interaction between several components of the platform and scale effects are kept out of the scope of this present work. The presence of currents is treated as an additional source of viscous origin. The relative velocity concept is taken as a further tool in solving the problem of a moored semi-submersible. All hydrodynamic aspects related to potential effects at zero speed are treated via 3-D potential theory with approximate modifications due to forward speed effects in the mean wave drift force calculations.

For a submerged structure like the pontoon of a semi-submersible, viscous effects on the mean drift force are not considered because the time averaged value of the drag force term of the Morison equation is zero but in a wave-current coexisting flow field, even a small magnitude of current velocity would cause the viscous drift force. In case of a vertical cylinder such as the column of a semi-submersible, wave elevation up to the instantaneous sea level is considered as the source of the viscous drift force due to waves only but in a wave-current coexisting flow field the fluid particle velocity is to be increased by superimposing the current velocity. In order to eliminate the uncertainties in the selection of the (mean) drag coefficient C_{D0} , not (oscillating) drag coefficient C_D , in a waves-only field and in a wave-current coexisting flow field, attention is paid to the experimental assessment of such complex force coefficients. Use of the linear (Airy) theory is made in conjunction with the Morison equation to model the hydrodynamic force.

Accordingly, the cylinder is considered divided into two parts namely the splash zone (from the mean water level to the actual sea level) and the submerged zone (from the mean water level down to the bottom of the cylinder). The splash zone is thus defined as the region that the free surface profile of a nominal progressive wavetrain can envelope for any given structural form. The pontoon is also considered a submerged zone in addition to the constantly submerged zone of the column. Force coefficients may be directly obtained from a fit to the Fourier coefficients via experimental measurements obtained from an instrumented segment located in the splash zone and in the submerged zone of a vertical cylinder and also

from a completely submerged pontoon tested in a towing tank.

The flow velocities and accelerations are usually computed from a particular wave theory which has been matched to the wave shape. The traditional linear wave theory attributed to Airy is in general inadequate for predicting the kinematics of water particles in the splash zone unless it is substantially modified for this purpose. The alternative is to develop nonlinear wave theories to provide more realistic estimates of the wave kinematics in the region where the Airy theory would at best be considered as a convenient approximation. In addition to the classical wave theories, some engineering methods have also been developed and those are the Wheeler's method (Wheeler 1970), Chakrabarti's method (Chakrabarti 1971) and Gudmestad's method (Gudmestad and Connor 1986).

Since different wave theories will, in general, produce different values of force coefficients for the same data, it is often suggested that their use be consistent in the selection of a wave theory. Many investigators have employed higher-order expansions in wave computations and report improved matching to the wave force. It is entirely possible that these improvements are only due to the additional terms in the curve fitting function and bear little relation to any improvements in the hydrodynamic description. For this reason and because actual kinematic measurements were not available for use in selecting a wave theory, it was felt that the linear wave theory would suffice for the purposes of this investigation. According to Gudmestad *et al.* (1988), simple linear theory gives reasonable agreement with the measurements while Wheeler's method and Chakrabarti's method do not give satisfactory results.

In dealing with the experimentally obtained force coefficients, it is essential that they are always expressed as function of some controlling hydrodynamic parameters. The Keulegan-Carpenter number is a direct measure of the drag force effect as it is again a function of the 'viscous parameter' ($\frac{H}{D}$) while the 'diffraction parameter' (kD) or ($\frac{D}{\lambda}$) determines the importance of the diffraction effect. When the 'viscous parameter' is large, the 'diffraction parameter' is small and vice versa. Thus, large diffraction effect means small drag effect and, inversely, when drag effect is large, the diffraction is negligible.

In the presence of currents, the velocity term in the drag force term of the Morison equation is normally replaced by the relative velocity term for an oscillating cylinder and the same concept is applied for a floating cylinder undergoing horizontal motions even in the presence of currents. However, an alternative form was proposed by Moe and Verley (1977) in which the

effect of current is separated from the oscillatory structure motion and, thus, resulting in a 'two term' drag force term. Sarpkaya *et al.* (1984) has shown, based on experimental findings, that the decomposition of the force exerted on a cylinder by the coexisting wave-current field is not very meaningful. Furthermore, the drag coefficients for the no-current case are not identical with those obtained for the current-harmonic-flow case (coexisting flow field), particularly, the wake biasing decreases the drag coefficient.

1.3 The Hypotheses

- For slender body type structures, viscous drag forces exist and are treated by means of the nonlinear drag force term of the Morison equation.
- In a waves-only flow field, the viscous mean force for a constantly submerged body is zero while due to relative wave elevation in the free surface (splash zone), the viscous mean force originates in a highly nonlinear (cubic not quadratic) way.
- The presence of small currents will result in an additional source of the viscous mean force even for the constantly submerged body.
- Oscillating drag coefficients C_D are not applicable while treating such problems of mean forces. Rather more appropriate mean drag coefficients C_{D0} are required.
- Force coefficients in regular waves can be applicable for the slowly varying (low frequency) force in irregular waves when the slowly varying wave envelope with associated frequencies is taken into consideration.
- The 'relative velocity' concept is applicable in the drag force term of the Morison equation in case of a floating body, even in the presence of currents.
- While the frequency domain analysis is sufficient to deal with the viscous mean drift force in regular waves, the time domain analysis is essential for the viscous low frequency drift force in irregular waves because of the highly nonlinear nature in its modeling.

1.4 The Objectives

The primary objective of this study is to evaluate the theoretical viscous mean and low frequency horizontal drift forces on a moored floating structure like a semi-submersible via its columns and pontoons separately.

Because of the newness of such a complex problem, a systematic series of experiments needs to be taken in hand to validate the theory and establish the force coefficients in regular wave model tests at zero speed and with forward speed before they can be applied to mean forces in regular waves and to irregular waves in connection with the viscous low frequency drift force.

In doing the exercise, the aim is also to keep looking at some other theories given so far in conjunction with the present experimental findings.

In addition to the above, some fundamental investigations like appropriate choice of force coefficients, their representation as function of proper controlling hydrodynamic parameters in line with fluid flow conditions are to be cared for.

1.5 The Outlines

In **Chapter 2**, details are presented of different model tests namely fixed vertical cylinders, fixed submerged pontoon, fixed semi-submersible and free floating (soft moored) semi-submersible. Model construction, test set-up and procedure, equipment and measurement, data acquisition and analysis are described in a comprehensive manner.

In **Chapter 3**, a theoretical study Dev (1992a) will be carried out for finding the viscous contributions to the horizontal mean drift force on a vertical cylinder in fixed and free floating conditions in regular waves. In theory, the value of the mean drag coefficient is suppressed by taking its value as unity. A series of model experiments with fixed segmented vertical cylinders of different diameter in still water, in waves and in waves and currents will be discussed and analyzed. The primary nonlinear viscous wave drift force is well demonstrated to be concentrated in the splash zone in waves only whereas even a small amount of currents gives further rise to the said force in the submerged zone. Such experimental evaluation validates the theory, i.e. the physical aspects and paves the way for ascertaining the values of the mean drag coefficients in a waves-only flow field and in a wave-current coexisting flow field. The appropriate definition and use of the

controlling hydrodynamic parameters in the respective fluid fields are also discussed in detail.

In **Chapter 4**, experimental analysis with a fully submerged fixed pontoon similar to the underwater hull of a semi-submersible is given. Theory concerning the viscous mean drift force for a fixed and floating pontoon in waves and currents will be discussed. Application of the mathematical modeling will be shown and compared with experimental results based on the experimentally obtained values of the mean drag coefficients.

In **Chapter 5**, the basis of a mathematical model for a semi-submersible in regular waves with and without currents is outlined which is a synthesis of the earlier tools described in Chapter 3 and Chapter 4. The computational method for calculating the forces on a semi-submersible in currents only will also be described. The final numerical model for predicting the additional hydrodynamic excitation force in the form of low frequency, viscous and potential, drift forces in irregular waves is presented. Computed and measured results of a fixed and a free floating semi-submersible in currents only will be discussed.

In **Chapter 6**, details of the results of experiments with a fixed semi-submersible (ITTC Model) in both head and beam seas at zero speed and with forward speed (simulating currents) will be given. The computational technique would be tested against experimental results before it is further applied to a moored semi-submersible in both regular and irregular waves. Because of the inherent complexity of the problems due to their viscous origin, the rational approach chosen is based on a simple mathematical background along with systematic experimental findings. The technique is finally applied and compared with model tests results and other published data.

References

- Arai, S. (1993). Forces and flows around a horizontal rectangular cylinder submerged in regular waves. In *Proceedings of the International Offshore and Polar Engineering Conference*, ISOPE, Singapore, pp. 288-293.
- Arai, S. (1995). Forces and circulation of horizontal cylinders submerged in regular waves. In *Proceedings of the International Offshore and Polar Engineering Conference*, ISOPE, The Hague, The Netherlands, pp. 348-355.
- Bearman, P. and J. Graham (1979). Hydrodynamic forces on cylindrical bodies in oscillatory flow. In *Proceedings of the International Conference on Behavior of Offshore Structures*, BOSS, London, England, pp. 309-322.
- Burns, G. E. (1983). Calculating viscous drift of a tension leg platform. In *Proceedings of the International Conference on Offshore Mechanics and Arctic Engineering*, OMAE, Houston, Texas, pp. 22-30.
- Chakrabarti, S. (1971). Dynamics of single point mooring in deep water (discussion). *Journal of Waterway, Port, Coastal and Ocean Engineering*, ASCE 97(WW3), 588-590.
- Chakrabarti, S. K. (1984). Steady drift force on vertical cylinder - viscous vs. potential. *Applied Ocean Research* 6(2), 73-82.
- Chaplin, J. R. (1984). Nonlinear forces on a horizontal cylinder beneath waves. *Journal of Fluid Mechanics* 147, 449-464.
- Chitrapu, A. S., R. C. Ertekin, and J. R. Paulling (1993). Viscous drift forces in regular and irregular waves. *Ocean Engineering* 20(1), 33-55.
- Denise, J.-P. F. and N. J. Heaf (1979). A comparison of linear and nonlinear response of a proposed tension leg production platform. In *Proceedings of the Annual Offshore Technology Conference*, OTC 3555, Houston, Texas, pp. 1743-1754.
- Dev, A. K. (1992). Evaluation of viscous mean drift forces on a vertical cylinder in waves and currents. Technical Report 927-M, Ship Hydromechanics Laboratory, Delft University of Technology, Delft, The Netherlands.
- Ferretti, C. and M. Berta (1980). Viscous effect contribution to the drift forces on floating structures. In *Proceedings of the International Sym-*

- posium of Ocean Engineering and Ship Handling*, SSPA, Gothenburg, Sweden, pp. 9:1-9:10.
- Gudmestad, O. and J. Connor (1986). Engineering approximations to nonlinear deepwater waves. *Applied Ocean Research* 8(2), 76-88.
- Gudmestad, O., J. Johnsen, J. Skjelbreia, and A. Torum (1988). Regular water wave kinematics. In *Proceedings of the International Conference on Behavior of Offshore Structures*, BOSS, Trondheim, Norway, pp. 789-803.
- Hamel-Derouich, D. (1993). *Hydrodynamic Forces on Rectangular Cylinders of Various Aspect Ratios Immersed in Different Flows*. Ph. D. thesis, Department of Naval Architecture and Ocean Engineering, University of Glasgow, Glasgow, Scotland.
- Huse, E. (1976). Wave induced mean force on platforms in direction opposite to wave propagation. *Interocean*, IO 76:221/01-IO 76:221/05.
- Ikeda, Y., K. Otsuka, and N. Tanaka (1988). Viscous forces acting on a semi-submersible. In *Proceedings of the International Conference on Offshore Mechanics and Arctic Engineering*, OMAE, Houston, Texas, pp. 101-108.
- Kato, S. and T. Kinoshita (1990). Nonlinear response of moored floating structures in random waves and its stochastic analysis; part 1 (theory and model experiments. Technical Report 27(4), Ship Research Institute, Ministry of Transport, Tokyo, Japan.
- Kobayashi, M., K. Shimada, and T. Fujihara (1985). Study on dynamic response of a tlp in waves. In *Proceedings of the International Conference on Offshore Mechanics and Arctic Engineering*, OMAE, Dallas, Texas, pp. 29-35.
- Koterayama, W. (1979). Wave forces exerted on submerged circular cylinders fixed in deep waves. Technical Report 84, Research Institute for Applied Mechanics, Kyushu University, Kyushu, Japan.
- Li, Y.-C. and H.-G. Kang (1992). Wave-current forces on slender circular cylinder. In *Proceedings of the International Conference on Offshore Mechanics and Arctic Engineering*, OMAE, Calgary, Alberta, Canada, pp. 117-125.
- Li, Y.-C. and M.-K. Xu (1989). Wave-current force on horizontal cylinder. In *Proceedings of the International Conference on Offshore Mechanics*

- and Arctic Engineering*, OMAE, The Hague, The Netherlands, pp. 7-12.
- Lundgren, H., S. E. Sand, and J. Kirkegaard (1982). Drift forces and damping in natural sea states- a critical review of the hydrodynamics of floating structures. In *Proceedings of the International Conference on Behavior of Offshore Structures*, BOSS, Cambridge, Massachusetts, pp. 592-607.
- Maruo, H. (1960). The drift of a floating body in waves. *Journal of Ship Research* 189, 149-157.
- Moe, G. and R. L. P. Verley (1977). Hydrodynamic damping of offshore structures in waves and currents. In *Proceedings of the Annual Offshore Technology Conference*, OTC 3798, Houston, Texas, pp. 37-44.
- Morison, J. R., J. R. O'Brien, M. P. Johnson, and S. A. Schaaf (1950). The force exerted by surface waves on piles. *Petroleum Transactions, AIME* 189, 149-157.
- Newman, J. N. (1967). The drift force and moment on ships in waves. *Journal of Ship Research* 11, 51-60.
- Otsuka, K., Y. Ikeda, and N. Tanaka (1990). Viscous forces acting on a horizontal circular cylinder in regular and irregular waves. In *Proceedings of the International Conference on Offshore Mechanics and Arctic Engineering*, OMAE, Houston, Texas, pp. 129-138.
- Otsuka, K., F. Niwa, and Y. Ikeda (1993). Viscous forces acting on oscillating roughened cylinders. In *Proceedings of the International Offshore and Polar Engineering Conference*, ISOPE, Singapore, pp. 436-443.
- Pijfers, J. G. L. and A. W. Brink (1977). Calculated drift forces of two semi-submersible platform type in regular and irregular waves. In *Proceedings of the Annual Offshore Technology Conference*, OTC 2977, Houston, Texas, pp. 155-164.
- Pinkster, J. (1974). Low frequency phenomena associated with vessels moored at sea. *Journal of the Society of Petroleum Engineers, AIME* (December), 1-16.
- Pinkster, J. A. (1980). *Low Frequency Second Order Wave Exciting Forces on Floating Structures*. Ph. D. thesis, Ship Hydromechanics Laboratory, Delft University of Technology, Delft, The Netherlands.

- Pinkster, J. A., A. Dercksen, and A. K. Dev (1993). Hydrodynamic aspects of moored semi-submersibles and ttps. In *Proceedings of the Annual Offshore Technology Conference*, OTC 7190, Houston, Texas, pp. 601-614.
- Ramberg, S. E. and J. M. Niedzwecki (1982). Horizontal and vertical cylinders in waves. *Ocean Engineering* 9(1), 1-15.
- Sarpkaya, T. (1981). A critical assessment of morison's equation. In *Proceedings of the International Symposium on Hydrodynamics in Ocean Engineering*, Trondheim, Norway, pp. 447-467.
- Sarpkaya, T., C. Bakmis, and M. A. Storm (1984). Hydrodynamic forces from combined wave and current flow on smooth and rough circular cylinders at high reynolds numbers. In *Proceedings of the Annual Offshore Technology Conference*, OTC 4830, Houston, Texas, pp. 455-462.
- Standing, R. G., W. J. Brendling, and G. E. Jackson (1991). Full scale measured and predicted low-frequency motions of the semi-submersible 'uncle john'. In *Proceedings of the International Offshore and Polar Engineering Conference*, ISOPE, Edinburgh, Scotland, pp. 434-441.
- Stokes, G. (1847). On the theory of oscillatory waves. In *Cambridge Philosophical Society*.
- Teng, C. C. and J. H. Nath (1985). Forces on horizontal cylinders towed in waves. *Journal of Waterway, Port, Coastal and Ocean Engineering* 111(6), 1022-1040.
- Teng, C. C. and J. H. Nath (1988). Periodic waves on horizontal cylinders. In *Proceedings of the International Conference on Offshore Mechanics and Arctic Engineering*, OMAE, Houston, Texas, pp. 391-398.
- Wheeler, J. D. (1970). Method for calculating forces produced by irregular waves. *Journal of Petroleum Technology, AIME* (March), 359-367.

Chapter 2

Model Tests

From the historical review presented in Chapter 1, it is found that no model tests were conducted specifically to understand the source of viscous contributions in the horizontal mean drift force especially in a waves only flow field. Though the free surface zone (splash zone) of surface piercing vertical cylinders has been hinted as the main source of viscous contributions as it is the direct result of the product of a wave force term, which is in proportion to a squared fluid velocity in the drag force term of the Morison equation, and a wave surface elevation. So, conducting experiments to validate this splash zone force was inevitable. At the same time, it was also necessary to establish that the constantly submerged zone of a cylinder and a pontoon in a waves only flow field does not attract any viscous contributions toward the horizontal mean drift force. Besides, it is essential to understand the change in viscous effects in the presence of currents. Apart from individual models of the structural components of a semi-submersible, the model tests with a fixed complete semi-submersible is necessary to make sure that the results from the individual models tests are consistent for the global case. A semi-submersible is mostly a moored floating structure in a seastate undergoing motions and drift due to the wave excitation forces. So, finally model tests with a free floating (soft moored) semi-submersible in a real seastate (irregular waves) was done.

The aims of the study were as follows:

- To understand the source of viscous effects and their magnitude
- The effects of the presence of currents on the drift forces

- Evaluation of the force coefficients as representative of hydrodynamic parameters

In particular the study was aimed at clarifying the followings:

- To check the validity of a computation method for the prediction of the mean and low frequency viscous drift forces on moored semi-submersibles in a seaway
- To check the validity of 3-dimensional computation method for prediction of the first order motions and the mean and low frequency wave (potential) drift forces.
- To provide guidelines on drift forces for a representative semi-submersible design

The experiments were performed with the following types of models:

1. Fixed, vertical, surface piercing and truncated cylinders of two different diameters – the larger diameter cylinder hereinafter referred to as the large cylinder and the smaller diameter cylinder hereinafter referred to as the small cylinder
2. Fixed submerged pontoon hereinafter referred to as the pontoon
3. Fixed semi-submersible
4. Free floating (soft moored) semi-submersible

The following investigations were carried out with the fixed models:

- Tests in still water (a uniform flow) to determine the current loads.
- Tests in regular waves (a waves-only flow) to determine the wave loads.
- Tests in regular waves and currents (a wave-current coexisting flow) to determine the total wave and current loads.

The wave loads in this case are the first order wave forces and the horizontal mean drift forces.

The following investigations were carried out with the free floating model of the semi-submersible:

- Tests in regular waves without and with currents (a waves-only flow and a wave-current coexisting flow) to determine the first order motion transfer functions (RAOs) and the horizontal mean drift forces.
- Tests in irregular waves without and with currents to determine the horizontal drift forces and the wave frequency motions.

2.1 The Towing Tanks

The experiments were carried out in the towing tanks of the Ship Hydromechanics Laboratory of Delft University of Technology (DUT) and in the Sea-keeping Basin of Maritime Research Institute Netherlands (MARIN). There are two towing tanks in the Ship Hydromechanics Laboratory hereinafter referred to as the Tank No.1 and the Tank No.2.

The tests with the large cylinder, the pontoon and the semi-submersibles were carried out in the Tank No.1. The dimensions of the tank are 142.0 m long, 4.22 m wide and 2.5 m maximum water depth. The tank is equipped with an electro-hydraulic plunger type wave maker fitted across the width at one end of the tank that generates regular and irregular waves in a wavelength range of 0.3 - 6.0 meter. The maximum wave height generated is 30 cm (depending on the chosen wave frequency). At the other end of the tank, a concrete beach in the form of a parabolic arc with transverse wooden beams is fitted to absorb the energy of the oncoming waves. The tank is also equipped with an electronically controlled motor driven towing carriage, with a manned observation platform, capable of traveling at a speed of up to 7 m/s.

In order to measure the undisturbed wave heights, a resistance type wave probe was placed on a small platform which can also be manually towed. Another two wave probes, one in front and one beside the model, in line with the model center of gravity, were mounted on the towing carriage for measuring wave heights, wave phase angles, etc. during the tests. All wave probes were portable type. The calibration of the wave probes was carried out by lifting up and lowering down the wave probes ± 6 cm and recording the corresponding signals.

On the observation platform of the towing carriage, several facilities are provided. During the model tests, the output from the model force transducers and the wave probes were first amplified and then filtered before they were recorded and processed by a personal computer using a data acquisition program named "DASTANK".

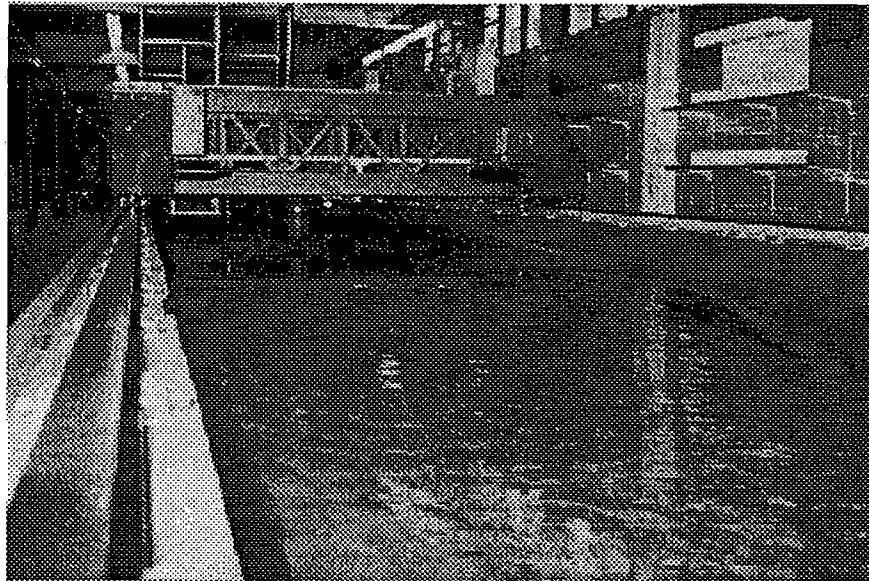


Figure 2.1: *The Towing Tank No.1 of DUT*

The Tank No.2, in which the tests with the small cylinder were carried out, is equipped like the Tank No.1 although the dimensions of the tank are different. The maximum carriage speed here is 3 m/s and the tank dimensions are 66.00 m long, 2.75 m wide and 1.25 m maximum water depth. The wave maker can generate both regular and irregular waves in a wavelength range of 0.4 - 6.5 meter and a wave amplitude of up to 15 cm (depending on the chosen wave frequency). The facilities on the carriage are similar to the Tank No.1.

The dimensions of the Seakeeping Basin of MARIN are Length x Breadth = 100.0 m x 24.5 m having a water depth of 2.5 m. The towing carriage, manned and motor driven, has a maximum speed of 4.5 m/s. The wave generator capability is regular and irregular waves in a wave period range of 0.7 - 3.0 s with a maximum wave height up to 0.3 m (significant), having wave directions between 180 - 270 and 0 - 90 and any angle in between. The wave maker is of the flap type. The beach is of a lattice type on circular arc plates. Portable electric resistance type wave probes were used for wave measurements.

The Tank No.1 of DUT and the Sea-keeping Basin of MARIN are shown in Figure 2.1 and Figure 2.2 respectively.

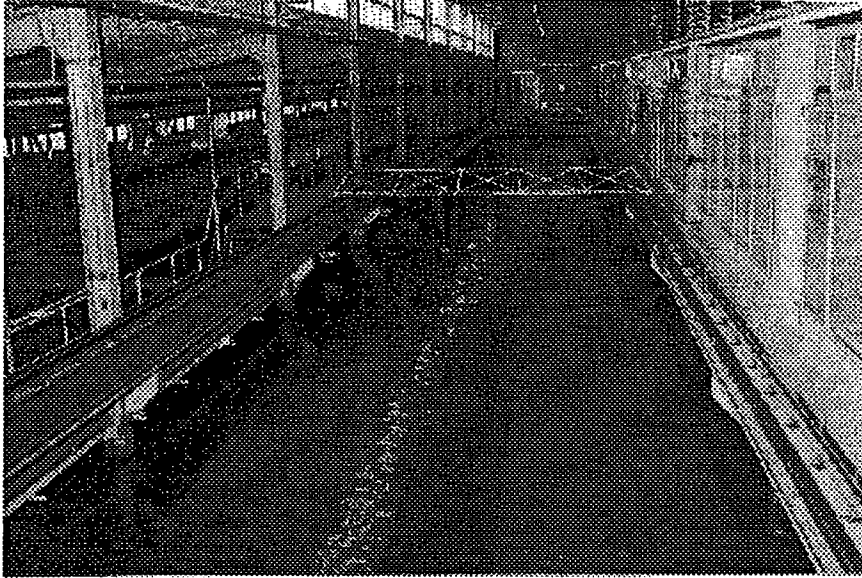


Figure 2.2: *The Sea-keeping Basin of MARIN*

2.2 The Models

2.2.1 The Small Cylinder

The model scale was 1 to 100. The small cylinder had a diameter of 7.5 cm and its total length was 91 cm. It was segmented into four sections, namely in order upper dummy, upper test, lower test and lower dummy, each mounted to a continuous rectangular steel beam inside. The top dummy section (20 cm long) and the bottom dummy section (11 cm long) were directly fixed to the beam. The two middle test sections (the upper one 40 cm long and the lower one 30 cm long) were each mounted to the beam by a small, double-shear type force transducer with a range of 180 Newton (upper test section) and 250 Newton (lower test section).

The clefts between the successive sections were closed and thus made watertight with thin rubber seals which were found to cause no couplings between the sections. The upper end of the steel beam served the purpose of supporting the complete model above water.

The arrangement of the fixed vertical small cylinder model in the Tank No.2 of DUT is shown in Figure 2.3.

Further details of the model tests namely construction of the model, test

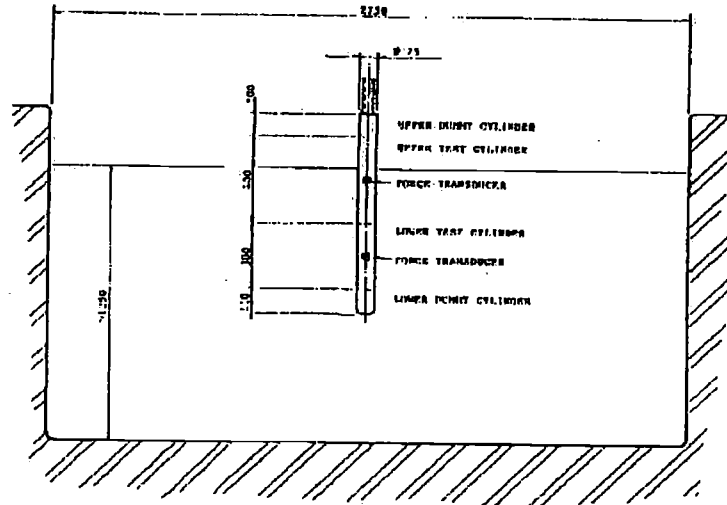


Figure 2.3: *The small cylinder model in the Tank No.2 of DUT*

set-up and procedure, experimental data are available in (Dev 1992b).

2.2.2 The Large Cylinder

The model scale was 1 to 35. This model was built up in a similar way like the small cylinder except the dimensions were different. All the sections, both dummy and test, were of 31.5 cm diameter. The bottom dummy section was 30 cm long. Both the test sections were also 30 cm long. The top dummy section was 15 cm long. Thus, the total model length was 105 cm.

The force transducers used, were temple-shaped type force transducers with a range of 200 Newton each. At each test section, two such transducers were mounted on each other, one was attached to the front face and the other to the side face to measure the in-line and transverse forces.

The arrangement of the fixed vertical large cylinder model in the Tank No.1 of DUT is shown in Figure 2.4.

Further details of the model tests namely construction of the model, test set-up and procedure, experimental data are available in (Dev 1992c; Dev 1993).

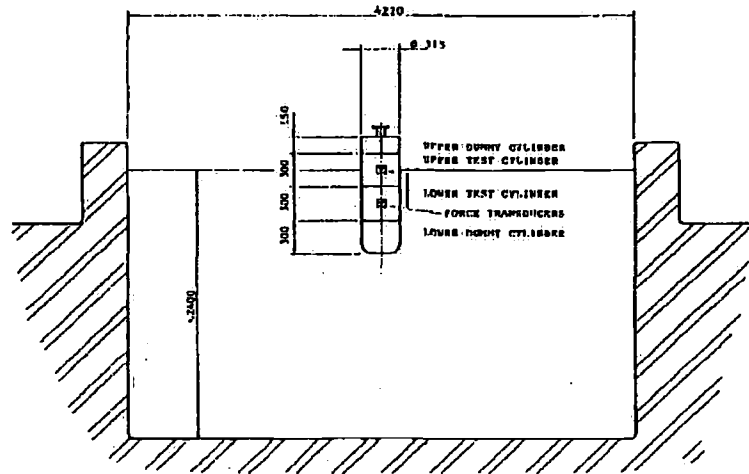


Figure 2.4: *The large cylinder model in the Tank No.1 of DUT*

2.2.3 The Pontoon

The model scale was 1 to 50. The pontoon was 2.3 m long, 30 cm wide and 18 cm high. Both ends of the model were made triangular shaped over a length of 14.6 cm and all the edges had a radius of about 1 cm. The pontoon was fixed on two vertical cylinders by two sets of force transducers (temple-shaped type). Each set contained three such force transducers for the inline, transverse and vertical forces. The force transducers were mounted on top of one another having mountings inside the pontoon and the cylinder. One set was mounted on a longitudinal sleigh to prevent distortion tension. The transducers with a range of 200 Newton each for the x-forces, 800 Newton each for the y-forces and 400 Newton each for the z-forces were used.

To prevent water ingress, the gaps between the pontoon and the cylinders were made watertight with thin rubber seals and also applying rubber coatings. The cylinders were 57.5 cm long and of 10.8 cm diameter. They were directly mounted to the carriage via steel beams.

The construction and arrangement of the fixed submerged pontoon model is shown in Figure 2.5.

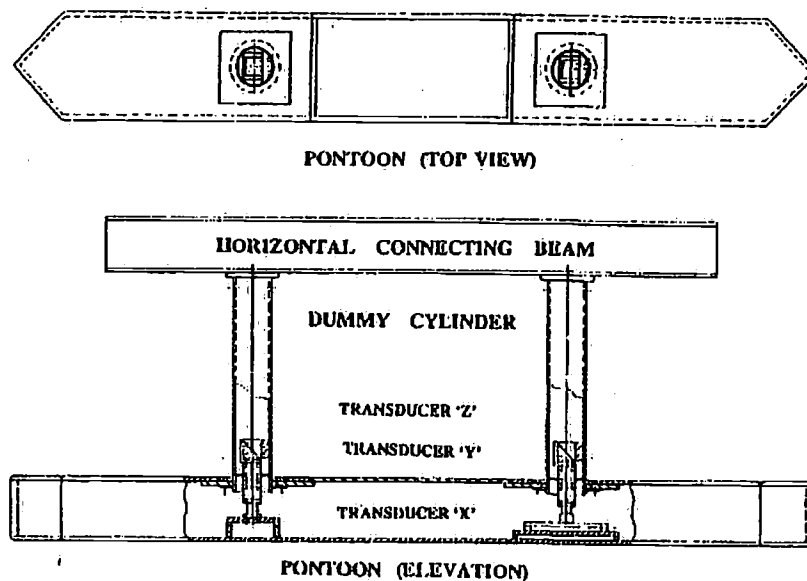


Figure 2.5: *The construction of the fixed submerged pontoon model*

Further details of the model tests namely construction of the model, test set-up and procedure, experimental data are available in (Dev 1993c).

2.2.4 The Fixed Semi-submersible

The model scale was 1 to 75. The model of the ITTC semi-submersible was constructed of steel for the columns and wood for the pontoon. Four out of eight columns were connected only to the deck structure and thus were made free from the pontoon top. These columns carried their individual force transducers with a range of 100 Newton each for measuring the horizontal force on the columns independently. For the deck structure, a steel frame was used to give enough structural rigidity and to fix the model to the carriage via steel beams. Besides, the model was fitted with six force transducers – three to measure the total horizontal force and three for the total vertical force. Besides, two wave probes were connected to the model to measure the relative wave elevation. All the force transducers used, were of the temple-shaped type. The transducers were fitted between the top of the columns and the steel frame. For the complete model, three sets of transducers, each

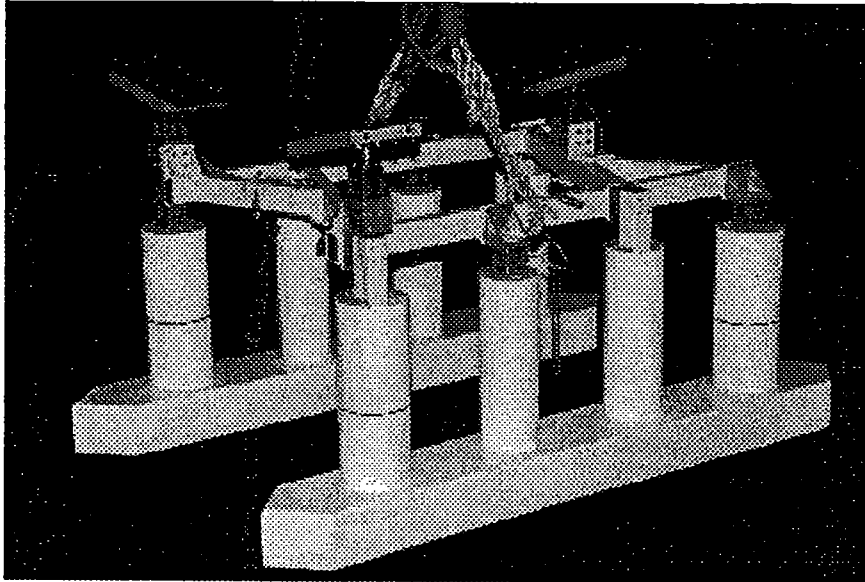


Figure 2.6: *The ITTC semi-submersible model for the fixed condition*

comprising two—one for the inline force and the other for the vertical force, were mounted on the deck steel frame. The transducers had a range of 200 Newton each.

Figure 2.6 and Figure 2.7 show the ITTC semi-submersible model configuration used for the experiments in the fixed condition.

Further details of the model tests namely construction of the model, test set-up and procedure, experimental data are available in (Dev 1995a).

2.2.5 The Free Floating (Moored) Semi-submersible

The basic construction was the same as the fixed semi-submersible except the deck construction was changed to a lighter material called Armhole F-Board (aluminum honeycomb core with woven glassy epoxy skin). Only the four columns were fitted with force transducers in a similar way as was done for the fixed semi-submersible. The model was weighed and dynamically balanced to measure the radii of gyration in air about the center of gravity. In the tank, inclining experiments were carried out to check the vertical position of the center of gravity. Natural periods of heave, pitch and roll were also measured. The particulars of the semi-submersible are given in Table 2.1.

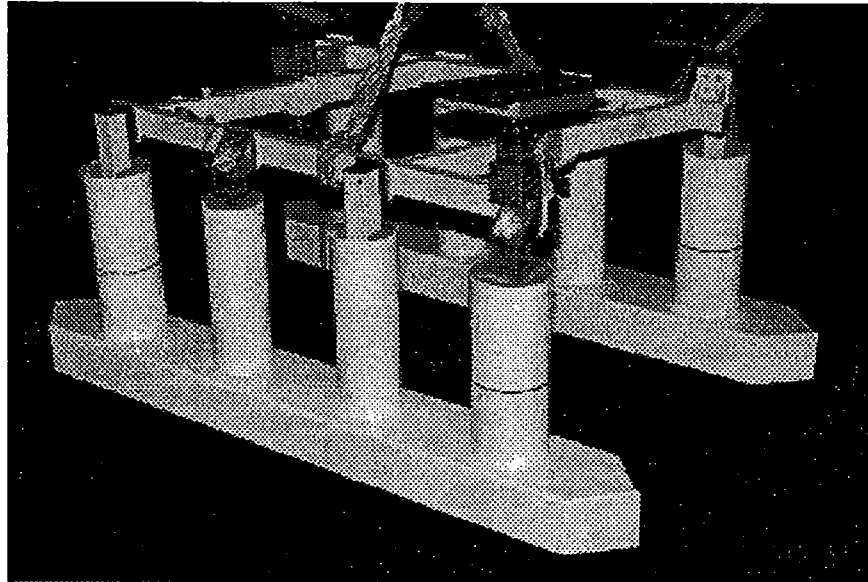


Figure 2.7: *The ITTC semi-submersible model for the fixed condition*

Further details of the model tests namely construction of the model, test set-up and procedure, experimental data are available in (Dev 1995c).

2.3 Test Set-up and Procedure

2.3.1 The Small Cylinder

The model tests were carried out in the Tank No.1 of the Ship Hydromechanics Laboratory. The model was fixed on to a cradle for raising up and lowering down the complete cylinder model. The cradle works on the rack-pinion principle.

For tests with the cylinders, the models were constructed in a unique way to represent the two separate hydrodynamic zones like the splash zone to represent the effects of the wave elevation during the crest and the trough phases and the submerged zone which is always immediately under the trough phase of the wave. During the experiment, the vertical position of the cylinder was adjusted so that the draft of the upper test section (splash zone) was equal to the amplitude of the incoming wave. Thus the trough of the passing wave always remained at the separation line between the splash zone and

Designation	Model	Prototype
<i>Lo.a.</i>	1.533 m	115.000 m
<i>Bo.a.</i>	1.000 m	75.000 m
<i>D</i>	0.600 m	45.000 m
Pontoon:		
<i>L_p</i>	1.533 m	115.000 m
<i>B_p</i>	0.200 m	15.000 m
<i>D_p</i>	0.120 m	9.000 m
Columns:		
<i>D_{cl}</i>	0.150 m	11.000 m
<i>D_{cs}</i>	0.125 m	9.500 m
<i>T</i>	0.2825m	21.1875m
Δ	0.089 t	37546.875 t
<i>KG</i>	0.277 m	20.775 m
<i>GM_t</i>	0.035 m	2.625 m
<i>GM_t</i>	0.029 m	2.175 m
<i>K_{xx}</i>	0.485 m	36.394 m
<i>K_{yy}</i>	0.451 m	33.816 m
<i>K_{zz}</i>	0.536 m	40.228 m
<i>T_x</i>	14.34 s	124.188 s
<i>T_y</i>	10.88 s	94.223 s
<i>T_z</i>	2.557 s	22.144 s
<i>T_φ</i>	7.120 s	61.661 s
<i>T_θ</i>	6.935 s	60.059 s

Table 2.1: Main Particulars of the ITTC semi-submersible

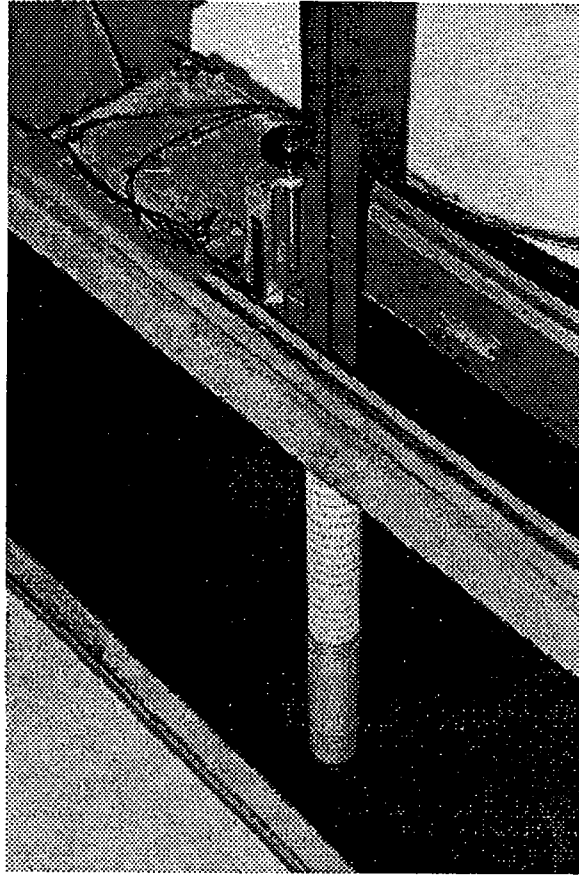


Figure 2.8: *The small cylinder model in the Tank No.2 of DUT*

the submerged zone. The submerged zone was always kept fully submerged throughout the experiment.

The test set-up of the small cylinder model in the Tank No.2 of DUT is shown in Figure 2.8.

Tests were first performed in still water at various speeds with a cylinder draft of up to 20 cm of the upper test cylinder. Tests were then conducted in regular waves for a wave frequency range of 3 - 10 rad/s. For each wave frequency, three wave amplitudes (ascending order) were used. The wave amplitudes were varied from 10 mm to 90 mm depending on the wave frequencies used. At every intermediate wave amplitude for each frequency, tests were also conducted for positive and negative currents in still water

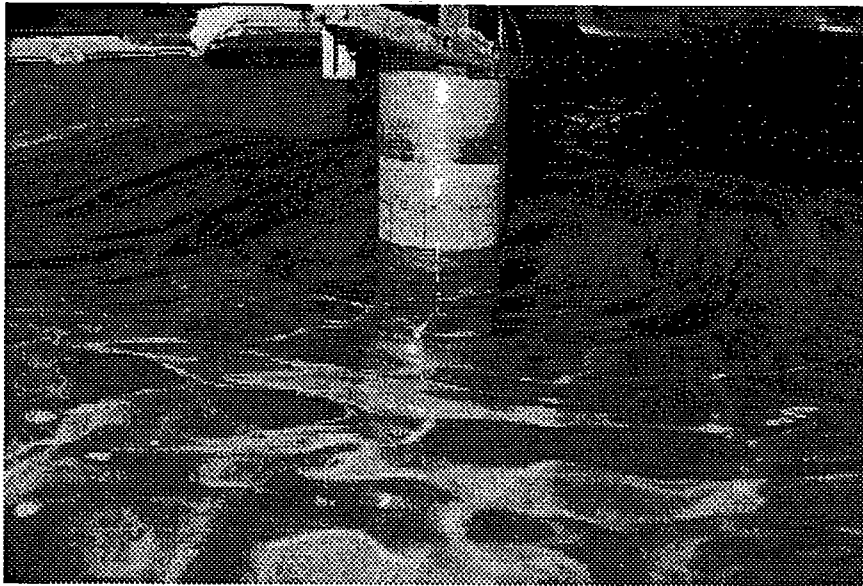


Figure 2.9: *The large cylinder model in the Tank No.1 of DUT*

as well as in the presence of waves. Two uniform velocities were used and those were ± 0.15 m/s and ± 0.30 m/s ($+$ means towing the carriage towards the wave maker, i.e. into the waves simulating waves and currents in the same direction and $-$, away from the wave maker, i.e. out of the waves simulating waves and currents in the opposite direction). As the wave amplitudes were different for different wave frequencies, tests were done in still water for different immersion (draft) of the splash zone equal to the different wave amplitudes used with positive and negative currents using the aforementioned carriage speeds.

2.3.2 The Large Cylinder

The model tests were carried out in the Tank No.1 of the Ship Hydromechanics Laboratory and also in the Seakeeping Basin of MARIN.

The test set-up of the large cylinder model in the Tank No.1 of DUT is shown in Figure 2.9.

The cylinder model was connected to a beam across the towing carriage and both ends of the beam were further connected to two cradles for sliding up and down the complete cylinder model. The model itself was also firmly held in its vertical position by additional supports to two other fixed beams

connected to the towing carriage. The two cradles were supported on one of the two fixed beams. The said arrangement was adopted while carrying out the tests in the Ship Hydromechanics Laboratory.

Tests were first performed in still water at different speeds with a cylinder draft of up to 15 cm for the upper test cylinder. Tests were then conducted in regular waves for a wave frequency range of 3.25 - 6.50 rad/s. For each wave frequency, three wave amplitudes were utilized. The wave amplitudes were varied from 20 mm to 135 mm depending on the chosen wave frequencies. At each wave frequency for each wave amplitude, tests were carried out for both positive and negative currents in the presence of regular waves. For each wave frequency and for each wave amplitude, three different carriage speeds were used, namely 0.173 m/s, 0.261 m/s and 0.348 m/s. Similar to the small cylinder model, as the wave amplitudes were different for different wave frequencies, tests were done in still water for different immersion (draft) of the splash zone equal to the different wave amplitudes used with positive and negative currents using the aforementioned carriage speeds. Besides the above, some additional tests were carried out in regular waves only using a few different wave amplitudes in order to gather more data in a waves-only field. The said experiment was conducted in Tank No.1 of the Ship Hydromechanics Laboratory.

Limited tests were conducted in the Seakeeping Basin of MARIN where the set-up arrangement was slightly different because of the variations in the towing carriage construction. A U-shaped construction was made up of steel beams connected to each other while the horizontal beam was used to hold the cylinder model by means of a single cradle. The two vertical beams were fixed to the carriage construction members thus providing the strong structural rigidity of the entire set-up.

The test set-up of the large cylinder in the Sea-keeping Basin of MARIN is shown in Figure 2.10.

Tests were conducted in regular waves for a wave frequency range of 2.66 - 5.32 rad/s. For each wave frequency, two to three different wave amplitudes were used as before. The wave amplitudes were varied from 50 mm to 135 mm. For each wave frequency at each wave amplitude, tests were conducted for both positive and negative currents in the presence of regular waves. One carriage speed of 0.261 m/s was used.

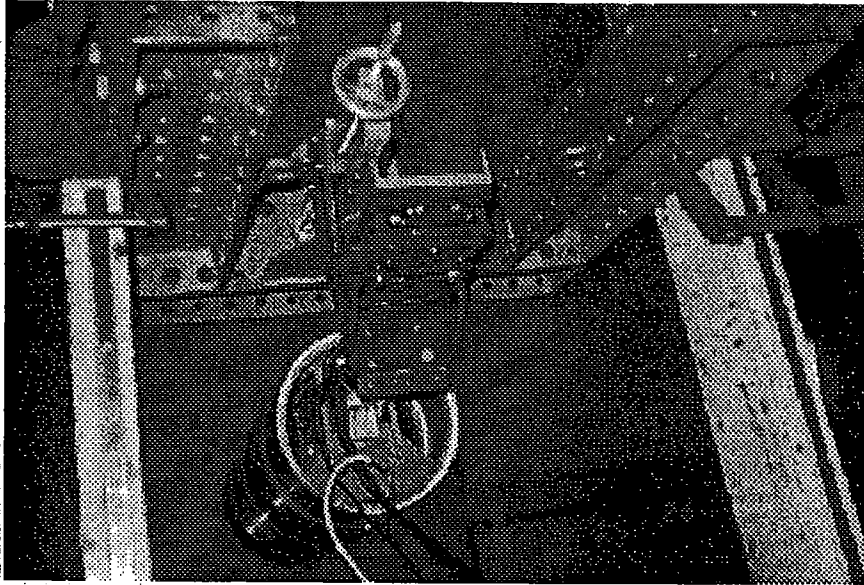


Figure 2.10: *The large cylinder model in the Sea-keeping Basin*

2.3.3 The Pontoon

The model tests were conducted in the Tank No.1 of the Ship Hydromechanics Laboratory. The model itself was submerged and the draft amounted to 40 cm. In fact the cylinders were not in any way connected to the pontoon body so as not to attract any load. The cylinders were rather used to connect the entire rig to the carriage via fixed steel beams. Tests were performed for both head seas and beam seas.

The test set-up of the fixed submerged pontoon in the Tank No.1 of DUT in head seas and in beam seas are shown in Figure 2.11 and Figure 2.12 respectively.

Tests were first performed at various speeds in still water. Tests were then conducted in regular waves for a wave frequency range of 3.54 - 7.07 rad/s. For each wave frequency, five wave amplitudes were employed. At each wave frequency for three wave amplitudes, tests were carried out for both positive and negative currents in the presence of regular waves. Three carriage speeds of 0.146 m/s, 0.218 m/s and 0.291 m/s were used.

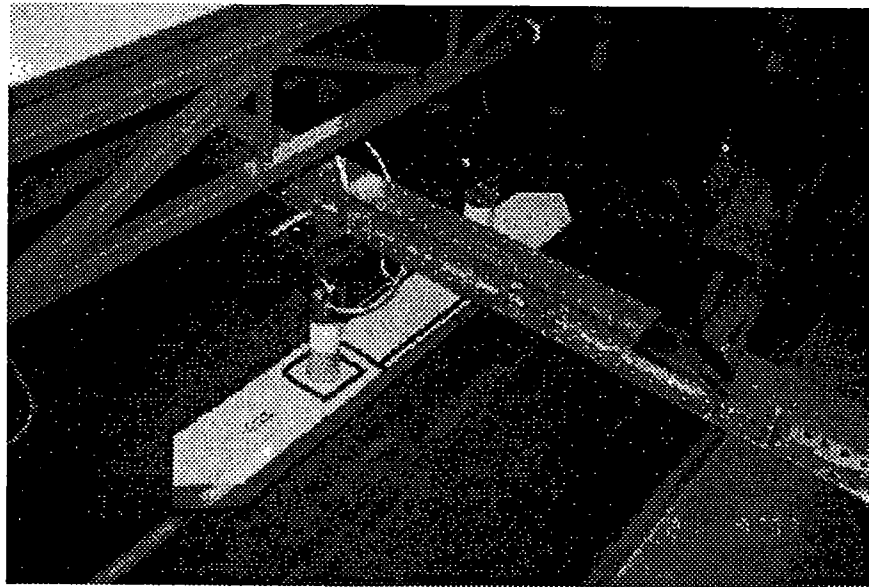


Figure 2.11: *The fixed submerged pontoon model in head seas*

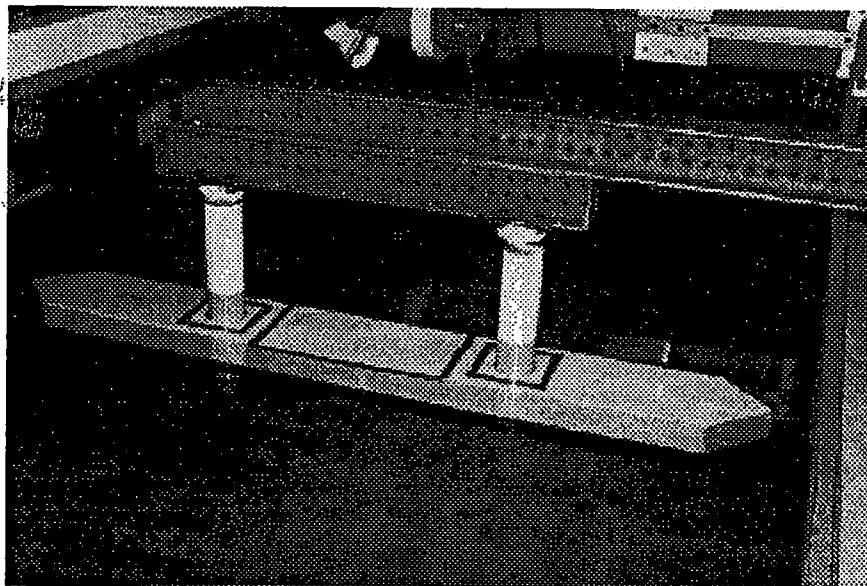


Figure 2.12: *The fixed submerged pontoon model in beam seas*

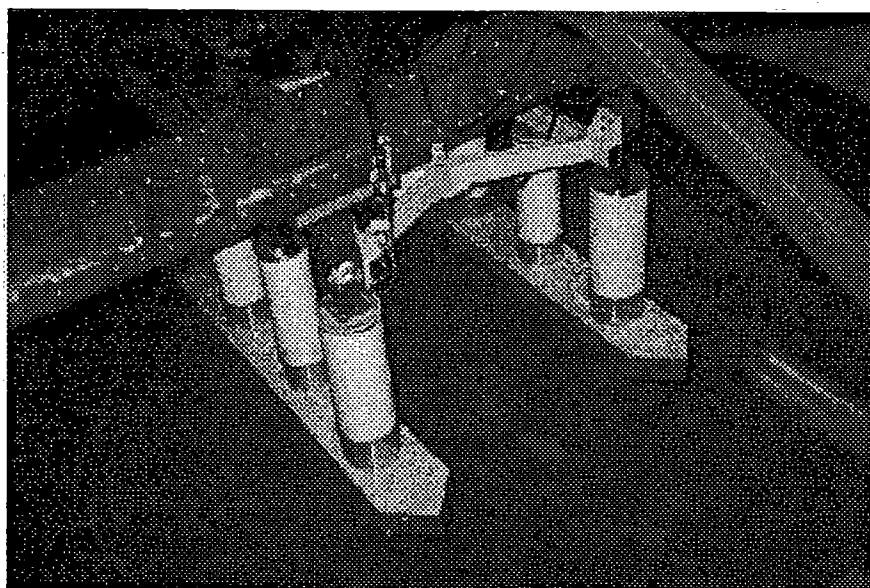


Figure 2.13: *The fixed ITTC semi-submersible model in head seas*

2.3.4 The Fixed Semi-submersible

The model tests were carried out in the Tank No.1 of the Ship Hydromechanics Laboratory. The model was fixed on to the steel beams via mounting base plates connected to the force transducers. The draft of the model was 28 cm. Tests were performed for both head seas and beam seas.

The test set-up of the fixed ITTC semi-submersible model in the Tank No.1 of DUT in head seas and in beam seas are shown in Figure 2.13 and in Figure 2.14 respectively.

Tests were first conducted in still water at various speeds. Tests were then conducted in regular waves for a wave frequency range of 3.464 - 6.928 rad/s. At least three wave amplitudes were used for each wave frequency and two carriage speeds of 0.118 m/s and 0.178 m/s were used to simulate positive and negative currents.

Figure 2.15 and Figure 2.16 show the perspective view of the model set-up in beam seas and in head seas respectively. Figure 2.17 and Figure 2.18 show again the top view of the model in the tank indicating the identity of the vertical columns.

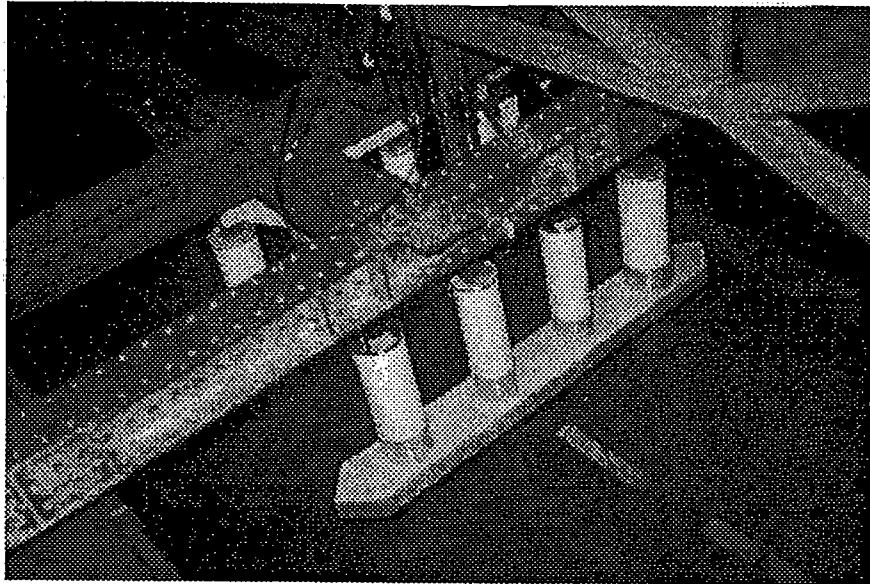


Figure 2.14: *The fixed ITTC semi-submersible model in beam seas*

2.3.5 The Free Floating (Moored) Semi-submersible

The model tests were carried out in the Tank No.1 of the Ship Hydromechanics Laboratory. The model was soft moored to simulate the free floating behavior. The model was connected to two force transducers - fore and aft - by means of two horizontally deployed springs between the model and each force transducer. Two potentiometers connected to pulleys having vertical threads connected to the deck at one end and having suspended weight at the other end were used to measure the vertical (heave) and angular (pitch and roll in head seas and in beam seas respectively) motions. Besides, two other potentiometers were used having horizontal threads connected to the fore and aft end of the model deck and passing through pulleys in order to measure the horizontal (surge and sway in head seas and in beam seas respectively) motions. The draft of the model was 28.25 cm.

The test set-up of the moored ITTC semi-submersible model in the Tank No. 1 of DUT in head seas and in beam seas are shown in Figure 2.19 and in Figure 2.20 respectively.

Tests were performed in still water at various speeds and then in regular waves. Wave frequency range for regular waves and carriage speeds were the same as that for the fixed semi-submersible model except that a few more

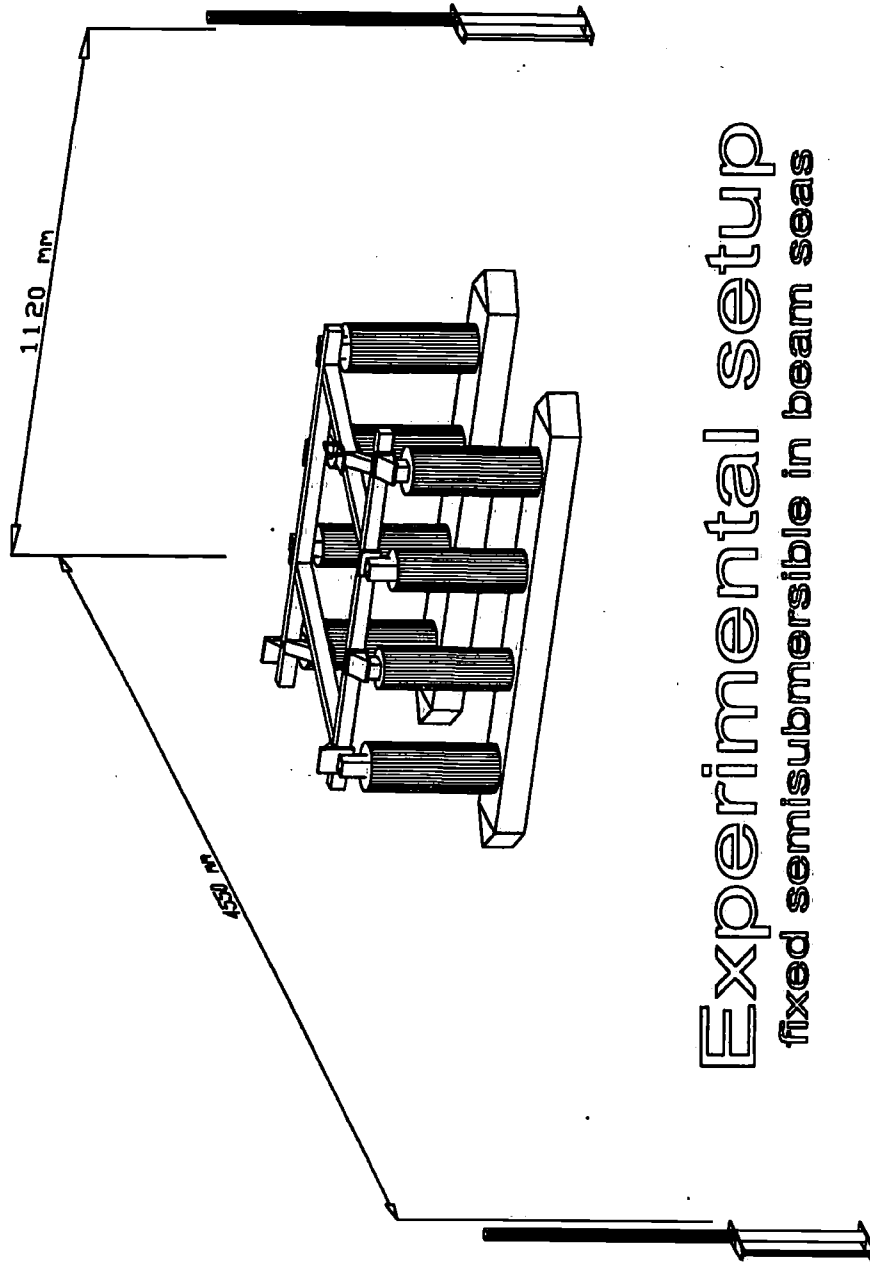


Figure 2.15: Perspective view of the fixed semi-submersible in beam seas

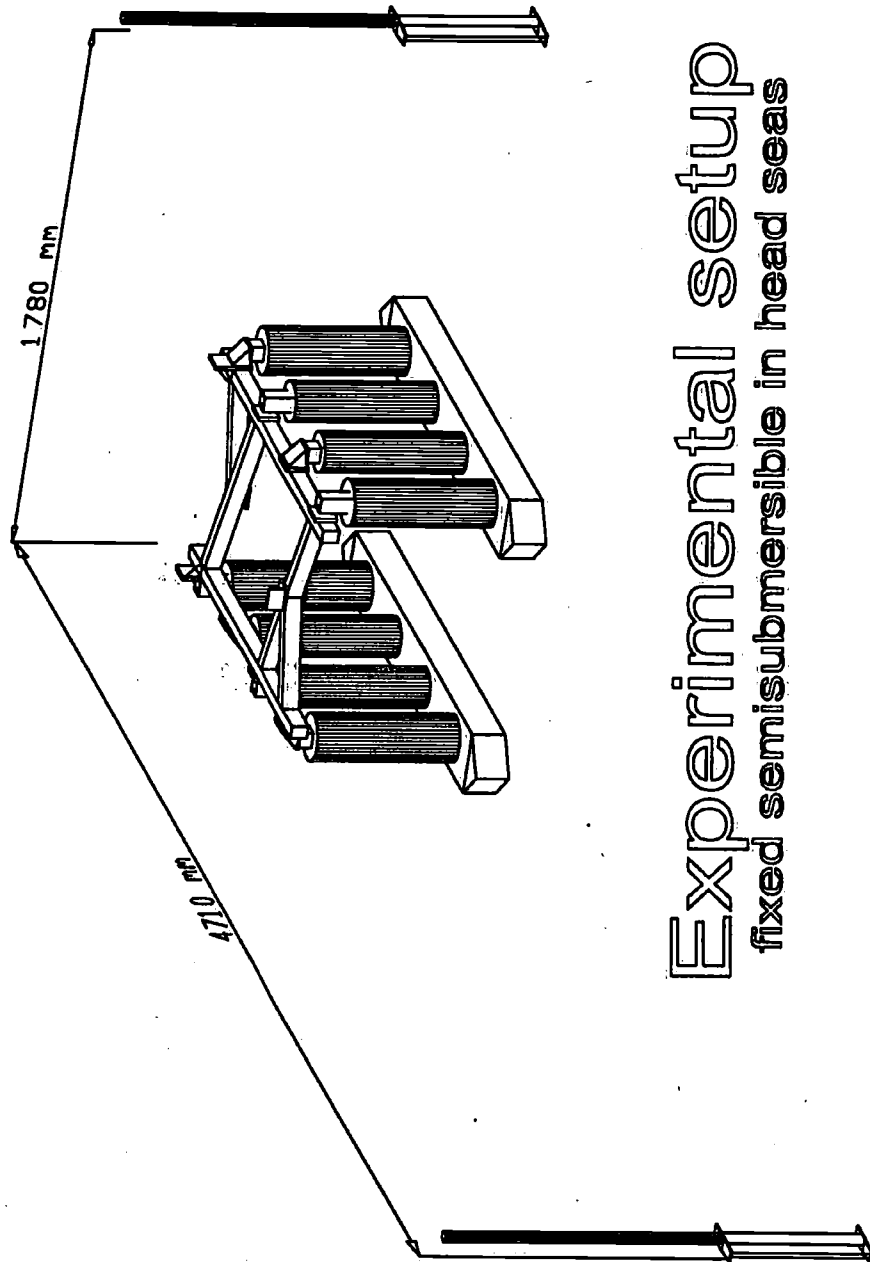


Figure 2.16: *Perspective view of the fixed semi-submersible in head seas*

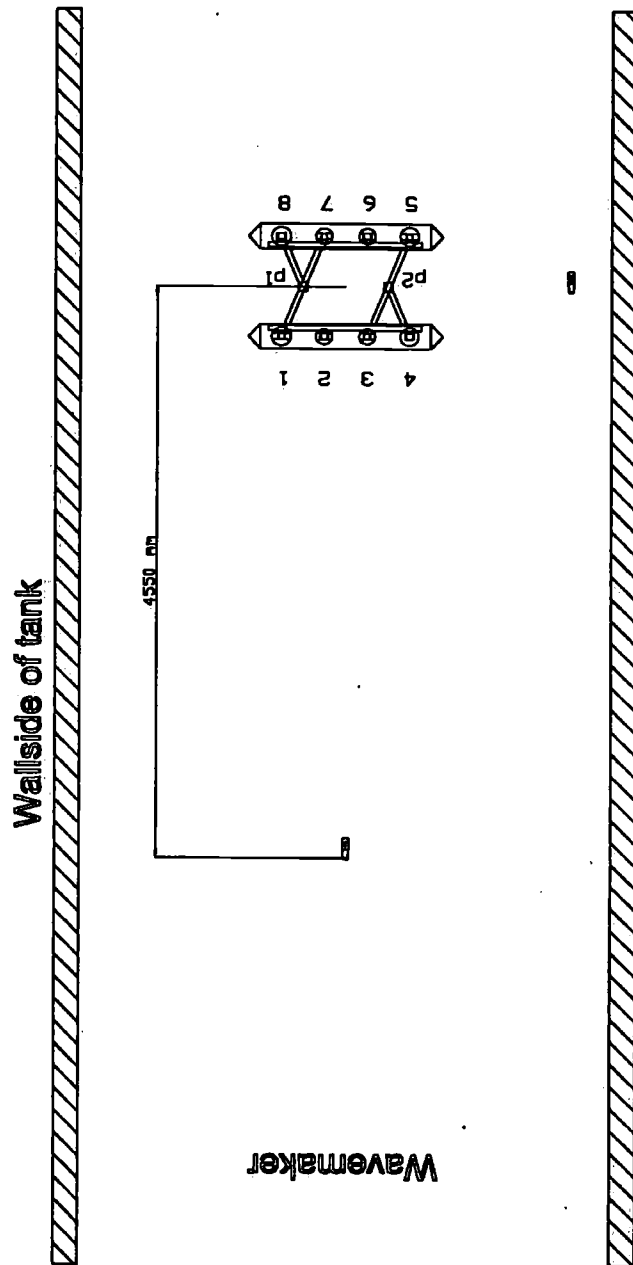


Figure 2.17: Top view of the fixed semi-submersible in beam seas

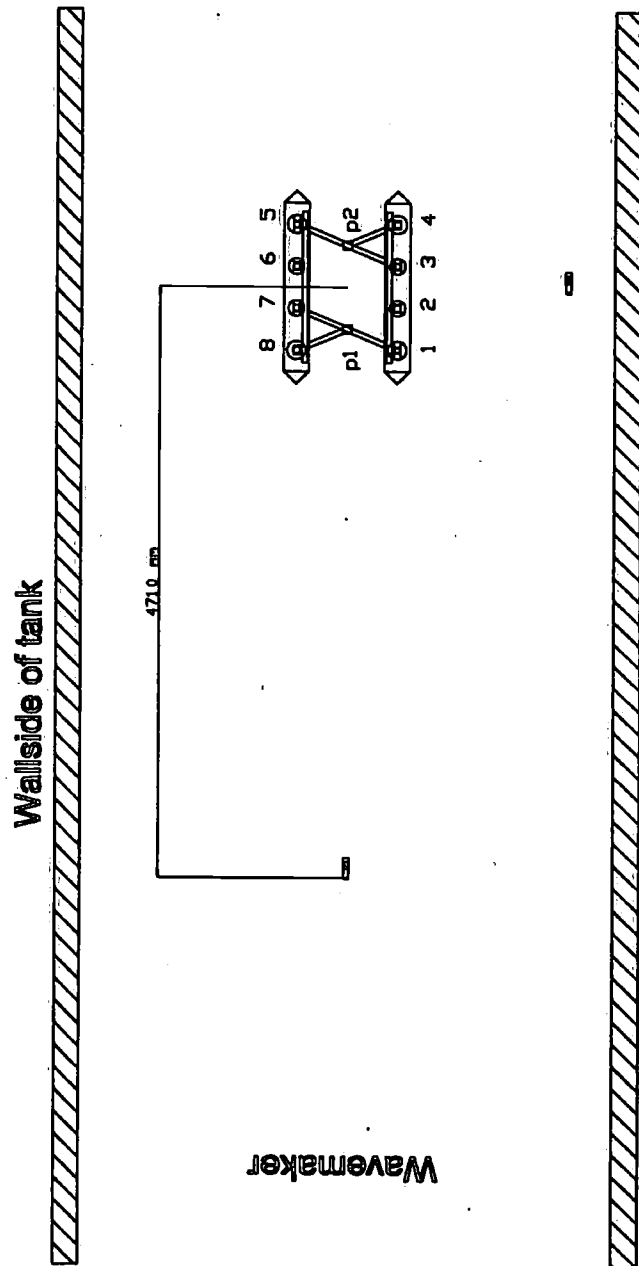


Figure 2.18: Top view of the fixed semi-submersible in head seas

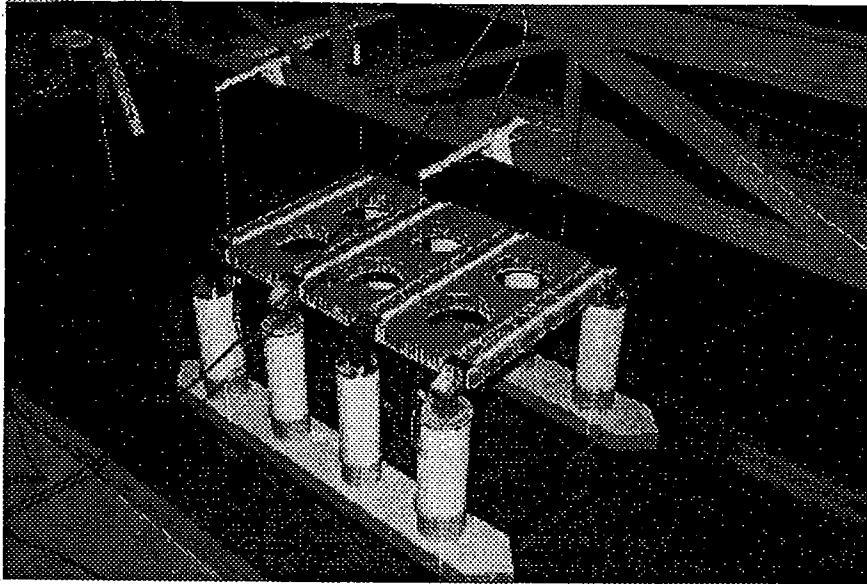


Figure 2.19: *The moored ITTC semi-submersible model in head seas*

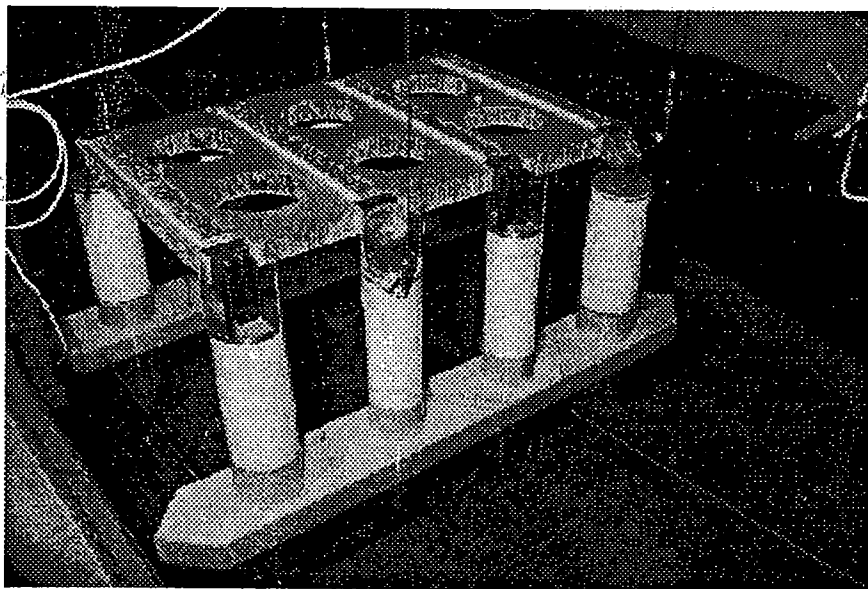


Figure 2.20: *The moored ITTC semi-submersible model in beam seas*

wave frequencies were used. Tests in irregular waves were conducted for a sea condition having a significant wave height of 0.163 m and a peak period of 1.83 s with a mean zero crossing period of 1.59 s.

Figure 2.21 and Figure 2.22 show the perspective view of the model set-up in beam seas and in head seas respectively.

2.3.6 The Simulated Flow Fields

The uniform flow field was produced by towing the model in still water at various speeds. Thus, it represented different Reynolds Numbers.

The waves-only flow field was created by the wave maker generating regular waves of different wavelengths and wave heights. During the tests, the models were held stationary in such regular wave trains. The waves were first measured without the presence of the models at a predetermined location where the models were to be placed. After the calibration of the undisturbed incident waves, the models were then placed in the predetermined location. For a fixed wave frequency, the wave heights were varied by changing the voltage from the input signal of the wave maker. Thus a range of Keulegan-Carpenter Numbers and values of β -parameter (a ratio of the Reynolds number to the Keulegan-Carpenter number) were obtained for a waves-only field.

The presence of currents in waves, the wave-current coexisting flow field, was simulated by towing the models into the waves, i.e. towards the wave maker and out of the waves, i.e. away from the wave maker. Thus, the wave-current coexisting flow field was created with positive and negative currents. During the tests, the models were either placed forward (for negative currents) or aft (for positive currents) of the predetermined position so that the models passed the predetermined position halfway the data acquisition time. Such offset distance from the predetermined location was dependent on the carriage speed. Because of the presence of currents, a range of Moe-Verley Numbers, also known as reduced velocity, and modified Keulegan-Carpenter Numbers were obtained for a wave-current coexisting flow field.

The irregular waves were generated using a pseudo-random generator followed by an analogue shaping filter. This filter was set to provide the transfer function required to obtain the desired spectral properties of the waves. Due to the length of the pseudo-random white noise sequence (approximately 29 hours), there was no danger of the waves repeating themselves during an experiment.

During all the experiments in regular waves, once the required flow field

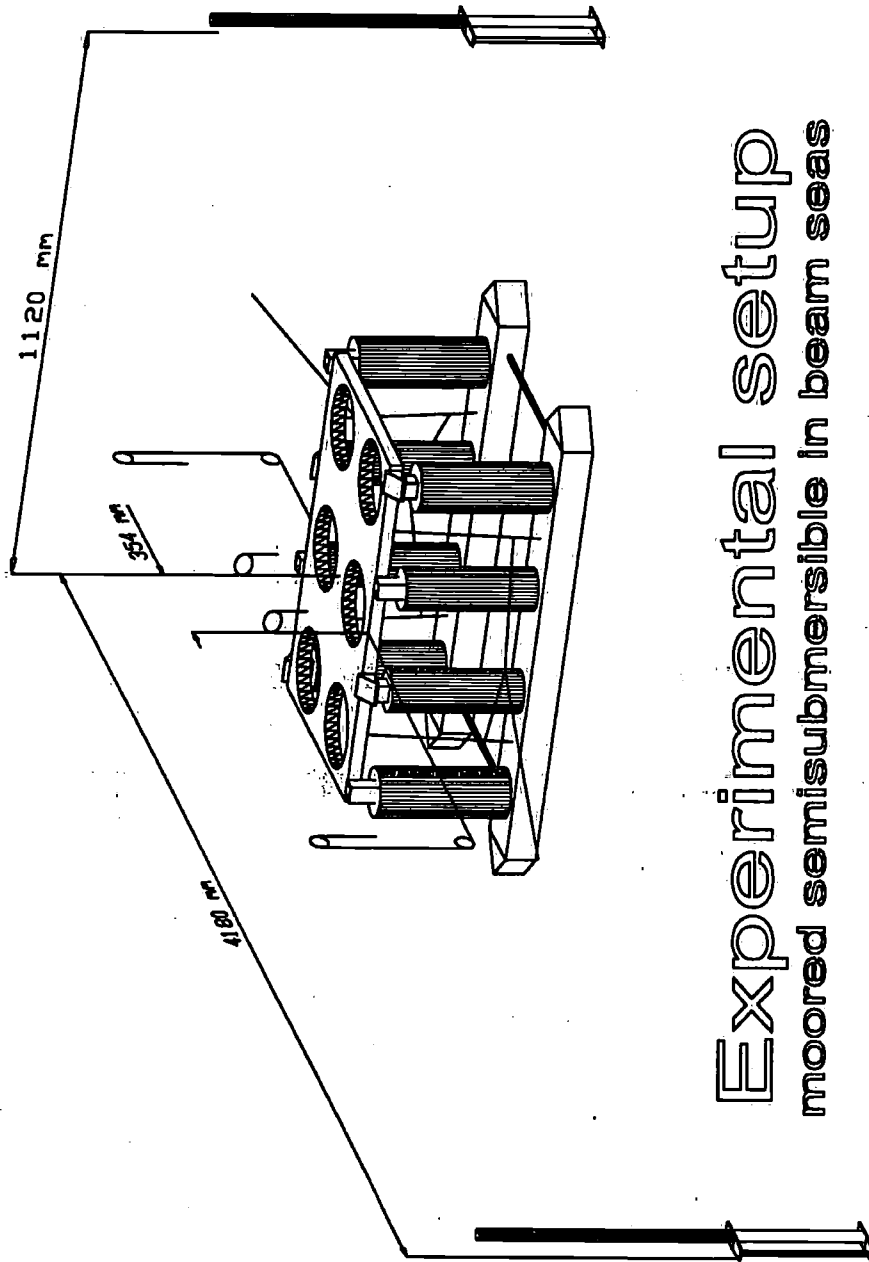


Figure 2.21: *Perspective view of the moored semi-submersible in beam seas*

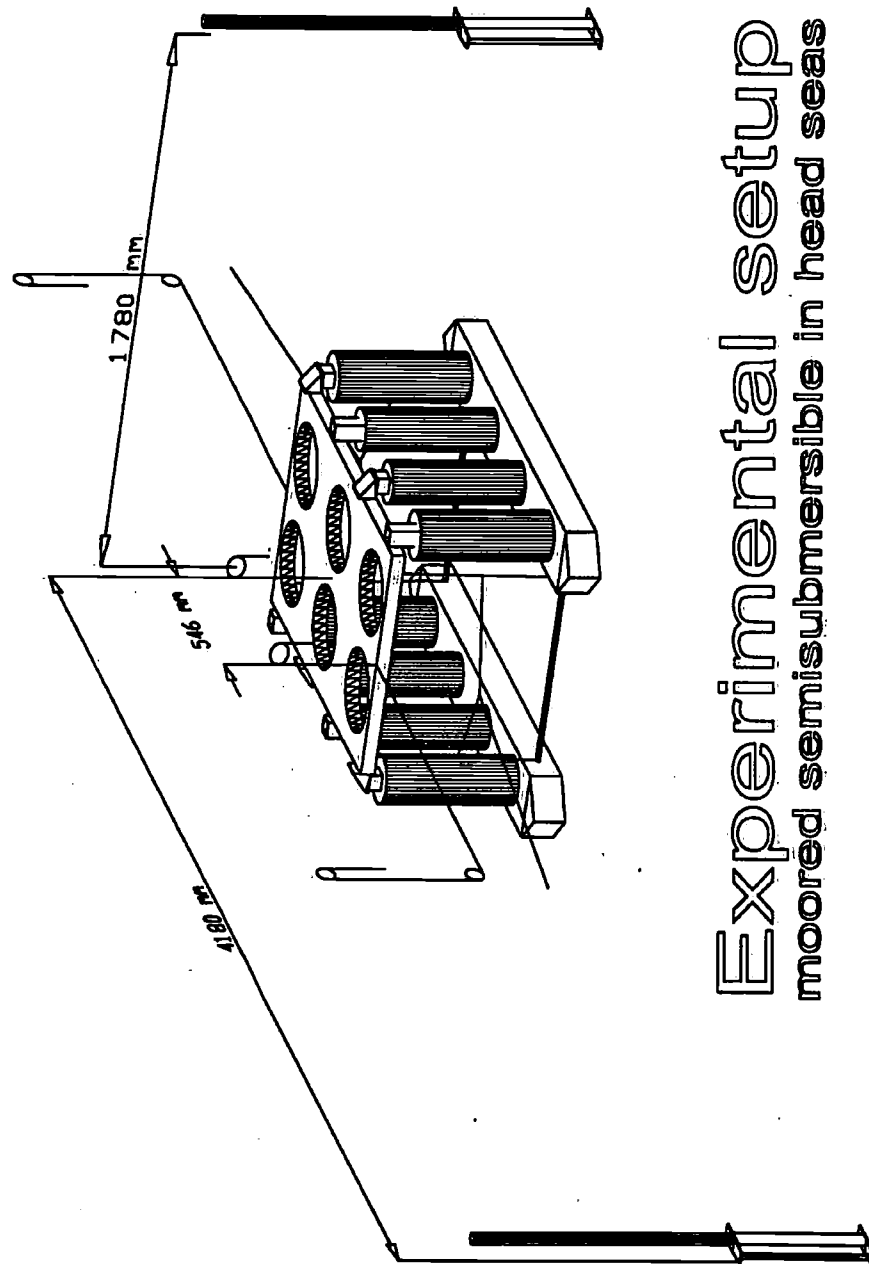


Figure 2.22: Perspective view of the moored semi-submersible in head seas

had been established around the models, the data were collected for a minimum period of 20 seconds. In irregular waves, the data acquisition time was for a minimum period of 300 seconds.

2.4 Test Equipment and Measurement

2.4.1 Instrumentation

The Double-Shear Force Transducer: This force transducer can be applied to measure both forces and bending moments on two axes but only the force signals were required for the tests with the small cylinder. The force transducer is built up of four square shaped legs between two platforms. The legs are connected by thin shear plates on which the strain gauges are glued for measuring the forces.

The Temple-Shaped Force Transducer: This force transducer consists of two platforms connected by four legs, with strain gauges on each leg forming a Wheatstone bridge and is sensitive only in one direction. The outside dimensions are 5 x 5 x 5 cm. The nominal capacities are 50, 100, 200, 400 or 800 Newton.

2.4.2 Data Acquisition

The signals of the force transducers, in the order of millivolt, were fed to an amplifier with high impedance differential input stage and high common mode rejection ratio. The signals from the amplifier were then taken to a low pass filter set for a cut off frequency of 10 Hertz which removed any noise present in the signals. The filter was a variable state 2 pole Butterworth filter and had, with this setting, an attenuation of 28 dB at 50 Hertz thus filtering out any mains hum on the signals.

The force transducers were individually calibrated in air before assembly by applying different weights and checking that they behaved similarly. Then a calibration factor was found for each force transducer and used later in the computer program analysis to convert digital data into forces. Once the force transducers were built into the models, calibration of the force transducers was further tested in air by a system comprising a frictionless pulley mounted on a vertical traverse and a set of weights. Once the models were positioned in the right orientation in the tank, they were carefully aligned and calibrated for further verification of the force transducers. Any

variation found was accounted for by the analysis program in the computer. The sensitivity of each signal depended on the force transducer type used and the chosen amplifier range.

All the filtered signals, were connected to the inputs of a data acquisition system in the computer. These signals also included those of the different wave probes. The wave signals were used for measuring wave phase angles, wave heights, etc.

2.5 Data Analysis of Measurements

The measured forces in waves only or in waves and currents can be expanded in a Fourier Series up to third order as follows:

$$F = F_0 + \sum_{n=1}^3 (F_{I_n} \sin n\omega t + F_{D_n} \cos n\omega t) \quad (2.1)$$

One of the main objectives is to find the viscous contribution towards the measured mean force, i.e. to express the measured mean force as the following $F_0 = F_{P0} + F_{D0}$.

The potential mean drift force on the splash zone is due to the contribution, of the relative wave elevation and the second order pressure (velocity squared term of Bernoulli's equation) and is calculated by the Program DELFRAC, a 3-dimensional linear radiation-diffraction program developed by the department of Ship Hydromechanics. So, the viscous mean drift force is calculated out as follows $F_{D0} = F_0 - F_{P0}$.

From the above, the time averaged mean drag coefficients can be obtained by using the theoretical expressions for the viscous mean drift forces on a fixed cylinder and a submerged pontoon which will be outlined in detail in Chapter 3 and Chapter 4 respectively. However for the splash zone of a cylinder, corrections are to be made for the mean drift force due to the second order pressure. For the submerged zone of the cylinder and for the submerged pontoon in a waves-only field, the contribution to the mean force is purely of potential origin and can thus be calculated using the second order pressure as mentioned before. For the models in waves and currents, similar treatment can be applied except that the theoretical viscous mean drift forces need to be considered for the conditions when U is greater or equal to u_a or less than u_a . Potential contributions are to be considered properly with forward speed effects using the equations proposed by Clark

et al. (1993). The values of the mean drag coefficients can then be obtained from the measured mean forces and the theoretical ones.

For the semi-submersible, an identical approach was used except that the theoretical mean force on the individual columns due to potential effects were obtained for those columns fitted with a force transducer by using the relative wave elevation around them and the second order pressure. For the floating semi-submersible, motions were measured directly. The pitch motion has been derived based on the two vertical displacements measured fore and aft and the distance between them. Horizontal motions were measured at deck level and accordingly the theoretical calculations at the center of gravity were corrected for the deck reference point.

In the case of the moored semi-submersible in irregular waves, the total spring force is not equal and opposite to the low frequency wave exciting force and this phenomenon results into low frequency horizontal motions of the model. Accordingly, the measured spring (restraining) force must be corrected for the effects of low frequency horizontal motions of the model in order to obtain the true drift forces on the model. Details of correction methods will be presented in Chapter 6.

The force coefficients obtained from the model tests' results will be used for the full scale predictions. The phenomenon of "scale effects" for the time being will not be considered though it is important when dealing with viscous effects.

References

- Clark, P. J., S. Malenica, and B. Molin (1993). An heuristic approach to wave drift damping. *Applied Ocean Research* 15(1), 53-55.
- Dev, A. K. (1992a). Experimental investigation of viscous mean drift forces on a fixed vertical cylinder in waves and currents; part-i. Technical Report 928-M, Ship Hydromechanics Laboratory, Delft University of Technology, Delft, The Netherlands.
- Dev, A. K. (1992c). Experimental investigation of viscous mean drift forces on a fixed vertical cylinder in waves and currents; part-iii. Technical Report 943-M, Ship Hydromechanics Laboratory, Delft University of Technology, Delft, The Netherlands.
- Dev, A. K. (1993a). Experimental investigation of viscous mean drift forces on a fixed vertical cylinder in waves and currents; part-v. Technical Report 972-M, Ship Hydromechanics Laboratory, Delft University of Technology, Delft, The Netherlands.
- Dev, A. K. (1993c). Hydrodynamic forces on a fixed submerged rectangular pontoon in waves and currents; part-i. Technical Report 987-I-M, Ship Hydromechanics Laboratory, Delft University of Technology, Delft, The Netherlands.
- Dev, A. K. (1995a). Hydrodynamic forces on a fixed semi-submersible in waves and currents; part i (computations & model tests). Technical Report 1011-M, Ship Hydromechanics Laboratory, Delft University of Technology, Delft, The Netherlands.
- Dev, A. K. (1995c). Motion behaviour of a floating semi-submersible in waves and currents; part i (computations & model tests). Technical Report 1012-M, Ship Hydromechanics Laboratory, Delft University of Technology, Delft, The Netherlands.

Chapter 3

Viscous Mean Drift Forces on a Vertical Cylinder

In this chapter a theoretical evaluation (Dev 1992a) will be carried out for finding viscous contributions to the horizontal mean drift force on a surface piercing truncated vertical cylinder in both fixed and floating condition in waves as well as in waves and currents. In floating condition, it is considered to be moored undergoing horizontal and vertical motions.

The purpose is to relate the results of such an analysis to the vertical columns of a semi-submersible. The cylinder is considered divided into two parts namely the splash zone (from the mwl up to the instantaneous sea level) and the submerged zone (from the mwl down to the bottom of the cylinder). In this way it is possible to treat the splash zone separately from the constantly submerged zone of a cylinder and to find which of the zones comes out as the contributor to viscous effects. In theoretical evaluation for the purpose of qualitative analysis, the value of the mean drag coefficient, C_{D0} , will be taken as unity.

In Section 3.1, some results of computations are shown in order to give a qualitative indication of the influence of viscous effects on the total mean drift forces with and without current effects.

3.1 Theoretical Evaluation

3.1.1 Viscous Mean Drift Forces on a Fixed Cylinder

Regular wave kinematics for deep water conditions are incorporated using the following expressions. Constant velocity in the wave crest of the linear (Airy) wave theory is applied. Wave amplitude and water particle velocity are shown at mean water level.

$$\phi = \frac{\zeta_a g}{\omega} e^{kz} \sin(kx - \omega t) \quad (3.1)$$

$$\zeta = \zeta_a \cos(kx - \omega t) \quad (3.2a)$$

$$u = \zeta_a \omega \cos(kx - \omega t) \quad (3.2b)$$

$$= u_a \cos(kx - \omega t) \quad (3.2c)$$

In Waves Only

The viscous drag force term of the Morison equation produces a zero mean force over any submerged part of the cylinder. In order to find the viscous contribution towards the mean drift force, the splash zone has to be taken into consideration because of the in-phase part of the force with the crest velocity. For a fixed cylinder, the oscillating viscous drag force for a unit length due to regular waves in the Morison equation is as follows:

$$F_D(t) = \frac{1}{2} \rho C_D D u |u| \quad (3.3)$$

After replacing u by $u_a \cos \omega t$, the Equation 3.3 becomes:

$$F_D(t) = \frac{1}{2} \rho C_D D (u_a \cos \omega t) |u_a \cos \omega t| \quad (3.4a)$$

$$= \frac{1}{2} \rho C_D D \zeta_a^2 \omega^2 \frac{8}{3\pi} \cos \omega t + \text{higher harmonic terms} \quad (3.4b)$$

This shows that according to the Morison equation, no mean force of viscous origin is exerted on a constantly submerged cylinder section.

Splash Zone: A non-zero mean drift force component due to viscous effects in the splash zone is found by integrating the unit length force on the cylinder over the splash zone as follows:

$$F_{D0} = \frac{4}{3\pi} \rho C_{D0} D \zeta_a^2 \omega^2 \frac{1}{T} \int_0^T \int_0^{\zeta} \cos \omega t \, dz \, dt \quad (3.5a)$$

$$= \frac{2}{3\pi} \rho \omega^2 C_{D0} D \zeta_a^3 \quad (3.5b)$$

The viscous mean drift force on the splash zone is thus found to vary with the cube of the wave height and for a particular wave height, it would increase linearly with wave frequency squared.

$$\frac{F_{D0}}{\rho g C_{D0} D \zeta_a^2} = \frac{1}{3\pi} (kD) \left(\frac{H}{D} \right) \quad (3.6)$$

Furthermore from Equation 3.6, it can be seen that the quadratic mean force transfer function (similar to potential mean drift force transfer function) is now a function of either the viscous parameter ($\frac{H}{D}$) and the diffraction parameter (kD) or a combination of them, i.e. wave steepness (kH).

In Currents Only

As currents produce nonlinear forces of viscous origin, it may be termed as the 'drift' force due to currents only. The velocity profile of currents from the mean water level to the sea bed normally varies according to a power law. However, for simplicity the profile to be considered here is horizontally and vertically uniform along the draft of the cylinder. The 'drift' force due to currents only is:

$$F_{DC} = \frac{1}{2} \rho C_{DC} A_P U^2 \quad (3.7)$$

In Waves and Currents

It has been stated before that for a fixed cylinder in waves only, the mean drift force due to viscous effects on the submerged part is zero when the force is averaged over one cycle. But in the presence of currents, this is no longer true. Even the presence of a low magnitude of currents can account for the mean drift force due to viscous effects of the combined velocity of

waves and currents. As the interaction effects of a wave-current coexisting flow field are also of viscous origin, the nonlinear viscous drag force term of the Morison equation would be exploited again to compute the mean drift force. Though current is assumed to be present up to the mwl, its presence in the splash zone would also be investigated by considering it as a constant velocity in addition to the constant crest velocity. In the presence of positive or negative currents, the viscous drag force becomes as follows:

Splash Zone: The viscous drag force per unit length of the wetted cylinder in the presence of currents, U , is as follows:

$$F_D(t) = \frac{1}{2} \rho C_D D (u + U) |u + U| \quad (3.8)$$

After replacing u by $u_a \cos \omega t$, the Equation 3.8 becomes:

$$F_D(t) = \frac{1}{2} \rho C_D D (u_a \cos \omega t + U) |u_a \cos \omega t + U| \quad (3.9)$$

The application of Equation 3.9 depends on the magnitude of U with respect to that of u_a .

$$F_{D0} = \frac{1}{2} \rho C_{D0} D \frac{1}{T} \int_0^T \int_0^\zeta (U^2 + 2U u_a \cos \omega t + u_a^2 \cos^2 \omega t) dz dt \quad (3.10)$$

For $|U| \geq u_a$:

$$F_{D0} = \frac{1}{2} \rho C_{D0} D \zeta_a u_a^2 \gamma \quad (3.11)$$

For $|U| < u_a$:

$$F_{D0} = \frac{1}{2\pi} \rho C_{D0} D \zeta_a u_a^2 (d_1 + d_2 + d_3) \quad (3.12)$$

where

$$\begin{aligned} d_1 &= \frac{1}{6} (\sin 3\Theta + 9 \sin \Theta) \\ d_2 &= \gamma (2\Theta + \sin 2\Theta - \pi) \\ d_3 &= 2\gamma^2 \sin \Theta \\ \gamma &= \frac{U}{u_a} \end{aligned}$$

The value of Θ for positive U is $\cos^{-1}(-\frac{U}{u_a} = -\gamma)$ and for $-U$, the value of Θ is $\cos^{-1}(\frac{U}{u_a} = \gamma)$.

Submerged Zone: The submerged zone extends from the mwl to the bottom of the cylinder. At mwl, the water particle velocity is maximum and below the mwl, the water particle velocity will vary according to the exponential term e^{kz} . Similar to the splash zone, the expressions for the mean drift force are to be found for both $|U| \geq u_a$ and $|U| < u_a$. The expressions would be derived here at mwl, i.e. at maximum water particle velocity. However, in order to calculate the total mean drift force on the complete submerged zone, the computations are to be repeated for a number of vertical segments so that at each segment, the water particle velocity is calculated by taking account of the exponential term and consequently the wave-current interaction effects are considered accurately.

The viscous mean drift force per unit length of the cylinder due to a wave-current coexisting flow field at mwl ($z = 0$) is given by the following equations.

$$F_{D0} = \frac{1}{2} \rho C_{D0} D \frac{1}{T} \int_0^T (U^2 + 2Uu_a \cos \omega t + u_a^2 \cos^2 \omega t) dt \quad (3.13)$$

For $|U| \geq u_a$:

$$F_{D0} = \frac{1}{2} \rho C_{D0} D u_a^2 \left(\frac{1}{2} + \gamma^2 \right) \quad (3.14)$$

For $|U| < u_a$:

$$F_{D0} = \frac{1}{2\pi} \rho C_{D0} D u_a^2 (d_1 + d_2 + d_3) \quad (3.15)$$

where

$$d_1 = \frac{1}{2} (2\Theta + \sin 2\Theta - \pi)$$

$$d_2 = 4\gamma \sin \Theta$$

$$d_3 = \gamma^2 (2\Theta - \pi)$$

In the case of negative currents, the Equation 3.14 is to have a negative sign. In fact, Equation 3.12 and Equation 3.15 turn to Equation 3.11 and Equation 3.14 respectively when U equals u_a .

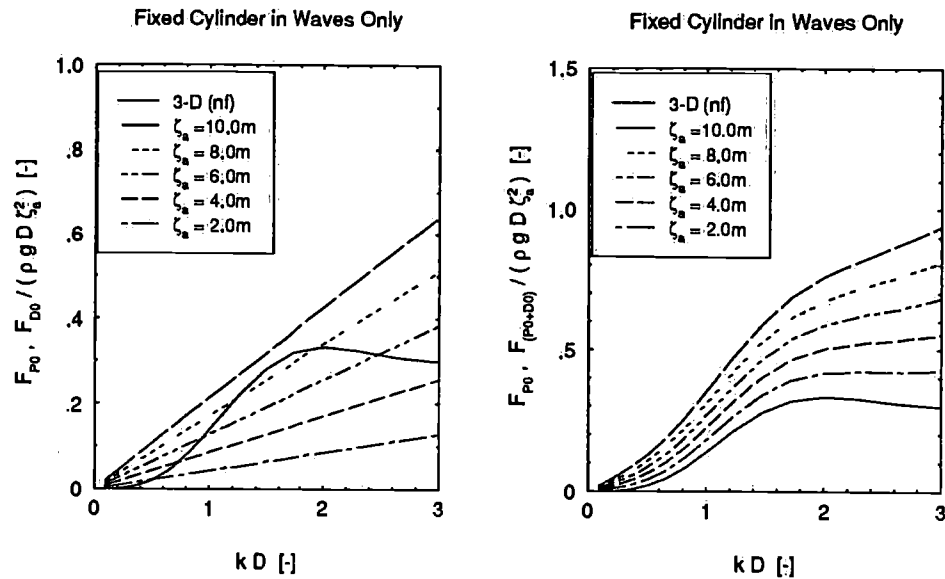


Figure 3.1: Potential, viscous and (potential plus viscous) mean drift forces on a fixed cylinder in waves only for different wave amplitudes

Computational Results

For a vertical cylinder of 10m diameter and 20m draft which is similar to a column of a semi-submersible or a tension leg platform, computations were carried out based on the above theory outlined. In doing so, the value of C_{D0} was taken as unity. For $(\frac{D}{\lambda} \leq 0.20)$, the first order drag forces cannot be disregarded and their effects on the total mean drift force can be equally or more important. Some results are presented here.

Figure 3.1 (left) shows the viscous mean drift force due to the viscous drag force term in the Morison equation. It is evident that with the increase of wave height, the viscous mean drift force increases with the cubic power.

A comparison between potential and viscous effects of the mean drift force is shown in Figure 3.1 (right). The total drift force calculations improve compared to potential contributions alone after viscous contributions are added. While considering the mean drift force due to viscous effects, it is no longer independent of the wave height and such trends are shown. On the other hand, the mean drift force due to potential effects, when nondimensionalized, is independent of the wave height. The mean drift force due to potential effects was calculated by DELFRAC (1992).

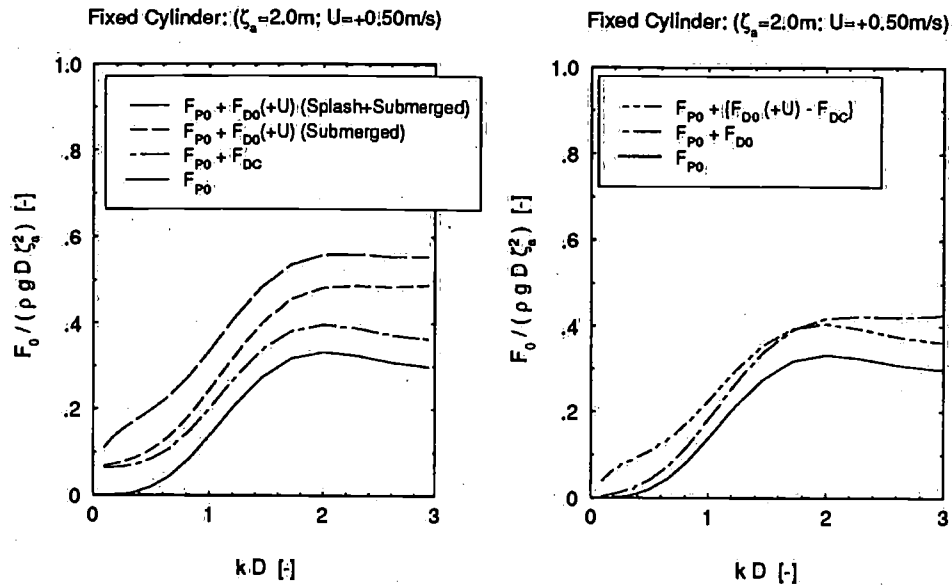


Figure 3.2: Potential and viscous mean drift forces on a fixed cylinder in waves only as well as in waves and currents

In Figure 3.2 (left), contributions due to currents alone (superposition theory) and the interaction effects of waves and currents are shown. The mean drift force progressively increases when all the contributions are added individually. But the interaction effects further increase the force. The contributions toward the mean drift force due to currents only were calculated in three ways: firstly the force due to currents alone were added; secondly the interaction effects were calculated for the submerged zone alone and thirdly the interactions effects were calculated for the splash zone and the submerged zone together respectively. Furthermore, in Figure 3.2 (right), the calculation of the viscous mean drift force, based on the idea that the subtraction of the force due to currents only from the force due to waves and currents on the submerged zone (Burns 1983; Chitrapu, Ertekin, and Paulling 1993; Pijfers and Brink 1977) is equal to the viscous drift force in waves only, is compared against the force calculated based on the idea of splash (free surface) zone. The former seems higher than the latter. However, such comparison fails to provide any substantial evidence when in both cases the values of the mean drag coefficient are considered unity or suppressed when nondimensionalizing the force.

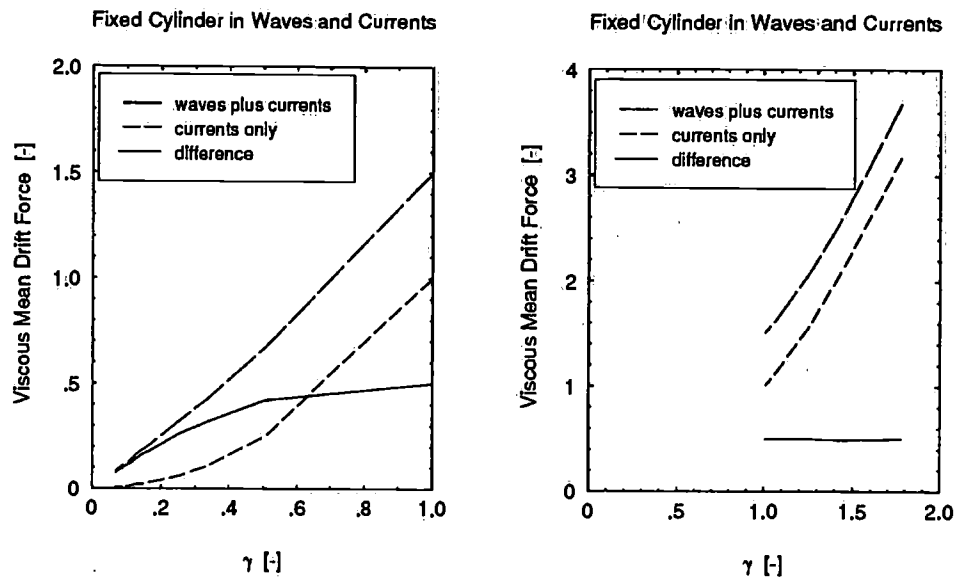


Figure 3.3: Viscous mean drift forces on a fixed cylinder at mean water level in currents only as well as in waves and currents

In Figure 3.3, the interaction effects are shown in waves and currents and also in waves and currents minus currents alone. For γ greater than unity, the difference is almost unchanged whereas for γ less than unity, the difference is mainly caused by the interaction effects. Such contributions are pronounced as the current velocity becomes smaller with respect to the water particle velocity.

For a fixed wave height, the wave-current interaction increases with an increase in the value of current velocities. Similar is the case where the magnitudes of wave amplitudes are varied for a fixed current velocity. The trend is exactly similar. These are shown in Figure 3.4.

So far the wave-current interaction effects are shown based on the computation results at mwl where the water particle velocity is maximum. Chakrabarti (1984) and Ferretti and Berta (1980) have also shown the wave-current interaction effects only at mwl. But it is essential to know the ultimate effects over the complete submerged zone of the cylinder.

In Figure 3.5, the forces due to waves and currents on the submerged zone of a fixed cylinder are shown compared to the force due to currents only for different wave frequencies, different wave amplitudes and for a fixed velocity of current. The forces appear to be to some extent linear with the

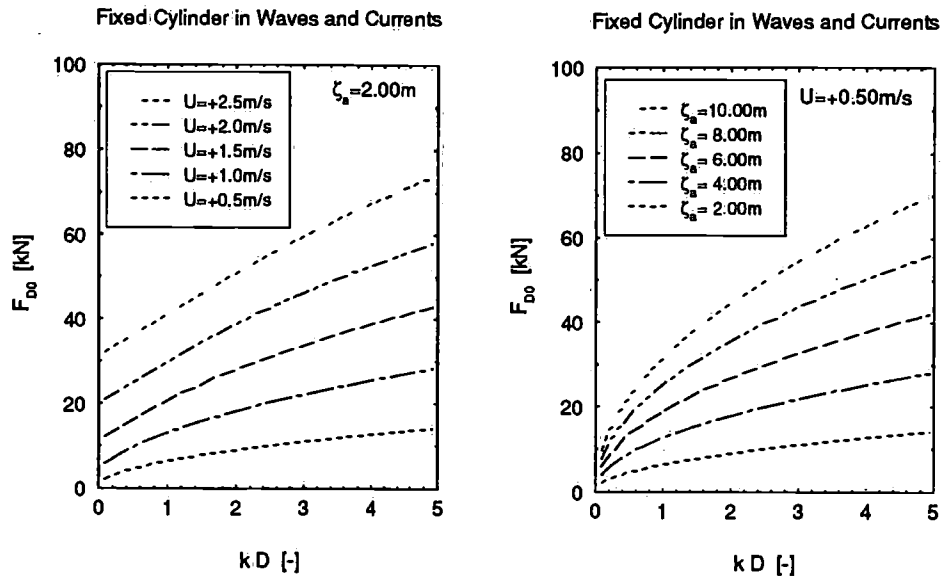


Figure 3.4: Effects of (left) velocity of currents and (right) wave amplitudes on viscous mean drift forces at mean water level in waves and currents

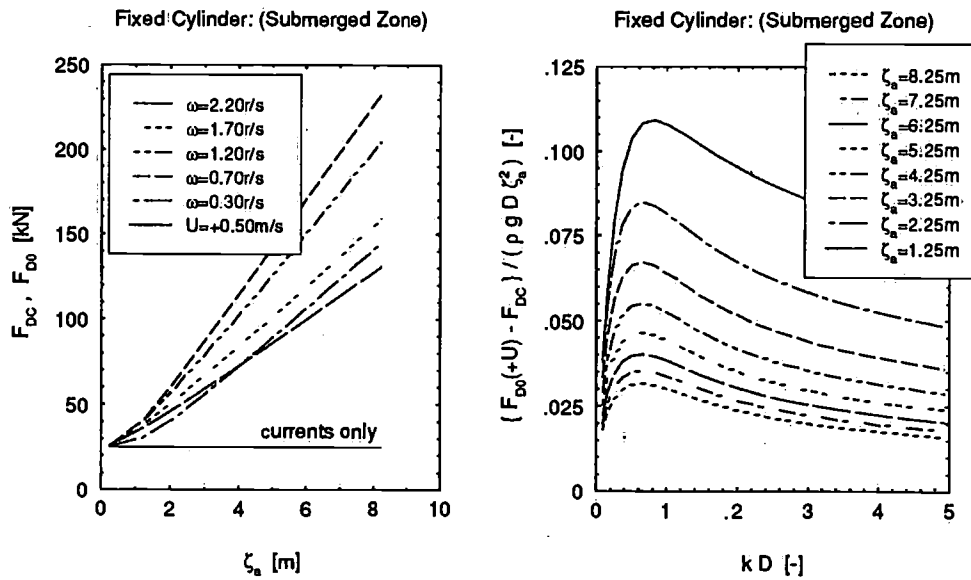


Figure 3.5: Viscous mean drift forces (left) in currents only as well as in waves and currents and (right) in waves and currents minus currents

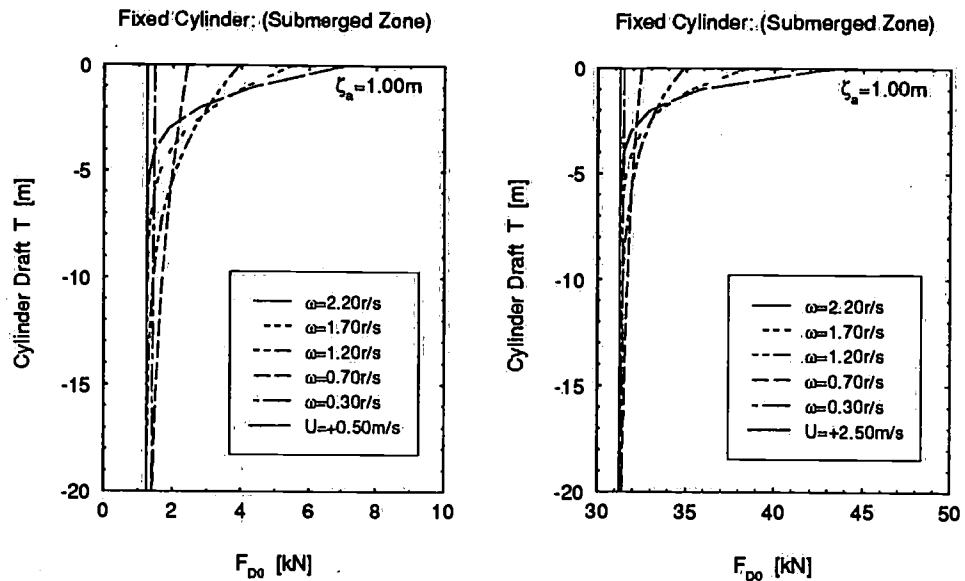


Figure 3.6: Effects of cylinder draft on viscous mean drift forces on the submerged zone of a fixed cylinder in waves and currents

increase in wave amplitude but unfortunately the quadratic transfer function of the forces after the force due to currents alone is subtracted still shows a marked nonlinearity, i.e. such transfer functions are still dependent on the wave amplitude. Burns (1983) showed that the viscous mean drift force can still be expressed as a quadratic transfer function similar to the mean drift force due to potential effects. This is to some extent true when $\gamma \geq 1$ but not when $\gamma < 1$. Perhaps it was possible to do so because of the simplification in the analytical expression when $\gamma < 1$.

Figure 3.6 clearly shows that the wave-current interaction is much more pronounced at or immediately below the mean water level. It increases with the increase of frequencies as well as with the wave height. As the draft below mwl increases, the interaction becomes weaker. The decrement is rather drastic in the sense that the higher the frequency, the higher the rate of decrement. This is due to the presence of the low magnitude current velocity. However, at higher current velocity, the trend is similar except that the rate of decrement is slower. Such phenomena are governed by the exponential term e^{kz} which is a function of both draft and frequency. It is worth mentioning here that assuming constant velocity for the submerged

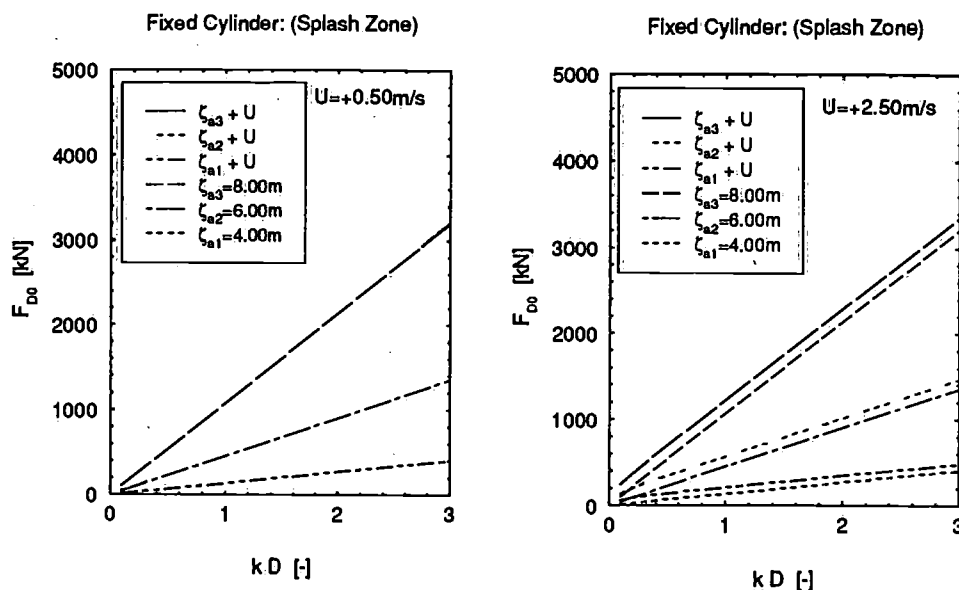


Figure 3.7: Effects of currents on viscous mean drift forces on the splash zone of a fixed cylinder in waves and currents

zone as mentioned in (Lundgren *et al.* 1982) would produce a much higher mean force and such characteristics of wave-current interaction as shown in the above mentioned figures would not be expected.

The effects of wave-current interaction on the splash zone can be seen in Figure 3.7. At lower velocity of current, the interaction effect is not at all noticeable. At higher velocity of current, there are some effects but still not appreciable. However, it should be considered first whether to assess such additional contribution neglecting it at this stage. Furthermore, an inappropriate choice of the mean drag coefficient which is taken as unity here may cause erroneous results as well.

3.1.2 Viscous Mean Drift Forces on a Floating Cylinder

In the case of a floating cylinder, only translatory motions, i.e. only horizontal and vertical modes of motions will be considered. Horizontal motions will cause a relative motion and vertical motions, a change in surface elevation, i.e. the cylinder would be subject to a relative surface elevation. Both of these relative motion effects seem to be significant.

The relative wave elevation ζ_r is replaced by $\zeta_{ra} \cos(\omega t + \epsilon_{\zeta_r,z})$.

$$\zeta_r(t) = \zeta(t) - z(t) \quad (3.16a)$$

$$\zeta(t) = \zeta_a \cos \omega t \quad (3.16b)$$

$$z(t) = z_a \cos(\omega t + \epsilon_{z\zeta}) \quad (3.16c)$$

$$\zeta_{ra} = \zeta_a \sqrt{\left\{1 + \left(\frac{z_a}{\zeta_a}\right)^2 - 2\left(\frac{z_a}{\zeta_a}\right) \cos \epsilon_{z\zeta}\right\}} \quad (3.17a)$$

$$\epsilon_{\zeta_r z} = \arctan \left[\frac{\left(\frac{z_a}{\zeta_a}\right) \sin \epsilon_{z\zeta}}{\left\{1 - \left(\frac{z_a}{\zeta_a}\right) \cos \epsilon_{z\zeta}\right\}} \right] \quad (3.17b)$$

The relative horizontal velocity u_r is replaced by $u_{ra} \cos(\omega t + \epsilon_{u_r \dot{x}})$.

$$u_r(t) = u(t) - \dot{x}(t) \quad (3.18a)$$

$$u(t) = u_a \cos \omega t \quad (3.18b)$$

$$x(t) = x_a \cos(\omega t + \epsilon_{x\zeta}) \quad (3.18c)$$

$$\dot{x}(t) = \dot{x}_a \cos(\omega t + \epsilon_{\dot{x}\zeta}) \quad (3.18d)$$

$$\text{where } \epsilon_{\dot{x}\zeta} = \left(\epsilon_{x\zeta} + \frac{\pi}{2} \right) \quad (3.18e)$$

$$u_{ra} = \zeta_a \omega \sqrt{\left\{1 + \left(\frac{x_a}{\zeta_a}\right)^2 - 2\left(\frac{x_a}{\zeta_a}\right) \cos \epsilon_{\dot{x}\zeta}\right\}} \quad (3.19a)$$

$$\epsilon_{u_r \dot{x}} = \arctan \left[\frac{\left(\frac{x_a}{\zeta_a}\right) \sin \epsilon_{\dot{x}\zeta}}{\left\{1 - \left(\frac{x_a}{\zeta_a}\right) \cos \epsilon_{\dot{x}\zeta}\right\}} \right] \quad (3.19b)$$

In Waves Only

Splash Zone: Similar to a fixed cylinder except that u is replaced by u_r . The mean drift force due to viscous effects on a floating cylinder is now as follows:

$$F_{D0} = \frac{1}{2} \rho C_{D0} D \frac{1}{T} \int_0^T \int_0^{\zeta_r} \times$$

$$\{u_{ra}^2 \cos(\omega t + \epsilon_{ur\dot{x}}) | \cos(\omega t + \epsilon_{ur\dot{x}}) |\} dz dt \quad (3.20a)$$

$$= \frac{2}{3\pi} \rho C_{D0} D g k \zeta_{ra}^3 \cos(\epsilon_{\zeta rz} - \epsilon_{ur\dot{x}}) \quad (3.20b)$$

In Waves and Currents

$$F_D(t) = \frac{1}{2} \rho C_D D (u_r + U) |u_r + U| \quad (3.21)$$

Similar to the fixed cylinder, the application of Equation 3.21 is to be performed depending on the magnitude of the current velocity U with respect to that of the relative velocity u_{ra} .

Splash Zone:

$$F_{D0} = \frac{1}{2} \rho C_{D0} D \frac{1}{T} \int_0^T \int_0^{\zeta_r} \times \{U^2 + 2U u_{ra} \cos(\omega t + \epsilon_{ur\dot{x}}) + u_{ra}^2 \cos^2(\omega t + \epsilon_{ur\dot{x}})\} dz dt \quad (3.22)$$

For $|U| \geq u_{ra}$:

$$F_{D0} = \frac{1}{2} \rho C_{D0} D \zeta_{ra} u_{ra}^2 \gamma_r \cos(\epsilon_{\zeta rz} - \epsilon_{ur\dot{x}}) \quad (3.23)$$

For $|U| < u_{ra}$:

$$F_{D0} = \frac{1}{\pi} \rho C_{D0} \zeta_{ra} u_{ra}^2 (d_1 + d_2 + d_3) \quad (3.24)$$

where

$$d_1 = \frac{1}{6} [\sin 3\Theta \cos(\epsilon_{\zeta rz} + 2\epsilon_{ur\dot{x}}) + 3 \sin \Theta \{\cos(\epsilon_{\zeta rz} - 2\epsilon_{ur\dot{x}}) + 2 \cos \epsilon_{\zeta rz}\}]$$

$$d_2 = \gamma_r \{(2\Theta - \pi) \cos(\epsilon_{\zeta rz} - \epsilon_{ur\dot{x}}) + \sin 2\Theta \cos(\epsilon_{\zeta rz} + \epsilon_{ur\dot{x}})\}$$

$$d_3 = 2 \gamma_r^2 \sin \Theta \cos \epsilon_{\zeta rz}$$

Submerged Zone: The viscous mean drift on a floating cylinder at mean water level for a unit length is given by:

$$F_{D0} = \frac{1}{2} \rho C_{D0} D \frac{1}{T} \int_0^T \times$$

$$\{U^2 + 2Uu_{ra} \cos(\omega t + \epsilon_{u,r,\dot{x}}) + u_{ra}^2 \cos^2(\omega t + \epsilon_{u,r,\dot{x}})\} dt \quad (3.25)$$

For $|U| \geq u_{ra}$:

$$F_{D0} = \frac{1}{2} \rho C_{D0} D u_{ra}^2 \left(\frac{1}{2} + \gamma_r^2 \right) \quad (3.26)$$

For $|U| < u_{ra}$:

$$F_{D0} = \frac{1}{2\pi} \rho C_{D0} D u_{ra}^2 (d_1 + d_2 + d_3) \quad (3.27)$$

where

$$d_1 = \frac{1}{2} \{ (2\Theta - \pi) + \sin 2\Theta \cos 2\epsilon_{u,r,\dot{x}} \}$$

$$d_2 = 4\gamma_r \sin \Theta \cos \epsilon_{u,r,\dot{x}}$$

$$d_3 = \gamma_r^2 (2\Theta - \pi)$$

Similar to a fixed cylinder, Equation 3.26 is to have a negative sign in the presence of negative currents. Moreover, the exponential term in the horizontal water particle velocity has to take account of the draft when computations are to be carried out for the complete submerged zone divided into a number of vertical segments. This is essential in order to assess the value of γ_r so that appropriate consideration of wave-current interaction is maintained.

Computational Results

Calculations were performed by DELFRAC for the same cylinder, used in the fixed condition, in free floating condition to obtain motions and the potential mean drift force for a range of regular wave frequencies.

In Figure 3.8 (left), the potential mean drift forces on a fixed and floating cylinder is shown. The translatory motions, namely surge and heave, of a floating cylinder are also shown in Figure 3.8 (right).

In Figure 3.9, comparison is shown between the mean drift force due to viscous effects at unit wave amplitudes for a fixed and a floating cylinder. The difference is appreciable. But with an increase in wave height, the viscous effects would increase in a similar manner for a fixed cylinder. The mean drift force for a floating cylinder shows a blunt peak at the heave natural frequency. This is due to the maximum heave response.

Effects of a wave-current coexisting flow field are shown for the splash zone and mwl between a fixed and a floating cylinder in Figure 3.10. The

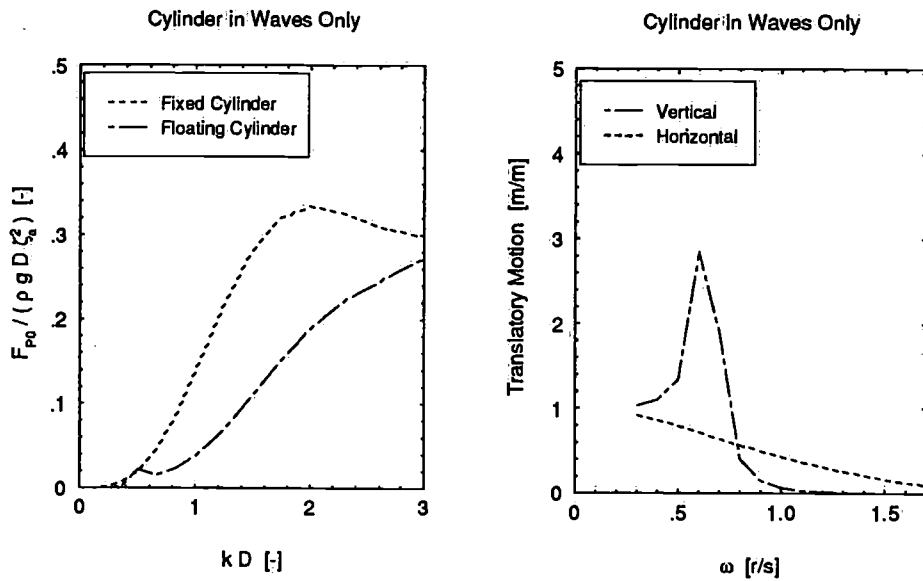


Figure 3.8: (left) Potential mean drift forces on a cylinder in waves only and (right) motions of a floating cylinder in waves only

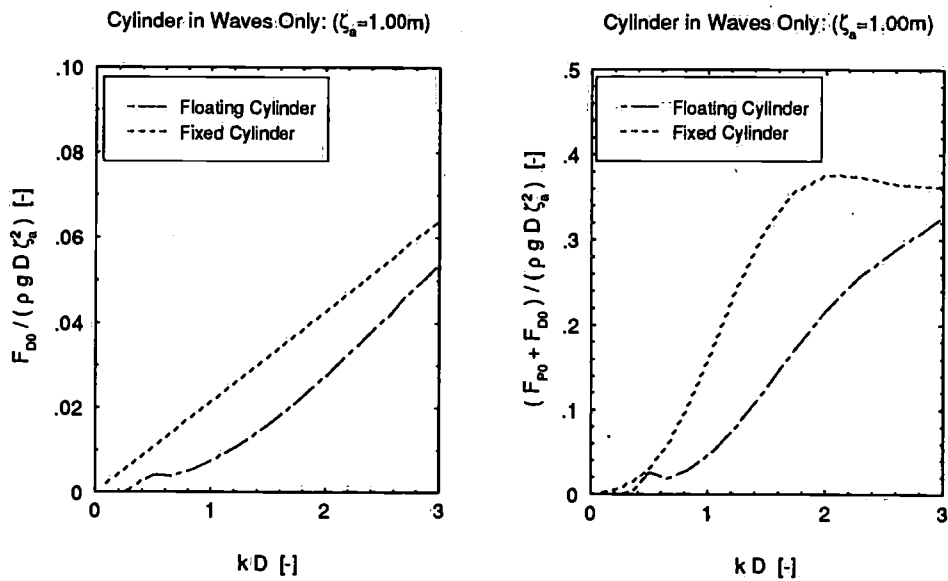


Figure 3.9: (left) Viscous mean drift forces in waves only and (right) potential plus viscous mean drift forces on a cylinder in waves only

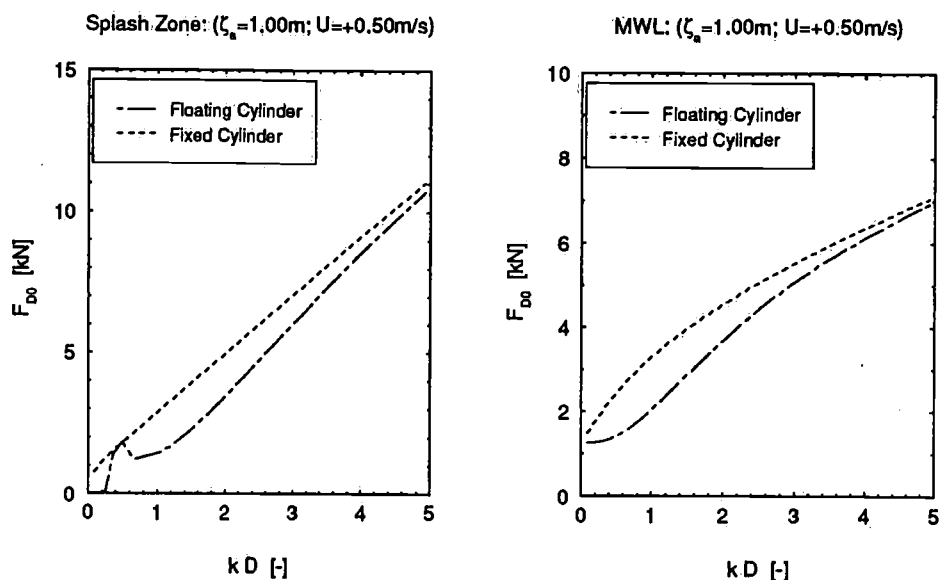


Figure 3.10: Viscous mean drift forces (left) on the splash zone and (right) on the submerged zone at mwl of a cylinder in waves and currents

peak is still observed at the heave natural frequency. However, such effects again depend on the magnitude of the wave particle velocity as well as the current velocity.

In Figure 3.11 (left), effects of a wave-current coexisting flow field are shown for the submerged zone of a floating cylinder for different wave amplitudes. The viscous mean drift forces between a fixed and a floating cylinder are shown in Figure 3.11 (right).

In Figure 3.12 (left), effects of velocities of currents for a constant wave amplitude are shown. The trend is similar to a fixed cylinder except in magnitude. Similar trends are shown in Figure 3.12 for different amplitudes for a fixed velocity of current.

3.1.3 Wave Stretching

In the linear (Airy) wave theory, the amplitude of the wave is assumed small and both kinematic and dynamic free surface boundary conditions are simplified. The boundary conditions are further simplified by considering them not at the unknown free surface $z = \zeta$ rather at still water level $z = 0$. Such inherent assumptions lead all calculations up to the still water level.

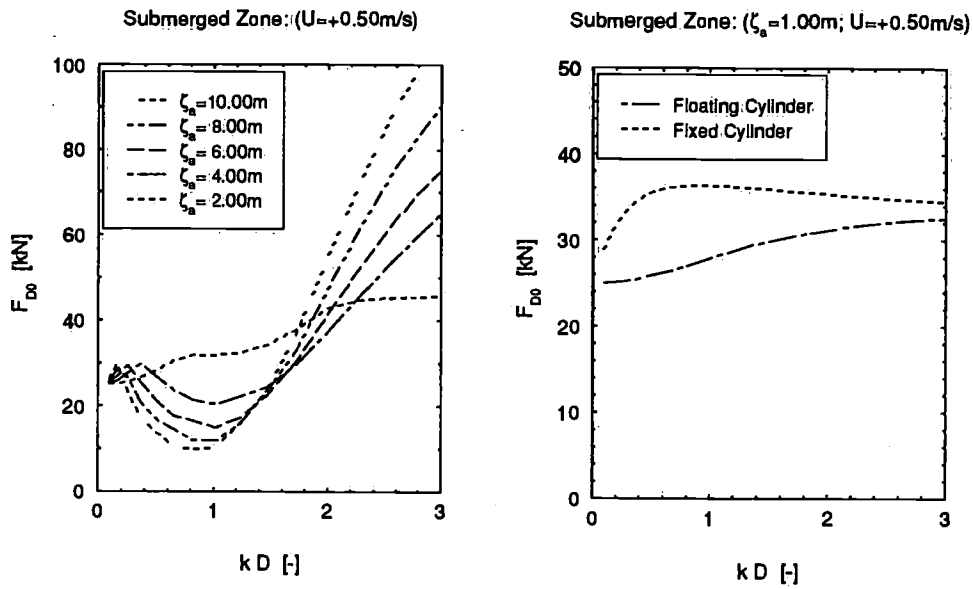


Figure 3.11: (left) Effects of wave amplitudes on viscous mean drift forces on a floating cylinder and (right) viscous mean drift forces on a cylinder

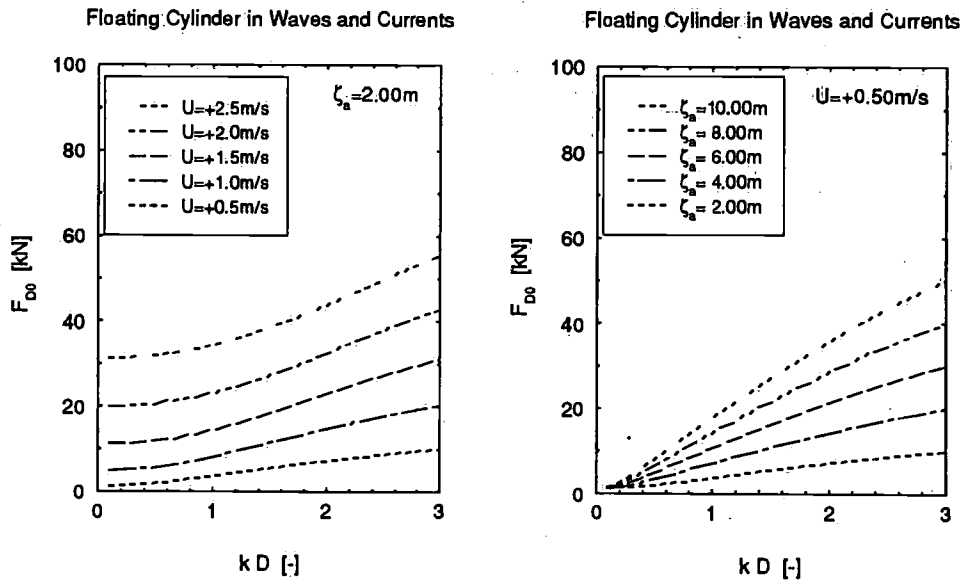


Figure 3.12: Effects of (left) velocity of currents and (right) wave amplitudes on a floating cylinder at mean water level in waves and currents

Under such assumptions of the linear (Airy) wave theory, the pressure is zero when the wave crosses the mwl ($z = 0, \zeta = 0$). On the other hand, at other points ($z = 0$), the pressure is equal to $\rho g z$ and thus the decay above mwl may be assumed linear (hydrostatic).

In practice, many offshore structures lie at the free surface and it is sometimes considered necessary to incorporate the changing free surface effect to calculate the response correctly. Chakrabarti (1984) has suggested a linear free surface correction to modify the linear (Airy) wave theory with 'stretching' by means of which, the kinematics of the water surface is stretched up and down to the free surface. According to Chakrabarti (1971) the modified formulation results in a better pressure distribution near the free surface.

Under the above criteria, an attempt will be made here to calculate the mean viscous drift force on a fixed vertical cylinder using the linear wave theory and the same with wave stretching. In doing so, shallow water velocity potential has been used so that effects of water depth on the viscous mean drift force can also be verified.

According to the linear (Airy) wave theory, the horizontal water particle velocity is as follows:

$$u = \frac{\zeta_a g k}{\omega} \frac{\cosh k(z+h)}{\cosh kh} \cos(kx - \omega t) \quad (3.28)$$

According to the modified linear (Airy) wave theory with stretching as proposed by Chakrabarti (1984), the horizontal water particle velocity will be as follows:

$$u = \frac{\zeta_a g k}{\omega} \frac{\cosh k(z+h)}{\cosh k(h+\zeta)} \cos(kx - \omega t) \quad (3.29)$$

Further modification is done for the denominator and the altered expression now takes the following form:

$$u = \frac{\zeta_a g k}{\omega} \frac{\cosh k(z+h) \{h/(h+\zeta)\}}{\cosh kh} \cos(kx - \omega t) \quad (3.30)$$

The expression in Equation 3.30 has also been proposed by Wheeler (1970).

For the splash zone of a fixed truncated surface piercing vertical cylinder, the viscous drag force for a unit height is as follows:

$$F_D(t) = \frac{1}{2} \rho C_D D u |u| \quad (3.31)$$

Taking origin at the center of the cylinder and after replacing u by Equation 3.29 and linearization, the viscous mean drift force in the splash zone is obtained from the following equation:

$$F_{D0} = \frac{8}{3\pi} \rho C_{D0} D g k \zeta_a^2 \frac{1}{\sinh 2kh} \frac{1}{T} \times \int_0^T \int_0^\zeta \cosh^2 k(z+h) \cos \omega t \, dz \, dt \quad (3.32a)$$

$$= \frac{2}{3\pi} \rho C_{D0} D g k \zeta_a^3 \left[\frac{1}{\sinh 2kh} + \{1 + S(2k\zeta_a)\} \coth 2kh \right] \quad (3.32b)$$

where

$$S(2k\zeta_a) = \sum_{n=1}^{\infty} \frac{(2n+1)}{(2n+2)} \frac{(2k\zeta_a)^{2n}}{(2n+1)!}$$

Now similar to before except using Equation 3.30, the viscous mean drift force is obtained from the following equation:

$$F_{D0} = \frac{8}{3\pi} \rho C_{D0} D g k \zeta_a \frac{1}{\sinh 2kh} \frac{1}{T} \times \int_0^T \int_0^\zeta \cosh^2 k(z+h) \{h/(h+\zeta)\} \cos \omega t \, dz \, dt \quad (3.33a)$$

$$= \frac{2}{3\pi} \rho C_{D0} D g k \zeta_a^3 \left[\frac{1}{\sinh 2kh} + \frac{1}{2kh} \right] \quad (3.33b)$$

After having obtained two different expressions Equation 3.32b and Equation 3.33b for the viscous mean drift force on the splash zone, calculations are done for a cylinder of 10 meter diameter for different water depths. Computational results are presented in Figure 3.13 showing the nondimensional viscous mean drift force for different values of relative wave height. It is clearly demonstrated from those figures that relative wave height does not produce any significant effect on the force while using the linear (Airy) wave theory whereas with increasing water depth, the magnitude of the force reduces significantly while using the linear (Airy) theory modified with wave stretching. In fact, the force due to the splash zone should not be a function of water depth while using the constant crest velocity. The differences

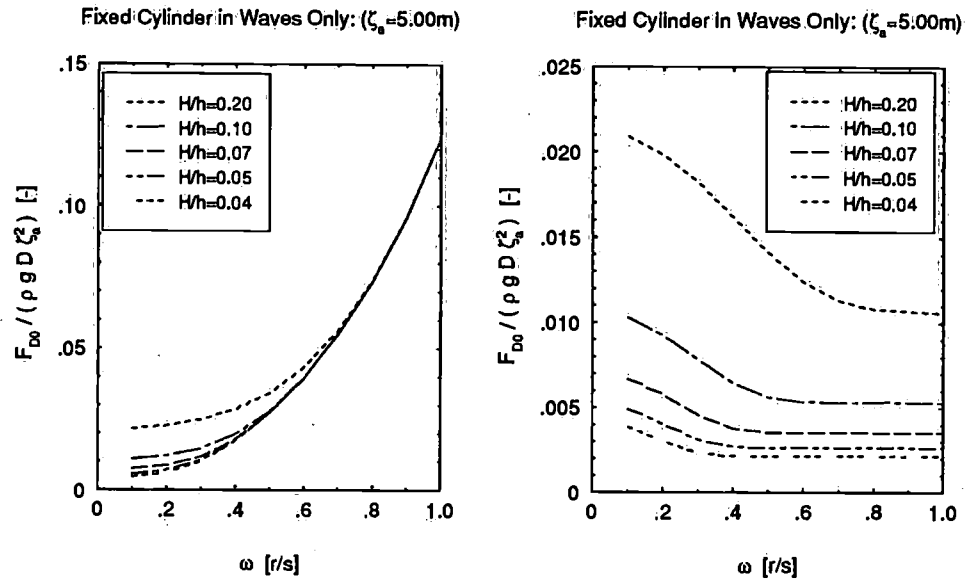


Figure 3.13: Viscous mean drift forces on a fixed cylinder in waves only using (left) the linear (Airy) wave theory and (right) the same with stretching.

observed for very shallow water are due to the fact that the exponential term has been used in the integration. However, these differences quickly diminish as the water depth increases. So, use of deep water velocity potential for computations is also justified. And surprisingly, the stretching phenomenon would cause the force to become zero for infinite water depth condition according to Equation 3.33b and that is why the viscous mean drift force becomes less and less as the water depth increases.

The governing parameters in Equation 3.32b and Equation 3.33b are ζ_a , k and h from the point of view of wave kinematics. Thus the viscous mean drift force becomes a function of dimensionless parameters like wave steepness (kH), relative wave height ($\frac{H}{h}$) and relative water depth (kh).

In Figure 3.19, Figure 3.25 and Figure 3.28 where relative water depth falls into the category of deep water condition, it is clearly demonstrated that the viscous mean drift force does exist even for deep water condition. So, the vertical wave stretching does not seem appropriate in such applications as assessing the viscous mean drift force.

3.2 Application of the Mean Drag Coefficient

In dealing with any viscous drag force, there are always uncertainties regarding its appropriate values. For uniform flow, the values of the drag coefficient are widely published even for different geometries. These values are expressed as a function of N_{Re} which takes account of the uniform velocity. Published data are also available for harmonically oscillating (bodies) flows. For oscillating (bodies) flows, the values of the drag coefficient are normally expressed as a function of N_{K-C} only or as a function of both N_{K-C} and N_{Re} , the combination of which is known as the 'frequency parameter' (β often known as the beta parameter) defined by Sarpkaya and Isaacson (1981). Both N_{Re} and N_{K-C} again depend on the maximum water particle velocity. Drag coefficients for oscillating (bodies) flows in uniform current are also available from many published test results. Most of the data available are for the first order forces like the inertia and also for the drag and the lift forces all of which have an oscillating nature and not a zero mean. Very few have dealt with the coefficients for the mean force. To the authors knowledge, Moe and Verley (1977), Chakrabarti (1984) and Koterayama (1984) have indicated the values of the mean drag coefficient relating to the viscous mean drift force in a wave-current coexisting flow field only which is shown again only for completely submerged bodies. No published results are available for the viscous mean drift force in a waves-only flow field.

Moe and Verley (1977) produced results for the drag coefficient for the mean force as a function of N_{M-V} and N_{K-C} . They interpreted both N_{M-V} and N_{K-C} as proportional to the ratio of vortex shedding frequency and the structural frequency. The mean drag coefficient was termed as the steady drag coefficient. Tests were carried out for a completely submerged horizontal cylinder oscillating in still water as well as in currents. Such test values can not be applied in evaluating the mean viscous drag force due to waves only on a surface piercing vertical cylinder because of the fact that drag coefficients mentioned for the oscillating cylinder in still water are not derived from the oscillating force. Furthermore, the hydrodynamic field created by a submerged cylinder with its axis parallel to wave crests is not equivalent to the one, by an oscillating cylinder in still water. Chakrabarti (1984) has mentioned only a single value of the mean drag coefficient which is 1.10 as a result of his tests for a vertical cylinder in waves and currents.

Pijfers and Brink (1977) considered the drag coefficient for the mean drift force in a wave-current coexisting flow field as an average value based

on N_{Re} and N_{K-C} as independent flow field. In the absence of any specific test results, such an approach seems reasonable although free surface effects are not considered. Also the value of the drag coefficient as a function of N_{K-C} has to be for the mean force, i.e. the drag coefficient should be a mean drag coefficient.

For bodies in waves and currents, both N_{Re} and N_{K-C} can be modified by adding the velocity of currents to the maximum water particle velocity as suggested by Sarpkaya and Isaacson (1981) and the mean drag coefficient can then be expressed as a function of these modified numbers or in terms of their combination, i.e. as a function of frequency parameter β though the latter would not change from the value in a waves-only flow field because of its inherent definition.

From the above references, it is clear that no systematic approach has yet been adopted or developed for the assessment of the values of mean drag coefficient for either surface piercing bodies or submerged bodies in a waves-only flow field as well as in a wave-current coexisting flow field. While, at present, the problem of predicting viscous mean drift forces is treated by the Morison equation, further deterioration in such approximate prediction methods should not be caused by the inappropriate or inaccurate choice of the the mean drag coefficient values.

The values of the mean drag coefficient for the viscous mean drift force due to waves only needs to be verified through experiments for a surface piercing vertical cylinder along with the effects of a wave-current coexisting flow field. For the viscous mean drift force on the submerged part due to waves and currents, published data by Moe and Verley (1977) and Kotera-ayama (1984) are quite useful in the absence of any appropriate experimental data for the submerged horizontal cylinder or for the constantly submerged zone of a vertical cylinder although they are limited in their nature.

3.3 Controlling Hydrodynamic Parameters

It has been observed from different studies that the Reynolds number is usually used for expressing hydrodynamic force coefficients in a uniform flow field. The Keulegan-Carpenter number is used similarly in a waves-only flow field whether the structure (hereinafter referred as a cylinder) is oscillating in the in-line direction in still water or fixed in a harmonically oscillating flow. The Strouhal Number is also a dominant parameter while considering the transverse force (lift force) due to vortex shedding phenomena. As N_{Re}

is a function of flow velocity, it is sometimes used for a waves-only flow field by replacing the uniform velocity term by the maximum water particle velocity amplitude. Thus for waves only, both N_{Re} and N_{K-C} again lead to a new hydrodynamic parameter known as frequency parameter β (a ratio of N_{Re} to N_{K-C}) as introduced by Sarpkaya and Isaacson (1981).

The viscous mean drift force in a waves-only flow field is in fact governed by the wave steepness (kH) which can be expressed as function of diffraction parameter (kD) and viscous parameter ($\frac{H}{D}$) so that force regimes can be well expressed whether they are dominated by diffraction effects or by viscous effects alone or by both of them. To the author's knowledge, no publication is available as to how to treat the viscous mean drag coefficient for a surface piercing body in waves only except taking the value as unity.

The objective of this present investigation is to determine, how and to what extent, which of the aforementioned hydrodynamic parameters is the predominant one for expressing hydrodynamic force coefficients like viscous mean drag coefficients in a wave-current coexisting flow field when current velocity can be either positive or negative with respect to the wave direction.

It has been revealed through different existing studies that only a few have dealt with the mean drag coefficient for the viscous mean drift force. Moe and Verley (1977) produced results for the mean drag coefficient as a function of the Moe-Verley Number and the Keulegan-Carpenter Number. Tests were carried out for a completely submerged horizontal oscillating cylinder in currents as well as in still water. Rather than considering interaction effects on the hydrodynamic parameters, they were treated separately. Koterayama (1984) used the same hydrodynamic parameters for the submerged zone of a surface piercing vertical cylinder in waves and currents.

Chakrabarti (1984) has mentioned a single value of viscous mean drag coefficient in a wave-current interaction field without mentioning any dominant hydrodynamic parameter.

Pijfers and Brink (1977) considered the drag coefficient for the mean drift force as an average value based on N_{Re} and N_{K-C} .

All the above mentioned works are related to completely submerged structures and do not necessarily take any account of the splash zone (free surface) effects while the cylinder in some practical problems can be surface piercing (vertical columns of a semi-submersible and a tension leg platform) and at the same time subject to viscous mean drift force due to a wave-current coexisting flow field which is different from a waves-only flow field.

Before proceeding further, the individual hydrodynamic parameter will be shown for an individual flow field and also in a coexisting flow field in

the conventional way. For either uniform flow or harmonically oscillating (bodies) flows, N_{Re} can be expressed as follows:

$$N_{Re} = \frac{\rho U D}{\mu} \quad \text{For a uniform flow field} \quad (3.34a)$$

$$= \frac{\rho u_a D}{\mu} \quad \text{For a waves-only flow field} \quad (3.34b)$$

For harmonically oscillating (bodies) flows, N_{K-C} is normally expressed as follows:

$$N_{K-C} = \frac{u_a T}{D} = \frac{u_a}{fD} \quad (3.35)$$

For harmonically oscillating (bodies) flows in a uniform flow, N_{M-v} is expressed by:

$$U_R = N_{M-v} = \frac{UT}{D} = \frac{U}{fD} \quad (3.36)$$

Moe and Verley (1977) described N_{M-v} (sometimes known as reduced velocity) as proportional to the ratio between the vortex shedding frequency and the structural (oscillating) frequency as the ratio $(\frac{U}{D})$ is proportional to the vortex shedding frequency in a uniform flow. In an indirect way, the Keulegan-Carpenter number has also been defined in a similar manner with the exception that the vortex shedding is governed by the cylinder only and not influenced by currents (a uniform flow). What is noticed above is that vortex shedding is a governing phenomenon influenced by the uniform velocity and the oscillating flow (body) frequency.

Sarpkaya and Isaacson (1981) have proposed a modified Keulegan-Carpenter number in a wave-current coexisting flow field which is defined as follows:

$$N_{K-C}^+ = \frac{(u_a + U)T}{D} = \frac{u_a T}{D} + \frac{UT}{D} = N_{K-C} + N_{M-v} \quad (3.37)$$

In fact, the modified N_{K-C}^+ is a combination of the same number for oscillating flows (bodies) and N_{M-v} for oscillating flow (bodies) fields in the presence of currents. In practice, U should be replaced by $|U|$ as the uniform flow (steady current) can be either positive or negative.

So, use of a modified Keulegan-Carpenter number obviates the necessity of introducing another hydrodynamic parameter N_{M-v} . Similar to

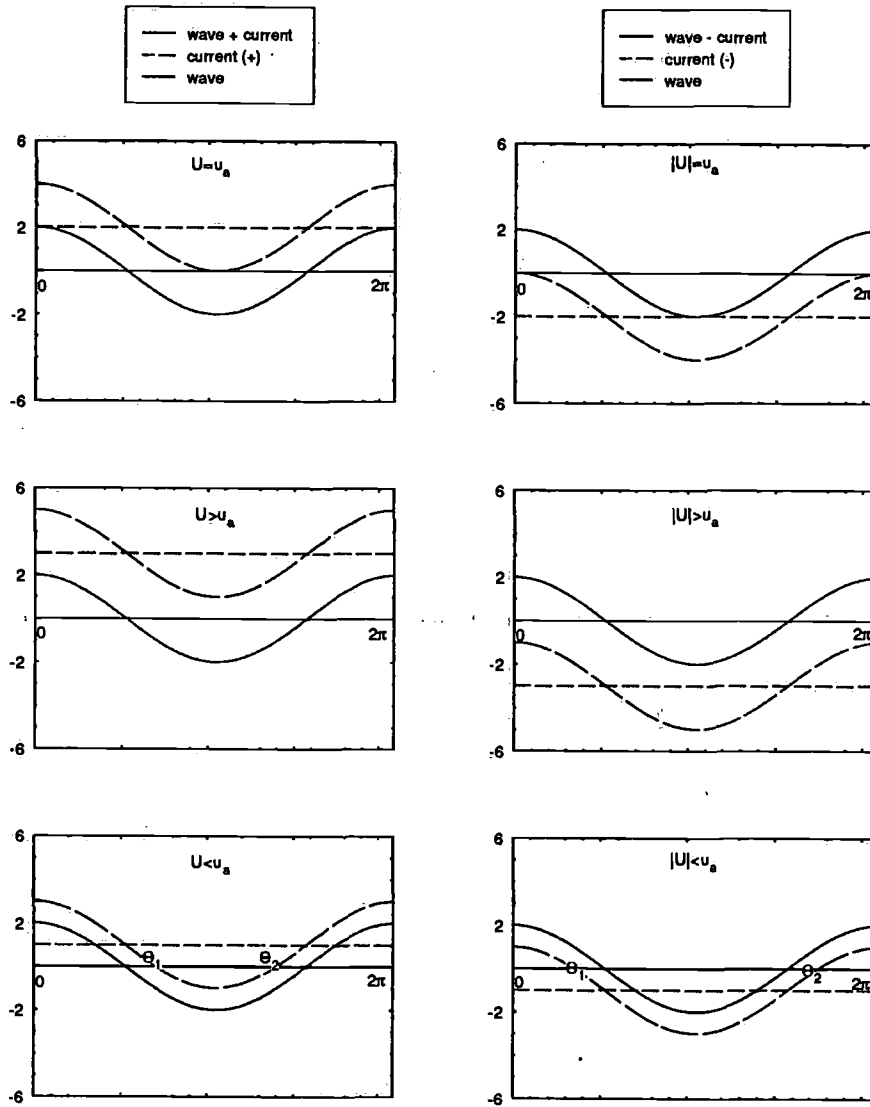


Figure 3.14: Effects of positive and negative velocities of currents on horizontal components of water particle velocities

the above, the Reynolds number can also be modified by replacing the velocity term by the combined velocity of waves and currents. Though the hydrodynamic terms in N_{Re} including the modified one can be linked to the vortex shedding phenomena, its use may not be suitable because of its large numerical value resulting in less significant variations over a frequency range. The frequency parameter β is not capable of showing any distinctive feature for a wave-current coexisting flow field because it is a ratio and so remains as an identical value both for a waves-only flow field as well as for a wave-current coexisting flow field. So, the only predominant hydrodynamic parameter left would be the Keulegan-Carpenter number. Now the remaining thing which needs further treatment is how the modified N_{K-C}^* behaves in a coexisting flow field rather than as defined earlier. The controlling factors to be chosen are the magnitude as well as the direction of the current velocity with respect to the water particle velocity and also the crest and trough phases of waves in a coexisting flow field.

Such newly proposed N_{K-C}^* would have the advantage of defining flow condition under a single parameter rather than introducing additional parameters. In addition, a flow field defined by a new Keulegan-Carpenter number for an interaction field can easily be compared to the similar flow field under a waves-only flow field.

The basic definition of the Keulegan-Carpenter number has been used for the newly proposed number, i.e its physical meaning is rather geometric which can be considered as the ratio of the moving distance of a water particle in one side direction of the cylinder S to the cylinder diameter D .

If U is either positive or negative and $U \geq u_a$: See Figure 3.14 (upper left & right and middle left & right)

$$N_{K-C}^* = \frac{\pi}{D} \left\{ 2 \int_0^{T/2} (u_a \cos \omega t \pm U) dt \right\} \quad (3.38a)$$

$$= \frac{\pi}{D} (\pm U) T \quad (3.38b)$$

$$= \pi |U| \frac{T}{D} \quad (3.38c)$$

If U is positive and $U < u_a$: See Figure 3.14 (lower left)

$$N_{K-C}^* = \frac{\pi}{D} \left\{ 2 \int_0^{T/2} (u_a \cos \omega t + U) dt \right\} \quad (3.39a)$$

$$= \frac{T}{D} u_a (\sin \Theta + \gamma \Theta) \quad (3.39b)$$

$$= N_{K-C} (\sin \Theta + \gamma \Theta) \quad (3.39c)$$

where

$$\Theta = \cos^{-1} \left(-\frac{U}{u_a} \right) = \cos^{-1}(-\gamma)$$

If U is negative and $|U| < u_a$: See Figure 3.14 (lower right)

$$N_{K-C}^* = \frac{\pi}{D} \left\{ 2 \int_{T/2}^T (|u_a \cos \omega t + U|) dt \right\} \quad (3.40a)$$

$$= \frac{T}{D} u_a \{ \sin \Theta + \gamma(\pi - \Theta) \} \quad (3.40b)$$

$$= N_{K-C} \{ \sin \Theta + \gamma(\pi - \Theta) \} \quad (3.40c)$$

where

$$\Theta = \cos^{-1} \left(\frac{U}{u_a} \right) = \cos^{-1}(\gamma)$$

From the above derivations, it can be seen that the Keulegan-Carpenter number for a waves-only flow field is quite different from that for a wave-current coexisting flow field not only by the additional magnitude of the combined velocity but also by the influence of crest and trough phases of the interacting waves. Furthermore, the Keulegan-Carpenter number in a wave-current coexisting flow field is governed by the magnitude as well as the direction of current velocity compared to water particle velocity in addition to the influence of the crest and trough phases of the waves.

Similar to the 'frequency parameter' β , the author has introduced another parameter called 'velocity parameter' γ (can be named as gamma parameter also) which is in fact a ratio of N_{M-V} and N_{K-C} or more precisely a velocity ratio of $\left(\frac{U}{u_a}\right)$. The value of γ would clearly indicate the strength of the individual flow field over the other in a coexisting flow field of waves and currents. Moreover, this new hydrodynamic parameter can be a more desirable variable as the value of γ being \gg than 1 or \ll 1

indicating strong current and no current condition thus revealing the fact of the force regime like drag or inertia being dominated.

$$\gamma = \frac{N_{M-V}}{N_{K-C}} = \frac{U}{u_a} \quad (3.41)$$

In order to show different definitions of the Keulegan-Carpenter number, Figure 3.15 has been produced for an arbitrary diameter of a cylinder. In this Figure (upper left and right), it is shown that the Keulegan-Carpenter number under a wave-current coexisting flow field (current velocity being less than the water particle velocity) ends up with the largest value. This maximum value occurs in the wave crest phase when U is positive (minimum value in the wave trough phase) and in the wave trough phase when U is negative (minimum value in the wave crest phase). But when current velocity is greater than water particle velocity, influence of either wave crest phase or trough phase is diminished thus resulting in the same value of the Keulegan-Carpenter number whether U is positive or negative. This is clearly shown in Figure 3.15 (lower left and right).

For the submerged zone in a wave-current coexisting flow field, the experimental (small cylinder) values of the mean drag coefficient are plotted in Figure 3.16 (left). N_{K-C}^+ used is based on the combined velocity of wave and current without taking into account any interaction effects. The values of C_{D0} were calculated for both positive and negative currents. Finally in Figure 3.16 (right), the values of the mean drag coefficient are plotted against the newly proposed N_{K-C}^* using the values of the crest phases for positive current and those of the trough phases for negative current. Comparing the two figures, it clearly indicates that the plot in Figure 3.16 (right) fits the values best.

From Figure 3.16 (right), it is further revealed that for the range of N_{K-C}^* up to around 8, the values of C_{D0} are around a more or less constant value and such a range corresponds to a pair of symmetric vortices in a waves-only flow field. Above this value, the values of the mean drag coefficient further increase which corresponds to the formation of a pair of asymmetric vortices and subsequently extremely asymmetric vortices with further increase in N_{K-C}^* . Such phenomena are also analogous to the classification of vortex pattern (Sawaragi and Nakamura 1979) in a waves-only flow field.

In waves only, N_{K-C} is governed by the water particle velocity (more precisely by the wave amplitude) only and the body's geometric dimensions. In Figure 3.34, the values of C_{D0} are plotted for values of N_{K-C} being less than or greater than 3 based on the measured forces on the splash

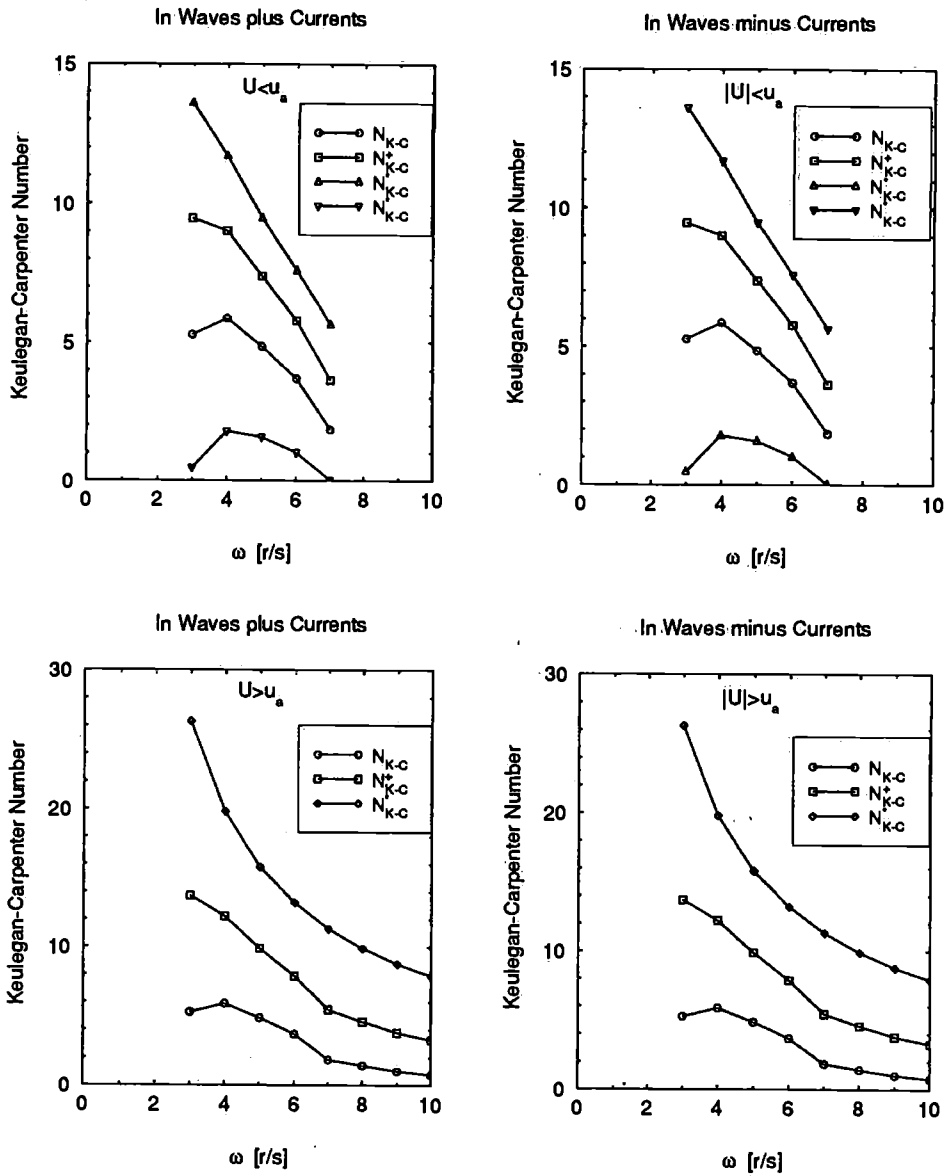


Figure 3.15: Various definitions of the Keulegan-Carpenter number in waves and currents and the Keulegan-Carpenter number in waves only

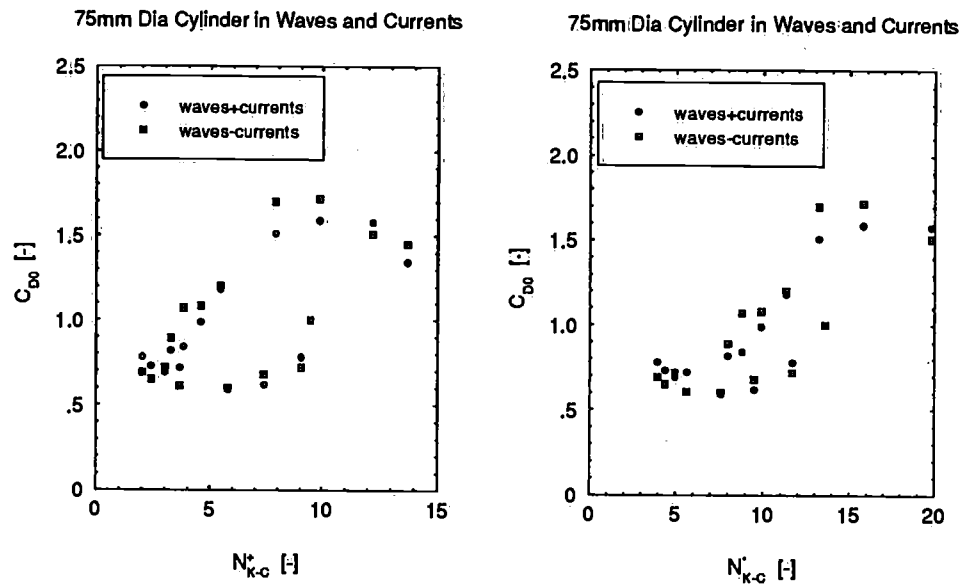


Figure 3.16: Experimental mean drag coefficients of the submerged zone of a fixed cylinder in waves and currents as function of the Keulegan-Carpenter number of different definitions

zone and the theoretical forces for the same condition. Some values seem scattered. Based on the values which fit close, it is clearly seen that the value of mean drag coefficient can be taken as an average value of 1.5 over the range ($3 \leq N_{K-C} < 8$) where the vortices are symmetric. The data seem scattered in the range ($0 < N_{K-C} < 3$). It has been indicated earlier that either the diffraction parameter and the viscous parameter or a combination of both govern the value of the mean drag coefficient. So, it is quite likely that for higher values of N_{K-C} , i.e. where the value of $(\frac{H}{D})$ is large, viscous effects dominate in low frequencies.

Table 3.1 along with Figure 3.17 can be referred to for more clarification.

3.4 Concluding Remarks

In this theoretical analysis the contributions have been evaluated of viscous effects in a waves-only flow field and also in a wave-current coexisting flow field (wave-current interaction effects) to the mean drift force for floating structures like semi-submersibles, tension leg platforms. From the results

Vortex Pattern	Outline	Sawaragi-Nakamura
V-1	No vortex generation	$N_{K-C} < 3$
V-2	A pair of symmetric vortices	$3 < N_{K-C} < 8$
V-3	A pair of asymmetric vortices	$8 < N_{K-C} < 13$
V-4	The third vortex generation	$13 < N_{K-C} < 20$ (weak asymmetry) $20 < N_{K-C} < 26$ (intensive asymmetry)
V-5	Pseudo Karman vortex street	$26 < N_{K-C}$

Table 3.1: Vortex pattern in waves only [Sawaragi and Nakamura (1979)]

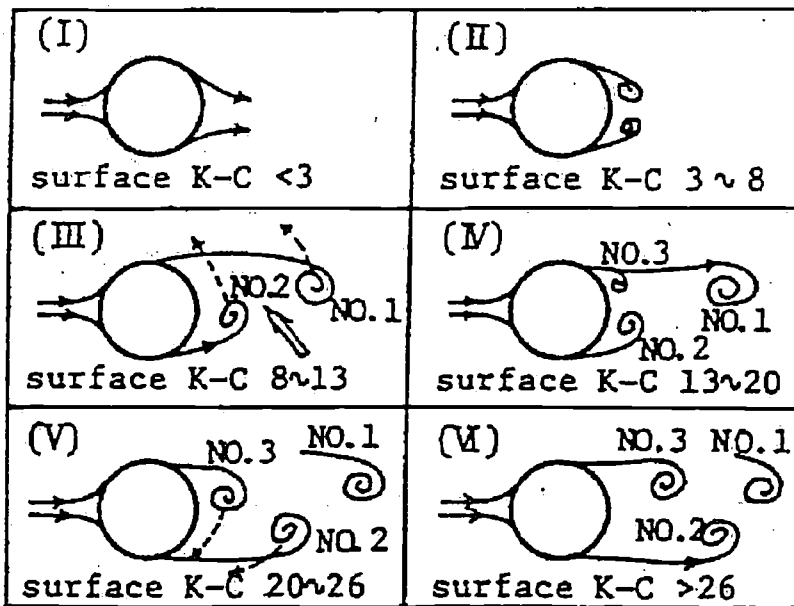


Figure 3.17: Schematic of the evolution of vortices in various ranges of the Keulegan-Carpenter number [Sawaragi and Nakamura (1979)]

presented, the following conclusions can be drawn:

1. Due to the splash zone nonlinearity, the mean drift force due to drag effects has been found to be proportional to wave height cubed. Its effectiveness is further enhanced with the increase of wave height.
2. A linear superposition method to consider wave-current interaction is not an appropriate approach because the presence of a small amount of current leads to a substantial increase of viscous drift force even for the submerged zone of a cylinder. Interaction effects seem to modify the force on the splash zone as well.
3. Prediction of viscous mean drift forces in a waves-only flow field based on the idea of subtracting the force due to currents only from that in a wave-current coexisting flow field shows much deviation from the present method which includes the splash zone (free surface zone) force.
4. For a floating cylinder, the relative velocity and the relative surface elevation concept considering their combined amplitude and phase seems to be sufficient to deal with the terms derived for a floating cylinder.
5. Great uncertainties still lie ahead with respect to the value of the mean drag coefficient. Though many published test results are available in existing literature, they are not suitable for direct application for such a mean force computation problem. Additional treatment is always necessary before they can be applied.
6. Systematic experimental investigation is necessary to validate the theory and also to understand other aspects before treating such a complex phenomenon of viscous origin.

3.5 Experimental Validation

In theoretical evaluation, all categories of viscous mean drift forces for either a fixed or a floating cylinder have been found to be a direct function of the mean drag coefficient apart from other hydrodynamic parameters which are the most controlling factors for the value of the mean drag coefficient. In almost all published work, the value of the mean drag coefficient has been taken as either unity or been suppressed while nondimensionalizing the

force without giving any clear indication as to how to treat such a problem with better accuracy. There have been many experiments concerning the inertia and drag coefficient in relation with first order forces while using the Morison equation. But very few experimental work has been done in order to investigate the values of the mean drag coefficient which is related to the viscous mean drift force while using the Morison equation.

To the author's knowledge, a few experiments were done to investigate the viscous mean force and all such experiments were done on the completely submerged test sections of either a vertical or a horizontal cylinder thus without giving any result on the splash zone which exists in the case of surface piercing vertical columns of a semi-submersible or a tension leg platform in addition to its constantly submerged zone.

The main objectives of the experimental investigations were:

- To assess the magnitude of the viscous mean drift force due to waves only as well as due to waves and currents on the two separate hydrodynamic zones of the cylinder.
- To obtain the values of the viscous mean drag coefficient over a dominant range of the wave frequencies in a waves-only flow field as well as in a wave-current coexisting flow field.
- To verify the suitability of the single controlling hydrodynamic parameter to express the viscous mean drag coefficient in a wave-current coexisting flow field so that the latter can be made analogous to the flow field due to a waves-only flow field.

In Section 2.2 and Section 2.3 of Chapter 2, details of experimental work have been given for fixed, truncated and surface piercing vertical cylinders. Further details can be found in (Dev 1992b; Dev 1992c; Dev 1993).

3.5.1 Small Cylinder

The range of the nondimensional hydrodynamic parameters of this experiment is as follows:

In a waves-only flow field:

$$N_{K-C} = 0.670 - 7.460$$

$$N_{Re} = 0.491 \times 10^4 - 0.243 \times 10^5$$

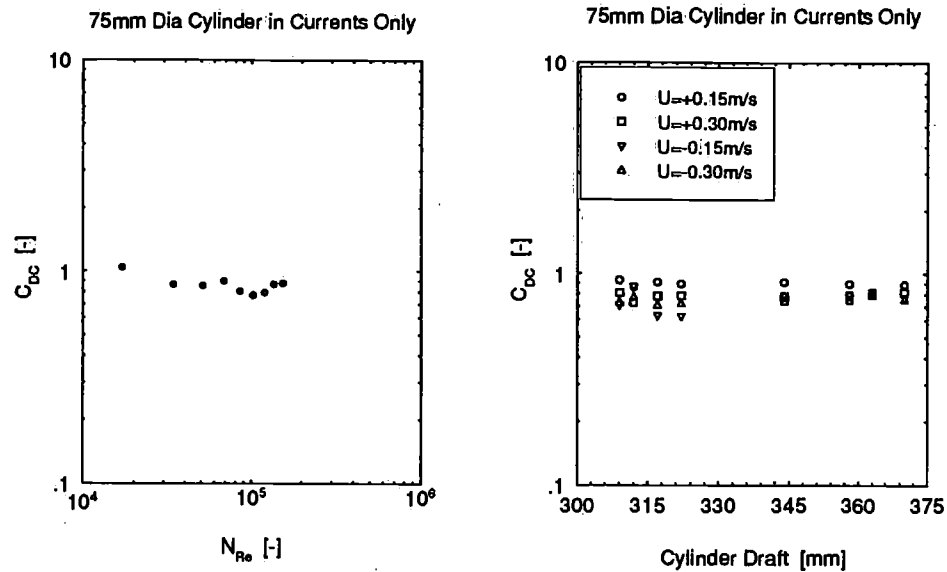


Figure 3.18: *Experimental drag coefficients of a fixed cylinder in currents only (left) for a constant draft and (right) for different drafts*

In a wave-current coexisting flow field:

$$N_{K-C}^+ = 2.010 - 13.700$$

$$N_{Re}^+ = 0.164 \times 10^5 - .395 \times 10^5$$

$$N_{M-V} = 12.600 - 83.800$$

$$N_{K-C}^* = 3.950 - 26.300$$

In Currents Only

The purpose of these tests was to observe any significant variation in the drag coefficient's values. Results of these tests are shown in Figure 3.18. The draft of the model cylinder was 500mm in Figure 3.18 (left). The draft of the model cylinder in Figure 3.18 (right) is a sum of the submerged zone (300mm) plus the varying splash zone (equal to different wave amplitudes) used in the experiment.

Splash Zone in Waves Only and also in Waves and Currents

In Figure 3.19 (left) the measured mean forces due to waves only (different wave amplitudes in ascending order of ζ_{a1} , ζ_{a2} and ζ_{a3}) on the splash zone

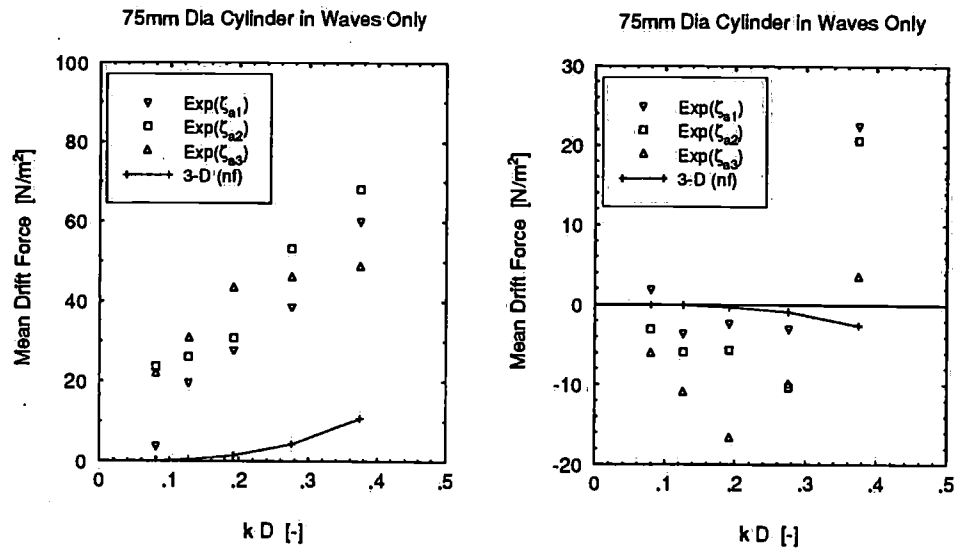


Figure 3.19: Potential vs. measured mean drift forces (left) on the splash zone and (right) the submerged zone for different wave amplitudes

are shown. Also shown in Figure 3.21 are the measured mean forces due to wave-current interaction effects. Mean forces due to potential effects were calculated by DELFRAC. The discretization of the cylinder is shown in Figure 3.20.

From the above mentioned figures, it is quite clear that mean drift forces due to viscous effects in the presence of waves only do exist and their magnitude is also considerable compared to potential effects. The presence of positive currents through interaction effects further contributes to such viscous effects related to mean forces. However, negative currents show the opposite trend resulting in less viscous effects than due to waves alone and such effects are further increased when the current velocity is increased.

The presence of currents further influences the mean drift force on the splash zone due to wave-current interaction effects as shown in Figure 3.21. However, negative currents show the opposite trend resulting in less viscous effects than due to waves only and such effects are further increased when the current velocity is increased.

The theoretical and experimental viscous mean drift forces due to wave-current interaction effects only on the splash zone are plotted again in Figure 3.22 (upper). In theoretical calculations, the value of the mean drag

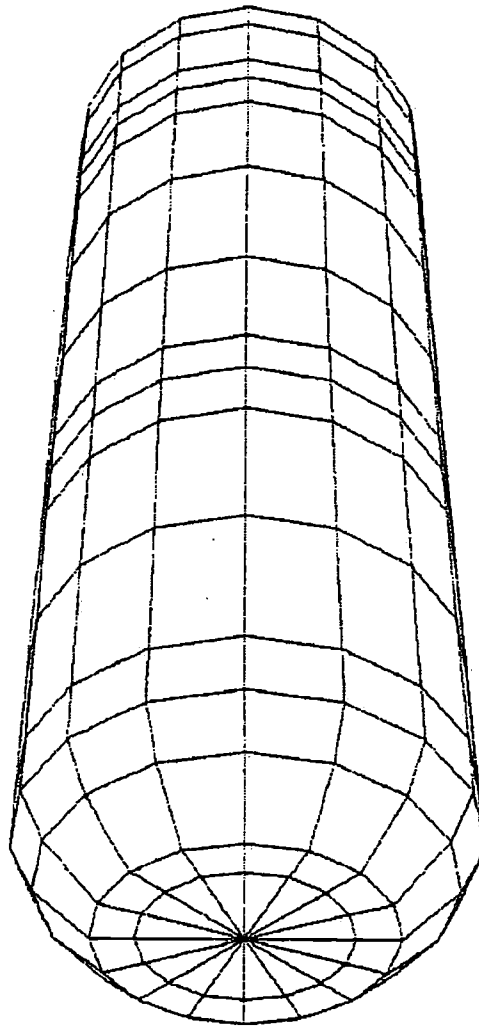


Figure 3.20: The panel distribution on the model cylinder

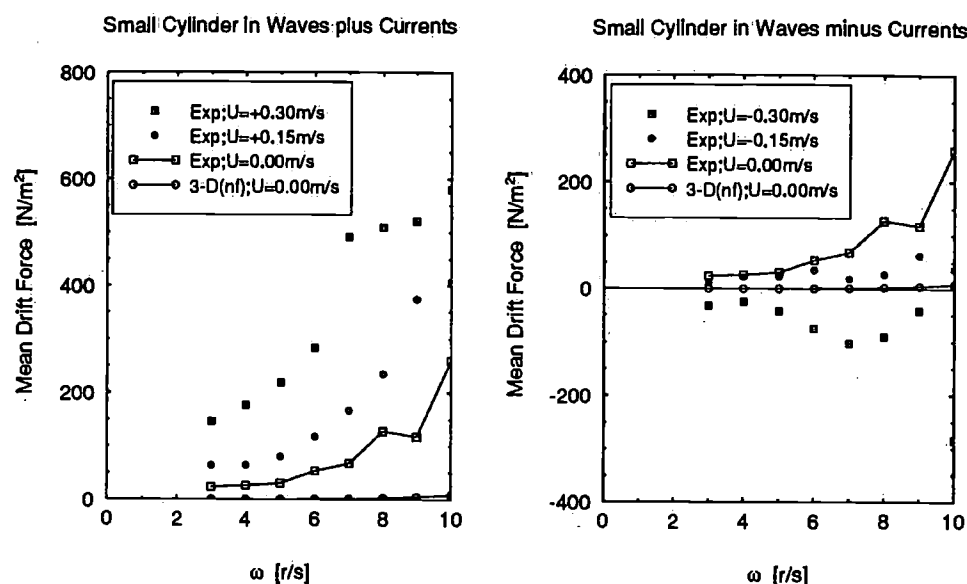


Figure 3.21: *Potential vs. measured mean drift forces on the splash zone of a fixed cylinder in waves and currents*

coefficient was used as 1.00. However, the trend of both theory and experiment seem quite similar. Discrepancies can be due to the inappropriate choice of the value of the mean drag coefficient.

Submerged Zone in Waves Only and also in Waves and Currents

The potential mean drift force on the submerged zone in waves only is due to the second order pressure (velocity squared term in the Bernoulli's equation). The magnitude of such potential mean force is very low compared to the one due to the wetted surface elevation on the splash zone. Figure 3.19 (right) shows the comparison between 3-D computation and measured mean forces. The differences are not consistent.

Figure 3.22 (lower) is produced for the submerged zone subject to waves and currents. The conclusions are similar to the behavior of the splash zone, that is, indicating similar trend between theory and experiment but differing again in magnitudes.

Out of the above presentation of the results, it can be firmly concluded that the viscous mean drift forces on a fixed vertical cylinder due to waves only field are theoretically zero while integration is performed up to the

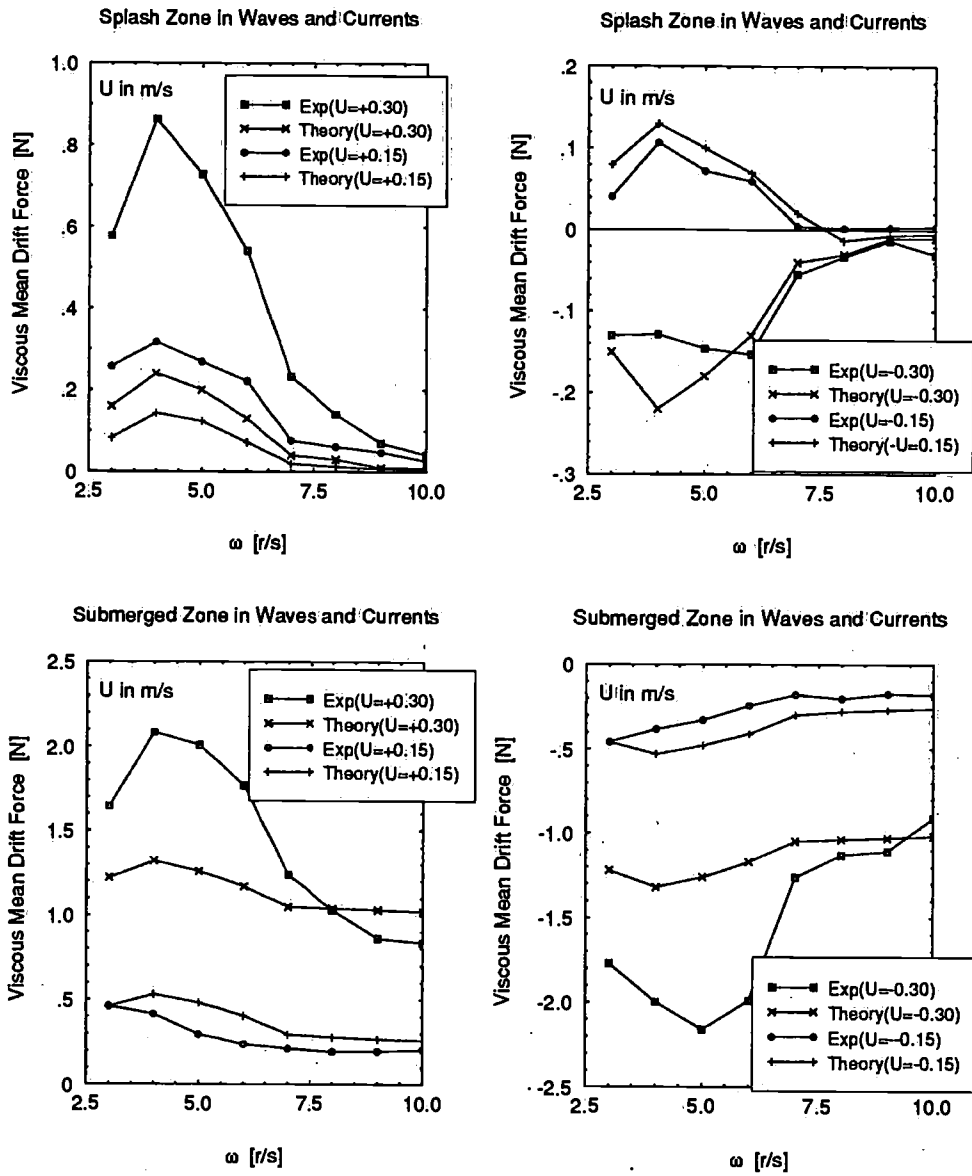


Figure 3.22: Theoretical ($C_{D0} = 1$) vs. experimental viscous mean drift forces on two different zones of a fixed cylinder in waves and currents

mwl. But due to the existence of the splash zone of a cylinder, viscous contributions towards the mean drift force do occur. Even a small presence of currents can again lead to the creation of viscous mean drift forces for the submerged zone of the cylinder as well. Furthermore, depending on the direction of currents with respect to waves, such viscous contributions on the splash zone further increase or decrease with much more pronounced effects depending on the magnitude of the current velocity also.

While comparing the results between theory and experiment, the main discrepancies have been found in connection with the magnitude of the forces which can be improved by applying suitable values of the drag coefficient based on the experimental results. This is why one of the main objectives of the experimental investigation was to find the values of the mean drag coefficient. The mean drag coefficient which is mainly a function of the flow field is normally expressed as a function of different hydrodynamic parameters like N_{Re} , N_{K-C} , N_{M-V} , β , etc. In a waves-only flow field, the Keulegan-Carpenter number is applicable as the oscillating nature is involved. However, for a wave-current coexisting flow field, the author has made an attempt to find a suitable parameter based on the basic definition of the Keulegan-Carpenter number.

Though flow visualization techniques were outside the scope of this experimental investigation, it was observed during the experiments that the water particle movement is quite symmetrical during the phases of the wave crest and wave trough in a waves-only flow field whereas in a wave-current coexisting flow field, the behavior is rather asymmetrical perhaps, due to the nonlinear effects of wave-current interactions. As a result of such difference in the inherent properties of the flow field under two different circumstances (crest phase and trough phase), the hydrodynamic mechanism of generating forces differs due to the complex properties of the flow field.

In Figure 3.23, the experimental viscous mean drift force in waves only is presented against the experimental mean drift forces in waves and currents after the forces due to currents alone have been deducted. It can be seen that the experimental viscous mean drift force in waves only is less than even from that due to the submerged zone alone and far less than from the total for the splash and the submerged zone together. So, a common theoretical approach used by many for instance Burns (1983), Chitrapu *et al.* (1993) and Pijfers and Brink (1977) for calculating the viscous mean drift force from that due to wave-current viscous mean drift force is not appropriate. Such discrepancies are due to the fact that in the presence of currents, wave-current interactions increase the force both in the submerged zone and in

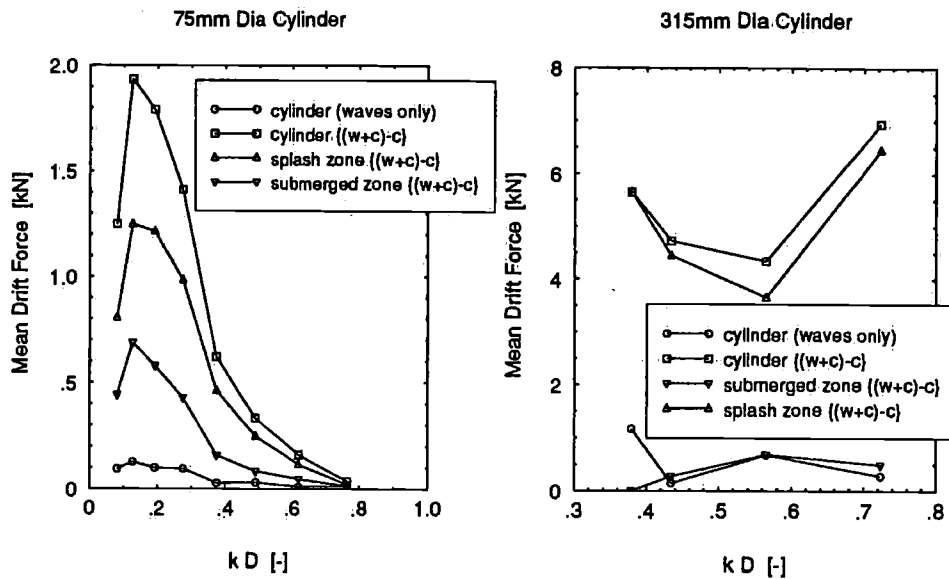


Figure 3.23: Experimental mean drift forces on a fixed cylinder in waves only as well as in waves and currents minus currents

the splash zone whereas in a waves-only flow field, the viscous mean drift force is mainly originated in the splash zone.

3.5.2 Large Cylinder at DUT

The range of the nondimensional hydrodynamic parameters of this experiment were as follows:

In a waves-only flow field:

$$N_{K-C} = 0.359 - 2.690$$

$$N_{Re} = 0.372 \times 10^5 - 0.126 \times 10^6$$

In a wave-current coexisting flow field:

$$N_{K-C}^+ = 0.930 - 4.830$$

$$N_{Re}^+ = 0.868 \times 10^5 - 0.225 \times 10^6$$

$$N_{M-V} = 0.530 - 2.100$$

$$N_{K-C}^* = 1.820 - 6.950$$

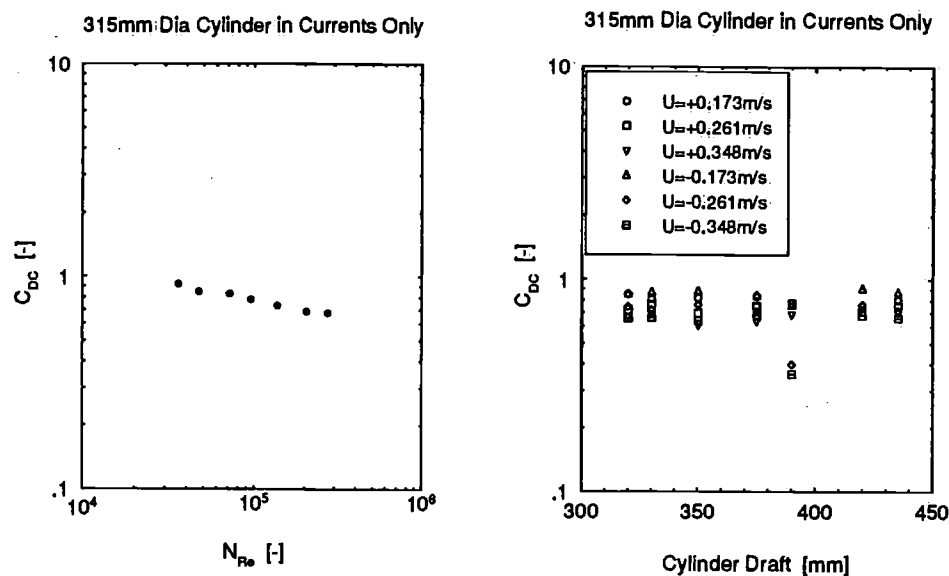


Figure 3.24: *Experimental drag coefficients of a fixed cylinder in currents only (left) for a constant draft and (right) for different drafts*

In Currents Only

As different wave amplitudes were used during the experiment for different frequencies in a waves-only flow field and also in wave-current coexisting flow field, it was felt necessary to conduct tests in currents only for different drafts of the splash zone resembling some of the wave amplitudes used. However, in such tests, the submerged zone always remained under the mwl. Tests were carried out for the following current velocities (carriage speeds) ($\pm 0.173\text{m/s}$, $\pm 0.261\text{m/s}$ and $\pm 0.348\text{m/s}$). Results are produced in Figure 3.25.

The draft of the model cylinder was 450mm in Figure 3.24 (left). The draft of the model cylinder in Figure 3.24 (right) was submerged zone (300mm) plus varying splash zone (equal to different wave amplitudes) used in the experiment.

In Waves Only

In Figure 3.25, results for the measured drift forces are shown against the potential (theoretical) mean drift force. Potential drift forces have been calculated by DELFRAC (1992) which also made possible the calculation

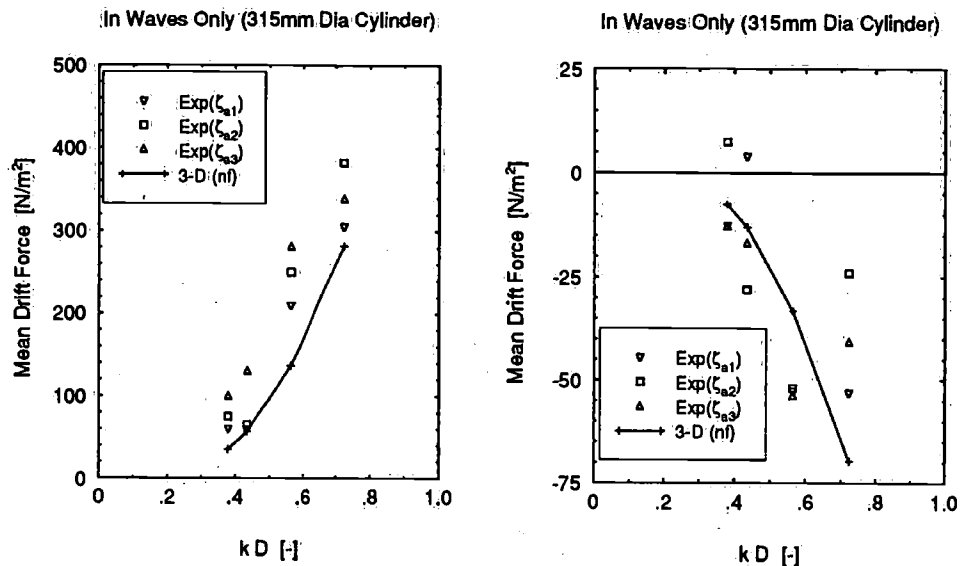


Figure 3.25: Potential vs. measured mean drift forces on (left) the splash zone and (right) the submerged zone for different wave amplitudes

of the mean drift force due to second order pressure effects. The differences between 3-dimensional computations and measured forces are not as high as was observed in the case of the small cylinder. Increase of diffraction parameter combined with a decrease in viscous parameter causes less effects of viscous origin. For the submerged zone, again the measured forces show some scatter but have a trend similar to 3-dimensional computations.

In Waves and Currents

Theoretical viscous mean drift forces were calculated using the same wave amplitudes used in the experiment for both the splash zone and the submerged zone considering the unit value of the mean drag coefficient. Subsequently, out of the measured mean forces, the experimental mean viscous forces have been obtained after deducting the potential part including forward speed effects. The results are compared in Figure 3.26. The anomaly observed is due to the unit value of the mean C_{D0} throughout the theoretical calculations which clearly indicates that the inappropriate choice of the mean drag coefficient will always lead to an erroneous result.

Similarly, Figure 3.27 demonstrates the comparison for the submerged

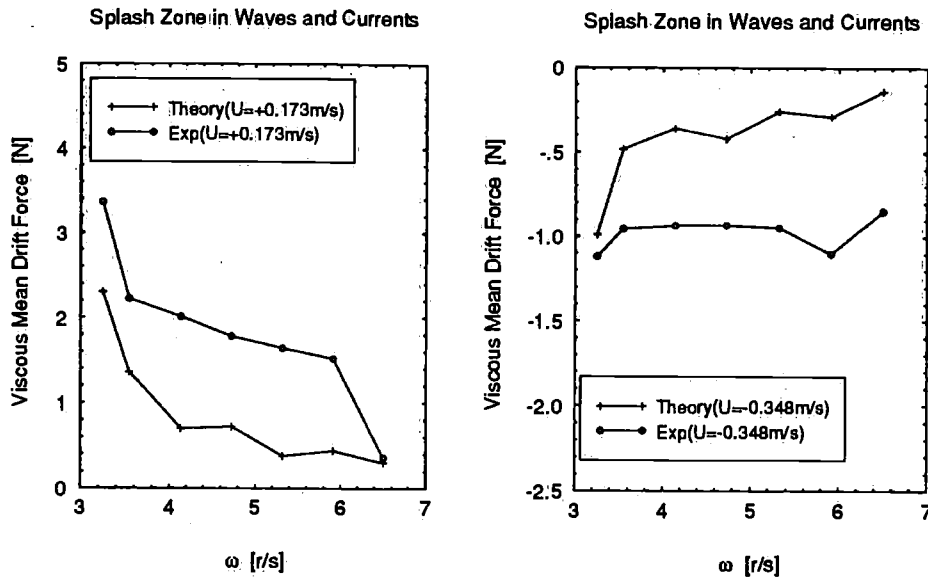


Figure 3.26: Theoretical ($C_{D0} = 1$) vs. experimental viscous mean drift forces on the splash zone of a fixed cylinder in waves and currents

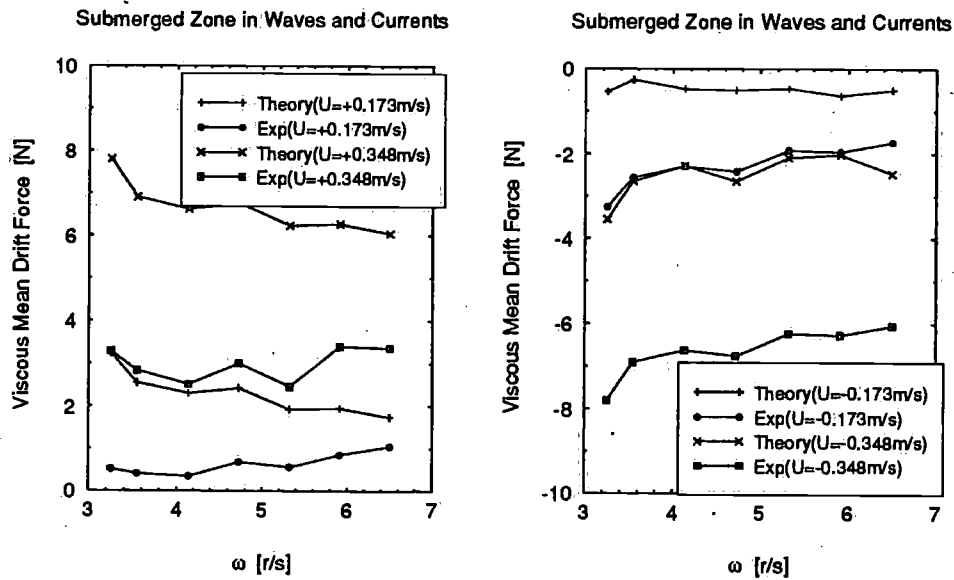


Figure 3.27: Theoretical ($C_{D0} = 1$) vs. experimental viscous mean drift forces on the submerged zone of a fixed cylinder in waves and currents

zone.

3.5.3 Large Cylinder at MARIN

Due to the limited width of the towing tank of DUT (Delft University of Technology) with respect to the diameter of the model cylinder, it was observed in the previous experiment that at zero speed tests, i.e. for a waves-only flow field, there could have been effects of wave reflections back from the tank wall. Under the above circumstances, it was then decided to repeat the experiment in the Sea-keeping BASIN of MARIN which is a much wider tank to remove any doubt in the investigation.

The range of the nondimensional hydrodynamic parameters of this experiment were as follows:

In a waves-only flow field:

$$N_{K-C} = 1.020 - 2.690$$

$$N_{Re} = 0.781 \times 10^5 - 1.600 \times 10^5$$

In a wave-current coexisting flow field:

$$N_{K-C}^{\dagger} = 2.000 - 3.950$$

$$N_{Re}^{\dagger} = 1.530 \times 10^5 - 2.350 \times 10^5$$

$$N_{M-V} = 0.970 - 1.200$$

$$N_{K-C}^* = 3.090 - 4.970$$

In Waves Only

In Figure 3.28, results for the measured drift forces are shown against the potential (theoretical) mean drift forces. Potential drift forces were calculated by DELFRAC which made it also possible to calculate the mean drift force due to the second order pressure effects. From the plots, it can be seen that for most cases, the measured drift forces are higher than the potential ones thus concluding that viscous contributions exist but not to the extent as seen in the case of the small cylinder. One of the reasons for such minimal difference between potential theory and the measured forces is the fact that because of the larger diameter of the model cylinder, the mean drift force is influenced by not only the viscous parameter ($\frac{H}{D}$) but also by the diffraction parameter (kD). Furthermore, the results appear consistent with those 3.25 from the tests with the same cylinder model at the Tank

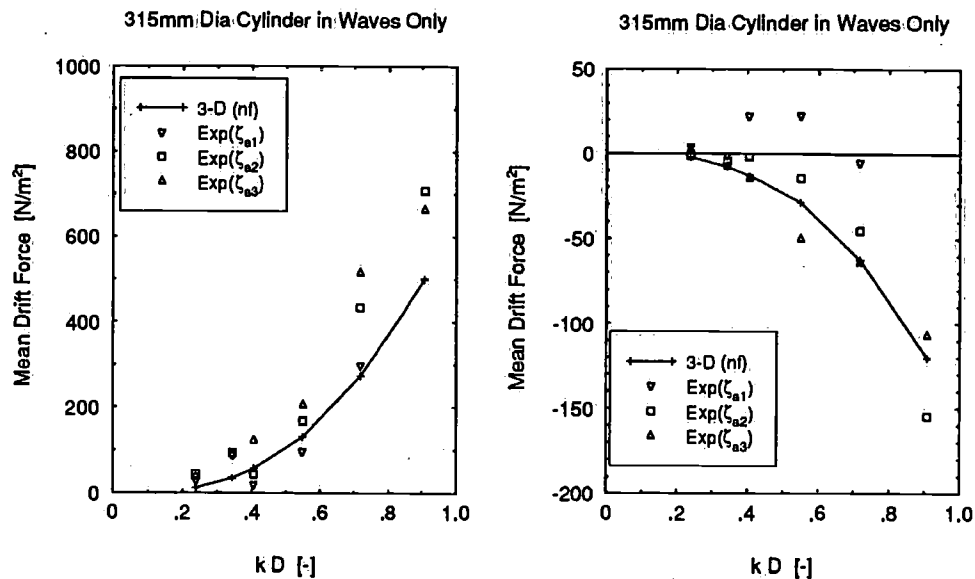


Figure 3.28: Potential vs. measured mean drift forces on (left) the splash zone and (right) the submerged zone for different wave amplitudes

No.1 of DUT. Accordingly, the wall effects do not appear significant in the previous test results at the Tank No.1 of DUT.

During the experiment, the relative wave elevation at the fore and aft of the cylinder was measured in order to verify them with the theoretical calculations. The results are presented in Figure 3.29. The comparison is quite satisfactory revealing the fact that the calculation of the mean drift force due to potential effects is justified. However, such relative wave elevation predicted by the theory would not be applicable when the cylinder is subject to a wave-current coexisting flow field and as such inherent errors would remain in the prediction of the viscous mean drift forces after deducting the potential part which is calculated for zero speed. Such a phenomenon could be overcome by the experimentally obtained mean drag coefficients.

In Waves and Currents

Similar to before, the theoretical mean viscous forces were calculated for both the splash zone and the submerged zone considering unit value of the mean drag coefficient. Subsequently, out of the measured mean forces, the experimental viscous mean forces were obtained after deducting the ap-

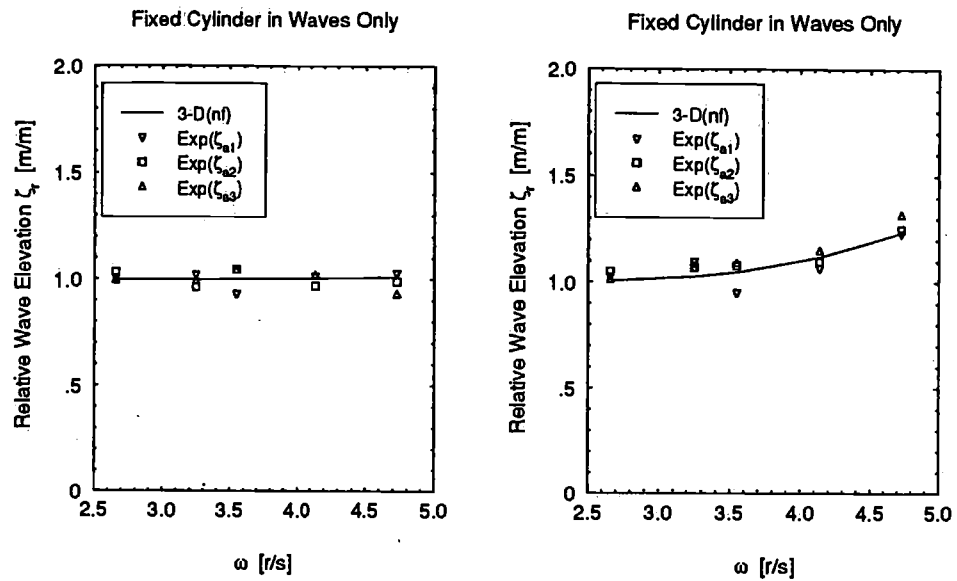


Figure 3.29: Relative wave elevation at the (left) aft and (right) fore of the cylinder in waves only for different wave amplitudes

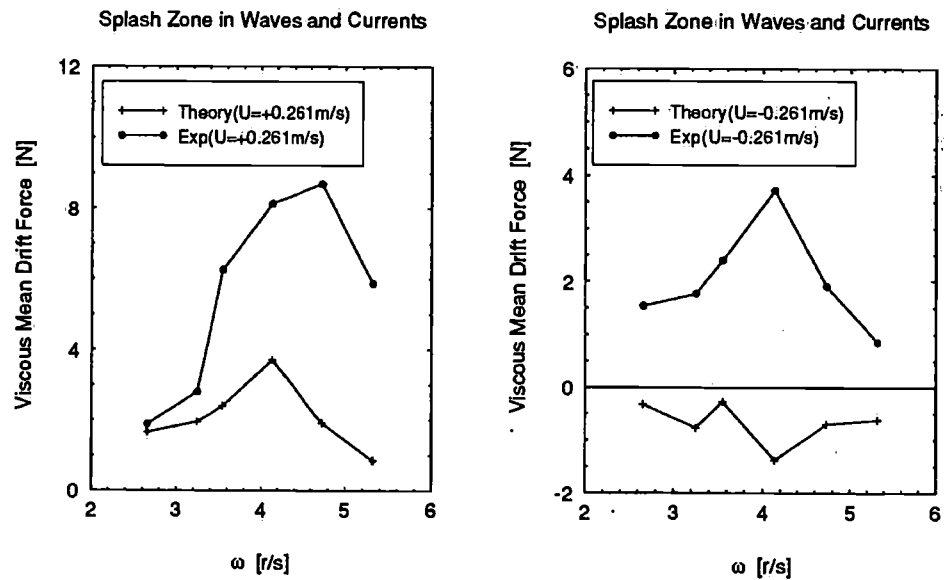


Figure 3.30: Theoretical ($C_{D0} = 1$) vs. experimental viscous mean drift forces on the splash zone of a fixed cylinder in waves and currents

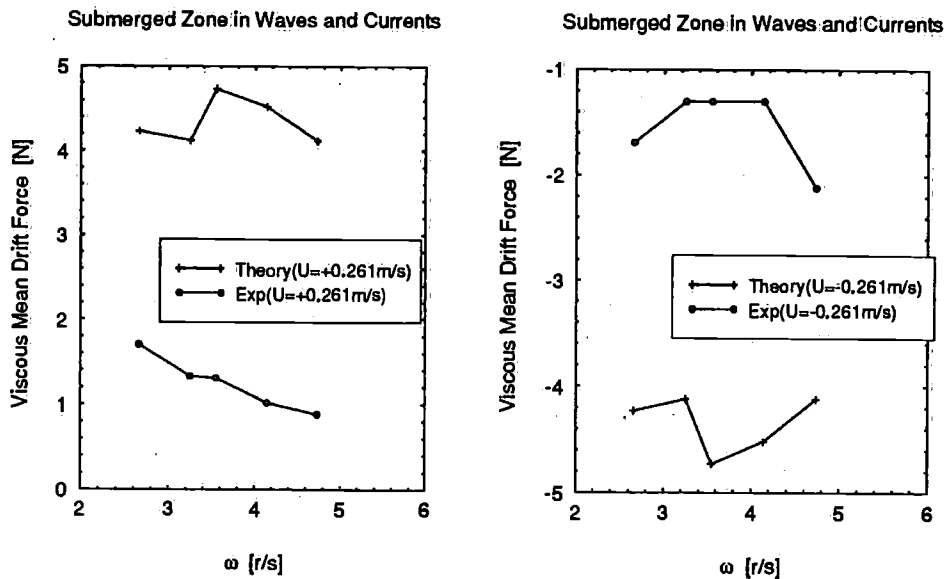


Figure 3.31: *Theoretical ($C_{D0} = 1$) vs. experimental viscous mean drift forces on the submerged zone of a fixed cylinder in waves and currents*

appropriate potential effects. Such comparison is made in Figure 3.26. The anomaly observed is due to the unit value of the mean drag coefficient throughout the theoretical calculations. However, the major deviation is when the current velocity is negative and when the absolute value of the current velocity is less than the water particle velocity. In this case, a negative force occurs due to the fact that over a complete cycle, the trough velocity is always higher. To overcome this, either the force under such circumstances is to be considered negative or the negative values of the mean drag coefficient are to be used.

Similarly, Figure 3.31 demonstrates the comparison for the submerged zone.

3.5.4 Mean Drag Coefficients

In Currents Only

From the experimentally obtained values of the drag coefficients in a currents-only flow field, it can be concluded that published data for the drag coefficient as a function of the Reynolds number for smooth circular cylinders

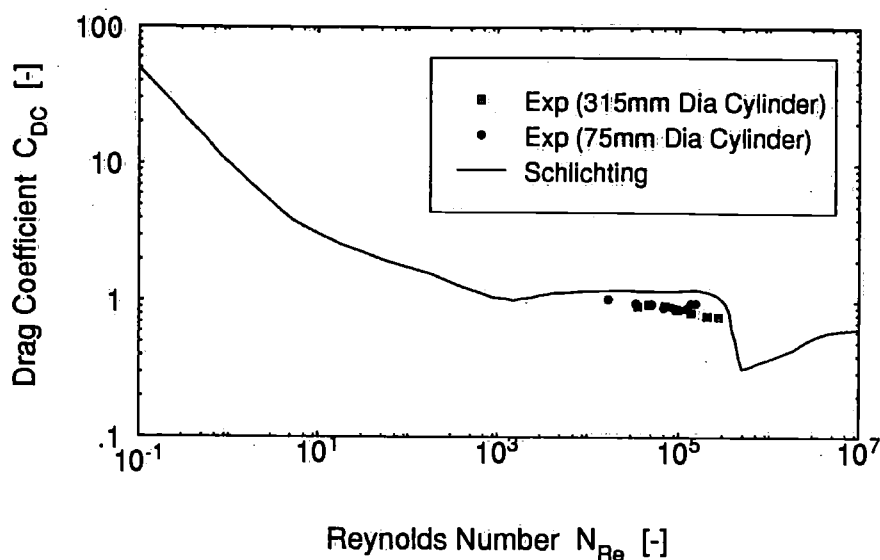


Figure 3.32: Drag coefficient for circular cylinders as a function of the Reynolds number [Schlichting (1968)]

can be used to calculate the force due to currents only. Figure 3.32 shows the comparison with the experimentally obtained values of the mean drag coefficient against the published data (Schlichting 1968).

In Waves Only

Based on the experimental data obtained from the three experiments, Figure 3.33 shows the three curves (theoretical ratio of viscous to potential mean drift force) equal to 5, 1 and $1/5$ represents 80% viscous, viscous equal to potential and 80% potential respectively. At $(\frac{H}{D} > 1)$ and at very low values of (kD) , the force is dominated mainly by viscous effects which is also indicated by the experimental results which were obtained from the tests with small cylinder. Around the line $(R_{ft} = 1)$, both viscous and potential drift forces are equally important. Experimental results from the small as well as the large cylinder show the trends with a few disparities. Figure 3.34 establishes the values of the mean drag coefficients in a waves-only field. In force regimes where both potential and viscous effects are equally important, the values of the mean drag coefficients are expected to be better expressed as function of viscous parameter $(\frac{H}{D})$, diffraction parameter (kD) and a combination of them, i.e. wave steepness (kH) .

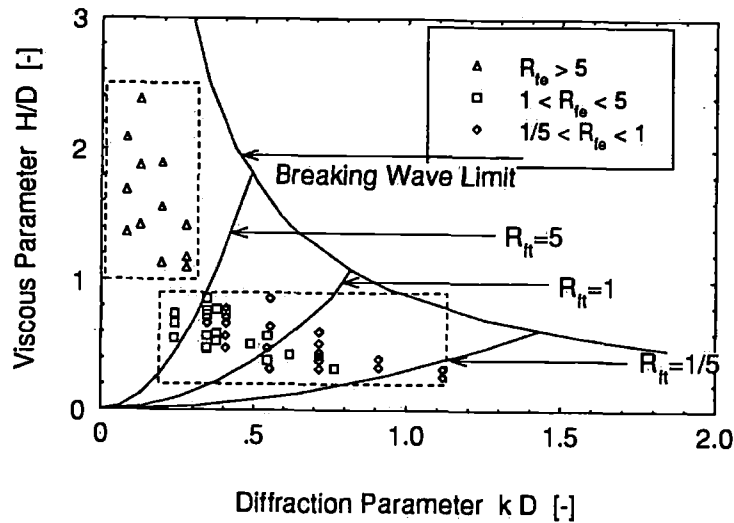


Figure 3.33: Viscous and potential mean drift regimes for the splash zone of both fixed model cylinders in waves only

In a waves-only flow field, the mean drag coefficient can be well represented as a function of a nondimensional hydrodynamic parameter like N_{K-C} based on wave parameters (wave amplitude and wave period) only.

In Figure 3.34 the values of the mean drag coefficients as obtained from the three experiments have been plotted as function of diffraction parameter (kD), viscous parameter ($\frac{H}{D}$) and wave steepness (kH) for ($N_{K-C} < 3$) where diffraction effects seem to dominate. However, for ($N_{K-C} \geq 3$), the values of C_{D0} show quite consistent results. As a result of the above, the values of C_{D0} in a waves-only flow field for vertical cylinders can be expressed as follows:

$$C_{D0} = c_1(kD) + c_2\left(\frac{H}{D}\right) + c_3(kH); (N_{K-C} < 3) \quad (3.42)$$

where

$$\begin{aligned} c_1 &= 1.863 \\ c_2 &= 0.433 \\ c_3 &= -1.373 \end{aligned}$$

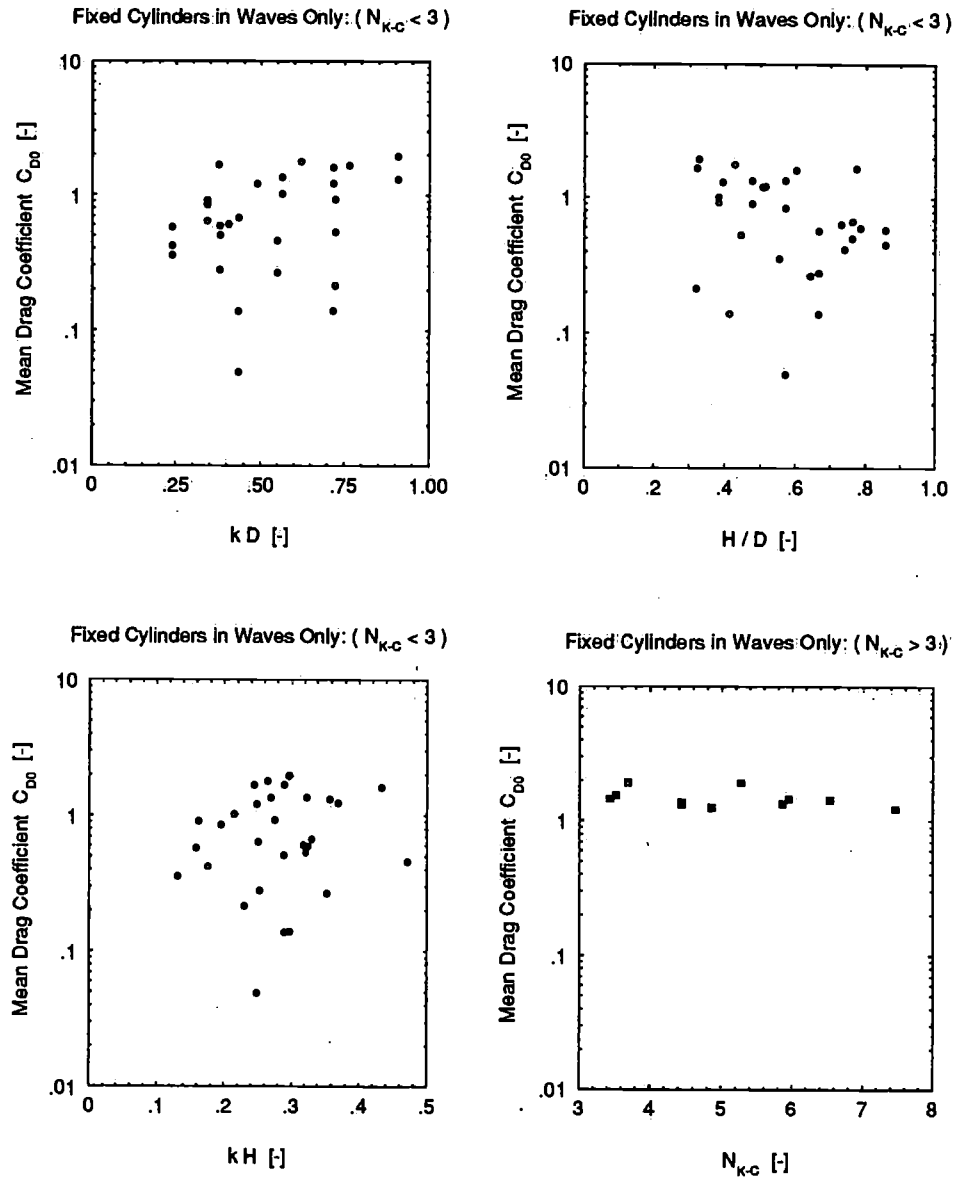


Figure 3.34: Experimental mean drag coefficients from both cylinder models in waves only as function of diffraction parameter (kD), viscous parameter ($\frac{H}{D}$), wave steepness (kH) and the Keulegan-Carpenter number (N_{K-C})

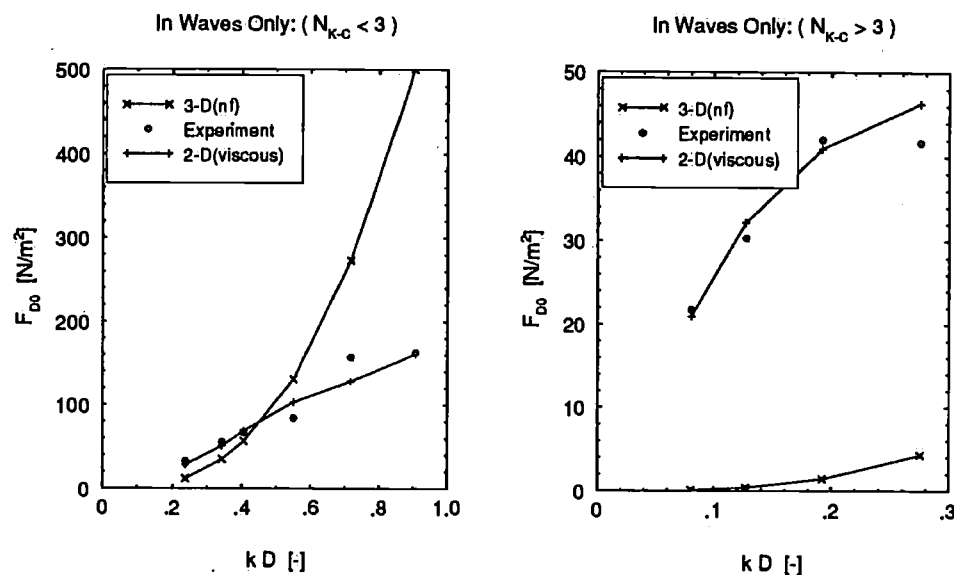


Figure 3.35: Potential vs. viscous (experimental C_{D0}) mean drift forces on both fixed cylinders (left: 315mm Dia and right: 75mm Dia) in waves only

$$C_{D0} = c_0 + c_1 N_{K-C}; \quad (3 \leq N_{K-C} < 8) \quad (3.43)$$

where

$$c_0 = 1.826$$

$$c_1 = -0.070$$

Applying Equation 3.42 and Equation 3.43 as appropriate, the viscous mean drift forces were calculated using the wave kinematics used in the experiment for the small and large cylinders and are compared with those in the experiments. From Figure 3.35, it can be seen that computations can be accurate enough while using the experimentally obtained values of the mean drag coefficients.

In Waves and Currents

However, in a wave-current coexisting flow field, the Keulegan-Carpenter number can be modified by including current velocity (Sarpkaya and Isaacson 1981) or it can be further modified taking into account the wave-current

interaction effects thus resulting in a new Keulegan-Carpenter number as proposed earlier. It has already been shown that the values of the mean drag coefficient matches suitably while using the newly proposed N_{K-C}^* in the case of the small cylinder in the previous experiment. So, accordingly the values of the mean drag coefficient are plotted against the newly proposed N_{K-C}^* in some figures. But it is also common to generate the values of the drag coefficient as a function of two nondimensional hydrodynamic parameters - one N_{K-C} based on water particle velocity only and the other N_{M-V} based on current velocity only. However, both the parameters are also treated with wave periods. Such representation can be found in much literature such as (Moe and Verley 1977; Sarpkaya and Isaacson 1981; Koterayama 1984), etc.

The only noticeable thing is that the value of the mean drag coefficient is very high for the splash zone in the presence of positive currents. For the submerged zone, not much difference is observed whether the current velocity is positive or negative. It is convenient to plot the values of the mean drag coefficient as a function of a single independent variable which in this case is the modified N_{K-C}^* which would enable more reliable data fitting because of more data.

In fact, presentation of the values of the mean drag coefficient against either the Keulegan-Carpenter number for different values of N_{M-V} and vice versa, much more data is necessary (which is better done with forced oscillation tests (Moe and Verley 1977; Koterayama 1984)). That is why the author has included in Figure 3.36 and Figure 3.37 the values of mean drag coefficient as a function of the newly proposed N_{K-C}^* which not only takes account of current velocity but also wave-current interaction effects.

Though N_{K-C}^* takes account of most of the hydrodynamic parameters, it does not take any account of the diffraction parameter (kD). So, the values of the mean drag coefficients have been presented as a function of (kD) and N_{K-C}^* .

$$C_{D0} = c_1(kD) + c_2 N_{K-C}^* \quad (3.44)$$

The values of the coefficients are produced in Table 3.2 through Table 3.9 for different hydrodynamic zones like splash zone and submerged zone and also for positive and negative currents with respect to their values compared to horizontal water particle velocity.

Viscous mean drift forces on a fixed cylinder (75mm Dia) in a wave-

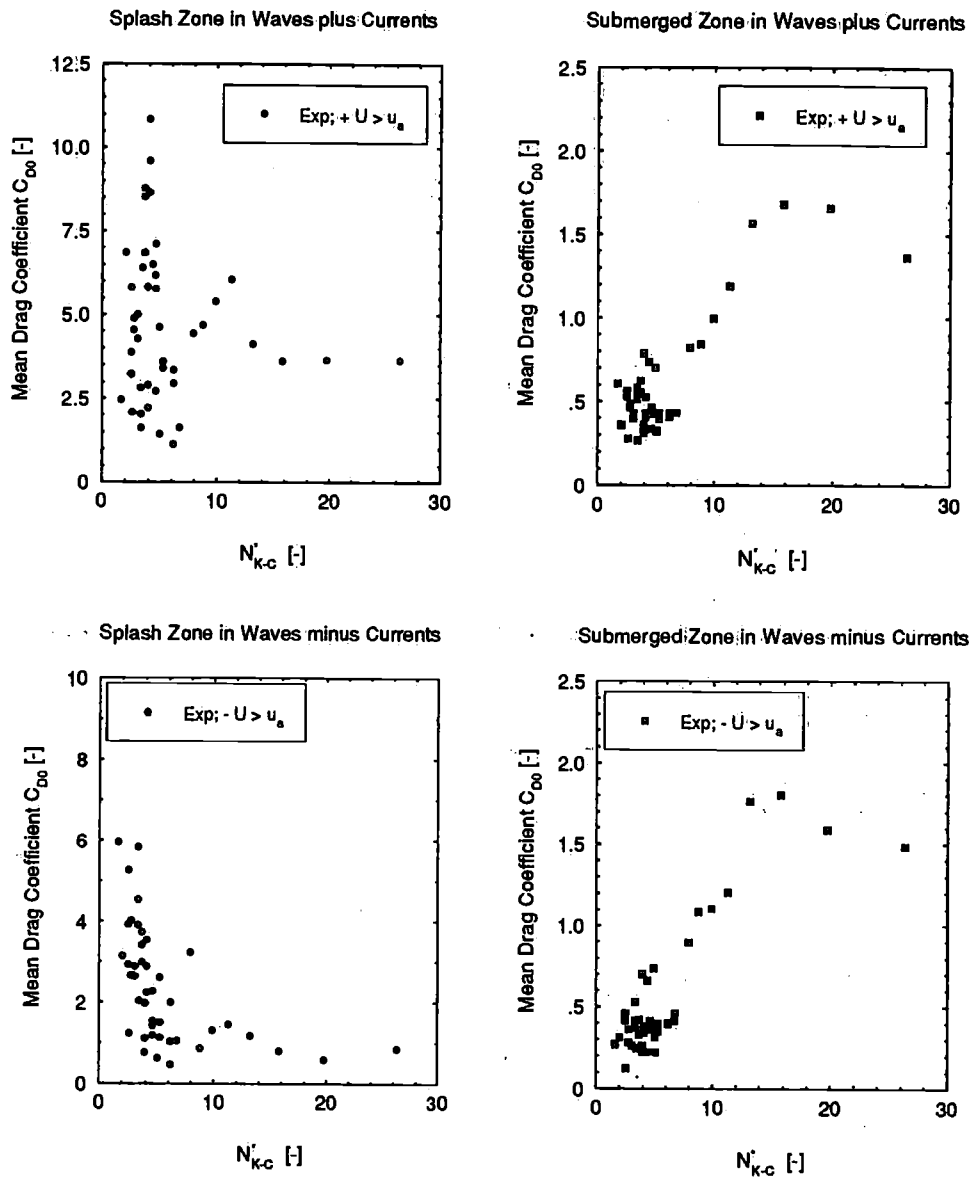


Figure 3.36: Experimental mean drag coefficients in waves plus currents for the splash and the submerged zones of fixed model cylinders

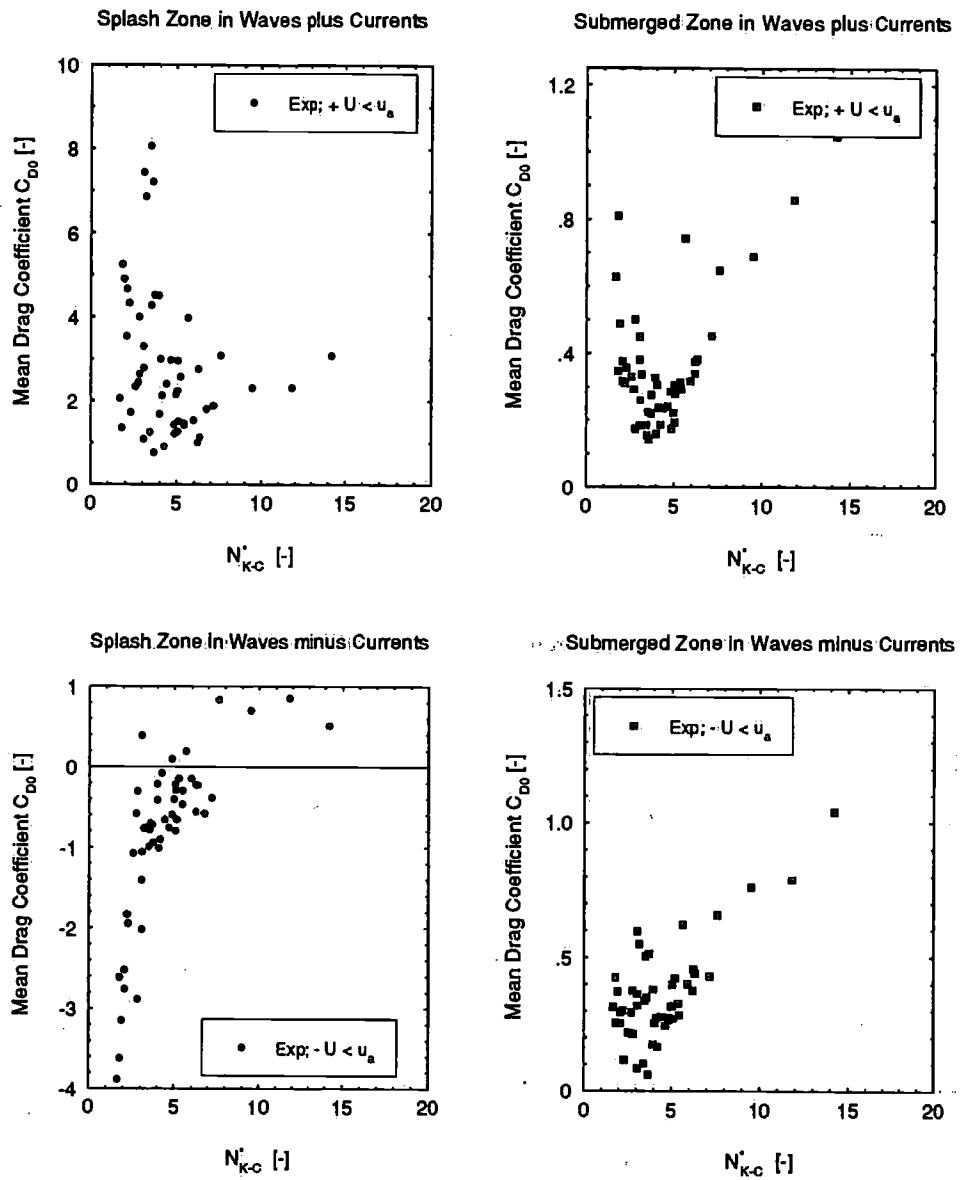


Figure 3.37: Experimental mean drag coefficients in waves plus currents for the splash and the submerged zones of model cylinders

Values of N_{K-C}^*	c_1	c_2
$N_{K-C}^* < 3$	1.317	1.104
$3 \leq N_{K-C}^* < 8$	4.424	0.311
$8 \leq N_{K-C}^* < 13$	4.521	0.284
$13 \leq N_{K-C}^* < 20$	10.25	0.110

Table 3.2: Values of coefficients for positive U and $U > u_a$ for the splash zone in waves and currents

Values of N_{K-C}^*	c_1	c_2
$N_{K-C}^* < 3$	4.514	-0.650
$3 \leq N_{K-C}^* < 8$	3.287	-0.066
$8 \leq N_{K-C}^* < 13$	0.313	0.098
$13 \leq N_{K-C}^* < 20$	1.869	0.025

Table 3.3: Values of coefficients for negative U and $|U| > u_a$ for the splash zone in waves and currents

Values of N_{K-C}^*	c_1	c_2
$N_{K-C}^* < 3$	1.729	0.692
$3 \leq N_{K-C}^* < 8$	6.897	-0.117
$8 \leq N_{K-C}^* < 13$	5.093	0.141

Table 3.4: Values of coefficients for positive U and $U < u_a$ for the splash zone in waves and currents

Values of N_{K-C}^*	c_1	c_2
$N_{K-C}^* < 3$	-3.390	0.478
$3 \leq N_{K-C}^* < 8$	-1.486	0.047
$8 \leq N_{K-C}^* < 13$	0.129	0.070

Table 3.5: Values of Coefficients for negative U and $|U| < u_a$ for the splash zone in waves and currents

Values of N_{K-C}^*	c_1	c_2
$N_{K-C}^* < 3$	0.406	0.002
$3 \leq N_{K-C}^* < 8$	0.393	0.008
$8 \leq N_{K-C}^* < 13$	0.609	0.008
$13 \leq N_{K-C}^* < 20$	4.547	0.003

Table 3.6: Values of coefficients for positive U and $U > u_a$ for the submerged zone in waves and currents

Values of N_{K-C}^*	c_1	c_2
$N_{K-C}^* < 3$	0.257	0.006
$3 \leq N_{K-C}^* < 8$	0.256	0.009
$8 \leq N_{K-C}^* < 13$	0.609	0.008
$13 \leq N_{K-C}^* < 20$	4.547	0.008

Table 3.7: Values of coefficients for negative U and $|U| > u_a$ for the submerged zone in waves and currents

Values of N_{K-C}^*	c_1	c_2
$N_{K-C}^* < 3$	0.495	-0.032
$3 \leq N_{K-C}^* < 8$	0.099	0.054
$8 \leq N_{K-C}^* < 13$	0.719	0.062

Table 3.8: Values of coefficients for negative U and $U < u_a$ for the submerged zone in waves and currents

Values of N_{K-C}^*	c_1	c_2
$N_{K-C}^* < 3$	0.235	0.026
$3 \leq N_{K-C}^* < 8$	0.286	0.046
$8 \leq N_{K-C}^* < 13$	0.719	0.062

Table 3.9: Values of coefficients for positive U and $U < u_a$ for the submerged zone in waves and currents

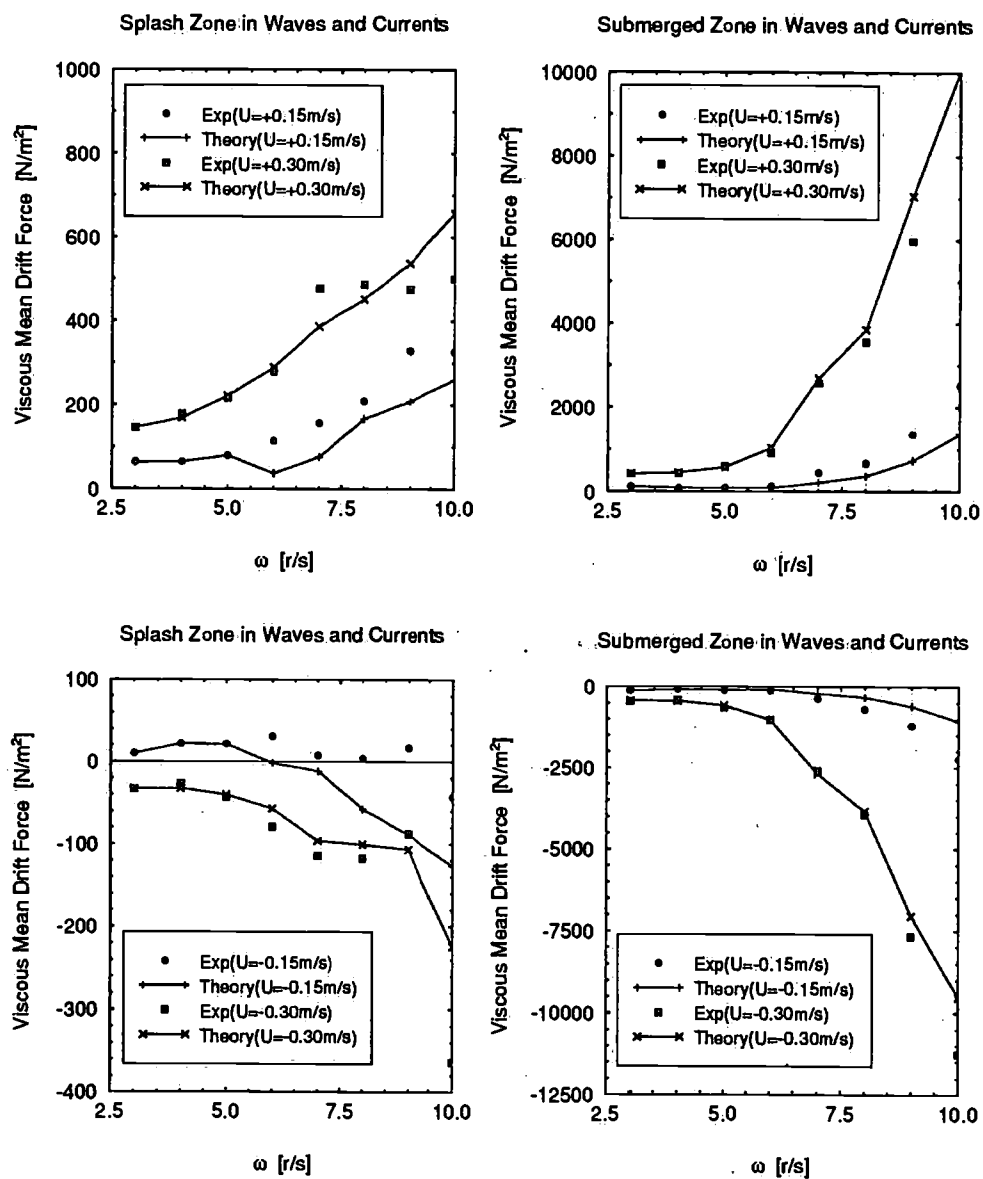


Figure 3.38: Viscous (using experimentally obtained C_{D0}) mean drift forces on a fixed cylinder (75mm Dia Cylinder) in waves and currents

current coexisting flow field were calculated by using the values of the mean drag coefficients obtained from the experimental results with the cylinder models. Results are compared in Figure 3.38. Comparisons are shown for both positive and negative currents for the splash zone and for the submerged zone respectively. Prediction improves compared to those calculations using a constant C_{D0} value of unity throughout.

Similar results of computations are shown for a fixed cylinder (315mm Dia) using the experimentally obtained values of the mean drag coefficient in Figure 3.39 and Figure 3.40. Though for the large cylinder, diffraction effects are dominant, yet the theoretical prediction improves.

3.6 Concluding Remarks

In this experimental validation, contributions of viscous effects in a waves-only flow field and also in a wave-current coexisting flow field (wave-current interaction effects) to the horizontal mean drift force have been investigated. From the results presented, the following conclusions can be drawn.

1. Due to the splash zone nonlinearity, the mean drift force due to viscous effects has been found to exist even in a waves-only flow field.
2. The constantly submerged zone which is not influenced by viscous effects in a waves-only flow field emerges as another important zone of the viscous mean drift force in the presence of a wave-current coexisting flow field.
3. Prediction of viscous mean drift forces in a waves-only flow field based on the idea of subtracting the force due to currents only from that in a wave-current coexisting flow field shows considerable deviations from that measured in a waves-only flow field. So, treatment of the viscous mean drift force for different flow fields has to remain independent.
4. Uncertainties in the choice of the values of the mean drag coefficient can be eliminated through systematic experimental investigations when hydrodynamic parameters are carefully chosen to treat them.
5. In the absence of any extensive numerical techniques, the present 2-D method along with experimental data should be sufficient enough to predict the viscous contributions towards the mean drift force originating from the surface piercing columns of a semi-submersible or a tension leg platform.

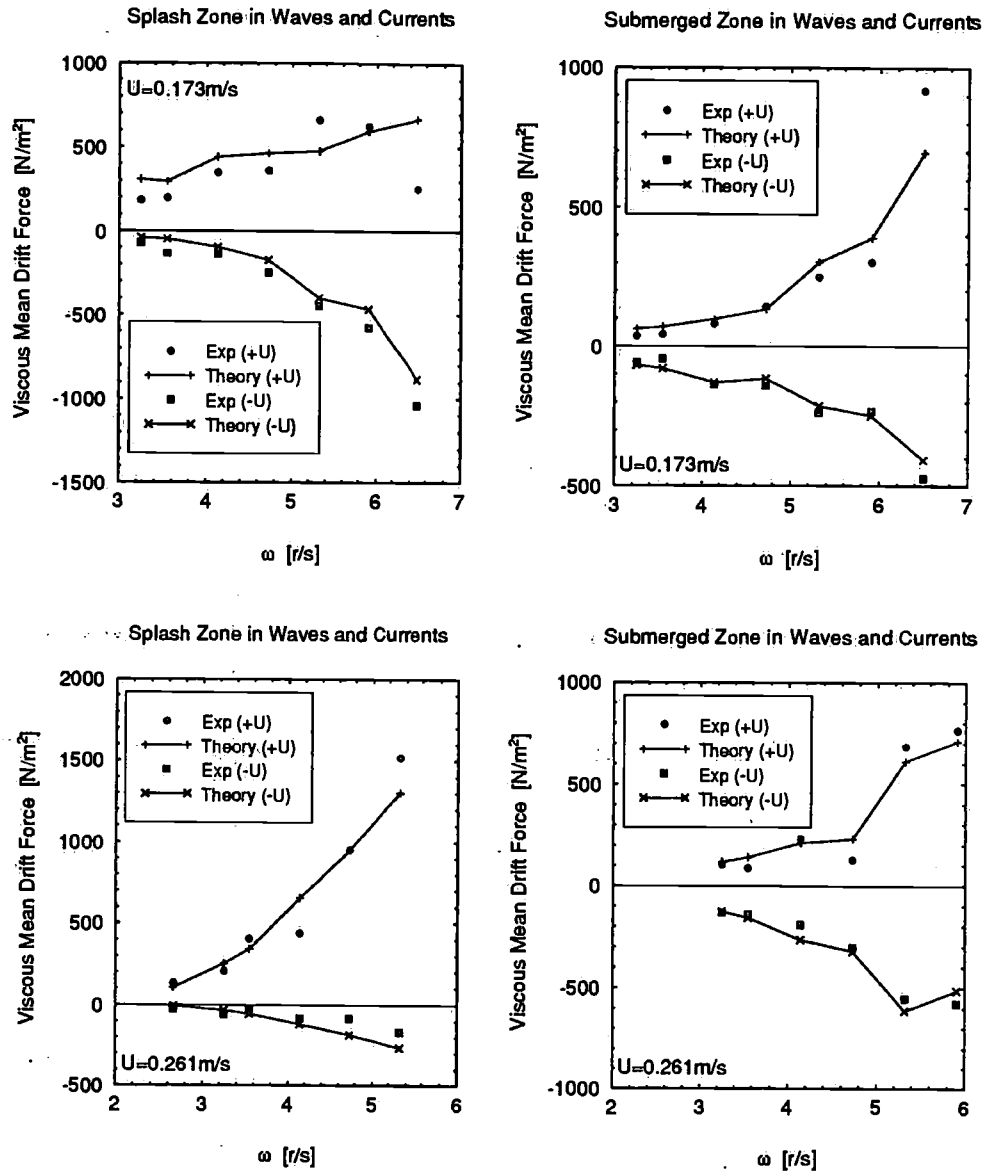


Figure 3.39: Viscous (using experimentally obtained C_{D0}) mean drift forces on a fixed cylinder (315mm Dia Cylinder at DUT) in waves and currents

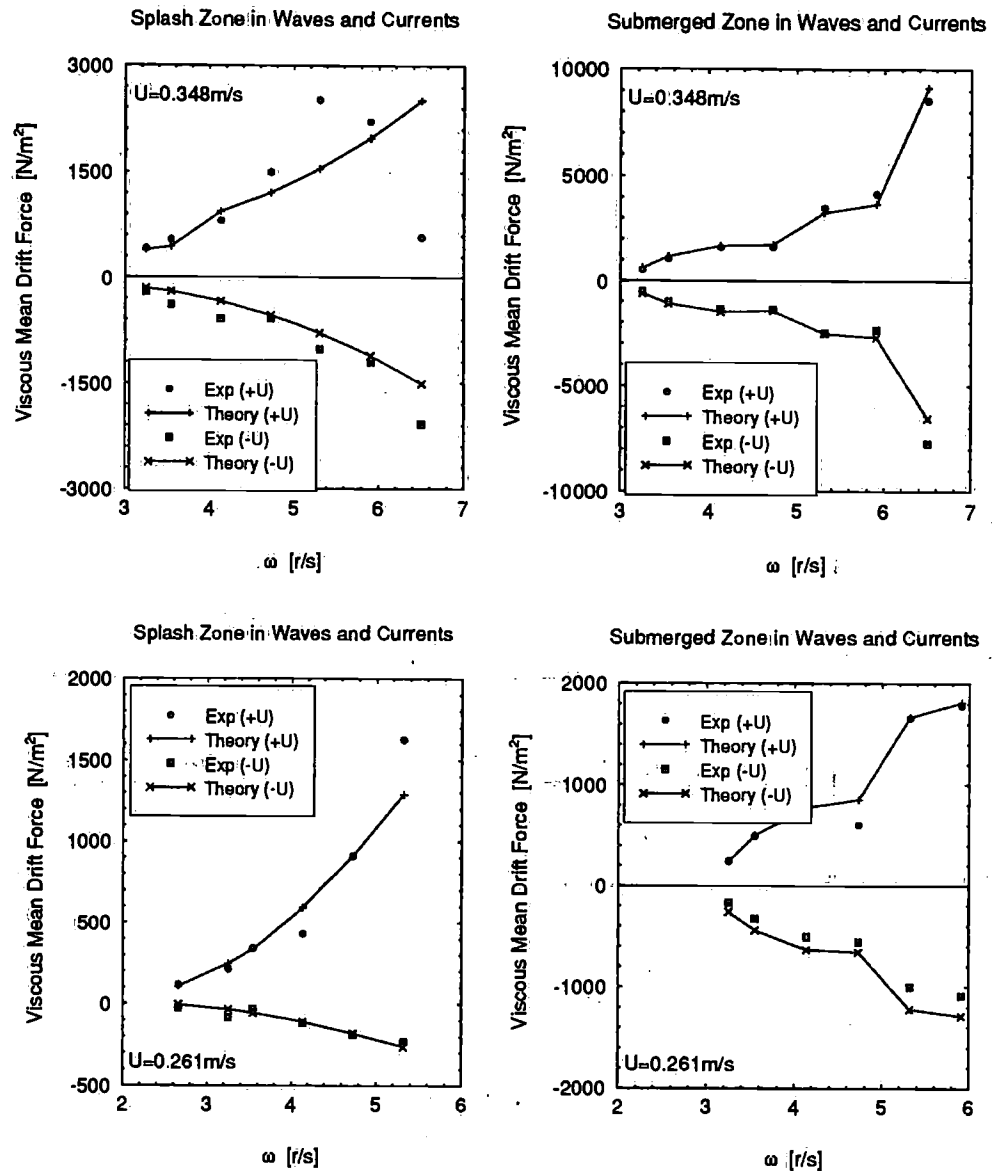


Figure 3.40: Viscous (using experimentally obtained C_{D0}) mean drift forces on a fixed cylinder (315mm Dia Cylinder (top) at DUT and (bottom) at MARIN).

References

- Burns, G. E. (1983). Calculating viscous drift of a tension leg platform. In *Proceedings of the International Conference on Offshore Mechanics and Arctic Engineering*, OMAE, Houston, Texas, pp. 22-30.
- Chakrabarti, S. (1971). Dynamics of single point mooring in deep water (discussion). *Journal of Waterway, Port, Coastal and Ocean Engineering*, ASCE 97(WW3), 588-590.
- Chakrabarti, S. K. (1984). Steady drift force on vertical cylinder - viscous vs. potential. *Applied Ocean Research* 6(2), 73-82.
- Chitrapu, A. S., R. C. Ertekin, and J. R. Paulling (1993). Viscous drift forces in regular and irregular waves. *Ocean Engineering* 20(1), 33-55.
- DELFRAC (1992). *A 3-D Diffraction Program*. Ship Hydromechanics Laboratory, Delft University of Technology, Delft, The Netherlands.
- Dev, A. K. (1992a). Evaluation of viscous mean drift forces on a vertical cylinder in waves and currents. Technical Report 927-M, Ship Hydromechanics Laboratory, Delft University of Technology, Delft, The Netherlands.
- Dev, A. K. (1992b). Experimental investigation of viscous mean drift forces on a fixed vertical cylinder in waves and currents; part-i. Technical Report 928-M, Ship Hydromechanics Laboratory, Delft University of Technology, Delft, The Netherlands.
- Dev, A. K. (1992c). Experimental investigation of viscous mean drift forces on a fixed vertical cylinder in waves and currents; part-iii. Technical Report 943-M, Ship Hydromechanics Laboratory, Delft University of Technology, Delft, The Netherlands.
- Dev, A. K. (1993). Experimental investigation of viscous mean drift forces on a fixed vertical cylinder in waves and currents; part-v. Technical Report 972-M, Ship Hydromechanics Laboratory, Delft University of Technology, Delft, The Netherlands.
- Ferretti, C. and M. Berta (1980). Viscous effect contribution to the drift forces on floating structures. In *Proceedings of the International Symposium of Ocean Engineering and Ship Handling*, SSPA, Gothenburg, Sweden, pp. 9:1-9:10.
- Koterayama, W. (1984). Wave forces acting on a vertical circular cylinder with a constant forward velocity. *Ocean Engineering* 11(4), 363-379.

- Lundgren, H., S. E. Sand, and J. Kirkegaard (1982). Drift forces and damping in natural sea states- a critical review of the hydrodynamics of floating structures. In *Proceedings of the International Conference on Behavior of Offshore Structures*, BOSS, Cambridge, Massachusetts, pp. 592-607.
- Moe, G. and R. L. P. Verley (1977). Hydrodynamic damping of offshore structures in waves and currents. In *Proceedings of the Annual Offshore Technology Conference*, OTC 3798, Houston, Texas, pp. 37-44.
- Pijfers, J. G. L. and A. W. Brink (1977). Calculated drift forces of two semi-submersible platform type in regular and irregular waves. In *Proceedings of the Annual Offshore Technology Conference*, OTC 2977, Houston, Texas, pp. 155-164.
- Sarpkaya, T. and M. Isaacson (1981). *Mechanics of Wave Forces on Offshore Structures*, Chapter 3, 6, pp. 93, 323. New York: Van Nostrand Reinhold Company Inc.
- Sawaragi, T. and T. Nakamura (1979). Analytical study of wave force on a cylinder in oscillatory flow. In *Proceedings of the Conference Coastal Structures 79*, Alexandria, Virginia, pp. 154-173.
- Schlichting, H. (1968). *Boundary Layer Theory* (Sixth ed.). New York: McGraw-Hill Book Co.
- Wheeler, J. D. (1970). Method for calculating forces produced by irregular waves. *Journal of Petroleum Technology, AIME* (March), 359-367.

Chapter 4

Hydrodynamic Forces on a Submerged Pontoon

The hydrodynamic force mechanisms in relation to the first order forces have been elaborated upon in a library of literature for the case of a vertical cylinder in regular deep-water waves with particle motions in circular orbits. The orbits are coplanar with the axis of the cylinder so that the velocity vector, constant in magnitude, has three orthogonal components namely the inline, the transverse and the vertical force. In general, the component parallel to the axis of the cylinder would not be expected to influence the flow phenomena external to the cylinder and is thus neglected.

In this chapter, consideration will be given to the idealized case of a horizontal cylindrical body (pontoon) completely submerged in regular, deep-water waves with particle motions in circular orbits and having the cylinder axis coplanar with orbital motions (in the head sea condition) and cylinder axis parallel to wave crests (in the beam sea condition).

In the former case (head seas), i.e. in the case of a horizontal pontoon coplanar with the orbital motions instead of orthogonal to them, again for regular waves and circular orbits, one finds that the vertical components of velocity and acceleration, z, \dot{z} and their periodic variations, are identical to those for the horizontal components, x, \dot{x} for the vertical cylinder, but with a phase shift of $\frac{\pi}{2}$. So, the periodic vertical forces on an element of this horizontal pontoon should in principle be the same as for the inline force on an element of a vertical cylinder at the corresponding position, again with a phase shift of $\frac{\pi}{2}$. The fundamental difference between the coplanar horizontal cylinder and a vertical cylinder is that the forces will

have a lengthwise periodic variation. This lengthwise variation can have a very important influence on the shedding and interaction of vortices. The forces transverse to the waves are associated only with the vortex effects and so will be directly affected by this influence. To the authors knowledge, this kind of study with coplanar submerged body has not been carried out yet but it would have its merits when it has practical significance.

In the latter case (beam seas), the situation has certain similarities to that for the vertical cylinder but also some differences. The differences include the fact that the plane of the orbits is now normal to the axis of the pontoon with no axial component of velocity. The forces associated with vortex shedding are now coplanar with the orbits and so there is no transverse force to the plane of the orbits. Thus there is a velocity vector, constant in magnitude, normal to the axis of the pontoon. The inertia, drag and vortex induced force vectors are in the same plane as the velocity vector. The velocity vector, the wake and the vortices tend to rotate around the cylinder depending on the orbital shape parameter which is the ratio of the maximum vertical velocity to the maximum horizontal velocity. The resulting total horizontal and vertical components do not differ from one another in principle (circular or square cylinder) but are of course orthogonal in phase.

The lower hull of a semi-submersible which is a horizontal pontoon and whose N_{K-C} is small seems to play an important role in the exciting mean force and the viscous effects on such a force need to be studied. The empirical Morison equation is used for the structures on which viscous effects are not negligible.

The geometry and configuration of the submerged pontoon used in this chapter is similar to the one used in the model tests. The pontoon has an overall length l , breadth b and height h . In addition, the longitudinal ends of the pontoon are triangular shaped having a length l_e at each end. Further details are available in Chapter 2.

4.1 Hydrodynamic Parameters

4.1.1 In Currents Only

The Reynolds number N_{Re} is the governing hydrodynamic parameter and is defined as

$$N_{Re} = \frac{\rho U l}{\mu}; \text{ head seas} \quad (4.1a)$$

$$N_{Re} = \frac{\rho U b}{\mu}; \text{ beam seas} \quad (4.1b)$$

4.1.2 In Waves Only

It is quite common to replace the steady flow velocity term in the Reynolds number N_{Re} by the wave (oscillatory flow) particle velocity in order to use N_{Re} as the governing hydrodynamic parameter and which is defined as

$$N_{Re} = \frac{\rho u_a l}{\mu}; \text{ head seas} \quad (4.2a)$$

$$N_{Re} = \frac{\rho v_a b}{\mu}; \text{ beam seas} \quad (4.2b)$$

Because of the oscillatory nature of the flow, another hydrodynamic parameter known as the Keulegan-Carpenter number N_{K-C} is more appropriate as the controlling hydrodynamic parameter in waves only and is defined as

$$N_{K-C} = \frac{u_a T}{l}; \text{ head seas} \quad (4.3a)$$

$$N_{K-C} = \frac{v_a T}{b}; \text{ beam seas} \quad (4.3b)$$

Now as u_a and v_a appear in both N_{Re} and N_{K-C} , the 'frequency parameter' or 'beta parameter' β as proposed by Sarpkaya and Isaacson (1981) is defined as follows:

$$\beta = \frac{N_{Re}}{N_{K-C}} = \frac{l^2}{(\nu T)}; \text{ head seas} \quad (4.4a)$$

$$\beta = \frac{N_{Re}}{N_{K-C}} = \frac{b^2}{(\nu T)}; \text{ beam seas} \quad (4.4b)$$

It is quite common to use cylinder diameter or width or ship length as the characteristic dimension in the Reynolds number. In line with this concept, the characteristic dimension l is used in the definition of the Keulegan-Carpenter number.

4.1.3 In Waves and Currents

Sarpkaya and Isaacson (1981) suggested that both N_{Re} and N_{K-C} be modified by changing the value of u_a by $(u_a \pm U)$. Such an approach would not affect the value of 'beta parameter'. In fact, the modified N_{Re} and N_{K-C} are similar to those in waves only plus an additional term due to the uniform flow velocity.

$$N_{Re}^+ = \frac{(u_a + U)l}{\nu}; \text{ head seas} \quad (4.5a)$$

$$N_{Re}^+ = \frac{(v_a + U)b}{\nu}; \text{ beam seas} \quad (4.5b)$$

$$N_{K-C}^+ = \frac{(u_a + U)T}{l}; \text{ head seas} \quad (4.5c)$$

$$N_{K-C}^+ = \frac{(v_a + U)T}{b}; \text{ beam seas} \quad (4.5d)$$

The additional term in N_{Re} is the same for the uniform flow field whereas the additional term in N_{K-C} is another hydrodynamic parameter known as the Moe-Verley number (reduced velocity) first introduced by Moe and Verley (1977) and is defined as

$$N_{M-V} = \frac{UT}{l}; \text{ head seas} \quad (4.6a)$$

$$N_{M-V} = \frac{UT}{b}; \text{ beam seas} \quad (4.6b)$$

The characteristic dimension D in original definition has been used as the diameter of a circular cylinder. In the case of a rectangular pontoon, D can be replaced by l or b depending on its orientation to the incoming flow field.

The 'velocity parameter' or 'gamma parameter' is defined as follows:

$$\gamma = \frac{N_{M-V}}{N_{K-C}} = \frac{U}{u_a} \quad (4.7)$$

The definition of a modified Keulegan-Carpenter number N_{K-C}^* for a vertical cylinder in a wave-current coexisting flow field has been described in detail in Chapter 3. A similar approach can be applied in the case of a cylinder (pontoon) in beam seas. The same idea will also be used for a cylinder (pontoon) in head seas by replacing the characteristic dimension

'diameter' or 'width' by 'length' keeping in mind certain hydrodynamic differences. The component of velocity resolved parallel to the axis of a vertical cylinder is expected to have only indirect effects on the external flow and hence on the hydrodynamic forces. Any influence due to these indirect effects is likely to be augmented when the periodic lengthwise variation along a cylinder (pontoon) coplanar with orbital motions would create a cell like behavior in the axial velocity with nodes and antinodes traveling along the cylinder with the progression of the waves. The presence of currents will have a further influence on the loads because of the convection of vortices and the way in which this can influence vortex interactions.

If U is either positive or negative and $U \geq u_a$:

$$N_{K-C}^* = \pi |U| \frac{T}{l} \quad (4.8)$$

If U is positive and $|U| < u_a$:

$$N_{K-C}^* = N_{K-C} (\sin \Theta + \gamma \Theta) \quad (4.9)$$

where

$$\Theta = \cos^{-1} \left(-\frac{U}{u_a} \right) = \cos^{-1}(-\gamma)$$

If U is negative and $|U| < u_a$:

$$N_{K-C}^* = N_{K-C} \{ \sin \Theta + \gamma(\pi - \Theta) \} \quad (4.10)$$

where

$$\Theta = \cos^{-1} \left(\frac{U}{u_a} \right) = \cos^{-1}(\gamma)$$

4.2 Force Formulations in Head Seas

4.2.1 In Currents Only in Head Seas

The force is directly proportional to the projected area and the flow velocity squared. The horizontal force on the fixed submerged pontoon due to currents only is then given by

$$F_{DCX} = \frac{1}{2} C_{DCX} \rho (b \times h) U^2 \quad (4.11)$$

4.2.2 In Waves Only in Head Seas

The velocity potential of a wave, based on linear wave theory, is given by

$$\phi = \frac{g\zeta_a}{\omega} e^{kz} \sin(kx - \omega t) \quad (4.12)$$

A wave profile is then given by

$$\zeta = -\frac{1}{g} \left(\frac{\partial \phi}{\partial t} \right)_{z=0} = \zeta_a e^{kz} \cos(kx - \omega t) \quad (4.13)$$

Water particle velocities and accelerations are given by

$$u = \zeta_a e^{kz} \omega \cos(kx - \omega t) \quad (4.14a)$$

$$w = \zeta_a e^{kz} \omega \sin(kx - \omega t) \quad (4.14b)$$

$$\dot{u} = \zeta_a e^{kz} \omega^2 \sin(kx - \omega t) \quad (4.15a)$$

$$\dot{w} = -\zeta_a e^{kz} \omega^2 \cos(kx - \omega t) \quad (4.15b)$$

$$u_a = w_a = \zeta_a e^{kz} \omega \quad (4.16)$$

$$\dot{u}_a = u_a \omega; \dot{w}_a = w_a \omega \quad (4.17)$$

Inertia Forces

Using the inertia term of the Morison equation, the horizontal and vertical inertia forces on the fixed submerged pontoon in a waves-only field is given as follows:

$$F_{IX}(t) = C_{MX} \rho (b \times h) \times \left\{ \frac{1}{2} \int_{-l/2}^{-(l-2l_e)/2} \dot{u} dx + \int_{-(l-2l_e)/2}^{+(l-2l_e)/2} \dot{u} dx + \frac{1}{2} \int_{+(l-2l_e)/2}^{+l/2} \dot{u} dx \right\} \quad (4.18a)$$

$$= -C_{MX} \rho (b \times h) \times \zeta_a e^{-kd} \omega^2 \frac{1}{k} \left\{ \sin \frac{kl}{2} + \sin k(l - 2l_e)/2 \right\} \sin \omega t \quad (4.18b)$$

Similarly, the vertical inertia force is given as follows:

$$F_{IZ}(t) = C_{MZ} \rho (b \times h) \times \left\{ \frac{1}{2} \int_{-l/2}^{-(l-2l_e)/2} \dot{w} dx + \int_{-(l-2l_e)/2}^{+(l-2l_e)/2} \dot{w} dx + \frac{1}{2} \int_{+(l-2l_e)/2}^{+l/2} \dot{w} dx \right\} \quad (4.19a)$$

$$= -C_{MZ} \rho (b \times h) \times \zeta_a e^{-kd} \omega^2 \frac{1}{k} \left\{ \sin \frac{kl}{2} + \sin \frac{k(l-2l_e)}{2} \right\} \cos \omega t \quad (4.19b)$$

Drag Forces

This case is different and is due to the projected area of the triangular faces of the pontoon's ends. As the horizontal water particle velocity varies along the length of the pontoon, the triangular length is divided into small strips of length dx with its own projected area ΔA_P being equal to $\frac{(b \times h)}{l_e} dx$. So, A_P for the two ends of the pontoon would be calculated as follows:

$$A_P = \frac{(b \times h)}{l_e} \left(\int_{-l/2}^{-(l-2l_e)/2} dx - \int_{+l/2}^{+(l-2l_e)/2} dx \right) \quad (4.20a)$$

$$= \frac{(b \times h)}{l_e} (I_N - I_P) \quad (4.20b)$$

where $(I_N - I_P)$ will take account of any variable which is a function of x .

Using the drag force term of the Morison equation, the horizontal viscous drag force on the fixed submerged pontoon in a waves-only flow field is given as follows:

$$F_{DX}(t) = \frac{1}{2} C_{DX} \rho \frac{(b \times h)}{l_e} \times \left(\int_{-l/2}^{-(l-2l_e)/2} u |u| dx - \int_{+l/2}^{+(l-2l_e)/2} u |u| dx \right) \quad (4.21a)$$

$$= \frac{8}{3\pi} C_{DX} \rho \frac{(b \times h)}{l_e} \times$$

$$\zeta_a^2 e^{-2kd} \omega^2 \frac{1}{k} \left\{ \sin \frac{kl}{2} - \sin \frac{k(l-2l_e)}{2} \right\} \cos \omega t \quad (4.21b)$$

Similarly, the vertical viscous drag force is given as follows:

$$\begin{aligned} F_{DZ}(t) &= \frac{1}{2} C_{DZ} \rho b \times \\ &\quad \left(\frac{1}{2} \int_{-l/2}^{-(l-2l_e)/2} w |w| dx + \int_{-(l-2l_e)/2}^{+(l-2l_e)/2} w |w| dx + \frac{1}{2} \int_{+(l-2l_e)/2}^{+l/2} w |w| dx \right) \end{aligned} \quad (4.22a)$$

$$= -\frac{4}{3\pi} C_{DZ} \rho b \zeta_a^2 e^{-2kd} \omega^2 \frac{1}{k} \left\{ \sin \frac{kl}{2} + \sin \frac{k(l-2l_e)}{2} \right\} \sin \omega t \quad (4.22b)$$

4.2.3 In Waves and Currents in Head Seas

In the presence of currents, there are interactions between waves and currents. But from an engineering point of view, the principle of superposition will be used for the combined velocity term. Based on a steady and uniformly distributed current, the independent and instantaneous horizontal water velocity would be $(u \pm U)$. The vertical water particle velocity is considered the same as in a waves-only flow field.

In the inertia term of the Morison equation, the term acceleration generally used is the local acceleration, i.e. no convective terms are normally taken into account. In the presence of currents, the additional convective term $U \frac{\partial u}{\partial x}$ can be appreciable when the value of U is large enough. But on the other hand, when the current velocity is large, the inertia force is almost negligible compared to the drag force and in that case the convective acceleration term is not significant anymore. So, whether to use the local acceleration or the total acceleration still remains debatable under those circumstances.

Effects of Currents on Wave Kinematics

Formulations will be presented which elaborate the motions of regular waves traveling on steady, uniform currents.

The water particle kinematics are generally predicted by means of a wave theory which itself is already based upon a number of simplifying assumptions. One of them is likely to be the notion that water is quiescent,

i.e. the only water motions are those induced by water waves. Though in reality ocean waves seldom propagate on quiescent water and rather more generally they travel on currents generated by winds, tidal forces or earth's gravity. Yet even when the presence of these currents is well recognized, it is quite common for designers to assume that there is no interaction between waves and currents. This is certainly not the case and such presence of currents will alter the wave celerity and thus will affect the relationship between the wave length and the observed wave period. In turn, there will be repercussions on the predicted water particle kinematics and wave induced forces.

Apparent and Relative Wave Frequencies

Let us assume a train of regular waves (wavelength λ , wave height H) traveling on a steady, horizontally and vertically uniform current. The current velocity is U and is defined as positive if it is in the direction of wave propagation.

In a stationary frame of reference containing the waves, there is a current with velocity U and the waves have an apparent celerity c and apparent period T . In contrast, in a frame of reference moving along the wave at velocity U , there is no current and the waves have celerity c_r and period T_r . Consequently,

$$c = c_r + U \quad (4.23a)$$

$$= \frac{\lambda}{T} \quad (4.23b)$$

$$c_r = \frac{\lambda}{T_r} \quad (4.24)$$

Combining the above two equations,

$$\omega = \omega_r + kU \quad (4.25)$$

where $\omega = \frac{2\pi}{T}$ is the apparent or total wave frequency noted by a stationary observer, $\omega_r = \frac{2\pi}{T_r}$ is the relative or intrinsic wave frequency and $k = \frac{2\pi}{\lambda}$ is the wave number.

In a moving frame of reference, the waves appear to be propagating on 'still' water and all the usual equations describing wave motions are valid. Thus according to the linear (Airy) wave theory

$$\omega_r^2 = gk \quad (4.26)$$

$$\omega = \omega_r + \frac{\omega_r^2}{g} U \quad (4.27)$$

In a moving frame of reference, the waves seem to be propagating on 'still' water and thus for small amplitude waves, the horizontal and vertical components of water particle velocities beneath waves are given by the linear (Airy) wave theory. Therefore to the stationary observer, the horizontal component of water particle velocity is given by:

$$u = u_r + U \quad (4.28a)$$

$$= \zeta_a e^{kz} (\omega - kU) \cos(kx - \omega t) + U \quad (4.28b)$$

Similarly, the vertical component of water particle velocity is :

$$w = w_r \quad (4.29a)$$

$$= \zeta_a e^{kz} (\omega - kU) \sin(kx - \omega t) \quad (4.29b)$$

The horizontal component of water particle acceleration may be obtained from the total derivative of u with respect to time:

$$\frac{du}{dt} = \frac{\partial u}{\partial t} + u \frac{\partial u}{\partial x} + v \frac{\partial u}{\partial y} + w \frac{\partial u}{\partial z} \quad (4.30)$$

in which v is the water particle velocity in y -direction parallel to the wave crests. If the current is steady, $\frac{\partial U}{\partial t} = 0$ and if it is both horizontally and vertically uniform then $\frac{\partial U}{\partial x} = 0$, $\frac{\partial U}{\partial y} = 0$ and $\frac{\partial U}{\partial z} = 0$. So, for small amplitude waves, the above equation becomes:

$$\frac{du}{dt} = \frac{\partial u_r}{\partial t} + U \frac{\partial u_r}{\partial x} \quad (4.31)$$

The remaining parts of the convective acceleration terms are negligible compared with the total acceleration term if the waves are small. Thus

$$\frac{du}{dt} \simeq \zeta_a e^{kz} \omega (\omega - kU) \sin(kx - \omega t) - \zeta_a e^{kz} kU (\omega - kU) \sin(kx - \omega t) \quad (4.32a)$$

$$\dot{u} = \zeta_a e^{kz} (\omega - kU)^2 \sin(kx - \omega t) \quad (4.32b)$$

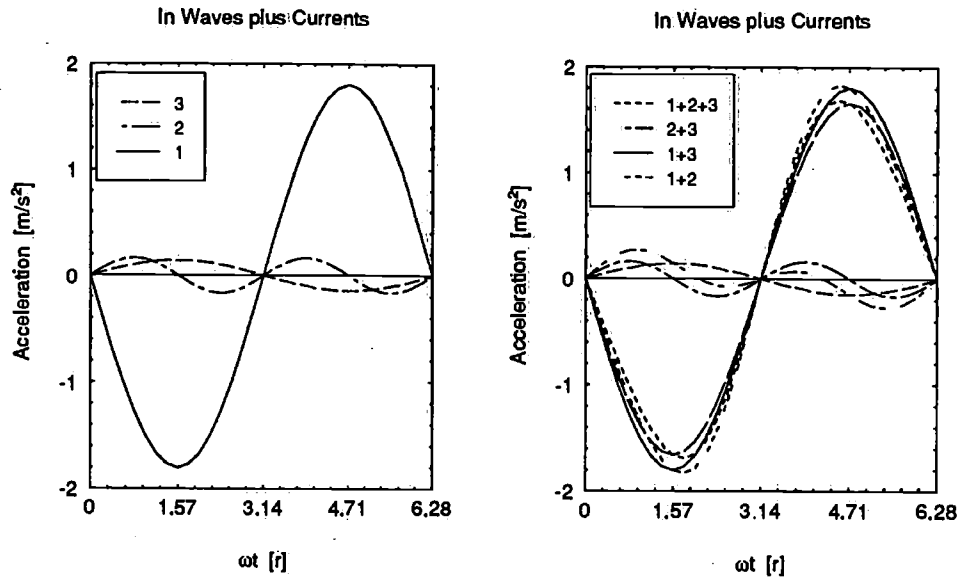


Figure 4.1: *Effects of currents on water particle accelerations (legend: 1 = $\frac{\partial u_x}{\partial t}$, 2 = $u_r \frac{\partial u_x}{\partial x}$ and 3 = $U \frac{\partial u_x}{\partial x}$)*

The vertical component of water particle acceleration may be determined similarly giving

$$\frac{dw}{dt} = -\zeta_a e^{kz} (\omega - kU)^2 \cos(kx - \omega t) \quad (4.33a)$$

$$\dot{w} = -\zeta_a e^{kz} (\omega - kU)^2 \cos(kx - \omega t) \quad (4.33b)$$

Figure 4.1 shows the variation of u and $\frac{du}{dt}$ through a wave cycle for currents + 1, 0 and -1.0 m/s for a unit wave amplitude with an arbitrary wave frequency. The variation of $\frac{du}{dt}$ is influenced by a current though its mean value remains zero.

Inertia Forces

The horizontal inertia force on the fixed submerged pontoon is given as follows:

$$F_{IX}(t) = -C_{MX} \rho (b \times h) \times$$

$$\zeta_a e^{-kd} (\omega - kU)^2 \frac{1}{k} \left\{ \sin \frac{kl}{2} + \sin \frac{k(l-2l_e)}{2} \right\} \sin \omega t \quad (4.34)$$

Similarly, the vertical inertia force is given as follows:

$$F_{IZ}(t) = -C_{MZ} \rho (b \times h) \times \zeta_a e^{-kd} (\omega - kU)^2 \frac{1}{k} \left\{ \sin \frac{kl}{2} + \sin \frac{k(l-2l_e)}{2} \right\} \cos \omega t \quad (4.35)$$

Drag Forces

The horizontal viscous drag force on the fixed pontoon is given as follows:

$$F_{DX}(t) = \frac{1}{2} C_{DX} \rho \frac{(b \times h)}{l_e} \times \left\{ \int_{-l/2}^{-(l-2l_e)/2} (u+U) |u+U| dx - \int_{+l/2}^{+(l-2l_e)/2} (u+U) |u+U| dx \right\} \quad (4.36)$$

For $|U| \geq u_a$:

$$F_{DX} = \frac{1}{2} \rho C_{DX} \frac{(b \times h)}{l_e} 2 u_a U \frac{2}{k} \left\{ \sin \frac{kl}{2} - \sin \frac{k(l-2l_e)}{2} \right\} \quad (4.37a)$$

$$= 2 \rho C_{DX} \frac{(b \times h)}{l_e} u_a^2 \gamma \frac{1}{k} \left\{ \sin \frac{kl}{2} - \sin \frac{k(l-2l_e)}{2} \right\} \quad (4.37b)$$

For $|U| < u_a$:

$$F_{DX} = \frac{1}{\pi} 2 \rho C_{DX} \frac{(b \times h)}{l_e} u_a^2 \left[\frac{1}{6} (\sin 3\Theta + 3 \sin \Theta) \times \left[\frac{1}{2k} \{ \sin kl - \sin k(l-2l_e) \} \right] + \sin \Theta l_e + \gamma (2\Theta + \sin 2\Theta - \pi) \times \left[\frac{1}{k} \left\{ \sin \frac{kl}{2} - \sin \frac{k(l-2l_e)}{2} \right\} \right] + \gamma^2 \sin \Theta l_e \right] \quad (4.38a)$$

$$= \frac{1}{\pi} 2 \rho C_{DX} \frac{(b \times h)}{l_e} u_a^2 (d_1 + d_2 + d_3) \quad (4.38b)$$

where

$$\begin{aligned}
 d_1 &= \frac{1}{6} (\sin 3\Theta + 3 \sin \Theta) \left[\frac{1}{2k} \{ \sin kl - \sin k(l - 2l_e) \} \right] + \sin \Theta l_e \\
 d_2 &= \gamma (2\Theta + \sin 2\Theta - \pi) \left[\frac{1}{k} \left\{ \sin \frac{kl}{2} - \sin \frac{k(l - 2l_e)}{2} \right\} \right] \\
 d_3 &= \gamma^2 \sin \Theta l_e
 \end{aligned}$$

Viscous Mean Drift Forces

The horizontal viscous mean drift force on the fixed submerged pontoon in a wave-current coexisting flow field is given as follows:

$$F_{D0X} = \frac{1}{T} \int_0^T F_{DX}(t) dt \quad (4.39)$$

For $|U| \geq u_a$:

$$F_{D0X} = \frac{1}{2} \rho C_{D0X} \frac{(b \times h)}{l_e} u_a^2 \left(\frac{1}{2} 2l_e + \frac{U^2}{u_a^2} l_e \right) \quad (4.40a)$$

$$= \frac{1}{2} \rho C_{D0X} \frac{(b \times h)}{l_e} u_a^2 (l_e + \gamma^2 l_e) \quad (4.40b)$$

$$= \frac{1}{2} \rho C_{D0X} (b \times h) u_a^2 (1 + \gamma^2) \quad (4.40c)$$

For $|U| < u_a$:

$$\begin{aligned}
 F_{D0X} &= \frac{1}{2\pi} \rho C_{D0X} \frac{(b \times h)}{l_e} u_a^2 \left[\frac{1}{2} \{ (2\Theta - \pi) + \sin 2\Theta \cos 2kx \} (I_N - I_P) \right. \\
 &\quad \left. + 4\gamma \sin \Theta \cos kx (I_N - I_P) + \gamma^2 (2\Theta - \pi) l_e \right] \quad (4.41a)
 \end{aligned}$$

$$\begin{aligned}
 &= \frac{1}{2\pi} \rho C_{D0X} \frac{(b \times h)}{l_e} u_a^2 \left[\frac{1}{2} (2\Theta - \pi) l_e + \sin 2\Theta \frac{1}{2k} \{ \sin kl - \sin k(l - 2l_e) \} \right. \\
 &\quad \left. + 4\gamma \sin \Theta \frac{1}{k} \left\{ \sin \frac{kl}{2} - \sin \frac{k(l - 2l_e)}{2} \right\} + \gamma^2 (2\Theta - \pi) l_e \right] \quad (4.41b)
 \end{aligned}$$

$$= \frac{1}{2\pi} \rho C_{D0X} \frac{(b \times h)}{l_e} u_a^2 (d_1 + d_2 + d_3) \quad (4.41c)$$

where

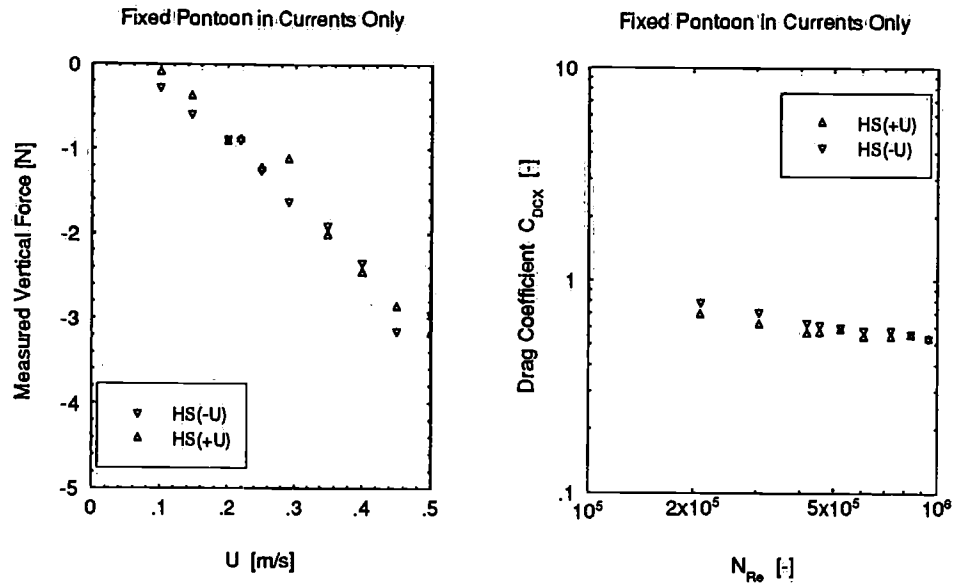


Figure 4.2: (left) Measured vertical forces on a fixed pontoon and (right) experimental drag coefficients of a fixed pontoon in currents only

$$d_1 = \frac{1}{2} (2\Theta - \pi) l_e + \sin 2\Theta \frac{1}{2k} \{ \sin kl - \sin k(l - 2l_e) \}$$

$$d_2 = 4\gamma \sin \Theta \frac{1}{k} \left\{ \sin \frac{kl}{2} - \sin \frac{k(l - 2l_e)}{2} \right\}$$

$$d_3 = \gamma^2 (2\Theta - \pi) l_e$$

4.3 Experimental Results in Head Seas

4.3.1 In Currents Only in Head Seas

In Figure 4.2, the measured vertical steady forces and the experimental drag coefficients in currents only are shown for both positive and negative currents. It is noticeable that the vertical mean force is a suction force often connected with the phenomena of the steady tilt of a semi-submersible. The drag coefficients in the horizontal force are found to be less than 1 and show a decreasing tendency with an increase in the Reynolds number.

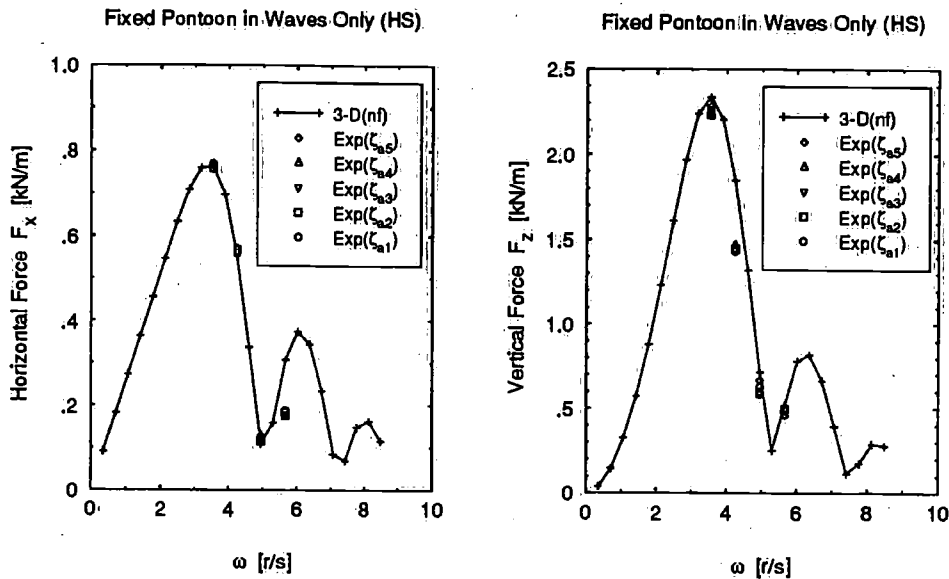


Figure 4.3: Computed and measured (left) horizontal and (right) vertical first order forces on a fixed pontoon in waves only in head seas

4.3.2 In Waves Only in Head Seas

The maximum amplitudes of the horizontal and vertical wave excitation forces including the inertia coefficients are shown in Figure 4.3 and in Figure 4.4 respectively. Some discrepancies between computations and measurements are clearly observed both in forces and in coefficients. From the comparison between the theoretical and experimental coefficients in Figure 4.4, it can be concluded that the inertia coefficient at certain wave frequencies is different from the theoretical values obtained from both 2-dimensional and 3-dimensional computations (3-D and 2-D values are shown on the minimum and the maximum values of the x-axis respectively). The author is not in a position to find similar findings from the available literature because they all deal with such submerged bodies in beam seas only.

In Figure 4.5, both horizontal and vertical mean drift forces are shown. Though data show scatter, there is no strong indication that the measured forces are higher than the theoretical computations by DELFRAC (1992). In addition, the mean drift force on such a fixed submerged body (only second order pressure contribution) is of comparatively lower magnitude which is more affected by the mean offset (noise) on the measurement system. In the

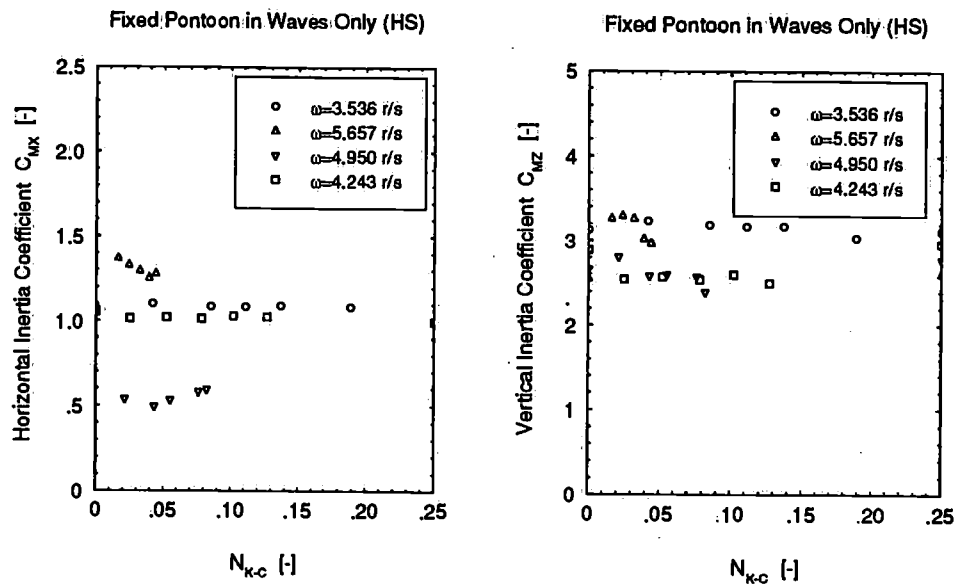


Figure 4.4: Experimental (left) horizontal and (right) vertical inertia coefficients of a fixed pontoon in waves only in head seas

case of vertical drift forces, the comparison seems quite satisfactory as far as potential contributions are concerned.

4.3.3 In Waves and Currents in Head Seas

In Figure 4.6 and in Figure 4.7, a comparison is shown between the theoretical and the measured forces. Certain differences are observed and most of them in the vertical forces. The differences noticed at some frequencies in waves only are retained in the presence of currents as well.

Though the horizontal mean drift force is seen to be subjected to only potential effects, the same is no longer true in the presence of currents. Currents with increasing order cause the horizontal mean drift force to increase as well. Figure 4.8 shows such effects for different sets of wave amplitudes.

In Figure 4.9, the measured drift forces are shown after deducting the measured forces due to currents (positive and negative) only. The resulting mean forces are different from the forces due to waves only. This does not indicate that the difference is the viscous mean drift force in waves only because the measured mean forces are found to be quite similar to the 3-D predictions. In fact, the difference is due to the the interaction

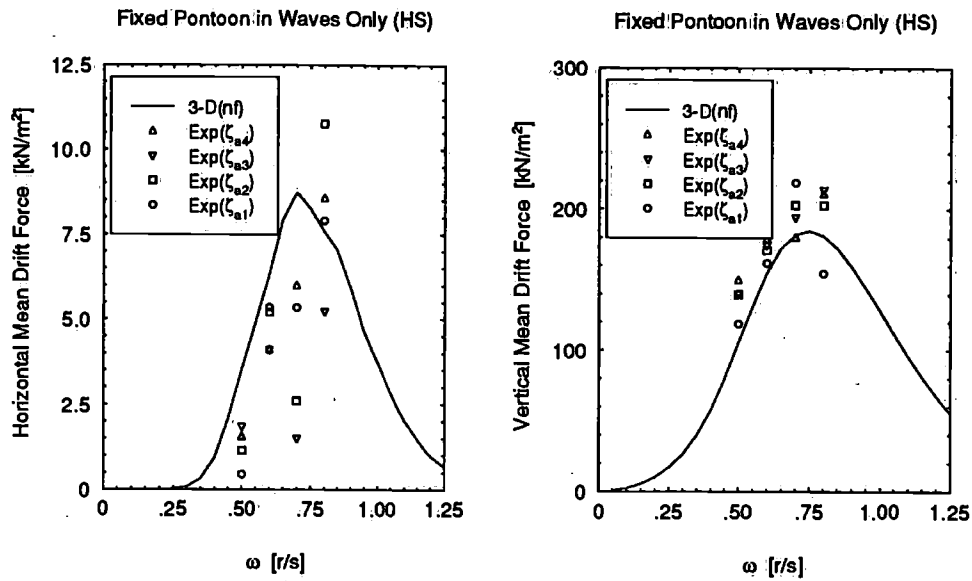


Figure 4.5: Computed and measured (left) horizontal and (right) vertical mean drift forces on a fixed pontoon in waves only in head seas

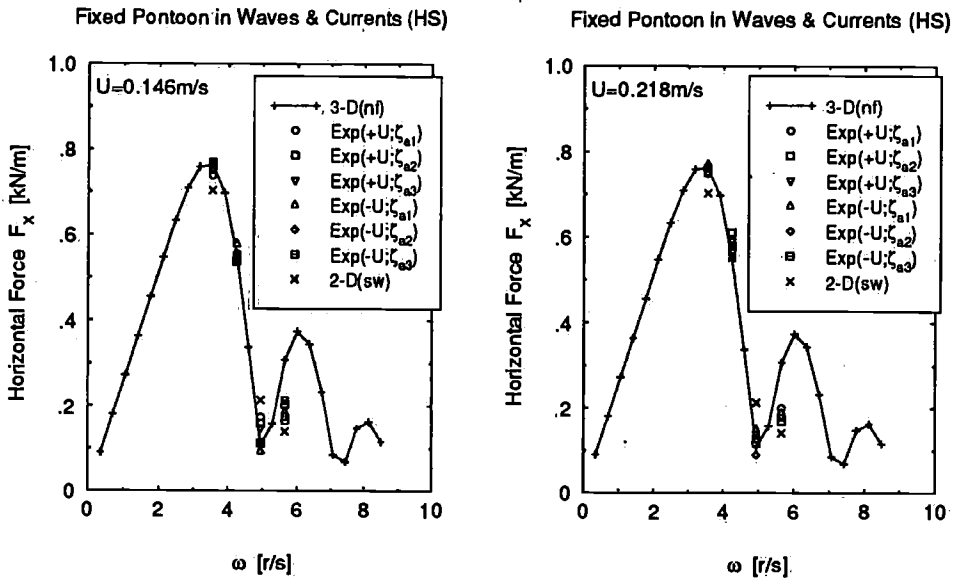


Figure 4.6: Computed and measured horizontal first order forces on a fixed pontoon in waves and currents in head seas

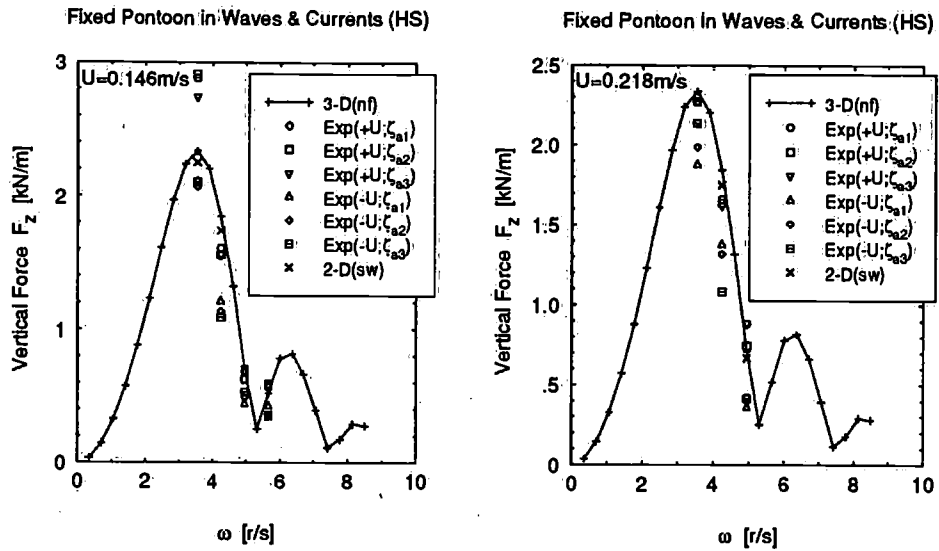


Figure 4.7: Computed and measured vertical first order forces on a fixed pontoon in waves and currents in head seas

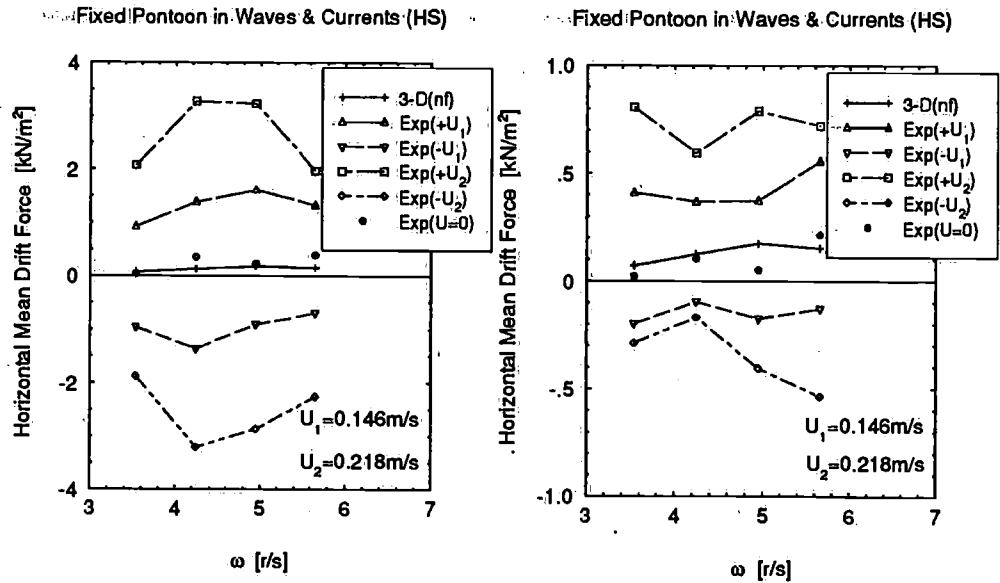


Figure 4.8: Computed (waves only) and measured (waves only; waves and currents) horizontal mean drift forces on a fixed pontoon in head seas

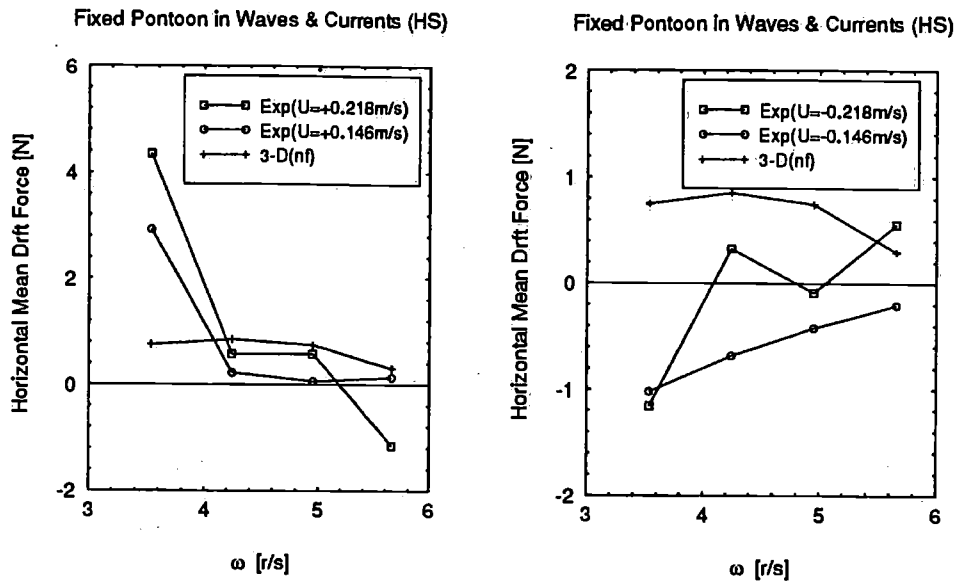


Figure 4.9: *Computed (waves only) and experimental (waves and currents minus currents) horizontal mean drift forces on a fixed pontoon in head seas*

effects between waves and currents. Similar trends are shown for the vertical cylinder as well.

In Figure 4.10 (left), the experimental values of the mean drag coefficients in waves and currents are produced. The limited data show some scatter yet they clearly indicate that the force coefficients are somewhat lower in values in negative currents than those in positive currents. A comparison between computed and measured results using the experimentally obtained mean drag coefficients is shown in Figure 4.10 (right). The calculations though show the similar tendency but not so comparable with the measured data. This might be due to the scatter in the force coefficients.

4.4 Force Formulations in Beam Seas

4.4.1 In Currents Only in Beam Seas

The force is directly proportional to the projected area and the flow velocity squared. The horizontal force due to currents only is thus given by

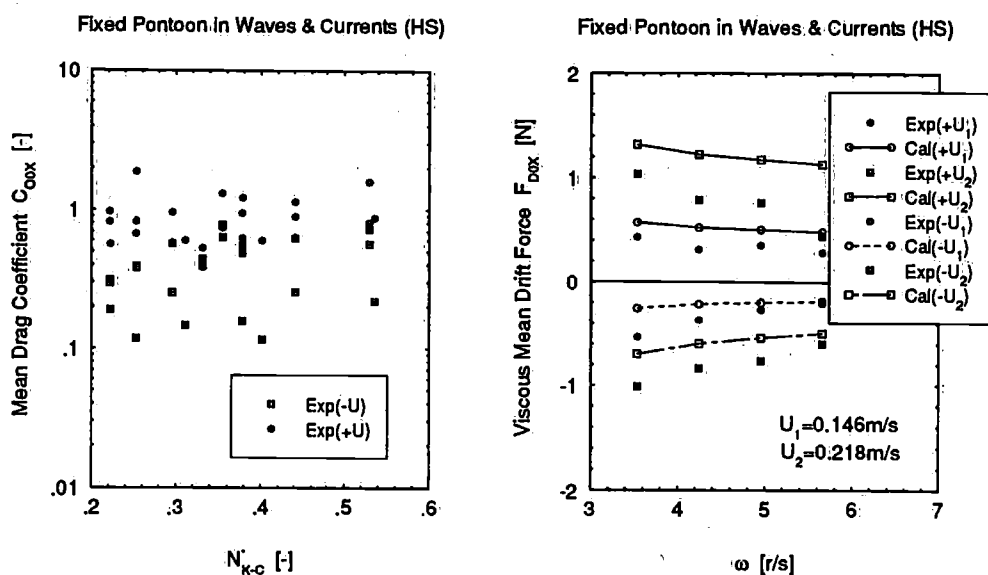


Figure 4.10: (left) Experimental mean drag coefficients and (right) computed and measured forces on a fixed pontoon in waves and currents in head seas.

$$F_{DCY} = \frac{1}{2} C_{DCY} \rho (l \times h) U^2 \quad (4.42)$$

4.4.2 In Waves Only in Beam Seas

The velocity potential of a wave, based on the linear wave theory, is given by

$$\phi = \frac{g \zeta_a}{\omega} e^{kz} \sin(ky - \omega t) \quad (4.43)$$

A wave profile is then given by

$$\zeta = -\frac{1}{g} \left(\frac{\partial \phi}{\partial t} \right)_{z=0} = \zeta_a e^{kz} \cos(ky - \omega t) \quad (4.44)$$

Water particle velocities and accelerations are given by

$$v = \zeta_a e^{kz} \omega \cos(ky - \omega t) \quad (4.45a)$$

$$w = \zeta_a e^{kz} \omega \sin(ky - \omega t) \quad (4.45b)$$

$$\dot{v} = \zeta_a e^{kz} \omega^2 \sin(ky - \omega t) \quad (4.46a)$$

$$\dot{w} = -\zeta_a e^{kz} \omega^2 \cos(ky - \omega t) \quad (4.46b)$$

$$v_a = w_a = \zeta_a e^{kz} \omega \quad (4.47)$$

$$\dot{v}_a = v_a \omega; \dot{w}_a = w_a \omega \quad (4.48)$$

For a submerged body like the submerged pontoon here, the velocity field is often expressed in terms of a rotating velocity vector like

$$\mathbf{V} = (v \vec{i} + w \vec{j}) \quad (4.49)$$

The use of a local velocity vector in place of an instantaneous and independent velocity field has been found in Koterayama (1979), Hamel-Derouich (1993), Teng and Nath (1985), Arai (1993) and Ramberg and Niedzwecki (1982).

On the other hand, Shankar *et al.* (1983), Rai and Khader (1983) and Otsuka *et al.* (1990) have used instantaneous horizontal and vertical velocity in order to calculate the drag force on a submerged cylinder. The latter approach will be followed by the author in this work.

In linear potential theory, the submerged pontoon would be subject to hydrodynamic forces like Froude-Krylov Forces, diffraction forces in the presence of waves only field. The computation of the aforementioned forces can be well accomplished by application of computer programs like SEAWAY (1992) and DELFRAC (1992). On the other hand, the inertia term of the Morison equation is well suited for slender structures to secure the similar hydrodynamic force prediction in a 2-D approach. However, no indication of forces due to damping is indicated in the Morison equation which is quite true in case the body is deeply submerged, i.e. not close to the free surface. But the Morison equation does indicate the other non-linear hydrodynamic force which is also anti phase with the inertia term and is known as the viscous drag force. So, for a body which is not deeply submerged, there exists the possibility of attracting both the forces like damping (potential and linear) and damping (viscous and non-linear) especially when the body is slender enough compared to the wave length. Apart from those mentioned above, there would be lift due to vortex shedding and that force, being perpendicular to the velocity vector, would be rotating around the body axis

due to the orbital motion of the water particles. As the period, the magnitude and the direction of the lift force are unknown, they are not added to the force components of the Morison equation as mentioned in (Teng and Nath 1985).

Inertia Forces

Using the inertia term of the Morison equation, the inertia force on the fixed submerged pontoon in waves only beam seas is as follows:

$$F_{IY}(t) = -C_{MY} \rho \{(l - l_e) \times b \times h\} \zeta_a e^{-kd} \omega^2 \sin \omega t \quad (4.50)$$

$$F_{IZ}(t) = -C_{MZ} \rho \{(l - l_e) \times b \times h\} \zeta_a e^{-kd} \omega^2 \cos \omega t \quad (4.51)$$

Drag Forces

Using the drag term of the Morison equation, the drag force on the fixed submerged pontoon in waves only in beam seas is given as follows:

$$F_{DY}(t) = \frac{1}{2} C_{DY} \rho (l \times h) v | v | \quad (4.52a)$$

$$F_{DY}(t) = \frac{4}{3\pi} C_{DY} \rho (l \times h) \zeta_a^2 e^{-2kd} \omega^2 \cos \omega t \quad (4.52b)$$

$$F_{DZ}(t) = \frac{1}{2} C_{DZ} \rho \{(l - l_e) \times b\} w | w | \quad (4.53a)$$

$$F_{DZ}(t) = -\frac{4}{3\pi} C_{DZ} \rho \{(l - l_e) \times b\} \zeta_a^2 e^{-2kd} \omega^2 \sin \omega t \quad (4.53b)$$

4.4.3 In Waves and Currents in Beam Seas

Effects of Currents on Wave Kinematics

Similar to head seas, the horizontal component of water particle velocity is given by:

$$v = v_r + U \quad (4.54a)$$

$$= \zeta_a e^{kz} (\omega - kU) \cos(ky - \omega t) + U \quad (4.54b)$$

Similarly, the vertical component of water particle velocity is :

$$w = w_r \quad (4.55a)$$

$$= \zeta_a e^{kz} (\omega - kU) \sin(ky - \omega t) \quad (4.55b)$$

The horizontal component of water particle acceleration may be obtained from the total derivative of v with respect to time:

$$\frac{dv}{dt} = \frac{\partial v}{\partial t} + u \frac{\partial v}{\partial x} + v \frac{\partial v}{\partial y} + w \frac{\partial v}{\partial z} \quad (4.56)$$

in which u is the water particle velocity in x-direction parallel to the wave crests. If the current is steady, $\frac{\partial U}{\partial t} = 0$ and if it is both horizontally and vertically uniform then $\frac{\partial U}{\partial y} = 0$, $\frac{\partial v}{\partial x} = 0$ and $\frac{\partial U}{\partial z} = 0$. So, for small amplitude waves, the above equation becomes:

$$\frac{dv}{dt} = \frac{\partial v_r}{\partial t} + U \frac{\partial v_r}{\partial y} \quad (4.57)$$

The remaining parts of the convective acceleration terms are negligible compared with the total acceleration term if the waves are small. Thus

$$\frac{dv}{dt} \simeq \zeta_a e^{kz} \omega (\omega - kU) \sin(ky - \omega t) - \zeta_a kU (\omega - kU) \sin(ky - \omega t) \quad (4.58a)$$

$$\dot{v} = \zeta_a e^{kz} (\omega - kU)^2 \sin(ky - \omega t) \quad (4.58b)$$

The vertical component of water particle acceleration may be determined similarly giving

$$\frac{dw}{dt} = -\zeta_a e^{kz} (\omega - kU)^2 \cos(ky - \omega t) \quad (4.59a)$$

$$\dot{w} = -\zeta_a e^{kz} (\omega - kU)^2 \cos(ky - \omega t) \quad (4.59b)$$

Inertia Forces

The horizontal and vertical inertia forces on the fixed submerged pontoon in a wave-current coexisting flow field is given by the following:

$$F_{FY}(t) = -C_{MY} \rho \{(l - l_e) \times b \times h\} \zeta_a e^{-kd} (\omega - kU)^2 \sin \omega t \quad (4.60)$$

$$F_{FZ}(t) = -C_{MZ} \rho \{(l - l_e) \times b \times h\} \zeta_a e^{-kd} (\omega - kU)^2 \cos \omega t \quad (4.61)$$

Drag Forces

The horizontal drag forces on the fixed submerged pontoon in a wave-current coexisting flow field is given by the following:

$$F_{DY}(t) = \frac{1}{2} C_{DY} \rho (l \times h) (v \pm U) |v \pm U| \quad (4.62)$$

where $-U$ represents opposing currents, i.e. against the direction of wave propagation.

For $|U| \geq v_a$:

$$F_{DY} = C_{DY} \rho (l \times h) v_a^2 \gamma \quad (4.63)$$

For $|U| < v_a$:

$$F_{DY} = \frac{1}{2\pi} \rho C_{DY} (l \times h) v_a^2 \left\{ \frac{1}{3} (\sin 3\Theta + 9 \sin \Theta) + 2\gamma (2\Theta + \sin 2\Theta - \pi) + 4\gamma^2 \sin \Theta \right\} \quad (4.64a)$$

$$= \frac{1}{2\pi} \rho C_{DY} (l \times h) 2v_a^2 \left\{ \frac{1}{6} (\sin 3\Theta + 9 \sin \Theta) + \gamma (2\Theta + \sin 2\Theta - \pi) + 2\gamma^2 \sin \Theta \right\} \quad (4.64b)$$

$$= \frac{1}{\pi} \rho C_{DY} (l \times h) v_a^2 (d_1 + d_2 + d_3) \quad (4.64c)$$

where

$$d_1 = \frac{1}{6} (\sin 3\Theta + 9 \sin \Theta)$$

$$d_2 = \gamma (2\Theta + \sin 2\Theta - \pi)$$

$$d_3 = 2\gamma^2 \sin \Theta$$

Viscous Mean Drift Forces

The horizontal viscous mean drift forces on the fixed submerged pontoon in a wave-current coexisting flow field is given by the following:

$$F_{DoY} = \frac{1}{T} \int_0^T F_{DY}(t) dt \quad (4.65)$$

For $|U| \geq v_a$:

$$F_{DoY} = \frac{1}{2} \rho C_{DoY} (l \times h) \left(\frac{1}{2} v_a^2 + U^2 \right) \quad (4.66a)$$

$$= \frac{1}{2} \rho C_{DoY} (l \times h) v_a^2 \left(\frac{1}{2} + \frac{U^2}{v_a^2} \right) \quad (4.66b)$$

$$= \frac{1}{2} \rho C_{DoY} (l \times h) v_a^2 \left(\frac{1}{2} + \gamma^2 \right) \quad (4.66c)$$

For $|U| < v_a$:

$$F_{DoY} = \frac{1}{2\pi} \rho C_{DoY} (l \times h) v_a^2 \left\{ \frac{1}{2} 2\Theta + \sin 2\Theta - \pi \right\} + 4\gamma \sin \Theta + \gamma^2 (2\Theta - \pi) \quad (4.67a)$$

$$= \frac{1}{2\pi} \rho C_{DoY} (l \times h) v_a^2 (d_1 + d_2 + d_3) \quad (4.67b)$$

where

$$d_1 = \frac{1}{2} (2\Theta + \sin 2\Theta - \pi)$$

$$d_2 = 4\gamma \sin \Theta$$

$$d_3 = \gamma^2 (2\Theta - \pi)$$

4.5 Experimental Results in Beam Seas

4.5.1 In Currents Only in Beam Seas

In Figure 4.11, the measured vertical steady forces and the experimental drag coefficients in currents only are shown. The horizontal drag coefficients

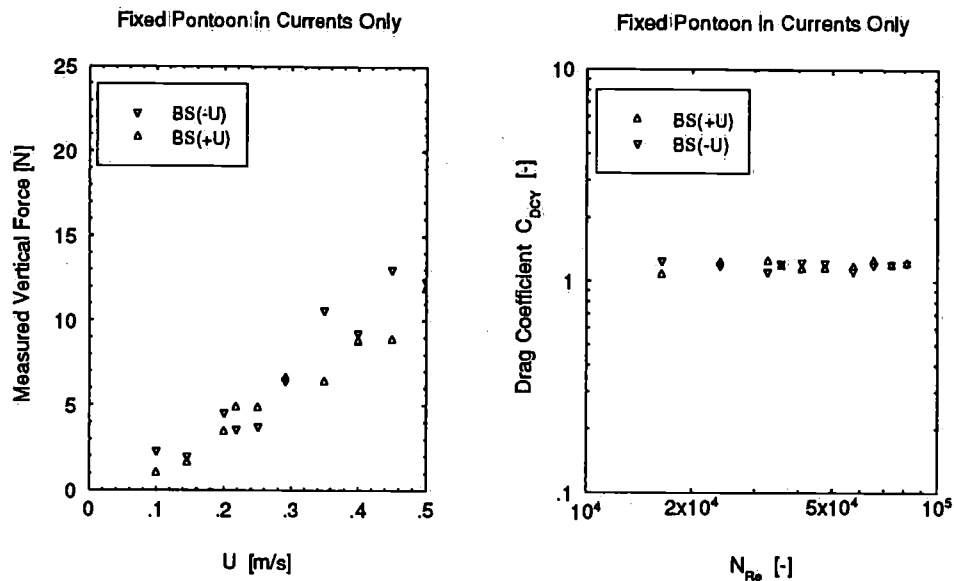


Figure 4.11: (Left) Measured vertical forces on a fixed pontoon and (right) experimental drag coefficients of a fixed pontoon in currents only

are found to be almost a constant value within the prescribed range of the Reynolds number.

4.5.2 In Waves Only in Beam Seas

In Figure 4.12, the measured horizontal and vertical forces are shown against the theoretical calculations. In most of the frequencies used, the nature of linearity of the predictions is not found. From Figure 4.13, it can be seen clearly that the inertia coefficients in horizontal and vertical directions decrease with increasing N_{K-C} (up to a value of 2 to 2.50 as pointed out by Otsuka *et al.* (1990) and Arai (1995) showing that the discrepancy in force measurements is caused by a reduction in the inertia forces. A similar tendency can be seen in experimental results in available literature. The cause of such reduction is the effect of a steady circulation due to oscillatory boundary layer around the cylinder. In the presence of water particle velocities, this circulation causes transverse forces to the incident flow. This is well known as 'Magnus Effect' in potential flow theory. These forces always reduce the inertia forces. So, the behavior of the inertia coefficients in waves is different from that of the same pontoon in a sinusoidal oscillation. The

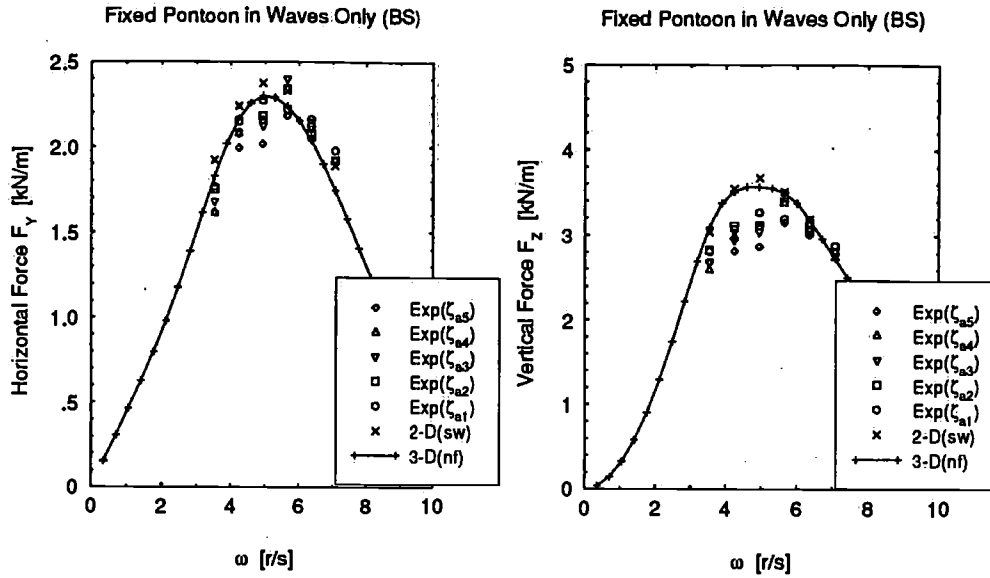


Figure 4.12: Computed and measured (left) horizontal and (right) vertical first order forces on a fixed pontoon in waves only in beam seas

hydrodynamic coefficients depend only on N_{K-C} in a waves only flow field.

Estimation of Circulation

If the circulation alone causes the reduction of the inertia forces, its value can roughly be estimated from the difference in the potential value of the inertia forces and the measured ones. If the reduction in the inertia coefficients is represented by the theoretical and the experimental values, the reduced inertia forces can be expressed by:

$$\rho \Delta C_M \{(l - l_e) \times b \times h\} \zeta_a e^{-kd} \omega^2 = \rho \Gamma l \zeta_a e^{-kd} \omega \quad (4.68)$$

Therefore,

$$\Gamma = \Delta C_M (b \times h) \left(\frac{l - l_e}{l} \right) \omega \quad (4.69)$$

Otsuka *et al.* (1990) proposed a nondimensional value K as the ratio of the circulating velocity to the rotating velocity of separated vortices where they assumed that the separated vortices rotate around the circular cylinder

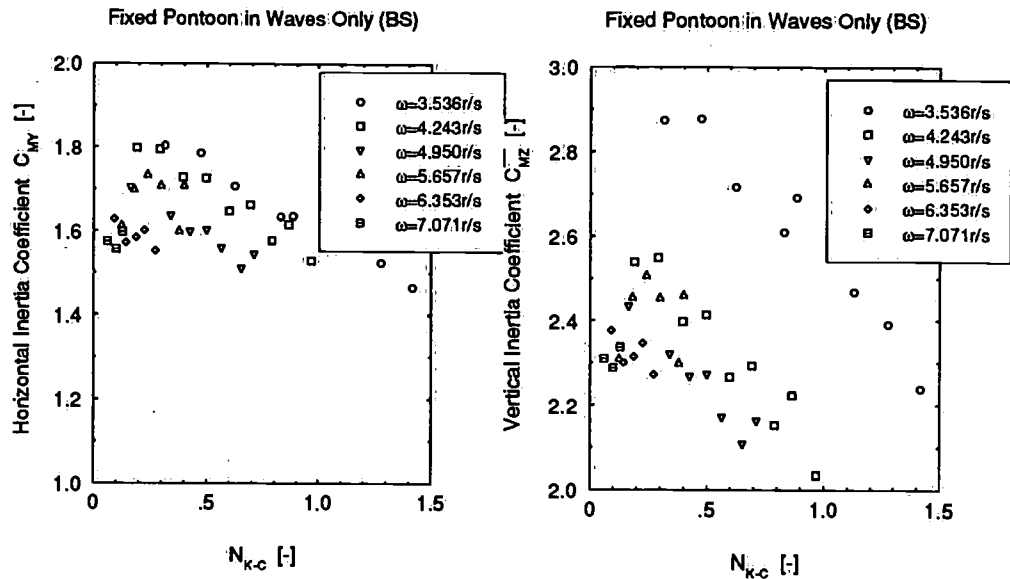


Figure 4.13: Experimental (left) horizontal and (right) vertical inertia coefficients of a fixed pontoon in waves only in beam seas

with the same cycle as the wave's. In the case of a rectangular pontoon, the nondimensional value K is obtained as follows:

$$K = \frac{\left\{ \frac{\Gamma}{2(b+h)} \right\}}{\left\{ \frac{2(b+h)}{T} \right\}} \quad (4.70a)$$

$$= \frac{\Gamma T}{\{2(b+h)\}^2} \quad (4.70b)$$

In Figure 4.14, the values of the non-dimensional coefficients are shown. The values obtained from horizontal forces show a more consistent pattern whereas those from vertical forces show some disparity though the basic pattern remains same.

It is not within the main scope of this work to find such anomaly in the first order forces on a submerged body. However, based on the existing literature, the author attempts here some empirical relations as proposed by Chaplin (1984), Otsuka and Ikeda (1993) and Arai (1995) to calculate the inertia forces including effects of circulation. The empirical relations gives an estimation of the inertia coefficients in the presence of circulation.

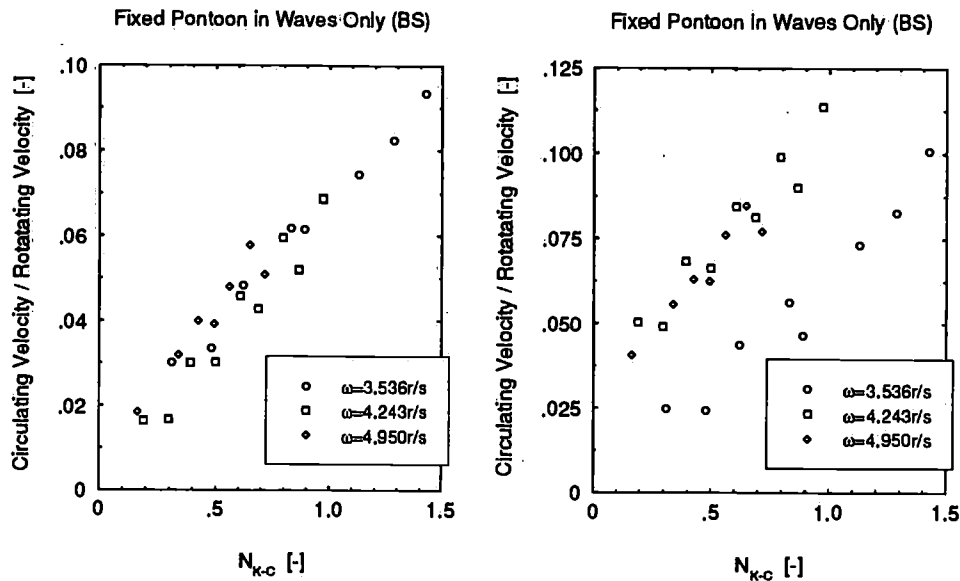


Figure 4.14: Circulation estimated from the measured (left) horizontal and (right) vertical first order forces in waves only in beam seas

$$C_M = 2.00 - 0.21 N_{K-C}^2; \text{ Chaplin} \quad (4.71)$$

$$C_M = 2.00 - \frac{2}{\pi^2} N_{K-C}^2; \text{ Otsuka and Ikeda} \quad (4.72)$$

Equation 4.71 and Equation 4.72 are based on investigations with circular cylinders and they are almost identical. It is shown that C_M of the pontoon behaves like the circular cylinders too, i.e. with the increase in the Keulegan-Carpenter number, C_M first decreases. As the orbital motion of a water particle is almost circular, the horizontal component of C_M is the same with the vertical one for a circular or a square cylinder. But in the case of a rectangular pontoon, however, the C_M values in the horizontal and in the vertical direction are expected to be different from each other because of the directional shape of the section. The proposed C_M values as given by Arai (1995) are as follows:

$$C_{MX} = 1.70 - 0.28 N_{K-C}^2 \quad (4.73a)$$

$$C_{MY} = 3.14 - 0.28 N_{K-C}^2 \quad (4.73b)$$

References	$\frac{b}{h}$	$\frac{r}{h}$	$d - \frac{h}{2}$
Dev	1.666	0.050	0.310m
Arai	1.875	0.000	0.093m
Ikeda, Otsuka and Tanaka	1.875	0.25	0.160m
Koterayama and Hu	1.625	0.125	-

Table 4.1: Model Pontoon Particulars

The author in his work has modified the Keulegan-Carpenter number with an equivalent diameter which can be done in different ways.

$$\pi D = 2(b + h) \quad (4.74)$$

$$D = \frac{\{2(b + h)\}}{\pi} \quad (4.75)$$

$$C_{Mc} \frac{\pi D^2}{4} = C_{Mp} (b \times h) \quad (4.76)$$

$$D = \sqrt{\frac{C_{Mp}}{C_{Mc}} \frac{4(b \times h)}{\pi}} \quad (4.77)$$

The values of C_{Mc} is equal to 2 and those for a pontoon of different aspect ratios are available in different literature. However, the author used the former one to find the equivalent diameter for the Keulegan-Carpenter number.

The results of the computations are shown in Figure 4.15 for the horizontal and vertical forces compared to the experimental ones. The correlation is found to be better when the formulations by Arai (1995) are used but still with anomalies. The reasons might be different experimental set-up, depth of submersion, wave frequencies and finally the model particulars including its corner radius. From the concerned references, a table 4.1 is produced where the relevant information are given.

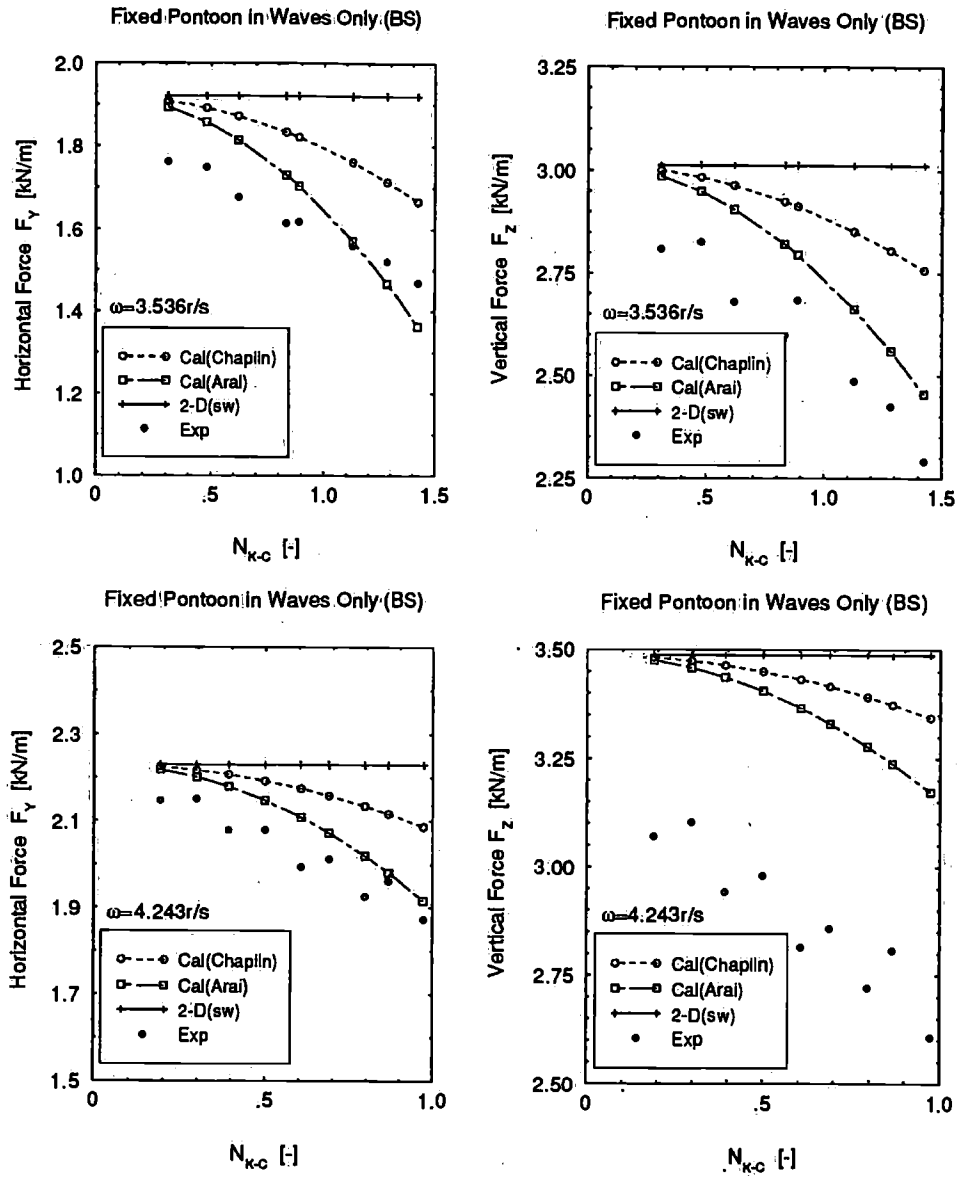


Figure 4.15: Computed and measured horizontal and vertical first order forces on a fixed pontoon in waves only in beam seas

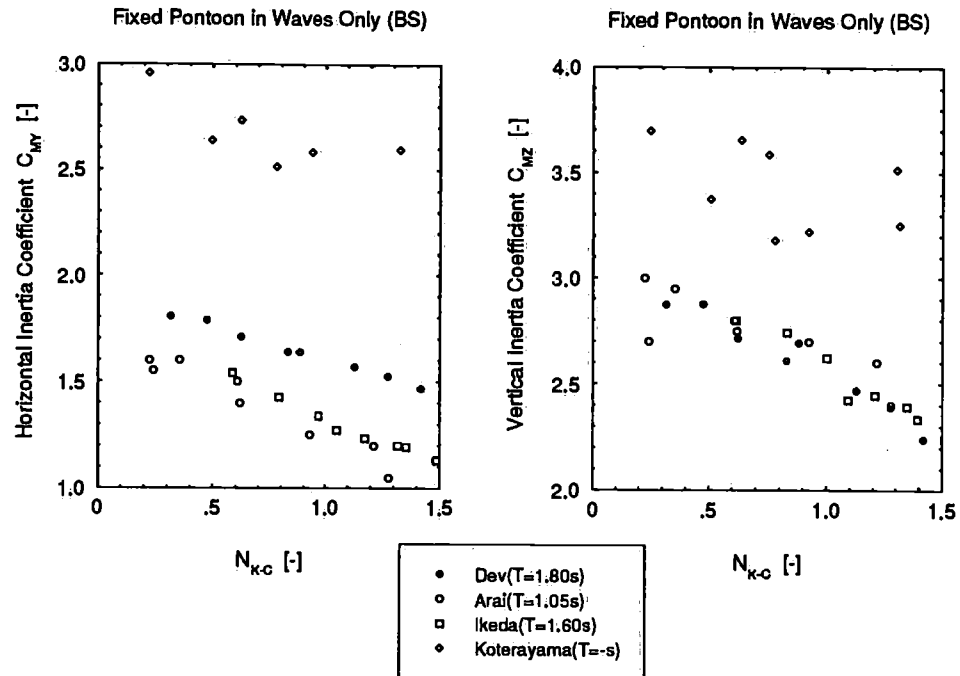


Figure 4.16: Comparison of experimental (left) horizontal and (right) vertical inertia coefficients of a fixed pontoon in waves only in beam seas

Comparison of experimental inertia coefficients from other published results including the author's ones are produced in Figure 4.16. The correlation among Arai (1995), Otsuka *et al.* (1990) and the author shows similar trends. But the values obtained from (Koterayama and Hu 1995) are quite high yet they show a decreasing tendency due to the presence of circulation. In this connection, Table 4.1 can be referred for the model particulars used in different experiments.

In spite of all these, it is evident that for a single cylindrical (circular or rectangular) submerged body having its axis parallel to the wave crests, the circulation phenomena exist and need to be taken care of for the reduction in the inertia force.

Both horizontal and vertical mean drift forces are shown in Figure 4.17. The trend is similar to what has been shown for the head sea condition. Though circulation phenomena do exist for such a single body cylindrical structure, its effects are still within the potential theory affecting only the

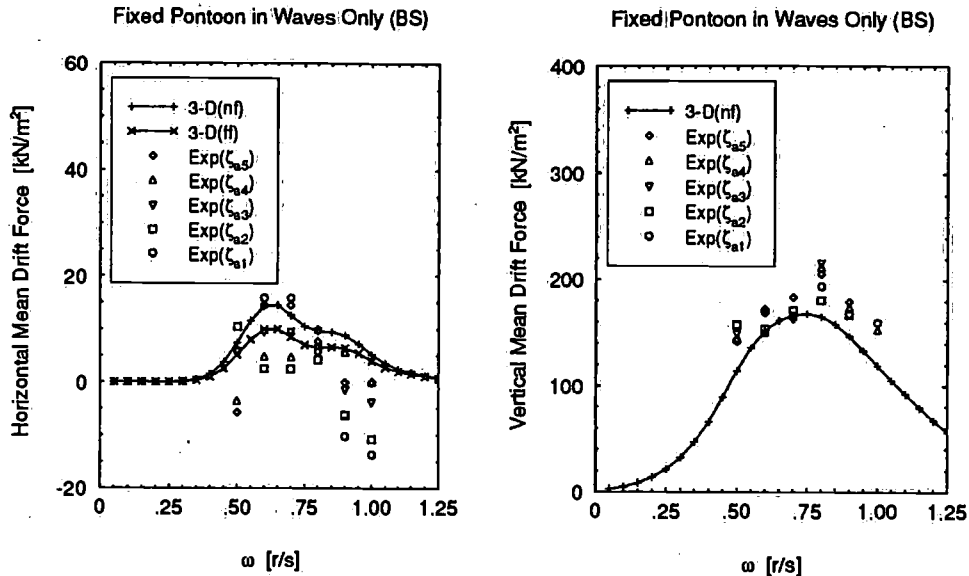


Figure 4.17: Computed and measured (left) horizontal and (right) vertical mean drift forces on a fixed pontoon in waves only in beam seas

inertia force causing non-linearity in first order horizontal and vertical forces.

4.5.3 In Waves and Currents in Beam Seas

The horizontal and vertical inertia forces are shown in Figure 4.18 and in Figure 4.19. Differences are still observed between the theoretical predictions and the measured values.

Figure 4.21 (left) shows the values of the experimentally obtained mean drag coefficients C_{D0Y} in a wave-current coexisting flow field for both positive and negative currents. The values are produced as function of N_{K-C}^* . The mean values can be taken as unity except for some higher wave amplitudes in positive currents in which case the values are slightly higher. Using the experimentally obtained values of the mean drag coefficients C_{D0Y} , a comparison is shown between the measured and the computed horizontal mean drift forces for different velocities of currents. Predictions appear well.

Similar to head seas, the measured mean drift forces are shown in Figure 4.22 after the measured forces due to currents (positive and negative) have been deducted from the forces in waves and currents. The results are

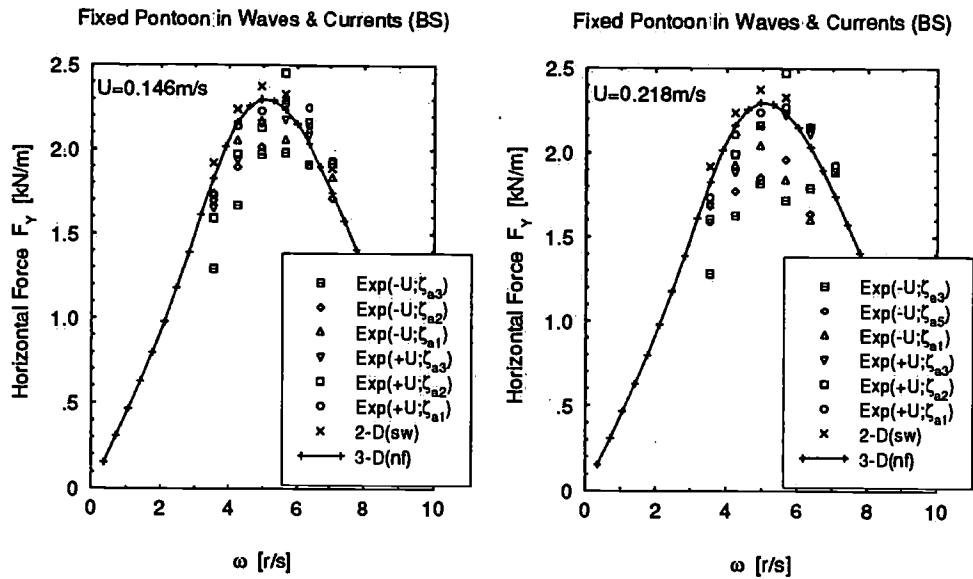


Figure 4.18: Computed and measured horizontal first order forces on a fixed pontoon in waves and currents in beam seas

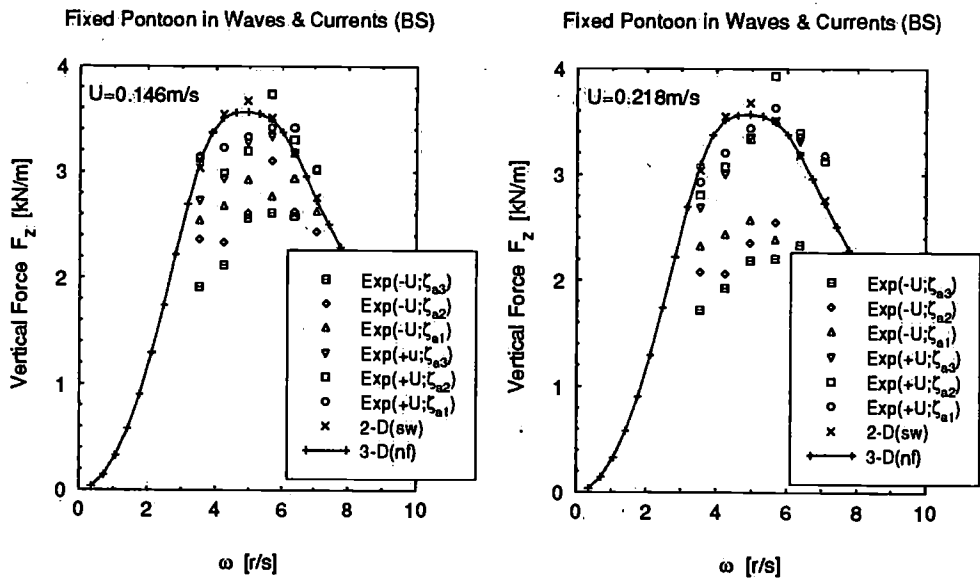


Figure 4.19: Computed and measured vertical first order forces on a fixed pontoon in waves and currents in beam seas

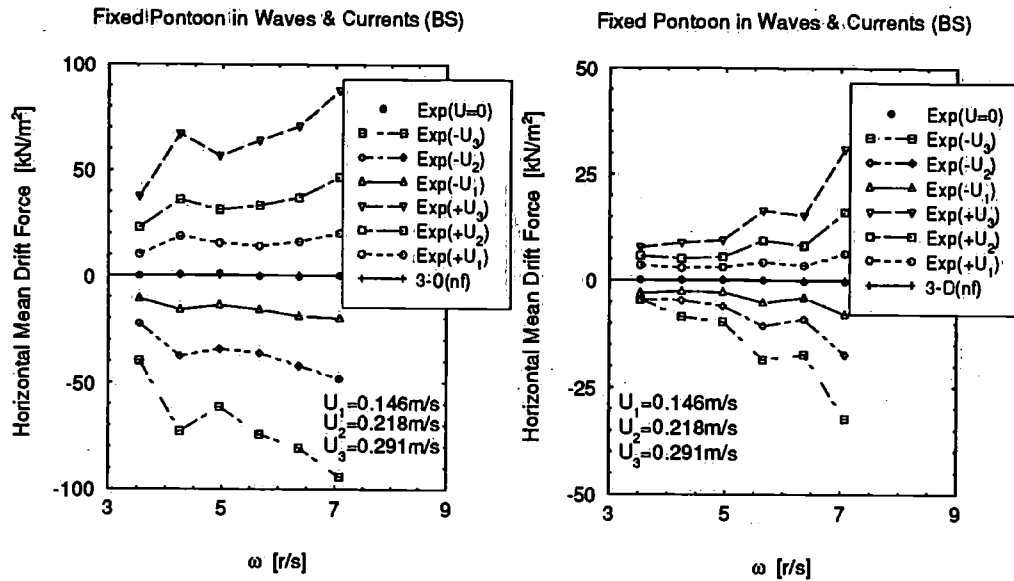


Figure 4.20: Computed and measured horizontal mean drift forces on a fixed pontoon in waves and currents in beam seas

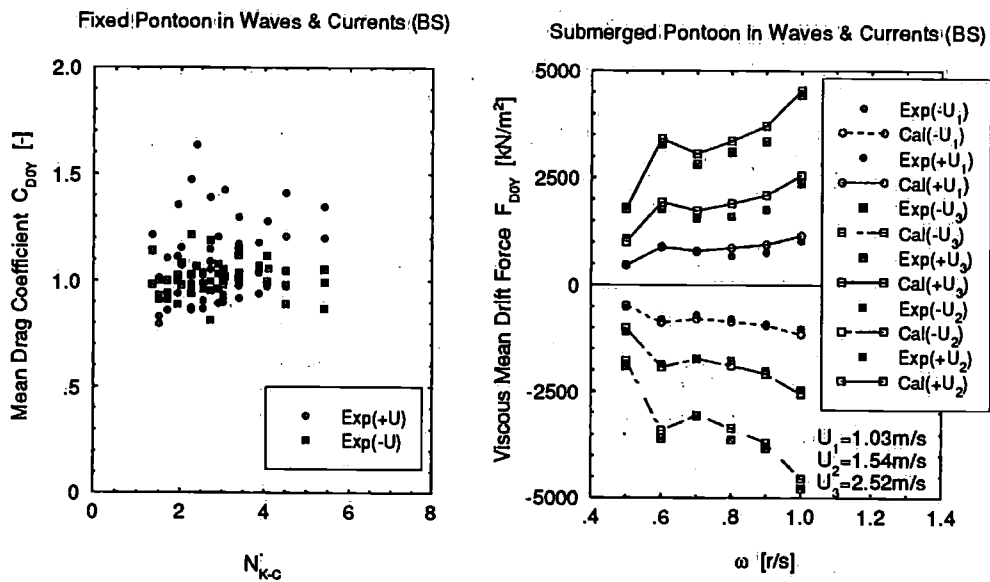


Figure 4.21: (left) Experimental mean drag coefficients and (right) computed and measured forces on a fixed pontoon in waves and currents in beam seas

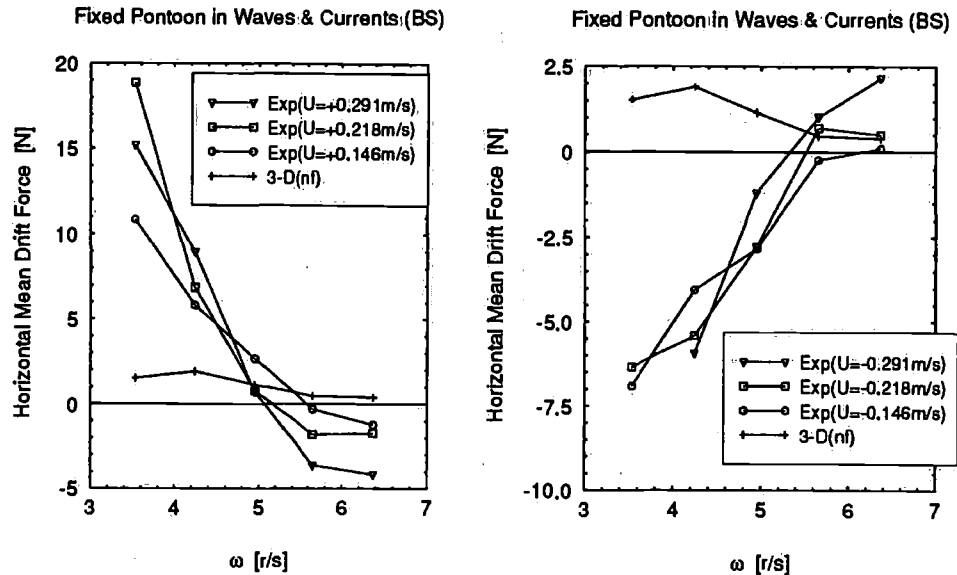


Figure 4.22: Computed (waves only) and experimental (waves and currents minus currents) horizontal mean drift forces on a fixed pontoon in beam seas

again different from the 3-D predictions. As the measured forces are similar in trend to those from 3-D predictions, such differences cannot be considered as the viscous drift forces due to a waves-only field on a constantly submerged zone.

4.6 Concluding Remarks

1. While comparing the measured mean forces with 3-dimensional predictions for a submerged pontoon in both head seas and beam seas, it is found that the contributions from potential effects are in sufficiently good agreement. No marked nonlinearity is observed and as such it is concluded that viscous effects do not play any substantial role for any constantly submerged body in a waves-only flow field.
2. In the presence of currents, the above phenomenon is no longer true and an additional source of viscous effects in the horizontal mean drift forces is established. Because of the absence of the free surface effects for a deeply submerged body, the wave current interactions in both positive and negative currents are quite similar resulting into almost

similar behavior in beam seas whereas in head seas differences still exist because of the lengthwise variation in the fluid velocity.

3. Beginning with the measured values of the mean forces on the cylinder, and on the pontoon in head seas and beam seas, it is consistently proved beyond any doubt that the origin of the viscous drift force for a structure cannot be treated by subtracting the mean force due to a currents-only flow field from the mean force due to a wave-current coexisting flow field and dealing with the difference as the viscous drift force in a waves-only flow field. Either an independent flow field or a coexisting flow field has its own mechanism of generating the viscous drift force. Neither an addition nor a subtraction is expected to result in either a coexisting (interacting) flow field or an independent flow field respectively.
4. First order forces at zero forward speed can be well predicted by either 3-D or 2-D computations in the head sea condition but in the beam sea condition the same computational methods fail due to the presence of the circulation phenomenon which has also been observed consistently in other experimental work. More systematic investigations, both numerical and experimental, are necessary for further insight into this hydrodynamic behavior.
5. First order forces in the presence of positive and negative currents are found again to be different from theoretical calculations. In the presence of currents, viscous effects influence inertia forces. Analysis of force coefficients based on the Morison force coefficients can help to overcome such differences in the low frequency range but at higher frequencies forward speed effects are necessary even in 3-D predictions.
6. The viscous mean drift force in a wave-current coexisting flow field can be predicted well when the experimentally obtained values of the mean drag coefficients are used in the theoretical calculations.

References

- Arai, S. (1993). Forces and flows around a horizontal rectangular cylinder submerged in regular waves. In *Proceedings of the International Offshore and Polar Engineering Conference*, ISOPE, Singapore, pp. 288-293.
- Arai, S. (1995). Forces and circulation of horizontal cylinders submerged in regular waves. In *Proceedings of the International Offshore and Polar Engineering Conference*, ISOPE, The Hague, The Netherlands, pp. 348-355.
- Chaplin, J. R. (1984). Nonlinear forces on a horizontal cylinder beneath waves. *Journal of Fluid Mechanics* 147, 449-464.
- DELFRAC (1992). *A 3-D Diffraction Program*. Ship Hydromechanics Laboratory, Delft University of Technology, Delft, The Netherlands.
- Hamel-Derouich, D. (1993). *Hydrodynamic Forces on Rectangular Cylinders of Various Aspect Ratios Immersed in Different Flows*. Ph. D. thesis, Department of Naval Architecture and Ocean Engineering, University of Glasgow, Glasgow, Scotland.
- Koterayama, W. (1979). Wave forces exerted on submerged circular cylinders fixed in deep waves. Technical Report 84, Research Institute for Applied Mechanics, Kyushu University, Kyushu, Japan.
- Koterayama, W. and C. Hu (1995). Wave forces on horizontal cylinders at low keulegan carpenter and reynolds numbers. In *Proceedings of the International Offshore and Polar Engineering Conference*, ISOPE, The Hague, The Netherlands, pp. 189-195.
- Moe, G. and R. L. P. Verley (1977). Hydrodynamic damping of offshore structures in waves and currents. In *Proceedings of the Annual Offshore Technology Conference*, OTC 3798, Houston, Texas, pp. 37-44.
- Otsuka, K. and Y. Ikeda (1993). An estimation of inertia coefficient of horizontal circular cylinder in waves at low kc number. *Journal of the Kansai Society of Naval Architects, Japan* 219, 135-141.
- Otsuka, K., Y. Ikeda, and N. Tanaka (1990). Viscous forces acting on a horizontal circular cylinder in regular and irregular waves. In *Proceedings of the International Conference on Offshore Mechanics and Arctic Engineering*, OMAE, Houston, Texas, pp. 129-138.

- Rai, S. P. and M. H. A. Khader (1983). Maximum wave force on a horizontal cylinder. In *Proceedings of Coastal Structures '83*, Arlington, Virginia, pp. 482-491.
- Ramberg, S. E. and J. M. Niedzwecki (1982). Horizontal and vertical cylinders in waves. *Ocean Engineering* 9(1), 1-15.
- Sarpkaya, T. and M. Isaacson (1981). *Mechanics of Wave Forces on Off-shore Structures*, Chapter 3, 6, pp. 93, 323. New York: Van Nostrand Reinhold Company Inc.
- SEAWAY (1992). *A 2-D Strip Theory Program*. Ship Hydromechanics Laboratory, Delft University of Technology, Delft, The Netherlands.
- Shankar, N. J., H. Raman, and V. Sundar (1983). Wave forces on a submerged cylinder near a plane boundary. In *Proceedings of Coastal Structures '83*, Arlington, Virginia, pp. 492-504.
- Teng, C. C. and J. H. Nath (1985). Forces on horizontal cylinders towed in waves. *Journal of Waterway, Port, Coastal and Ocean Engineering* 111(6), 1022-1040.

Chapter 5

Mathematical Model

In this chapter, the mathematical model for a complete semi-submersible in both regular and irregular waves will be discussed in connection with viscous effects in the mean and low frequency drift forces. No description in connection with either first order forces or motions will be given. These aspects of 3-Dimensional hydrodynamic theory have been treated by means of DELFRAC (1992).

The hydrodynamic theory concerning viscous effects in the horizontal mean drift forces on a vertical cylinder and on a submerged pontoon have been elaborated upon in Chapter 3 and Chapter 4 respectively. In those two chapters, it was shown that the basic mathematical model for a vertical cylinder and a submerged pontoon including the experimentally obtained force coefficients along with their controlling hydrodynamic parameters is sufficient to predict the viscous mean drift force in waves only and also in waves and currents in the frequency domain. Furthermore, it has become quite clear from the computations, the measurements and the validation that viscous effects either in an independent flow field or in a coexisting flow field should be treated exclusively in an independent manner. Neither a waves-only flow field can be created by eliminating a currents-only flow field from a wave-current coexisting flow field nor can a wave-current coexisting flow field be created by addition of two independent flow fields namely a waves-only flow field and a currents-only flow field. So, addition or subtraction of a currents-only flow field would thus lose its interaction effects resulting into severely erroneous results.

In line with the above facts, the present mathematical model has been developed by extending those fundamental concepts for a vertical cylinder

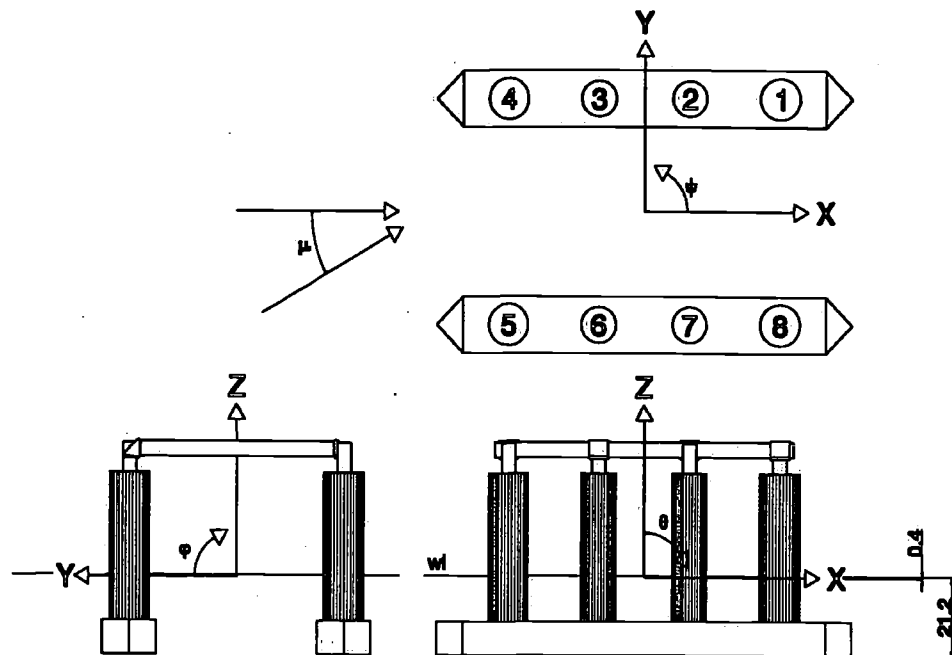


Figure 5.1: *Definition of wave direction and motions*

and a submerged pontoon. The main aspects will be to predict the viscous drift forces on a semi-submersible in regular waves and in irregular waves including the low frequency viscous drift force. The presence of currents alone or its interactions with waves will also be shown in the model.

The limitations of the model will be the exclusion of the interference effects between members, scale effects and inclusion of experimentally obtained values of force coefficients. Only some aspects of drag interference between the columns of a semi-submersible in a uniform flow field (currents only) will be treated by means of experimental findings and such results will be presented in this chapter.

The configuration and the direction of incident waves for the ITTC semi-submersible are shown in Figure 5.1.

5.1 Viscous Mean Drift Forces in Head Seas

5.1.1 Wave Kinematics

The undisturbed wave kinematics at the center of gravity of a semi-submersible is transferred to respective columns and pontoons in accordance with their orientations and layout.

Wave Surface Elevation at Columns

$$\zeta(t) = \zeta_a \cos(kx - \omega t) \quad (5.1a)$$

$$= \zeta_a \cos(\omega t - kx) \quad (5.1b)$$

$$\zeta_c(t) = \zeta(t) \quad (5.2a)$$

$$\zeta_c(t) = \zeta_{ca} \cos(\omega t + \epsilon_{\zeta_c \zeta}) \quad (5.2b)$$

$$\zeta_{ca} = \zeta_a \quad (5.3a)$$

$$\frac{\zeta_{ca}}{\zeta_a} = 1.0 \quad (5.3b)$$

$$\epsilon_{\zeta_c \zeta} = -kx_c \quad (5.3c)$$

Horizontal Water Particle Velocity at Columns

$$u(t) = \zeta_a \omega \cos(kx - \omega t) \quad (5.4a)$$

$$= u_a \cos(\omega t - kx) \quad (5.4b)$$

$$\text{where } u_a = \zeta_a \omega$$

$$u_c(t) = u(t) \quad (5.5a)$$

$$u_c(t) = u_{ca} \cos(\omega t + \epsilon_{u_c \zeta}) \quad (5.5b)$$

$$u_{ca} = u_a \quad (5.6a)$$

$$\frac{u_{ca}}{\zeta_a} = \omega \quad (5.6b)$$

$$\epsilon_{u_c \zeta} = -kx_c \quad (5.6c)$$

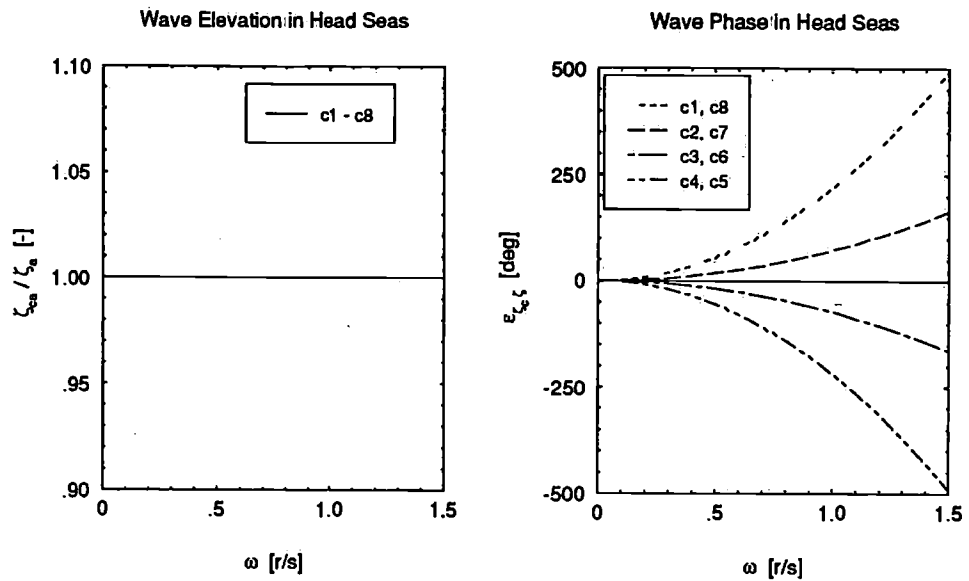


Figure 5.2: Undisturbed wave elevation and phases at the columns

Equations for the horizontal velocity at columns are shown at mwl for the free surface zone (splash zone) but for the submerged zone, the exponential term is to be included and the same will be done for a submerged pontoon.

Figure 5.2 and Figure 5.3 show the RAOs and phases of undisturbed wave elevation and horizontal water particle velocities at the respective columns in head seas.

Horizontal Water Particle Velocity at Pontoons

In the presence of currents, the horizontal projected areas at the pontoon's ends require the horizontal velocity to be calculated at those places.

$$u(t) = \zeta_a e^{kz} \omega \cos(kx - \omega t) \quad (5.7a)$$

$$= u_a \cos(\omega t - kx) \quad (5.7b)$$

$$\text{where } u_a = \zeta_a e^{kz} \omega$$

$$u_p(t) = u(t) \quad (5.8a)$$

$$u_p(t) = u_{pa} \cos(\omega t + \epsilon_{u_p \zeta}) \quad (5.8b)$$

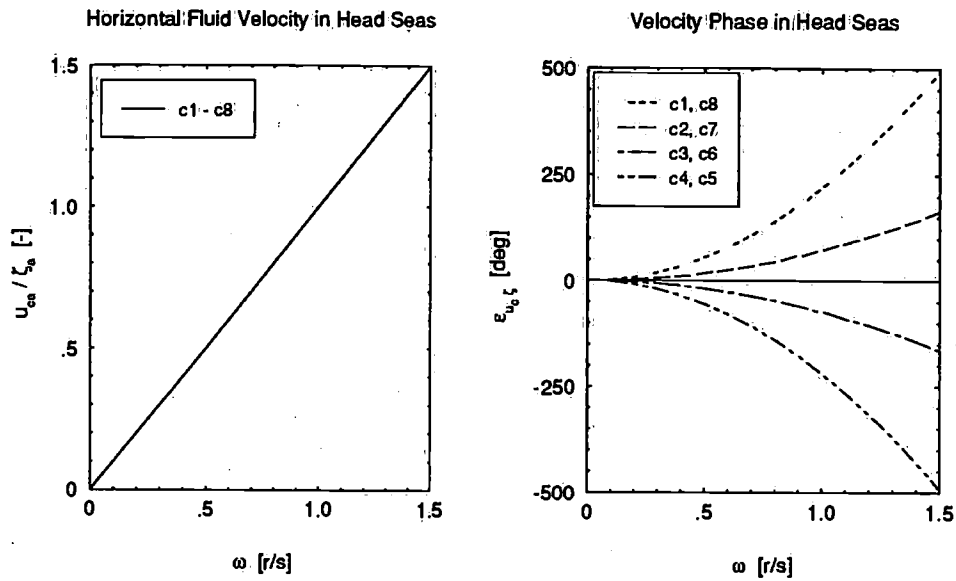


Figure 5.3: Undisturbed fluid velocities and phases at the columns

$$u_{pa} = u_a \quad (5.9a)$$

$$\frac{u_{pa}}{\zeta_a} = e^{kz} \omega \quad (5.9b)$$

$$\epsilon_{u_p \zeta} = -kx_p \quad (5.9c)$$

5.1.2 Horizontal Motions at Columns

Horizontal motions at any point on the center line of the columns are affected by the angular motion and the vertical distance between the center of gravity and a particular point.

$$x(t) = x_a \cos(\omega t + \epsilon_{x\zeta}) \quad (5.10a)$$

$$\theta(t) = \theta_a \cos(\omega t + \epsilon_{\theta\zeta}) \quad (5.10b)$$

$$x_c(t) = x(t) + z_{dc} \theta(t) \quad (5.11a)$$

$$x_c(t) = x_{ca} \cos(\omega t + \epsilon_{x_c \zeta}) \quad (5.11b)$$

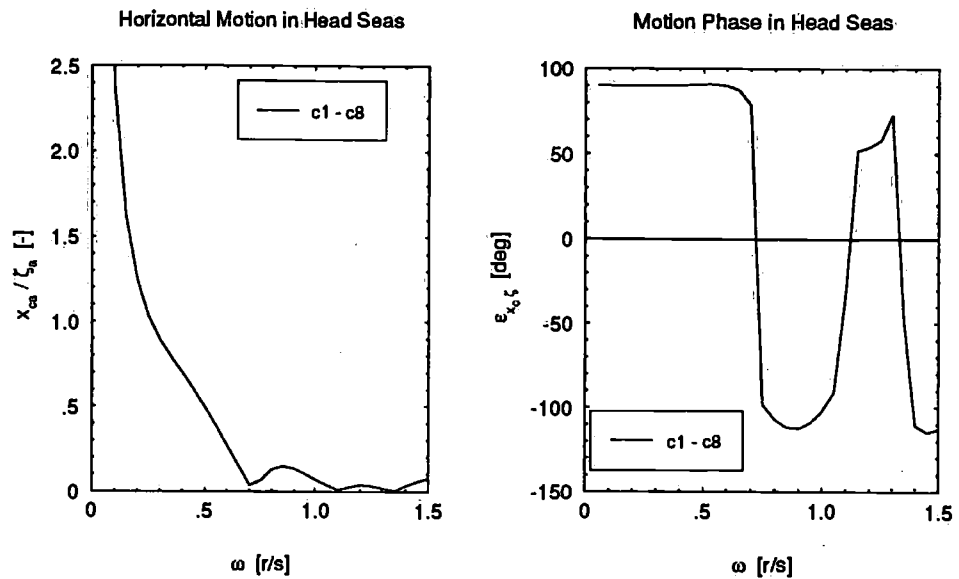


Figure 5.4: Horizontal motions and phases at the columns

$$\frac{x_{ca}}{z_a} = \sqrt{\left(\frac{x_a}{z_a}\right)^2 + \left\{z_{dc} \left(\frac{\theta_a}{z_a}\right)\right\}^2 + 2 \left(\frac{x_a}{z_a}\right) z_{dc} \left(\frac{\theta_a}{z_a}\right) \cos(\epsilon_{x\zeta} - \epsilon_{\theta\zeta})} \quad (5.12)$$

$$\epsilon_{x_c\zeta} = \arctan \left\{ \frac{\left\{\left(\frac{x_a}{z_a}\right) \sin \epsilon_{x\zeta} + z_{dc} \left(\frac{\theta_a}{z_a}\right) \sin \epsilon_{\theta\zeta}\right\}}{\left\{\left(\frac{x_a}{z_a}\right) \cos \epsilon_{x\zeta} + z_{dc} \left(\frac{\theta_a}{z_a}\right) \cos \epsilon_{\theta\zeta}\right\}} \right\} \quad (5.13)$$

Figure 5.4 shows the RAOs and phases of horizontal motion at the free surface of the respective columns in head seas.

5.1.3 Vertical Motions at Columns

In head seas, similar to horizontal motions at columns, the vertical motions are equally affected by the angular motion and the horizontal distance between the center of gravity and a particular point.

$$z(t) = z_a \cos(\omega t + \epsilon_{z\zeta}) \quad (5.14)$$

$$\theta(t) = \theta_a \cos(\omega t + \epsilon_{\theta\zeta}) \quad (5.15)$$

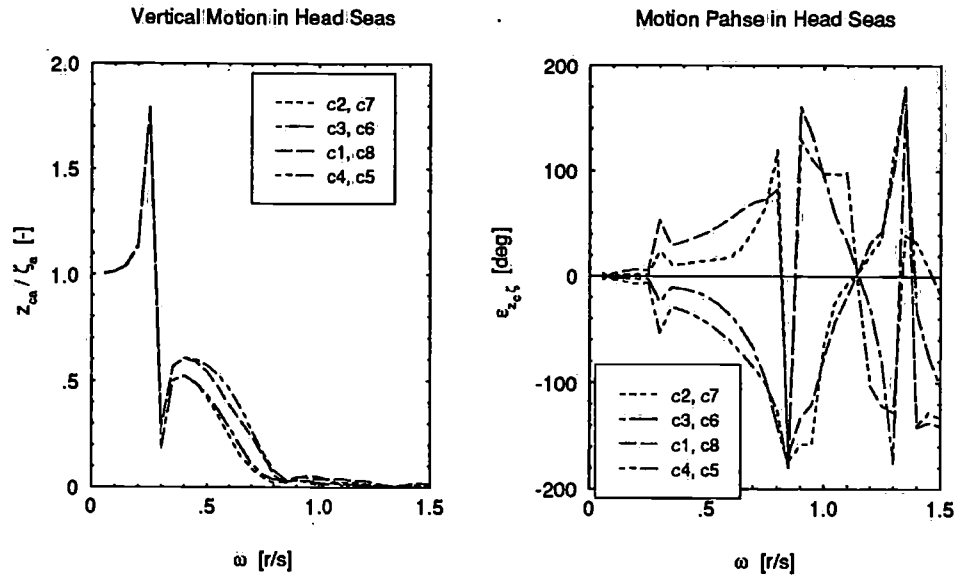


Figure 5.5: Vertical motions and phases at the columns

$$z_c(t) = z(t) - x_{dc} \theta(t) \quad (5.16a)$$

$$z_c(t) = z_{ca} \cos(\omega t + \epsilon_{zc}) \quad (5.16b)$$

$$\frac{z_{ca}}{\zeta_a} = \sqrt{\left(\frac{z_a}{\zeta_a}\right)^2 + \left\{x_{dc} \left(\frac{\theta_a}{\zeta_a}\right)\right\}^2 - 2 \left(\frac{z_a}{\zeta_a}\right) x_{dc} \left(\frac{\theta_a}{\zeta_a}\right) \cos(\epsilon_{z\zeta} - \epsilon_{\theta\zeta})} \quad (5.17)$$

$$\epsilon_{zc} = \arctan \left\{ \frac{\left\{ \left(\frac{z_a}{\zeta_a}\right) \sin \epsilon_{z\zeta} - x_{dc} \left(\frac{\theta_a}{\zeta_a}\right) \sin \epsilon_{\theta\zeta} \right\}}{\left\{ \left(\frac{z_a}{\zeta_a}\right) \cos \epsilon_{z\zeta} - x_{dc} \left(\frac{\theta_a}{\zeta_a}\right) \cos \epsilon_{\theta\zeta} \right\}} \right\} \quad (5.18)$$

Figure 5.5 shows the RAOs and phases of vertical motions at the free surface of the columns in head seas.

5.1.4 Relative Horizontal Velocity at Columns

$$u_r(t) = u(t) - \dot{x}(t) \quad (5.19a)$$

$$u_{rc}(t) = u_c(t) - \dot{x}_c(t) \quad (5.19b)$$

$$u_{rc}(t) = u_{rca} \cos(\omega t + \epsilon_{u_{rc}}) \quad (5.19c)$$

$$u_c(t) = u_{ca} \cos(\omega t + \epsilon_{u_c \zeta}) \quad (5.20a)$$

$$x_c(t) = x_{ca} \cos(\omega t + \epsilon_{x_c \zeta}) \quad (5.20b)$$

$$\dot{x}_c(t) = \dot{x}_{ca} \cos(\omega t + \epsilon_{\dot{x}_c \zeta}) \quad (5.20c)$$

$$\text{where } \epsilon_{\dot{x}_c \zeta} = \left(\epsilon_{x_c \zeta} + \frac{\pi}{2} \right)$$

$$u_{rca} = \zeta_{ca} \omega \sqrt{1 + \left(\frac{x_{ca}}{\zeta_{ca}} \right)^2 - 2 \left(\frac{x_{ca}}{\zeta_{ca}} \right) \cos(\epsilon_{u_c \zeta} - \epsilon_{\dot{x}_c \zeta})} \quad (5.21)$$

$$\epsilon_{u_{rc} \dot{x}_c} = \arctan \left\{ \frac{\left\{ \sin \epsilon_{u_c \zeta} - \left(\frac{x_{ca}}{\zeta_{ca}} \right) \sin \epsilon_{\dot{x}_c \zeta} \right\}}{\left\{ \cos \epsilon_{u_c \zeta} - \left(\frac{x_{ca}}{\zeta_{ca}} \right) \cos \epsilon_{\dot{x}_c \zeta} \right\}} \right\} \quad (5.22)$$

5.1.5 Relative Wave Elevation at Columns

$$\zeta_r(t) = \zeta(t) - z(t) \quad (5.23a)$$

$$\zeta_{rc}(t) = \zeta_c(t) - z_c(t) \quad (5.23b)$$

$$\zeta_{rc}(t) = \zeta_{rca} \cos(\omega t + \epsilon_{\zeta_{rc} z_c}) \quad (5.23c)$$

$$\zeta_c(t) = \zeta_{ca} \cos(\omega t + \epsilon_{\zeta_c \zeta}) \quad (5.24a)$$

$$z_c(t) = z_{ca} \cos(\omega t + \epsilon_{z_c \zeta}) \quad (5.24b)$$

$$\zeta_{rca} = \zeta_{ca} \sqrt{1 + \left(\frac{z_{ca}}{\zeta_{ca}} \right)^2 - 2 \left(\frac{z_{ca}}{\zeta_{ca}} \right) \cos(\epsilon_{\zeta_c \zeta} - \epsilon_{z_c \zeta})} \quad (5.25)$$

$$\epsilon_{\zeta_{rc} z_c} = \arctan \left\{ \frac{\left\{ \sin \epsilon_{\zeta_c \zeta} - \left(\frac{z_{ca}}{\zeta_{ca}} \right) \sin \epsilon_{z_c \zeta} \right\}}{\left\{ \cos \epsilon_{\zeta_c \zeta} - \left(\frac{z_{ca}}{\zeta_{ca}} \right) \cos \epsilon_{z_c \zeta} \right\}} \right\} \quad (5.26)$$

5.1.6 Horizontal Motions at pontoons

Similar to the vertical columns, horizontal motions are to be calculated at the pontoons ends by taking care of the angular motion.

$$x(t) = x_a \cos(\omega t + \epsilon_{x\zeta}) \quad (5.27)$$

$$\theta(t) = \theta_a \cos(\omega t + \epsilon_{\theta\zeta}) \quad (5.28)$$

$$x_p(t) = x(t) + z_{dp} \theta(t) \quad (5.29a)$$

$$x_p(t) = x_{pa} \cos(\omega t + \epsilon_{x_p\zeta}) \quad (5.29b)$$

$$\frac{x_{pa}}{\zeta_a} = \sqrt{\left(\frac{x_a}{\zeta_a}\right)^2 + \left\{z_{dp} \left(\frac{\theta_a}{\zeta_a}\right)\right\}^2 + 2 \left(\frac{x_a}{\zeta_a}\right) z_{dp} \left(\frac{\theta_a}{\zeta_a}\right) \cos(\epsilon_{x\zeta} - \epsilon_{\theta\zeta})} \quad (5.30)$$

$$\epsilon_{x_p\zeta} = \arctan \left\{ \frac{\left\{ \left(\frac{x_a}{\zeta_a}\right) \sin \epsilon_{x\zeta} + z_{dp} \left(\frac{\theta_a}{\zeta_a}\right) \sin \epsilon_{\theta\zeta} \right\}}{\left\{ \left(\frac{x_a}{\zeta_a}\right) \cos \epsilon_{x\zeta} + z_{dp} \left(\frac{\theta_a}{\zeta_a}\right) \cos \epsilon_{\theta\zeta} \right\}} \right\} \quad (5.31)$$

5.1.7 Vertical Motions at pontoons

Similar to the vertical columns, vertical motions are to be calculated at the pontoons ends by taking care of the angular motion.

$$z(t) = z_a \cos(\omega t + \epsilon_{z\zeta}) \quad (5.32)$$

$$\theta(t) = \theta_a \cos(\omega t + \epsilon_{\theta\zeta}) \quad (5.33)$$

$$z_p(t) = z(t) - x_{dp} \theta(t) \quad (5.34a)$$

$$z_p(t) = z_{pa} \cos(\omega t + \epsilon_{z_p\zeta}) \quad (5.34b)$$

$$\frac{z_{pa}}{\zeta_a} = \sqrt{\left(\frac{z_a}{\zeta_a}\right)^2 + \left\{x_{dp} \left(\frac{\theta_a}{\zeta_a}\right)\right\}^2 - 2 \left(\frac{z_a}{\zeta_a}\right) x_{dp} \left(\frac{\theta_a}{\zeta_a}\right) \cos(\epsilon_{z\zeta} - \epsilon_{\theta\zeta})} \quad (5.35)$$

$$\epsilon_{z_p\zeta} = \arctan \left\{ \frac{\left\{ \left(\frac{z_a}{\zeta_a}\right) \sin \epsilon_{z\zeta} - x_{dp} \left(\frac{\theta_a}{\zeta_a}\right) \sin \epsilon_{\theta\zeta} \right\}}{\left\{ \left(\frac{z_a}{\zeta_a}\right) \cos \epsilon_{z\zeta} - x_{dp} \left(\frac{\theta_a}{\zeta_a}\right) \cos \epsilon_{\theta\zeta} \right\}} \right\} \quad (5.36)$$

5.1.8 Relative Horizontal Velocity at pontoons

$$u_r(t) = u(t) - \dot{x}(t) \quad (5.37a)$$

$$u_{rp}(t) = u_p(t) - \dot{x}_p(t) \quad (5.37b)$$

$$u_{rp}(t) = u_{rpa} \cos(\omega t + \epsilon_{urp\dot{x}_p}) \quad (5.37c)$$

$$u_p(t) = u_{pa} \cos(\omega t + \epsilon_{up\zeta}) \quad (5.38a)$$

$$x_p(t) = x_{pa} \cos(\omega t + \epsilon_{xp\zeta}) \quad (5.38b)$$

$$\dot{x}_p(t) = \dot{x}_{pa} \cos(\omega t + \epsilon_{\dot{x}_p\zeta}) \quad (5.38c)$$

$$\text{where } \epsilon_{\dot{x}_p\zeta} = \left(\epsilon_{xp\zeta} + \frac{\pi}{2} \right)$$

$$u_{rpa} = \zeta_{pa} \omega \sqrt{1 + \left(\frac{x_{pa}}{\zeta_{pa}}\right)^2 - 2 \left(\frac{x_{pa}}{\zeta_{pa}}\right) \cos(\epsilon_{up\zeta} - \epsilon_{xp\zeta})} \quad (5.39)$$

$$\epsilon_{urp\dot{x}_p} = \arctan \left\{ \frac{\left\{ \sin \epsilon_{up\zeta} - \left(\frac{x_{pa}}{\zeta_{pa}}\right) \sin \epsilon_{xp\zeta} \right\}}{\left\{ \cos \epsilon_{up\zeta} - \left(\frac{x_{pa}}{\zeta_{pa}}\right) \cos \epsilon_{xp\zeta} \right\}} \right\} \quad (5.40)$$

5.1.9 Viscous Mean Drift Forces on a Column

Waves Only; Splash Zone

$$F_{D0X} = \frac{2}{3\pi} \rho C_{D0X} D g k \zeta_{rca}^3 \cos(\epsilon_{\zeta_{rcz_c}} - \epsilon_{u_{rc\dot{x}_c}}) \quad (5.41)$$

Waves and Currents; Splash Zone

For $|U| \geq u_{rca}$:

$$F_{D0X} = \frac{1}{2} \rho C_{D0} D \zeta_{rca} u_{rca}^2 \gamma_{rc} \cos(\epsilon_{\zeta_{rcz_c}} - \epsilon_{u_{rc\dot{x}_c}}) \quad (5.42)$$

For $|U| < u_{rca}$:

$$\begin{aligned} F_{D0X} = & \frac{1}{2\pi} \rho C_{D0} D \zeta_{rca} u_{rca}^2 \left[\frac{1}{6} \{ \sin 3\Theta \cos(\epsilon_{\zeta_{rcz_c}} + 2\epsilon_{u_{rc\dot{x}_c}}) + \right. \\ & 3 \sin \Theta \cos(\epsilon_{\zeta_{rcz_c}} - 2\epsilon_{u_{rc\dot{x}_c}}) + 6 \sin \Theta \cos \epsilon_{\zeta_{rcz_c}} \} + \\ & \left. \gamma_{rc} \{ (2\Theta - \pi) \cos(\epsilon_{\zeta_{rcz_c}} - \epsilon_{u_{rc\dot{x}_c}}) + \sin 2\Theta \cos(\epsilon_{\zeta_{rcz_c}} + \epsilon_{u_{rc\dot{x}_c}}) \} \right] + \end{aligned}$$

$$2 \gamma_{rc}^2 (\sin \Theta \cos \epsilon_{\zeta_{rc} z_c}) \quad (5.43a)$$

$$= \frac{1}{2\pi} \rho C_{D0} D \zeta_{rca} u_{rca}^2 (d_1 + d_2 + d_3) \quad (5.43b)$$

where

$$d_1 = \frac{1}{6} [\sin 3\Theta \cos(\epsilon_{\zeta_{rc} z_c} + 2\epsilon_{u_{rc} \dot{x}_c}) + 3 \sin \Theta \{\cos(\epsilon_{\zeta_{rc} z_c} - 2\epsilon_{u_{rc} \dot{x}_c}) + 2 \cos \epsilon_{\zeta_{rc} z_c}\}]$$

$$d_2 = \gamma_{rc} \{(2\Theta - \pi) \cos(\epsilon_{\zeta_{rc} z_c} - \epsilon_{u_{rc} \dot{x}_c}) + \sin 2\Theta \cos(\epsilon_{\zeta_{rc} z_c} + \epsilon_{u_{rc} \dot{x}_c})\}$$

$$d_3 = 2 \gamma_{rc}^2 (\sin \Theta \cos \epsilon_{\zeta_{rc} z_c})$$

Waves and Currents; Submerged Zone

For $|U| \geq u_{rca}$:

$$F_{D0X} = \frac{1}{2} \rho C_{D0} D \left(\frac{1}{2} u_{rca}^2 + U^2 \right) \quad (5.44a)$$

$$= \frac{1}{2} \rho C_{D0} D u_{rca}^2 \left(\frac{1}{2} + \frac{U^2}{u_{rca}^2} \right) \quad (5.44b)$$

$$= \frac{1}{2} \rho C_{D0} D u_{rca}^2 \left(\frac{1}{2} + \gamma_{rc}^2 \right) \quad (5.44c)$$

For $|U| < u_{rca}$:

$$F_{D0X} = \frac{1}{2\pi} \rho C_{D0} D u_{rca}^2 \left[\frac{1}{2} \{(2\Theta - \pi) + \sin 2\Theta \cos 2\epsilon_{u_{rc} \dot{x}_c}\} + 4 \gamma_{rc} \sin \Theta \cos \epsilon_{u_{rc} \dot{x}_c} + \gamma_{rc}^2 (2\Theta - \pi) \right] \quad (5.45a)$$

$$= \frac{1}{2\pi} \rho C_{D0} D u_{rca}^2 (d_1 + d_2 + d_3) \quad (5.45b)$$

where

$$d_1 = \frac{1}{2} \{(2\Theta - \pi) + \sin 2\Theta \cos 2\epsilon_{u_{rc} \dot{x}_c}\}$$

$$d_2 = 4 \gamma_{rc} \sin \Theta \cos \epsilon_{u_{rc} \dot{x}_c}$$

$$d_3 = \gamma_{rc}^2 (2\Theta - \pi)$$

5.1.10 Viscous Mean Drift Forces on a Pontoon

Waves and Currents

The viscous effects on a pontoon are only considered in the presence of currents, i.e. in a wave-current coexisting flow field.

This case is different and is due to the projected area of the triangular faces of the pontoon. As the relative horizontal fluid velocity would be different along the length of the pontoon, the force would be calculated for a number of small strips with their resulting projected area and calculating the relative horizontal fluid velocity at the middle of each strip including the proper vertical motions at the exponential term.

The projected area of one triangular end is $A_P = b \times h$. So, the ΔA_P for a small strip of length Δx is $\Delta A_P = \frac{(b \times h)}{l_e} \Delta x$ where $\Delta x = \frac{l_e}{N}$ where N is the number of small strips. So, $\Delta A_P = \frac{(b \times h)}{N}$ thus resulting in $A_P = \sum_{i=1}^N \Delta A_P$. Furthermore, as u_{rpa} is a function of x , it is to be calculated for both positive and negative x .

$$F_{DX}(t) = \frac{1}{2} \rho C_{DX} \sum_{i=1}^N \Delta A_P (u_{rp} + U) | (u_{rp} + U) | \quad (5.46)$$

For $|U| \geq u_{rpa}$:

$$F_{D0X} = \frac{1}{2} \rho C_{D0X} \sum_{i=1}^N \Delta A_P \left(\frac{1}{2} u_{rpa}^2 + U^2 \right) \quad (5.47a)$$

$$= \frac{1}{2} \rho C_{D0X} \sum_{i=1}^N \Delta A_P u_{rpa}^2 \left(\frac{1}{2} + \frac{U^2}{u_{rpa}^2} \right) \quad (5.47b)$$

$$= \frac{1}{2} \rho C_{D0X} \sum_{i=1}^N \Delta A_P u_{rpa}^2 \left(\frac{1}{2} + \gamma_{rp}^2 \right) \quad (5.47c)$$

For $|U| < u_{rpa}$:

$$F_{D0X} = \frac{1}{2\pi} \rho C_{D0X} \sum_{i=1}^N \Delta A_P u_{rpa}^2 \left[\frac{1}{2} \{ (2\Theta - \pi) + \sin 2\Theta \cos 2\epsilon_{u_{rp}\dot{x}_p} \} + 4 \gamma_{rp} \sin \Theta \cos \epsilon_{u_{rp}\dot{x}_p} + \gamma_{rp}^2 (2\Theta - \pi) \right] \quad (5.48a)$$

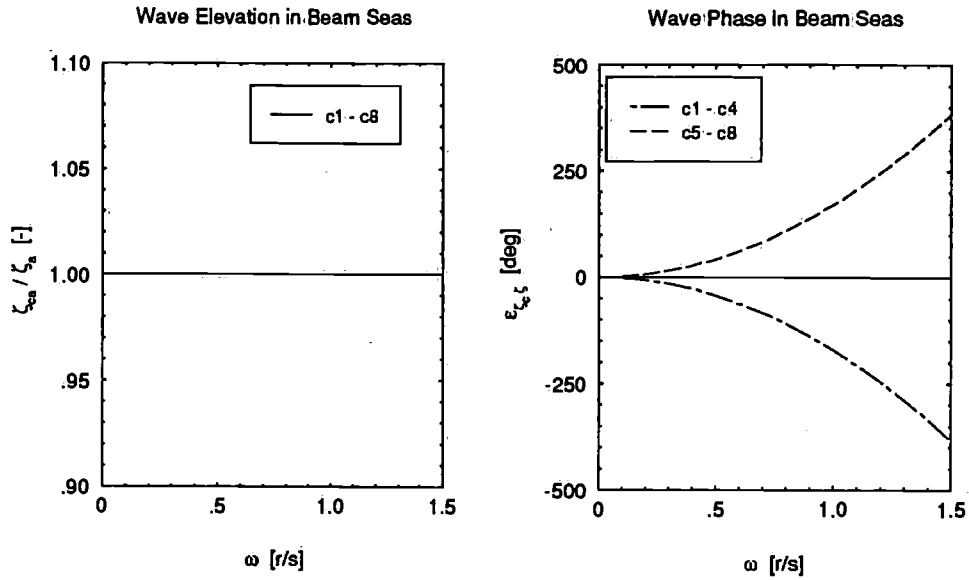


Figure 5.6: Undisturbed wave elevation and phases at the columns

$$= \frac{1}{2\pi} \rho C_{D0X} \sum_{i=1}^N \Delta A_P u_{rpa}^2 (d_1 + d_2 + d_3) \quad (5.48b)$$

where

$$\begin{aligned} d_1 &= \frac{1}{2} \{ (2\Theta - \pi) + \sin 2\Theta \cos 2\epsilon_{u_{rp}\dot{x}_p} \} \\ d_2 &= 4 \gamma_{rp} \sin \Theta \cos \epsilon_{u_{rp}\dot{x}_p} \\ d_3 &= \gamma_{rp}^2 (2\Theta - \pi) \end{aligned}$$

5.2 Viscous Mean Drift Forces in Beam Seas

The basic derivations for wave kinematics, horizontal motions and vertical motions and consequently the relative horizontal velocity and relative wave elevation are similar to head seas. The details are not produced again.

Figure 5.6 and Figure 5.7 show the RAOs and phases of undisturbed wave elevation and horizontal water particle velocities at columns in beam seas.

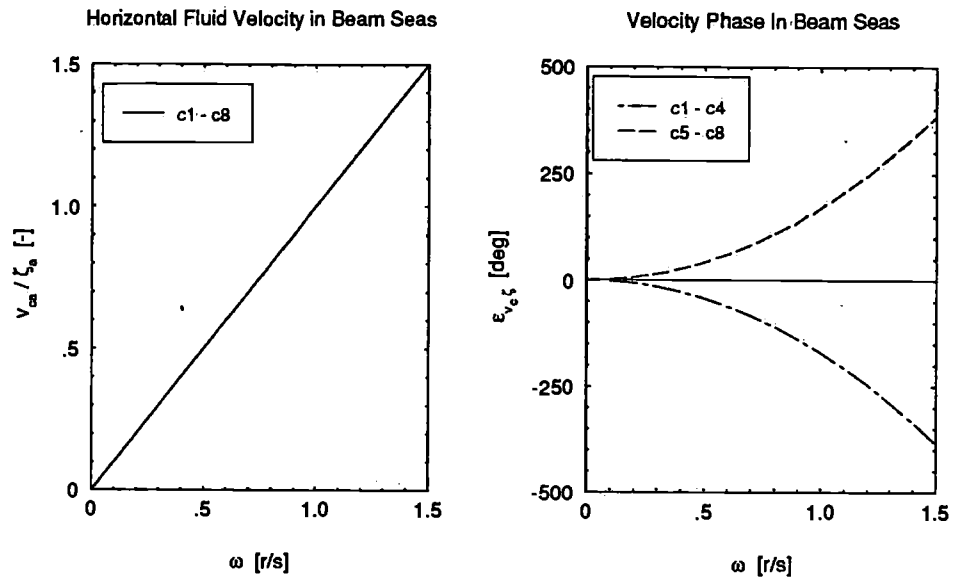


Figure 5.7: Undisturbed fluid velocities and phases at the columns

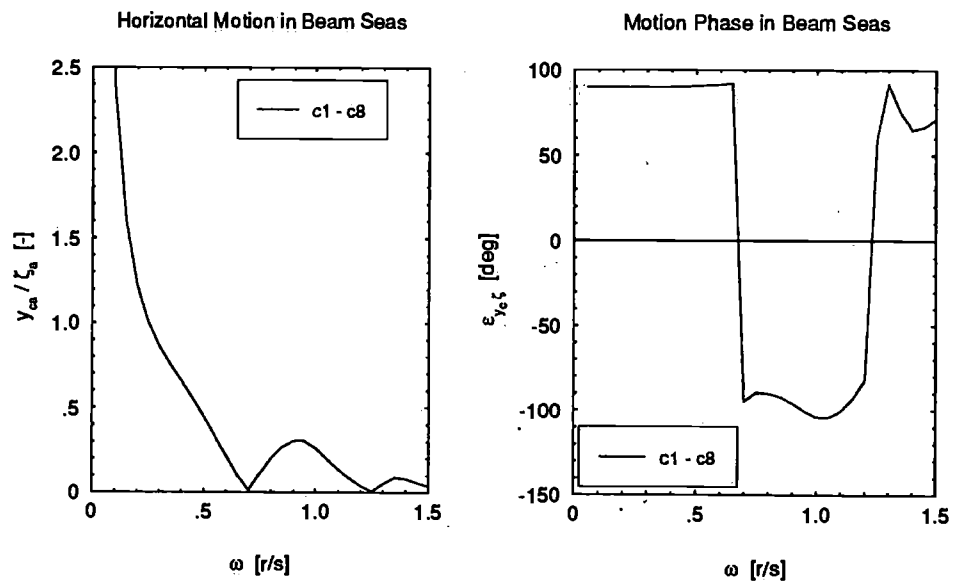


Figure 5.8: Horizontal motions and phases at the columns

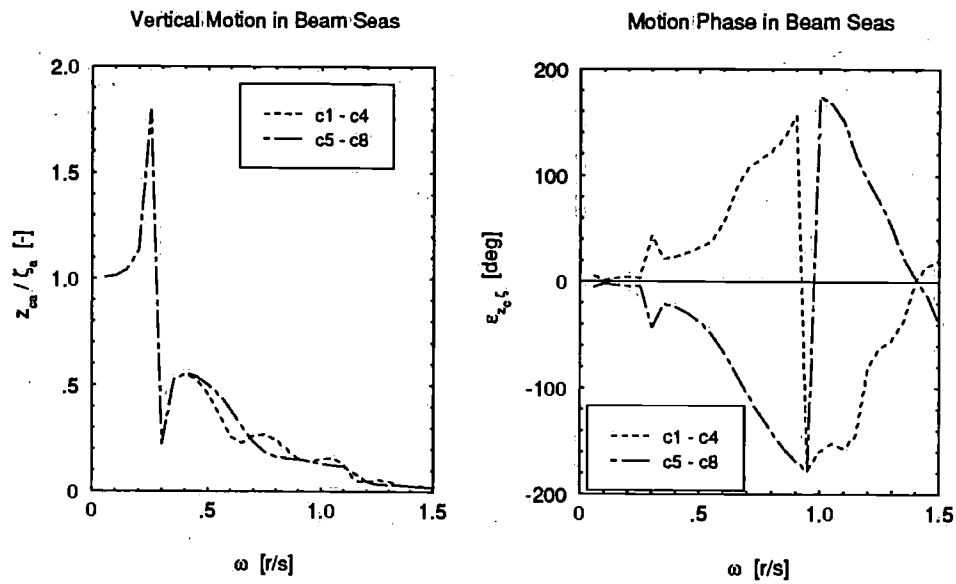


Figure 5.9: Vertical motions and phases at the columns

Figure 5.8 and Figure 5.9 show the RAOs and phases of horizontal and vertical motions at the free surface of the respective columns in beam seas.

5.2.1 Viscous Mean Drift Forces on a Column

Waves Only; Splash Zone

$$F_{D0Y} = \frac{2}{3\pi} \rho C_{D0} D g k \zeta_{rca}^3 \cos(\epsilon_{\zeta_{rc}z_c} - \epsilon_{v_{rc}\dot{y}_c}) \quad (5.49)$$

Waves and Currents; Splash Zone

For $|U| \geq v_{rca}$:

$$F_{D0Y} = \frac{1}{2} \rho C_{D0} D \zeta_{rca} v_{rca}^2 \gamma_{rc} \cos(\epsilon_{\zeta_{rc}z_c} - \epsilon_{v_{rc}\dot{y}_c}) \quad (5.50)$$

For $|U| < v_{rca}$:

$$F_{D0Y} = \frac{1}{2\pi} \rho C_{D0} D \zeta_{rca} v_{rca}^2 \left[\frac{1}{6} \{ \sin 3\Theta \cos(\epsilon_{\zeta_{rc}z_c} + 2\epsilon_{v_{rc}\dot{y}_c}) + 3 \sin \Theta \cos(\epsilon_{\zeta_{rc}z_c} - 2\epsilon_{v_{rc}\dot{y}_c}) + 6 \sin \Theta \cos \epsilon_{\zeta_{rc}z_c} \} + \right]$$

$$\gamma_{rc} \left\{ (2\Theta - \pi) \cos(\epsilon_{\zeta_{rc}z_c} - \epsilon_{v_{rc}y_c}) + \sin 2\Theta \cos(\epsilon_{\zeta_{rc}z_c} + \epsilon_{v_{rc}y_c}) \right\} + 2\gamma_{rc}^2 (\sin \Theta \cos \epsilon_{\zeta_{rc}z_c}) \quad (5.51a)$$

$$= \frac{1}{2\pi} \rho C_{D0} D \zeta_{rca} v_{rca}^2 (d_1 + d_2 + d_3) \quad (5.51b)$$

where

$$d_1 = \frac{1}{6} [\sin 3\Theta \cos(\epsilon_{\zeta_{rc}z_c} + 2\epsilon_{v_{rc}y_c}) + 3 \sin \Theta \{ \cos(\epsilon_{\zeta_{rc}z_c} - 2\epsilon_{v_{rc}y_c}) + 2 \cos \epsilon_{\zeta_{rc}z_c} \}]$$

$$d_2 = \gamma_{rc} \{ (2\Theta - \pi) \cos(\epsilon_{\zeta_{rc}z_c} - \epsilon_{v_{rc}y_c}) + \sin 2\Theta \cos(\epsilon_{\zeta_{rc}z_c} + \epsilon_{v_{rc}y_c}) \}$$

$$d_3 = 2\gamma_{rc}^2 (\sin \Theta \cos \epsilon_{\zeta_{rc}z_c})$$

Waves and Currents; Submerged Zone

For $|U| \geq v_{rca}$:

$$F_{D0Y} = \frac{1}{2} \rho C_{D0} D \left(\frac{1}{2} v_{rca}^2 + U^2 \right) \quad (5.52a)$$

$$= \frac{1}{2} \rho C_{D0} D v_{rca}^2 \left(\frac{1}{2} + \frac{U^2}{v_{rca}^2} \right) \quad (5.52b)$$

$$= \frac{1}{2} \rho C_{D0} D v_{rca}^2 \left(\frac{1}{2} + \gamma_{rc}^2 \right) \quad (5.52c)$$

For $|U| < v_{rca}$:

$$F_{D0Y} = \frac{1}{2\pi} \rho C_{D0} D v_{rca}^2 \left[\frac{1}{2} \{ (2\Theta - \pi) + \sin 2\Theta \cos 2\epsilon_{v_{rc}y_c} \} + 4\gamma_{rc} \sin \Theta \cos \epsilon_{v_{rc}y_c} + \gamma_{rc}^2 (2\Theta - \pi) \right] \quad (5.53a)$$

$$= \frac{1}{2\pi} \rho C_{D0} D v_{rca}^2 (d_1 + d_2 + d_3) \quad (5.53b)$$

where

$$d_1 = \frac{1}{2} \{ (2\Theta - \pi) + \sin 2\Theta \cos 2\epsilon_{v_{rc}y_c} \}$$

$$d_2 = 4\gamma_{rc} \sin \Theta \cos \epsilon_{v_{rc}y_c}$$

$$d_3 = \gamma_{rc}^2 (2\Theta - \pi)$$

5.2.2 Viscous Mean Drift Forces on a Pontoon

5.2.3 Waves and Currents

Similar to head seas, the origin of viscous drift forces is considered only in a wave-current coexisting flow field. Relative horizontal velocity along with the effects of vertical motions at the exponential term will be considered.

$$F_{DY}(t) = \frac{1}{2} \rho C_{DY} (l \times h) (v_{rp} + U) | (v_{rp} + U) | \quad (5.54)$$

For $|U| \geq v_{rpa}$:

$$F_{D0Y} = \frac{1}{2} \rho C_{D0Y} (l \times h) \left(\frac{1}{2} v_{rpa}^2 + U^2 \right) \quad (5.55a)$$

$$= \frac{1}{2} \rho C_{D0Y} (l \times h) v_{rpa}^2 \left(\frac{1}{2} + \frac{U^2}{v_{rpa}^2} \right) \quad (5.55b)$$

$$= \frac{1}{2} \rho C_{D0Y} (l \times h) v_{rpa}^2 \left(\frac{1}{2} + \gamma_{rp}^2 \right) \quad (5.55c)$$

For $|U| < v_{rpa}$:

$$F_{D0Y} = \frac{1}{2\pi} \rho C_{D0Y} (l \times h) v_{rpa}^2 \left[\frac{1}{2} \{ (2\Theta - \pi) + \sin 2\Theta \cos 2\epsilon_{v_{rp}\dot{y}_p} \} + 4\gamma_{rp} \sin \Theta \cos \epsilon_{v_{rp}\dot{y}_p} + \gamma_{rp}^2 (2\Theta - \pi) \right] \quad (5.56a)$$

$$= \frac{1}{2\pi} \rho C_{D0Y} (l \times h) v_{rpa}^2 (d_1 + d_2 + d_3) \quad (5.56b)$$

where

$$d_1 = \frac{1}{2} \{ (2\Theta - \pi) + \sin 2\Theta \cos 2\epsilon_{v_{rp}\dot{y}_p} \}$$

$$d_2 = 4\gamma_{rp} \sin \Theta \cos \epsilon_{v_{rp}\dot{y}_p}$$

$$d_3 = \gamma_{rp}^2 (2\Theta - \pi)$$

5.3 Low Frequency Viscous Drift Forces

In the foregoing mathematical model, it was shown that the viscous mean drift forces in regular waves can be treated in the frequency domain by

calculating the same for each column with its respective relative horizontal velocity and relative vertical wave surface elevation using the appropriate mean drift force coefficient. Summing up all the contributions, the total viscous mean drift force on a moored semi-submersible is then obtained. In the presence of currents, additional contributions from the submerged pontoon are to be included in order to compute the total viscous mean drift force in a wave-current coexisting flow field.

In irregular waves, due to the difference frequencies, the low frequency phenomenon exists. The computations cannot be handled accurately in the frequency domain due to the highly nonlinear (cubic) nature of the transfer functions in a waves only flow field. In the presence of currents, even the qtf's do not show any linearity. In order to remove these difficulties, the frequency domain approach often used in dealing with only potential effects in the mean and low frequency wave drift forces is avoided and instead, the time domain approach will be adopted for the low frequency viscous drift forces.

The fundamental concept is still based on the Morison equation approach for the local drag force combined with a relative horizontal velocity and relative wave surface elevation. Effects of angular motions are well taken into account while calculating the horizontal and vertical motions at any point on the centerline of the columns and the pontoons.

The viscous contribution to the drift force in the time domain will then be determined from the following relation:

$$F_{vis}(t) = \frac{1}{2} \rho C_{D0}(t) D \zeta_r(t) u_r(t) |u_r(t)| \quad (5.57)$$

From the foregoing regular wave transfer functions at columns, for any arbitrary time records of input waves relating to any sea spectrum, time records of the relative wave elevation and relative horizontal velocity can be generated using the FFT technique. Similar to regular waves, the total viscous drift force on a semi-submersible is thus obtained after all the individual contributions are added. Finally, all traces of the signals generated by the FFT and the measured irregular sea records will be subject to a lpf (low pass filter). The computed signals of the potential (wave drift force) and viscous (viscous drift force) contributions will be added together (samplewise) and then be compared with the measured low frequency drift force.

The effect of currents on the viscous contribution to the drift force can be taken into account by adding the current velocity to the relative horizontal

velocity.

In Figure 5.11 and Figure 5.12, the computed low frequency potential and viscous drift force on the floating ITTC semi-submersible in irregular waves in head seas and beam seas respectively is shown. The magnitude of the low frequency viscous drift force is quite large compared to the low frequency wave (potential) drift force especially in the region where higher wave groups are present. However, such large magnitude is based on a constant value of the mean drag coefficient of unity which has been followed in many work. But it is essential that such low frequency viscous drift forces need to be treated with appropriate mean drag coefficients at each column depending on the slowly varying wave kinematics.

5.3.1 Hydrodynamic Parameters

One noticeable thing in Equation 5.57 is the expression of the mean drag coefficient in the time domain. In regular waves, it is quite straightforward to deal with the mean drag coefficient with its controlling hydrodynamic parameters using regular wave kinematics like wave frequency, wave amplitude, current velocity, etc. In the case of floating bodies, relative horizontal velocity based on the wave frequency motions can again be used for calculating the relevant hydrodynamic parameters.

On the other hand, in irregular waves the amplitude of the motion of water particles changes in each wave cycle. It is not convenient to define a certain N_{K-C} through the measured waves of a particular seastate. In addition, in the low frequency domain, it is further complicated by the presence of a slowly varying wave envelope with its associated frequencies.

It is possible to modify the Keulegan-Carpenter number by replacing the maximum horizontal velocity u_a by significant wave height H_s and peak wave frequency ω_p (Li and Kang 1992). For a particular sea spectrum, this approach will produce a single value of the mean drag coefficient. For a large number of wave spectra of varied H_s and ω_p with different geometries, this approach may be suitable to deal with first order force coefficients in irregular waves. This does not take any account of the low frequency phenomenon present in the hydrodynamic field. On the other hand Otsuka *et al.* (1990) proposed an alternative approach for irregular waves. If the original definition of N_{K-C} is retained, that is, defining it in terms of each half wave cycle for an irregular wave, then the Keulegan-Carpenter number can be defined in terms of the moving distance of water particles in each swing. The approach is similar to the building block method of dealing with slowly

varying drift force in irregular waves by Hsu and Blenkarn (1970). But still such definitions will not be sufficient while dealing with the low frequency phenomenon. Perhaps these approaches might be suitable for treating first order forces in irregular waves in connection with expressing first order force coefficients like C_M and C_D . In literature, no other formulations are available regarding any other kind of definition of appropriate hydrodynamic parameters associated with the low frequency behavior of a floating body like semi-submersibles.

The slowly varying wave envelope with its associated frequencies can then be used to calculate the appropriate hydrodynamic parameters. Formulations are given below for calculating the wave envelope and its associated frequencies (Pinkster 1974).

An irregular, long-crested sea may be considered as the sum of a large number of regular wave components:

$$\zeta(t, x) = \sum_{i=1}^N \zeta_i \cos(\omega_i t - k_i x + \varepsilon_i) \quad (5.58)$$

This expression may also be written as follows:

$$\zeta(t, x) = A(t, x) \cos\{\omega_0 t + \varepsilon(t, x)\} \quad (5.59)$$

where the wave envelope is expressed by

$$A(t, x) = \left[\sum_{i=1}^N \sum_{j=1}^N \zeta_i \zeta_j \cos\{(\omega_i - \omega_j)t - (k_i - k_j)x + (\varepsilon_i - \varepsilon_j)\} \right]^{\frac{1}{2}} \quad (5.60)$$

$$\varepsilon(t, x) = \arctan \left[\frac{\sum_{i=1}^N \zeta_i \sin\{(\omega_i - \omega_0)t - k_i x + \varepsilon_i\}}{\sum_{i=1}^N \zeta_i \cos\{(\omega_i - \omega_0)t - k_i x + \varepsilon_i\}} \right] \quad (5.61)$$

If the spectral density of the irregular waves is narrow, i.e. if the highest and the lowest frequencies present in the waves differ only slightly from some centrally chosen frequency ω_0 , then the wave envelope amplitude $A(t, x)$ and its phase $\varepsilon(t, x)$ are of a slowly varying form.

From the above expression, the slowly varying wave frequency $\omega(t, x)$ can be defined as follows:

$$\omega(t, x) = \omega_0 + \frac{\partial \varepsilon(t, x)}{\partial t} \quad (5.62)$$

Equation 5.62 leads to the following

$$\omega(t, x) = \frac{\sum_{i=1}^N \sum_{j=1}^N \zeta_i \zeta_j \frac{(\omega_i + \omega_j)}{2} \cos\{(\omega_i - \omega_j)t - (k_i - k_j)x + (\varepsilon_i - \varepsilon_j)\}}{\sum_{i=1}^N \sum_{j=1}^N \zeta_i \zeta_j \cos\{(\omega_i - \omega_j)t - (k_i - k_j)x + (\varepsilon_i - \varepsilon_j)\}} \quad (5.63)$$

In Figure 5.10 the wave envelope, without and with lpf, is shown for a measured time record. Further shown are the associated frequencies and the wave steepness. Using the above mentioned slowly varying wave kinematics, hydrodynamic parameters like the viscous parameter, diffraction parameter and the Keulegan-Carpenter number can be obtained for the respective columns to ascertain the values of the mean drag coefficients including the fact that the time derivative of the low frequency motion is negligible in the relative velocity term.

5.4 Low Frequency Wave Drift Forces

The mean low frequency wave drift forces due to potential effects are computed with 3-dimensional theory using the direct integration method (Pinkster 1980). By this method the wave drift forces are found from the second order term in the following expression for the hydrodynamic forces:

$$\vec{F}^1 = - \int \int_S p \vec{N} dS \quad (5.64)$$

The expression of the second order wave forces:

$$\begin{aligned} \vec{F}^2 = & - \int_{WL} \frac{1}{2} \rho g \zeta_r^{(1)2} \vec{n} dl + \vec{\alpha} \times (M \ddot{X}_g^{(1)}) \\ & - \int \int_{S_0} - \frac{1}{2} \rho |\vec{\nabla} \phi^{(1)}|^2 \vec{n} dS - \int \int_{S_0} \rho (\vec{X}^{(1)} \vec{\nabla} \phi_t^{(1)}) \vec{n} dS \\ & - \int \int_{S_0} \rho (\phi_{wt}^{(2)} + \phi_{dt}^{(2)}) \vec{n} dS \end{aligned} \quad (5.65)$$

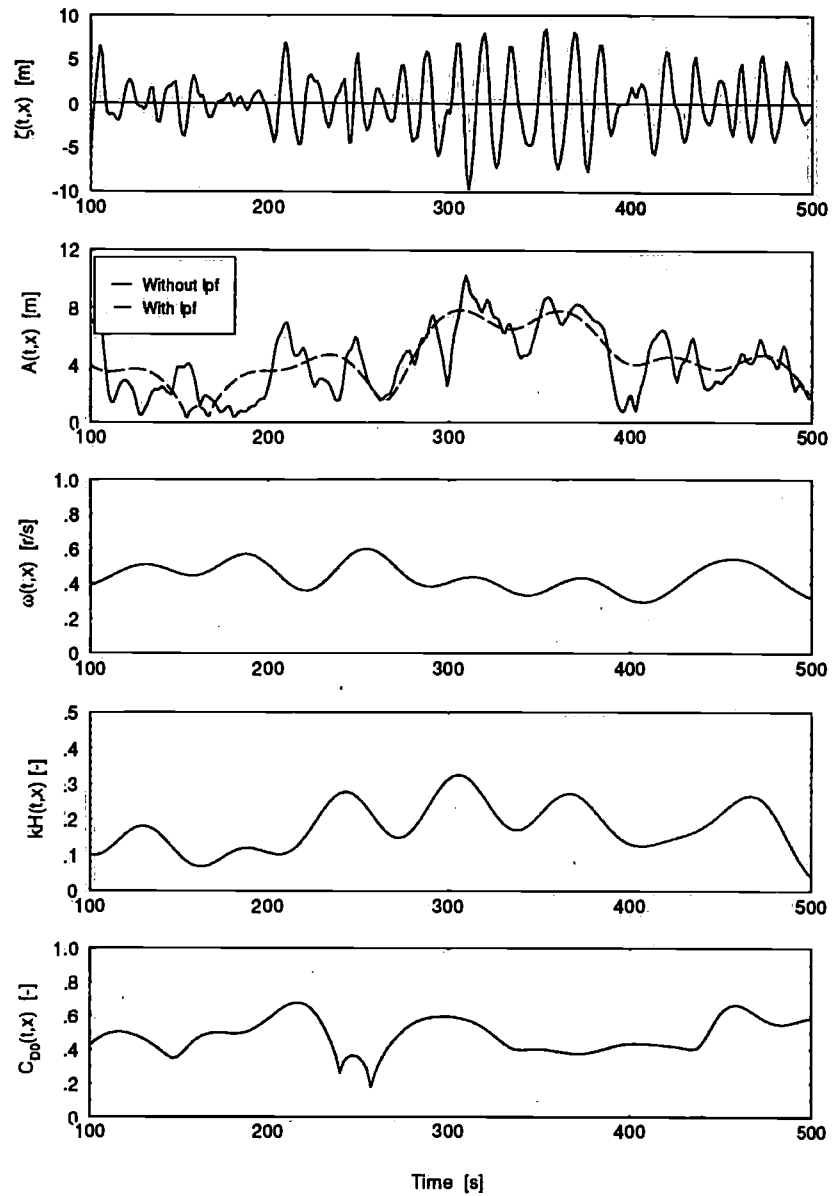


Figure 5.10: *Wave kinematics of slowly varying wave envelope, wave frequency, wave steepness and mean drag coefficient in irregular waves for a particular column of a semi-submersible*

It is convenient to use Equation 5.65 to compute frequency domain transfer functions which, in turn can be transformed into time domain second order impulse response functions. These second order impulse response functions when convoluted with the undisturbed wave train, produce time records of the second order drift force (Dalzell 1976).

5.4.1 Quadratic Transfer Functions

From the aforesaid, it follows that the total second order force in waves contains the following components:

I: Relative wave height contribution

$$-\frac{1}{2} \rho g \int_{WL} \zeta_r^{(1)2} \bar{n} d\ell$$

II: Pressure drop contribution due to velocity squared

$$-\frac{1}{2} \rho \iint_{S_0} -|\vec{\nabla} \phi^{(1)}|^2 \bar{n} dS$$

III: Pressure contribution due to the product of gradient of first order pressure and first order motion

$$-\rho \iint_{S_0} (\vec{X}^{(1)} \vec{\nabla} \phi_t^{(1)}) \bar{n} dS$$

IV: Pressure due to the product of angular motion and inertia forces

$$\vec{\alpha} \times (M \ddot{X}_g^{(1)})$$

V: Contribution due to the second order potential

$$-\rho \iint_{S_0} (\phi_{w_t}^{(2)} + \phi_{d_t}^{(2)}) \bar{n} dS$$

The procedure to obtain the qtfs of the forces dependent on first order quantities (*I*, *II*, *III*, *IV*) will be illustrated by taking the low frequency part of the longitudinal component of the force contribution due to the relative wave elevation:

$$F_{1r}^{(2)} = F_{1r}^{(2)}(t) = - \int_{WL} \frac{1}{2} \rho g \zeta_r^{(1)2}(t, \ell) n_1(\ell) d\ell \quad (5.66)$$

In irregular long crested waves the elevation, to first order, of the incoming undisturbed waves, referred to the mean position of the cog of a floating body, may be written as:

$$\zeta^{(1)}(t) = \sum_{i=1}^N \zeta_i^{(1)} \cos(\omega_i t + \varepsilon_i) \quad (5.67)$$

The first order relative wave elevation at a point ℓ on the waterline of the body may be written as:

$$\zeta_r^{(1)}(t, \ell) = \sum_{i=1}^N \zeta_i^{(1)} \zeta_{r_i}^{(1)'}(\ell) \cos\{\omega_i t + \varepsilon_i + \varepsilon_{r_i}(\ell)\} \quad (5.68)$$

Substituting Equation 5.68 in Equation 5.66 leads to the following:

$$\begin{aligned} F_{1I}^{(2)}(t) = & \sum_{i=1}^N \sum_{j=1}^N \zeta_i^{(1)} \zeta_j^{(1)} P_{ijI} \cos\{(\omega_i - \omega_j)t + (\varepsilon_i - \varepsilon_j)\} + \\ & \sum_{i=1}^N \sum_{j=1}^N \zeta_i^{(1)} \zeta_j^{(1)} Q_{ijI} \sin\{(\omega_i - \omega_j)t + (\varepsilon_i - \varepsilon_j)\} + \\ & \text{high frequency terms} \end{aligned} \quad (5.69)$$

where P_{ijI} and Q_{ijI} are the in-phase and out-of-phase components of the time dependent transfer function with:

$$P_{ijI} = P_I(\omega_i, \omega_j) = \int_{WL} \frac{1}{4} \rho g \zeta_{r_i}'(\ell) \zeta_{r_j}'(\ell) \cos\{\varepsilon_{r_i}(\ell) - \varepsilon_{r_j}(\ell)\} n_1(\ell) d\ell \quad (5.70)$$

$$Q_{ijI} = Q_I(\omega_i, \omega_j) = - \int_{WL} \frac{1}{4} \rho g \zeta_{r_i}'(\ell) \zeta_{r_j}'(\ell) \sin\{\varepsilon_{r_i}(\ell) - \varepsilon_{r_j}(\ell)\} n_1(\ell) d\ell \quad (5.71)$$

Taking the low frequency part of the square of the wave elevation given by Equation 5.67 results in:

$$\zeta^{(1)2}(t)_\ell = \sum_{i=1}^N \sum_{j=1}^N \frac{1}{2} \zeta_i^{(1)} \zeta_j^{(1)} \cos\{(\omega_i - \omega_j)t + (\varepsilon_i - \varepsilon_j)\} \quad (5.72)$$

Comparison with Equation 5.69 shows that P_{ijI} and Q_{ijI} are transfer functions which give that part of the wave drifting force which is in-phase

and out-of-phase respectively with the low frequency part of the square of the incident wave elevation.

It will be clear that similar developments can be made for other contributions to the wave drifting forces which depend only on first order quantities. The contribution V due to second order potentials is approximated using results of first order wave loads (Pinkster 1980). The total in-phase and out-of-phase transfer functions are found by simple summation of the contributions from the five components. The wave drifting forces may thus be represented as transfer functions which, as can be seen from the foregoing, are a function of two frequencies. In general, the qtf's will also be functions of the direction of the waves.

Based on a wave elevation as given by Equation 5.67 the total wave drift force is found from:

$$F_1^{(2)}(t) = \sum_{i=1}^N \sum_{j=1}^N \zeta_i^{(1)} \zeta_j^{(1)} P_{ij} \cos\{(\omega_i - \omega_j)t + (\varepsilon_i - \varepsilon_j)\} + \sum_{i=1}^N \sum_{j=1}^N \zeta_i^{(1)} \zeta_j^{(1)} Q_{ij} \sin\{(\omega_i - \omega_j)t + (\varepsilon_i - \varepsilon_j)\} \quad (5.73)$$

in which P_{ij} and Q_{ij} are found by summation of contributions I through V .

5.4.2 Drift Force in a Regular Wave Group

The first order wave elevation in a regular wave group consisting of two regular waves with frequency ω_i and ω_j is given by:

$$\zeta^{(1)}(t) = \sum_{i=1}^2 \zeta_i^{(1)} \cos(\omega_i t + \varepsilon_i) \quad (5.74a)$$

$$= \zeta_1^{(1)} \cos(\omega_1 t + \varepsilon_1) + \zeta_2^{(1)} \cos(\omega_2 t + \varepsilon_2) \quad (5.74b)$$

The second order force associated with such a wave train has the following form:

$$F_1^{(2)}(t) = \sum_{i=1}^2 \sum_{j=1}^2 \zeta_i^{(1)} \zeta_j^{(1)} P_{ij} \cos\{(\omega_i - \omega_j)t + (\varepsilon_i - \varepsilon_j)\} +$$

$$\sum_{i=1}^2 \sum_{j=1}^2 \zeta_i^{(1)} \zeta_j^{(1)} Q_{ij} \sin\{(\omega_i - \omega_j)t + (\varepsilon_i - \varepsilon_j)\} \quad (5.75a)$$

$$= \zeta_1^{(1)2} P_{11} + \zeta_2^{(1)2} P_{22} +$$

$$\zeta_1^{(1)} \zeta_2^{(1)} (P_{12} + P_{21}) \cos\{(\omega_1 - \omega_2)t + (\varepsilon_1 - \varepsilon_2)\} +$$

$$\zeta_1^{(1)} \zeta_2^{(1)} (Q_{12} - Q_{21}) \sin\{(\omega_1 - \omega_2)t + (\varepsilon_1 - \varepsilon_2)\} \quad (5.75b)$$

From Equation 5.75b it is seen that the second order forces contain two constant components. Each of these components represents the constant force which would be found if the wave train consisted of a single regular wave with frequency ω_1 or ω_2 respectively. This shows that, although the force is a non-linear phenomenon, the constant and the mean second order force in a wave train consisting of a superposition of regular waves is the sum of the mean forces found for each of the component waves. The quadratic transfer functions:

$$P_{11} = P(\omega_1, \omega_1) \quad (5.76)$$

gives the mean second order force in regular waves with frequency ω_1 . In literature dealing with the mean second order forces on floating bodies in regular or in irregular waves this is often expressed as a function dependent on one frequency ω_1 . The above equations show that the transfer function for the mean or constant part is, however, only a specific case of the general quadratic transfer function $P(\omega_1, \omega_2)$ for the force in regular wave groups.

Besides the constant parts the second order force contains low frequency parts with a frequency corresponding to the difference frequency $(\omega_1 - \omega_2)$ of the component regular waves. It is seen that the amplitudes of the in-phase and out-of-phase parts depend on the sum of the in-phase qtf's P_{12} and P_{21} and the difference of the out-of-phase functions Q_{12} and Q_{21} .

5.4.3 Symmetry of the Quadratic Transfer Functions

From Equation 5.75b it is seen that the transfer functions do not appear in isolation but rather in pairs. In general, the in-phase and out-of-phase components of the qtf's as determined from components I through IV for combinations of ω_1 and ω_2 will be so that, for instance:

$$P(\omega_1, \omega_2) \neq P(\omega_2, \omega_1) \quad (5.77)$$

However, since the force as given in Equation 5.75b depends on the sum or difference of the components of the quadratic transfer functions these may be so reformulated that the following symmetry relations are valid:

$$P(\omega_1, \omega_2) = P(\omega_2, \omega_1) \quad (5.78)$$

$$Q(\omega_1, \omega_2) = -Q(\omega_2, \omega_1) \quad (5.79)$$

The in-phase component $P(\omega_1, \omega_2)$ of the quadratic transfer function of the total second order force takes the form of a matrix which is symmetrical about the diagonal for which ω_1 is equal to ω_2 while the out-of-phase component $Q(\omega_1, \omega_2)$ is anti-symmetric about the diagonal.

5.4.4 Evaluation of the Quadratic Transfer Functions

Evaluation of the various components of the quadratic transfer functions of the low frequency wave drift forces requires detailed knowledge of the first order body motions and fluid motions. For instance, as shown by Equation 5.70 and Equation 5.71, evaluation of contribution I requires knowledge of the relative wave elevation amplitudes and phase angles around the waterline.

5.4.5 Time Domain Representation

According to Dalzell (1976), the low frequency second order forces can be computed given the qtf and the time record of the wave elevation using the following relationship:

$$F_1^{(2)}(t) = \int_{-\infty}^{+\infty} \int_{-\infty}^{+\infty} g^{(2)}(t_1, t_2) \zeta^{(1)}(t - t_1) \zeta^{(1)}(t - t_2) dt_1 dt_2 \quad (5.80)$$

The quadratic impulse response function $g^{(2)}(t_1, t_2)$ is derived from the following expression:

$$g^{(2)}(t_1, t_2) = \frac{1}{2\pi^2} \int_{-\infty}^{+\infty} \int_{-\infty}^{+\infty} e^{(i\omega_1 t_1 - i\omega_2 t_2)} G^{(2)}(\omega_1, \omega_2) d\omega_1 d\omega_2 \quad (5.81)$$

in which

$$\begin{aligned} G^{(2)}(\omega_1, \omega_2) &= \text{complex quadratic transfer function} \\ &= P(\omega_1, \omega_2) + iQ(\omega_1, \omega_2) \end{aligned} \quad (5.82)$$

From Equation 5.80 it is seen that if the quadratic impulse response function $g^{(2)}(t_1, t_2)$ is known the time record of the low frequency second order forces can be computed for arbitrary wave elevation records. The applicability of this technique has been demonstrated extensively by Dalzell (1975) using quadratic transfer functions for the second order forces obtained from tests in irregular waves using cross-bi-spectral analysis techniques.

Time records of second order wave drift forces in irregular waves can also be generated based on Equation 5.73. In such cases it is assumed that the irregular waves are described by the spectral density $S_\zeta(\omega)$. The amplitudes ζ_i are found from the following relationship:

$$\zeta_i = \sqrt{2 S_\zeta(\omega_i) \Delta\omega} \quad (5.83)$$

The phase angles ε_i are random with a homogeneous distribution function from 0 to 2π . The wave elevation follows from Equation 5.67. The wave drift force record is found from Equation 5.73.

Computational efforts for the evaluation of the wave drift force record according to Equation 5.73 can be drastically reduced by choosing equidistant frequencies ω_i to describe the wave spectrum. If the frequency step used to describe the wave spectrum is $\Delta\omega$ then the wave record and hence the wave drift force record become periodic with a period of $T = \frac{2\pi}{\Delta\omega}$.

According to Fourier's theorem the wave drift forces record can then be written in the form of a single summation as follows:

$$F_1^{(2)}(t) = \sum_{k=0}^M \{A_k \cos \omega_k t + B_k \sin \omega_k t\} \quad (5.84)$$

where $\omega_k = k \Delta\omega$ and from Equation 5.73 A_k and B_k are found to be:

$$A_k = \delta_k \sum_{j=1}^{N-k} \zeta_{j+k} \zeta_j \{P_{j+k,j} \cos(\varepsilon_{j+k} - \varepsilon_j) + Q_{j+k,j} \sin(\varepsilon_{j+k} - \varepsilon_j)\} \quad (5.85)$$

$$B_k = \delta_k \sum_{j=1}^{N-k} \zeta_{j+k} \zeta_j \{Q_{j+k,j} \cos(\varepsilon_{j+k} - \varepsilon_j) - P_{j+k,j} \sin(\varepsilon_{j+k} - \varepsilon_j)\} \quad (5.86)$$

with

$$\delta_k = 1 \text{ for } k = 0$$

$$\delta_k = 2 \text{ for } k \neq 0$$

N = number of wave frequencies used to describe the wave spectrum

$$M = N - 1$$

Use of Equation 5.84 instead of Equation 5.73 involves computing the coefficients A_k and B_k according to Equations 5.83, 5.85 and 5.86 using data on the qtf's P_{ij} and Q_{ij} . Once these coefficients are computed and stored, the time record of the wave drift force is computed from the single summation of Equation 5.84.

In Figure 5.11 and Figure 5.12, the computed low frequency wave (potential) drift force on the floating ITTC semi-submersible in irregular waves in head seas and beam seas respectively is shown.

5.5 Forces in Currents Only

The scope of this section is to provide an overview of the calculation procedures of environmental design loads due to currents, i.e. the mechanisms by which they originate hydrodynamic loads in the most conventionally used methods (empirical methods) of load calculations. Numerical estimation of steady loads like current loads is hardly possible and as such is beyond the scope of this presentation. The traditional methods widely used in the world are the Rules and Regulations of the International Classification Societies like (DnV 1990; GL 1990; ABS 1988).

The calculation of the above forces is mainly complicated by the need for an appropriate selection of non-dimensional force coefficients like drag force and lift force coefficients, shielding effects, effects of interference, etc.

5.5.1 Classification of Geometry

In the case of offshore floating platforms like semi-submersibles, there are two major buoyant items - one is the submerged hulls and the other is the surface piercing vertical columns. Other than these two major elements, there are randomly oriented horizontal and inclined circular tubes (bracing) whose main contributions are to the structural reliability and compatibility. Nevertheless, they fortunately contribute to the increased hydrodynamic viscous damping also.

The submerged hulls (often called pontoons) can be of either circular or rectangular cross-section. Sometimes, cross-sections of a rectangle with

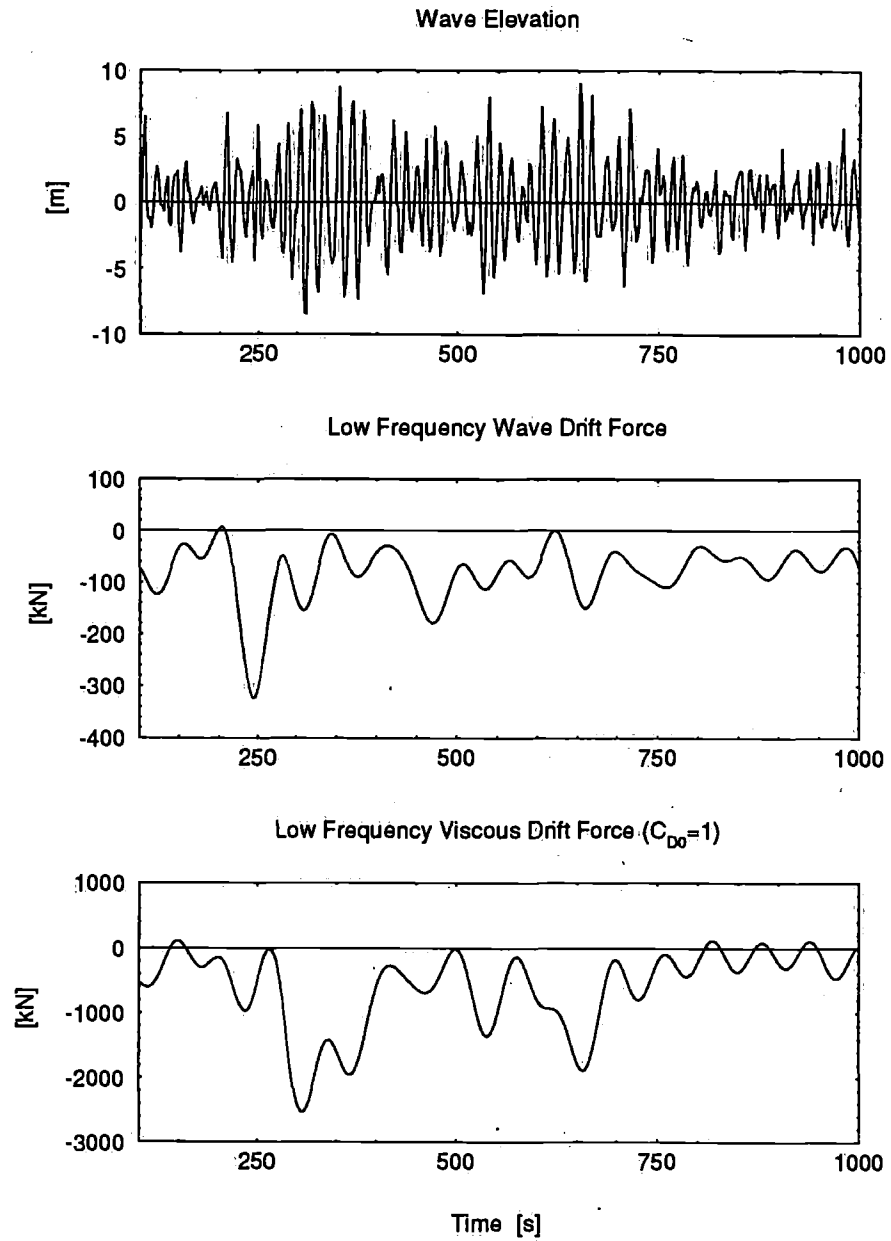


Figure 5.11: Computed low frequency wave (potential) and viscous drift forces on the moored ITTC semi-submersible in irregular head seas

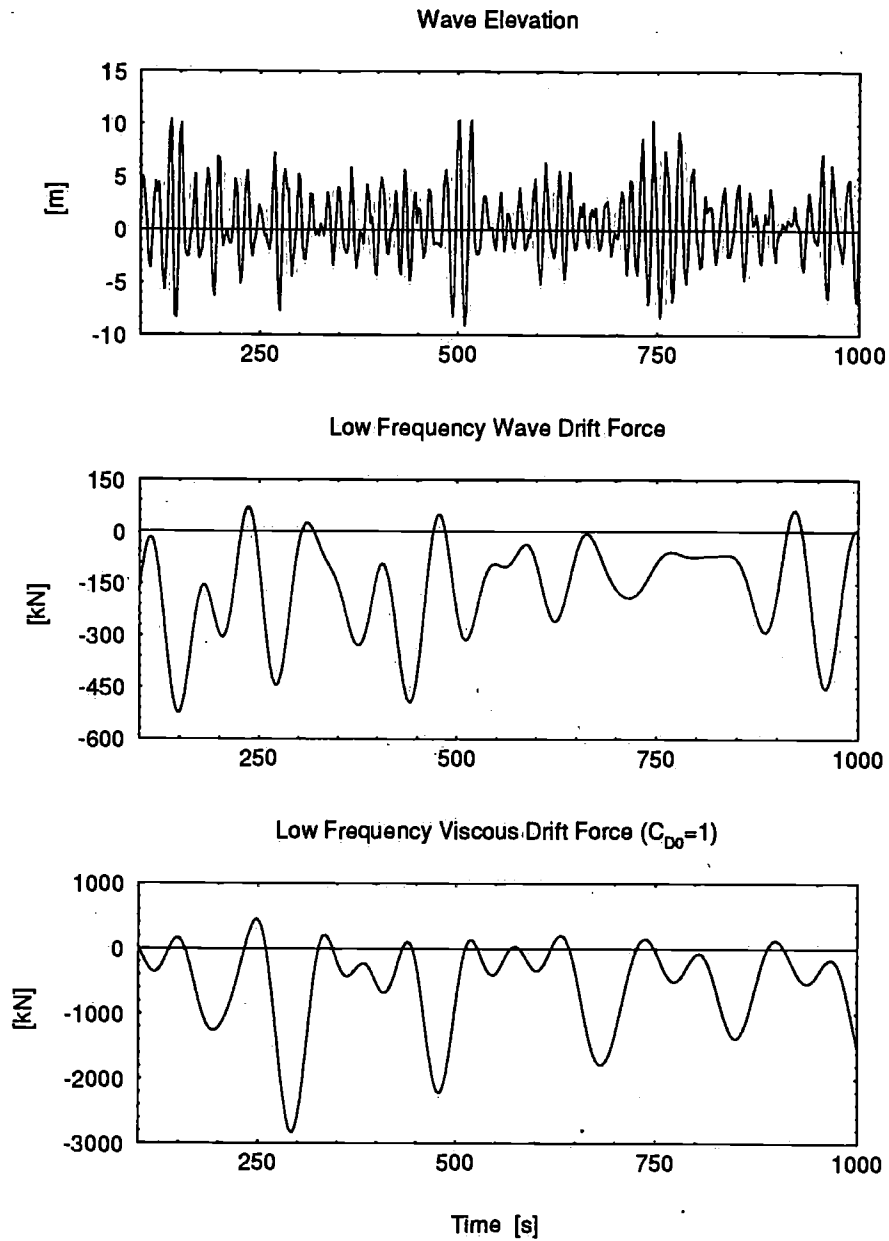


Figure 5.12: Computed low frequency wave (potential) and viscous drift forces on the moored ITTC semi-submersible in irregular beam seas

semi-circular ends are adopted. In some early designs of semi-submersibles, instead of having two hulls, a number of submerged floaters (caissons) were used. Their shapes were also cylindrical, spherical, rectangular, etc. and there were at least three of them. Such designs need more randomly oriented bracing tubes. Semi-submersibles can also have a continuous hull, e.g. a ring hull semi-submersible having columns connected to its toroidal hull.

Surface piercing vertical columns for semi-submersibles can be of either circular or rectangular cross-section.

5.5.2 System of Axes and Definitions

The earth-fixed system of axes is $O_0X_0Y_0Z_0$ which is right-handed with O_0Z_0 vertically upwards. The X_0Y_0 plane lies on the undisturbed water level.

The second system of body-fixed axes $OXYZ$ is also right-handed. The OX axis is chosen in the forward direction, the OY axis to port and the OZ axis vertically upwards through the center of gravity G of the complete floating structure. In the equilibrium condition, the OXY plane coincides with the undisturbed water level. ψ is the heading angle of the structure with respect to the earth-fixed system of axes $O_0X_0Y_0Z_0$.

With respect to the body-fixed co-ordinate system $OXYZ$, F_{DCX} and F_{DCY} are the current forces along the fixed horizontal X - and Y -axis and current moments are M_{DCX} , M_{DCY} and M_{DCZ} about the body fixed X -, Y - and Z -axis. There is also a current force along the vertical Z -axis. According to Maeda *et al.* (1985), lift forces occur at almost all current directions. Obviously, such steady lift forces generally contribute to the overturning moments.

5.5.3 Forces and Moments

The existence of viscosity causes flow separation and gives rise to additional hydrodynamic forces. These viscous forces in line with the flow direction are commonly known as drag forces. They are of the greatest importance for structural members with slender dimensions and under flow conditions where high fluid particle velocities exist. In addition to the in-line drag force, the wake formation as a consequence of flow separation also gives rise to a lift force normal to the flow direction. Lift forces can be of either a steady or oscillatory nature. Due to the cross-flow principle, steady lift forces occur for a submerged cylindrical body (Hoerner 1965). For a vertical

surface column, oscillatory lift forces occur due to the shedding of vortices into the wake. In the following calculation methods, steady lift forces will be assumed as far as practical.

Under the above circumstances, the underwater geometry of a semi-submersible is subject to hydrodynamic loads due to current flow. The basis of the mathematical model will be to compute the forces and moments by sub-dividing the structure into some typical members and summing up the forces and moments due to those individual members. Interference effects will be considered between the shielded members.

A short description of force and moment formulations are given here. Further details are available in (Dev 1993; Dev 1994).

Forces and Moments on Horizontal pontoons

The current forces and moments about the body-fixed co-ordinate system $OXYZ$ of the pontoon.

$$F_{DCX'} = 0.50\rho U^2 A_{PX'} C_{DCX} \cos^2 \mu_C \quad (5.87)$$

$$F_{DCY'} = 0.50\rho U^2 A_{PY'} C_{DCY} \sin^2 \mu_C \quad (5.88)$$

The above two expressions seem reasonable from the point of view of mathematics. But the hydrodynamic phenomenon is rather different which needs some explanation here. In fact, in case of a uniform flow (current) to a deeply submerged infinitely long cylindrical body with an oblique angle to the longitudinal axis, lift force is also associated with the drag force having neither of the forces perpendicular to the body axis. Such hydrodynamic phenomena are due to the cross-flow principle (Hoerner 1965).

That is why it is more practical to use the following equation by just taking the normal component of the lift and the drag forces rather than using Equation 5.87 and Equation 5.88. After some trigonometry, in fact, the result would be the same as Equation 5.87 and Equation 5.88 but keeping them separate facilitates the independent use of lift and drag coefficients according to published data (Hoerner 1965). So, in the calculation, the following equation will be used.

$$F_{DCY'} = 0.50\rho U^2 A_{PY'} \{(C_{DCB} \sin^3 \mu_C + 0.02) \cos(90 - \mu_C) + C_{DCB} \sin^2 \mu_C \cos \mu_C \cos \mu_C\} \quad (5.89)$$

On the other hand, if the component forces of lift and drag are taken along the axis, they would cancel each other because of their opposite directions provided the term 0.02 for friction is neglected.

$$F_{DCX'} = 0.50 \rho U^2 A_{PX'} \{ (C_{DCB} \sin^3 \mu_C) \sin(90 - \mu_C) - C_{DCB} \sin^2 \mu_C \cos \mu_C \sin \mu_C \} \quad (5.90)$$

Doing so, Equation 5.90 will be sufficient to calculate the force along the cylindrical axis.

Now the current forces and the moments with the body-fixed $X - Y$ co-ordinates and the cylinder axis- Z' respectively are as follows:

$$F_{DCX} = F_{DCX'} \quad (5.91)$$

$$F_{DCY} = F_{DCY'} \quad (5.92)$$

$$M_{DCZ'} = F_{DCY'} \cdot X'_{LP} \quad (5.93)$$

where X'_{LP} is the distance between the point of application of the force and the axes origin O' .

A good approximation as suggested in (Pijfers 1975) is the following relation $X'_{LP} = 0.0038 L_P (90 - |\mu_C - 180|)$ where μ_C in degrees; $0 < \mu_C < 180$ and $180 < \mu_C < 360$.

The moments about the body-fixed X -, Y - and Z -axis are respectively.

$$M_{DCX} = F_{DCY} \cdot Z'_i \quad (5.94)$$

$$M_{DCY} = -F_{DCY} \cdot Z'_i \quad (5.95)$$

$$M_{DCZ} = M_{DCZ'} - F_{DCX} \cdot Y'_i + F_{DCY} \cdot X'_i \quad (5.96)$$

Forces and Moments on Vertical Columns

Rectangular Cross Section For rectangular cross-sections, the horizontal forces and moments about the body-fixed axes are expressed as follows:

$$F_{DCX} = F_{DCX'} = 0.50 \rho U^2 A_{PX'} \cos^2 \mu_C \quad (5.97)$$

$$F_{DCY} = F_{DCY'} = 0.50 \rho U^2 A_{PY'} \sin^2 \mu_C \quad (5.98)$$

$$M_{DCX} = F_{DCY} \cdot Z'_i \quad (5.99)$$

$$M_{DCY} = -F_{DCY} \cdot Z'_i \quad (5.100)$$

$$M_{DCZ} = -F_{DCX} \cdot Y'_i + F_{DCY} \cdot X'_i \quad (5.101)$$

Circular Cross Section For circular cross-sections, the horizontal forces and moments about the body-fixed axes are expressed as follows:

$$F_{DCX} = F_{DCX'} = 0.50 \rho U^2 A_P \cos \mu_C \quad (5.102)$$

$$F_{DCY} = F_{DCY'} = 0.50 \rho U^2 A_P \sin \mu_C \quad (5.103)$$

$$M_{DCX} = F_{DCY} \cdot Z'_i \quad (5.104)$$

$$M_{DCY} = -F_{DCX} \cdot Z'_i \quad (5.105)$$

$$M_{DCZ} = -F_{DCX} \cdot Y'_i + F_{DCY} \cdot X'_i \quad (5.106)$$

Forces and Moments on Tubular Bracing

Randomly oriented tubes are normally of two types - horizontal and vertically inclined. Though horizontal, they have different orientations, i.e. they have rotations about the Z' -axis only. On the other hand inclined bracing have two different orientations - rotation about the Z' -axis as well as rotation about the Y' -axis. The angle of rotation about the Z' -axis is α , i.e. the X' -axis is the tube axis and the Y' -axis is situated in the horizontal $O'XY$ plane. Consequently α represents the angle in the horizontal plane between the X' -axis and the X -axis. Similarly rotation about the Y' -axis is β , i.e. this is the angle between the X' -axis with the horizontal XY -plane. The origin O' is the point of application of the force acting on the tube due to the current velocity U . Now if the current velocity vector in the $O'XYZ$ system of axes is \vec{U} and in the $O'X'Y'Z'$ system of axes \vec{U}' respectively, then the following relation can be written.

$$\vec{U} = A\vec{U}' \quad (5.107)$$

where

$$\vec{U} = (U \cos \mu_C, U \sin \mu_C, 0)$$

A = Matrix of orthonormal basis transformation

$$A = \begin{pmatrix} \cos \alpha \cos \beta & \sin \alpha & -\cos \alpha \sin \beta \\ -\sin \alpha \cos \beta & \cos \alpha & -\sin \alpha \sin \beta \\ \sin \beta & 0 & \cos \beta \end{pmatrix}$$

The velocity vector \vec{U}' with respect to the bracing axis $O'X'Y'Z'$ is:

$$\vec{U}' = A^{-1}\vec{U} \quad (5.108)$$

Since the matrix A is orthonormal, the inverse or transpose of matrix A are similar.

$$A^{-1} = A^T = \begin{pmatrix} \cos \alpha \cos \beta & -\sin \alpha \cos \beta & \sin \beta \\ -\sin \alpha & \cos \alpha & 0 \\ -\cos \alpha \sin \beta & \sin \alpha \sin \beta & \cos \beta \end{pmatrix}$$

Now, if \vec{F}'_C is the force vector with respect to the bracing axis, then

$$\vec{F}'_{DC} = \begin{pmatrix} f_{X'} \cdot \vec{U}'_{X'} \\ f_{Y'} \cdot \vec{U}'_{Y'} \\ f_{Z'} \cdot \vec{U}'_{Z'} \end{pmatrix}$$

in which $\vec{U}'_{X'}$, $\vec{U}'_{Y'}$, and $\vec{U}'_{Z'}$ are the components of the velocity vector \vec{U}' .

$$f_{DX'} = 0.50 \rho C_{DX'} A_{PX'} |\vec{U}'_{X'}| \quad (5.109)$$

$$f_{DY'} = 0.50 \rho C_{DY'} A_{PY'} |\vec{U}'_{Y'}| \quad (5.110)$$

$$f_{DZ'} = 0.50 \rho C_{DZ'} A_{PZ'} |\vec{U}'_{Z'}| \quad (5.111)$$

When the bracing ends at other platform members, the value is zero and so $F'_{DCX'} = 0$.

The force vector \vec{F}'_{DC} with respect to the body-fixed $O'XYZ$ -axis system and the moment vector \vec{M}'_{DC} with the body-fixed $OXYZ$ -axis system are now as follows:

$$\vec{F}'_{DC} = A \vec{F}'_{DC} \quad (5.112)$$

$$\vec{M}'_{DC} = B \vec{F}'_{DC} \quad (5.113)$$

where B is the translational matrix from origin O' to O .

$$B = \begin{pmatrix} 0 & Z'_1 & Y'_1 \\ -Z'_1 & 0 & -X'_1 \\ -Y'_1 & X'_1 & 0 \end{pmatrix}$$

5.5.4 Interference of Drag between Bodies

In semi-submersibles where surface piercing vertical columns are placed side by side and also one behind another, shielding effects between them become increasingly important. For pairs of bodies placed one behind the other, the drag of the one placed in the wake produced by the first one is usually less because of reduced dynamic pressure. The drag can even be negative due to the suction behind the first one. Similarly, in the case of a pair of cylinders placed side by side, the resulting vortex street becomes a combined one out of that of a pair originating independently from each cylinder.

For shielded members in a row, DnV (1990) rules provide the appropriate reduction in the values of the drag coefficients according to the cross-sectional dimension of the shielded member and the center to center distance between such members. Some information regarding interference effects is also available in (Hoerner 1965).

5.5.5 Theoretical and Experimental Results

Horizontal Forces

In order to validate the theoretical analysis, a comparison was made with some published experimental data for the semi-submersible I for both head seas ($\mu_C = 180$ deg) and beam seas ($\mu_C = 90$ deg) conditions.

The results of the theoretical calculations for full scale dimensions are compared in Figure 5.13 with those based on the model tests. This comparison shows quite good agreement.

Furthermore, experiments were carried out with a semi-submersible (ITTC Model) for both head seas and beam seas conditions in the Towing Tank No.1 of the Ship Hydromechanics Laboratory of Delft University of Technology. Details have been discussed in Chapter 2.

The geometry and the principal particulars of semi-submersible I and ITTC semi-submersible are shown in Figure 5.14 and in Figure 5.15 respectively.

The values of the measured drag coefficients based on the measured forces are plotted in Figure 5.16. For the beam sea condition, the measured coefficients of the four individual columns are shown in Figure 5.16 (left). It is clearly noticeable that the forces on the two columns situated aft in the vortex stream created by the two forward columns are considerably less. However, the interference effects between the columns placed side by side is

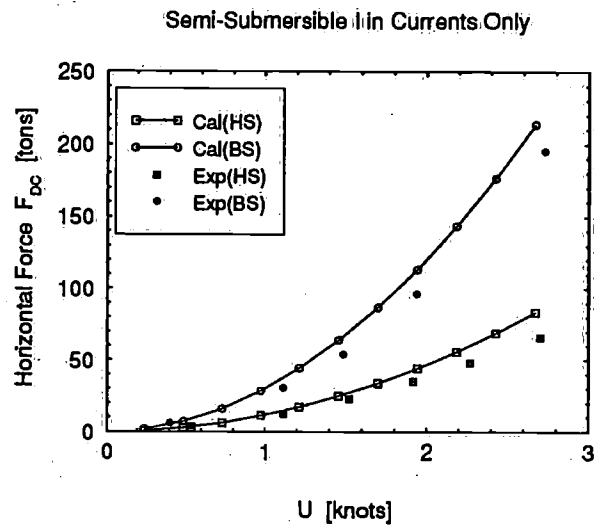


Figure 5.13: *Theoretical and measured horizontal forces on the moored semi-submersible I in currents only in head seas and beam seas*

not that significant. Finally in Figure 5.17 (left), the measured forces for the complete model are compared with the theoretical calculations. Calculations based on the published values of the drag coefficients show higher values than those measured. On the other hand, when using the experimentally obtained values of the drag coefficients, the theoretical predictions match very well with the experimental results.

For the head sea condition, the columns on each pontoon are placed in a row. In such a case, the distance between the columns is much less than what it was for the beam sea condition. Under such circumstances, the interference effects are expected to play a much more dominant role. In Figure 5.16 (right), the corresponding values of the drag coefficients based on the measured forces are shown. The coefficients on Column #8 are the largest because it is subject to free stream velocity. The coefficients on Column #2 are even negative because of its immediate vicinity to Column #1 forward of it. The coefficients on the other two columns are also different according to their individual position. Finally in Figure 5.17 (right), the total measured forces for the complete model are compared with the theoretical calculations. Again the theory using published values of drag coefficients overpredicts the experimental results. However, the comparison improves after the experimentally obtained values of the drag coefficients were used

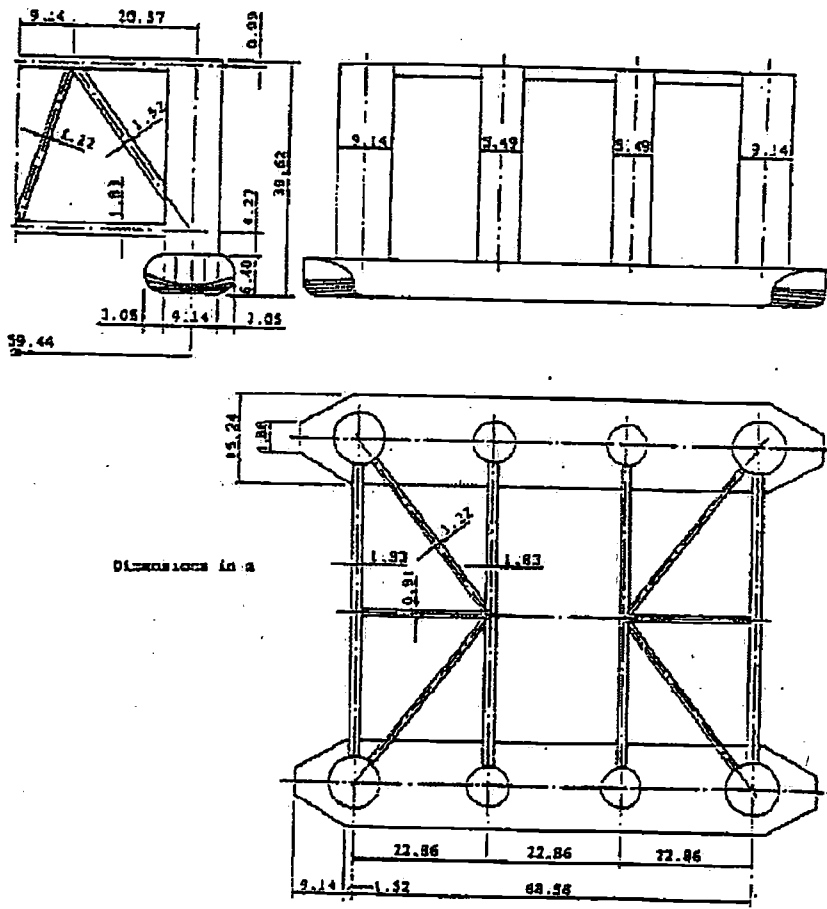


Figure 5.14: Geometry and particulars of the semi-submersible I

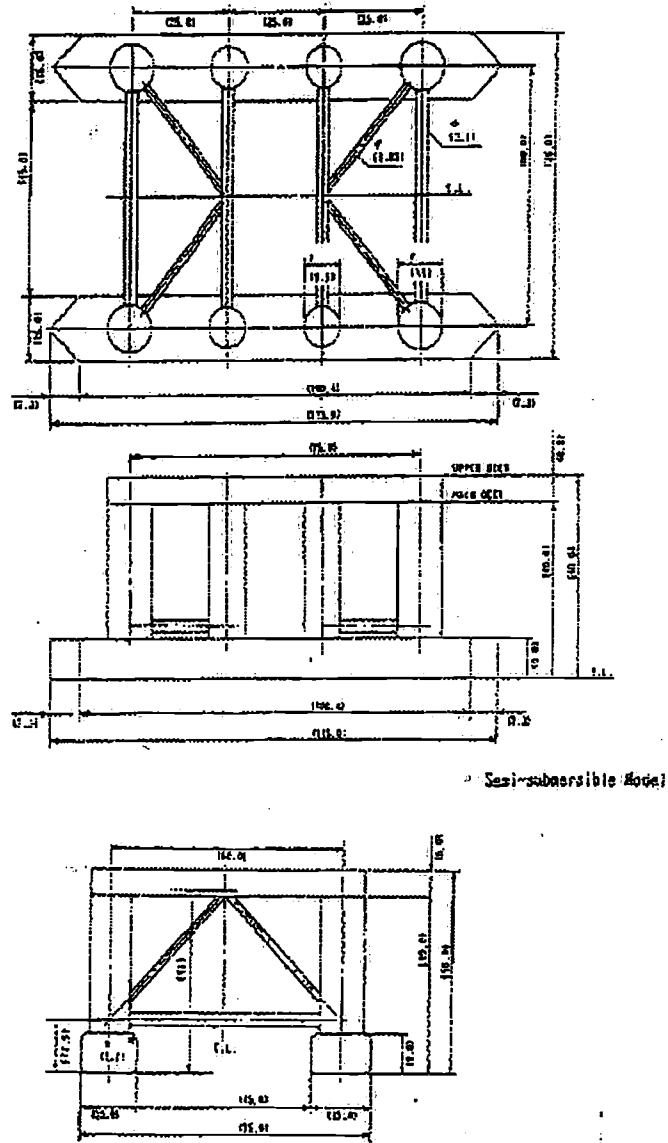


Figure 5.15: Geometry and particulars of the ITTC semi-submersible

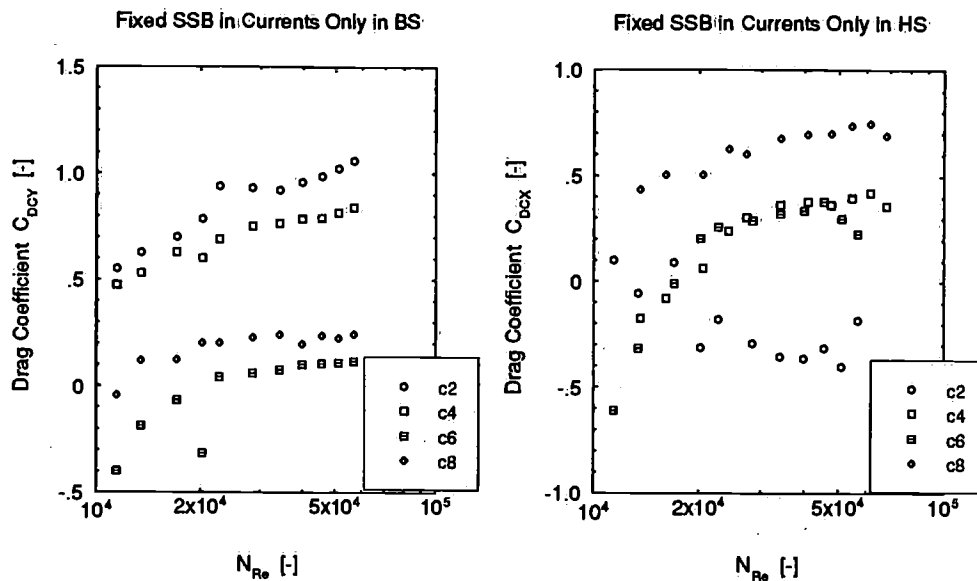


Figure 5.16: Experimental drag coefficients on different columns of the fixed ITTC semi-submersible in currents only in beam seas and head seas

in the theoretical prediction.

From Table 5.1, it is seen that for semi-submersibles with circular columns and rectangular pontoons with tapered ends, the global force coefficients for the head and beam seas are close and they can be used for calculating the force for $N_{Re} < 10^5$.

Forces in currents only were also measured for the free floating (moored) ITTC semi-submersible model in head and in beam seas. Lower current velocities were used because higher values cause the model to tilt due to the vertical forces which results in different immersion of the columns. The

	Semi-submersible 'P'	Semi-submersible 'ITTC MODEL'
Projected Area \perp to X	1337.0 m ²	0.2240 m ²
Projected Area \perp to Y	2292.0 m ²	0.5440 m ²
Force Coefficient C_{DCX}	0.642	0.603
Force Coefficient C_{DCY}	0.961	0.962

Table 5.1: Total projected area and global force coefficients

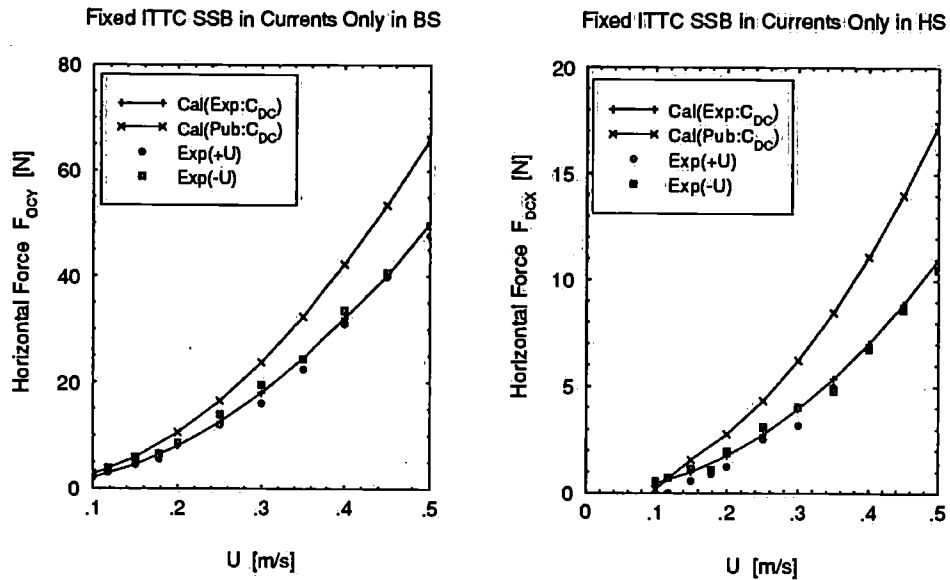


Figure 5.17: *Theoretical and measured horizontal forces on the fixed ITTC semi-submersible in currents only in beam seas and head seas*

comparison between the measured forces and theoretical forces is shown in Figure 5.18. Theoretical predictions using experimentally obtained drag coefficient values match quite well.

Vertical Forces

During the model tests with the fixed ITTC semi-submersible, the vertical forces were also measured for the complete model. Such vertical forces are believed to be mainly caused by the velocity squared term of the Bernoulli's equation in the potential regime. In the case of semi-submersibles such contributions are only attributed to the completely submerged pontoons. However viscous effects might play a role as well. A complete mathematical model for calculating such vertical forces is beyond the scope of this work and therefore experimentally obtained coefficients for vertical forces for a completely submerged fixed pontoon which has been discussed in Chapter 4, were used to predict the same for the semi-submersible model. Coefficients were obtained through a power regression analysis for the force as a function of the Reynolds Number. Comparison between calculated and measured values are shown in Figure 5.19. Theoretical predictions for the

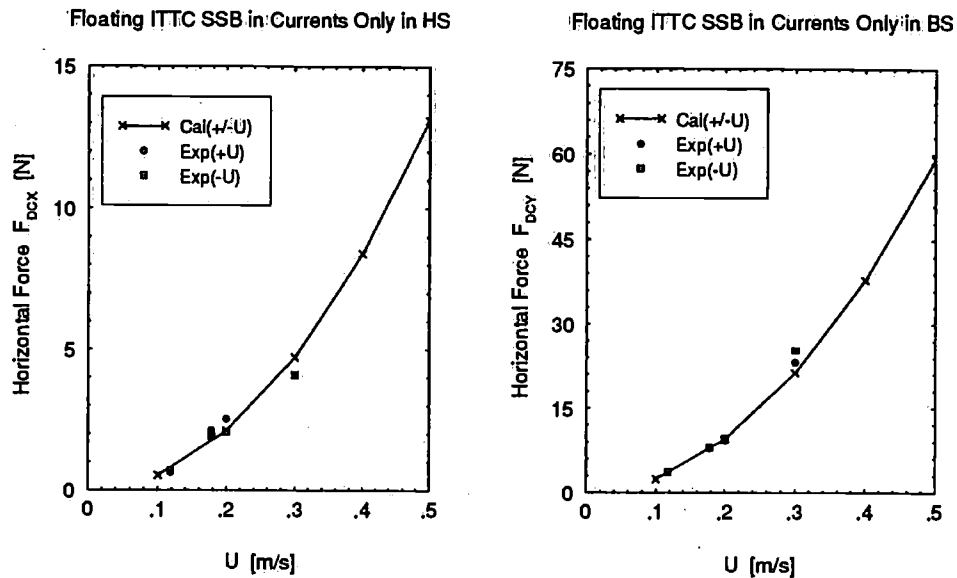


Figure 5.18: Theoretical and measured horizontal forces on the fixed ITTC semi-submersible in currents only in head seas and beam seas

semi-submersible model both in beam seas and head seas condition show good agreement when the experimentally obtained values of the force coefficients were employed.

5.5.6 Concluding Remarks

Depending on the design code available in the Rules and Regulations of different International Classification Societies like Det Norske Veritas, Germanischer Lloyds and American Bureau of Shipping, the developed mathematical model can be used to calculate the current loads on offshore floating structures like semi-submersibles and tension leg platforms.

Data from other literature and results of different model tests were utilized in order to achieve results as accurate as possible. Redundancy is bound to be expected in the results but the aim was to keep them as little as possible.

If the elemental force coefficients involving interaction effects and the velocity profile are suitably treated, the procedures described for summing up the elemental forces are useful for the estimation of the total loads on the structures. The force coefficients used in the theoretical calculations are not

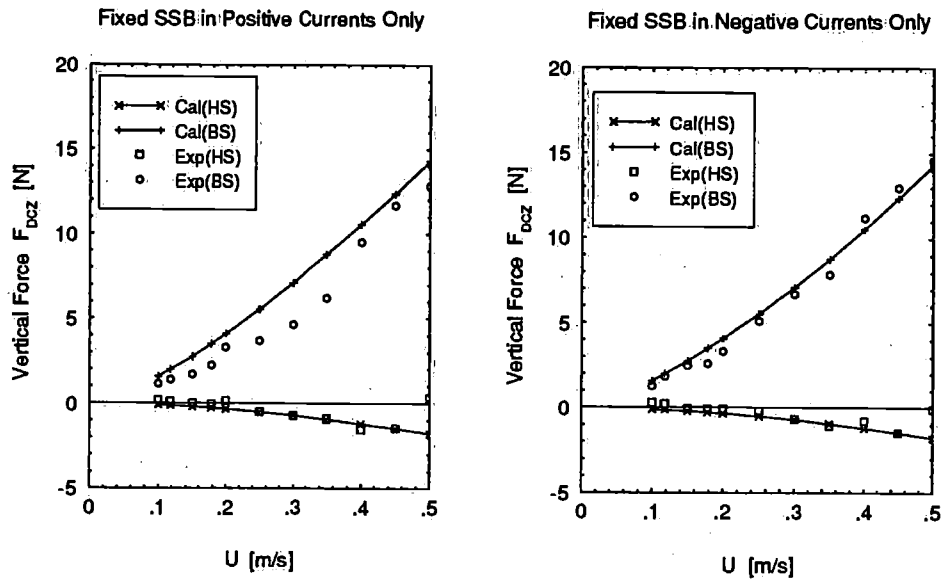


Figure 5.19: Theoretical and measured vertical forces on the fixed ITTC semi-submersible in currents only in head seas and beam seas

exaggerated; it is the overall geometry which as a whole results in less force due to interference/interaction among different structural members because of their close proximity.

Enormous criticisms nowadays exist due to conservative code of practice by the International Classification Societies. Unfortunately, so far no alternative rule has either been proposed or yet fully established itself to further the present state-of-the-art of the Rules and Regulations. Choice of drag coefficients based on interference effects should be incorporated in details in Rules and Regulations of the International Classification Societies.

How effective the model tests would be to predict the behavior of the full scale structure, when there are questions of scale effects, blockage effects and also to some extent employment of dubious techniques while performing the tests, still remains obscure. The widely used traditional (empirical) methods seem much more efficient in computation compared to individual model tests. However important findings from different model test results can be incorporated where relevant towards a more reliable prediction using computational methods.

References

- ABS (1988). *Rules for Building and Classing Mobile Offshore Drilling Units*, Chapter 3. USA: American Bureau of Shipping.
- Dalzell, J. (1975). The applicability of the functional polynomial input-output model to ship resistance in waves. Technical Report SIT-DL-75-1794, Davidson Laboratory, Stevens Institute of Technology, USA.
- Dalzell, J. (1976). Application of the functional polynomial model to the ship added resistance. In *Proceedings of the International Conference on Numerical Ship Hydrodynamics*, London, England, pp. 279-347.
- DELFRAC (1992). *A 3-D Diffraction Program*. Ship Hydromechanics Laboratory, Delft University of Technology, Delft, The Netherlands.
- Dev, A. K. (1993). Current and wind loads on semi-submersibles (ssbs) and tension leg platforms (tlps). Technical Report 971, Ship Hydromechanics Laboratory, Delft University of Technology, Delft, The Netherlands.
- Dev, A. K. (1994). Hydrodynamic loading on semi-submersibles and tension leg platforms in steady currents. In *Proceedings of the 10th International Offshore South East Asia Conference*, OSEA, Singapore, pp. 855-875.
- DnV (1990). *Rules for Classification of Mobile Offshore Units*, Chapter 1, Sec.4. Norway: Det Norske Veritas. Pt.3.
- GL (1990). *Rules for Classification and Construction - Offshore Technology*, Chapter 2, Sec.1 and Sec.4. Germany: Germanischer Lloyd. Pt.2.
- Hoerner, S. (1965). *Fluid Dynamic Drag*, Chapter III, IV. Brick Town, N.J.: Hoerner Fluid Dynamics.
- Hsu, F. and K. Blenkarn (1970). Analysis of peak mooring force caused by slow vessel drift oscillation in random seas. In *Proceedings of the Annual Offshore Technology Conference*, OTC 1159, Houston, Texas, pp. I:136-I:146.
- Li, Y.-C. and H.-G. Kang (1992). Wave-current forces on slender circular cylinder. In *Proceedings of the International Conference on Offshore Mechanics and Arctic Engineering*, OMAE, Calgary, Alberta, Canada, pp. 117-125.

- Maeda, H., K. Nishimoto, and S. Eguchi (1985). A study of components of wind and current loads on semi-submersibles. *Naval Architecture and Ocean Engineering, SNAJ 23*, 53-65.
- Otsuka, K., Y. Ikeda, and N. Tanaka (1990). Viscous forces acting on a horizontal circular cylinder in regular and irregular waves. In *Proceedings of the International Conference on Offshore Mechanics and Arctic Engineering*, OMAE, Houston, Texas, pp. 129-138.
- Pijfers, J. G. L. (1975). Calculation of the environmental loads, thrust and power requirements of two dynamically positioned semi-submersibles. Report No.11499.
- Pinkster, J. (1974). Low frequency phenomena associated with vessels moored at sea. *Journal of the Society of Petroleum Engineers, AIME* (December), 1-16.
- Pinkster, J. A. (1980). *Low Frequency Second Order Wave Exciting Forces on Floating Structures*. Ph. D. thesis, Ship Hydromechanics Laboratory, Delft University of Technology, Delft, The Netherlands.

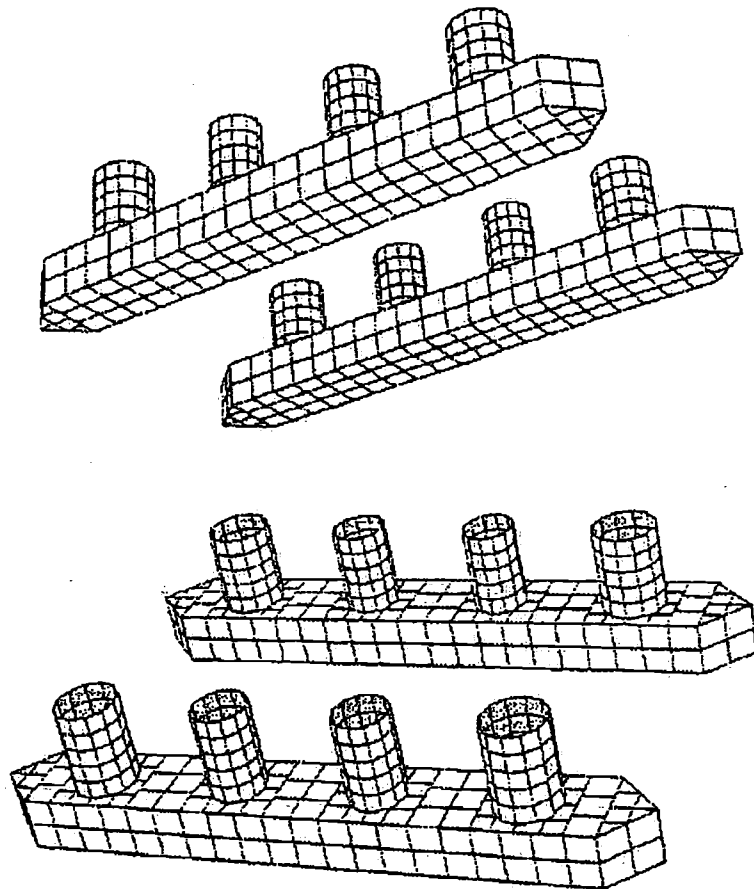
Chapter 6

Results of Computations and Measurements

The mathematical model which has been presented in Chapter 5 was the basis for developing a computer code in Fortran 77. The computer program is able to calculate the viscous drift forces on a semi-submersible in both regular waves in the frequency domain and in irregular waves in the time domain. Furthermore, the wave (potential) mean drift force results in regular waves are also used for the frequency domain analysis in a waves only field as well as in a wave-current coexisting flow field. The program was developed in line with the configuration of the ITTC semi-submersible. However, it is suitable for any twin-hull semi-submersible with a maximum number of five columns on a pontoon. For the free floating condition, any standard output of regular wave motions and phases can be used. In this study, such results from DELFRAC (1992) have been used. The discretization of the ITTC semi-submersible is shown in Figure 6.1. The values of the mean drag coefficient are those obtained from the experiments with vertical cylinders and a submerged pontoon in different flow fields and they are treated appropriately via controlling hydrodynamic parameters.

Details of all experiments have been elaborated upon in Chapter 2. Before developing the final computer code for a semi-submersible, independent computer code for a fixed vertical cylinder and a fixed submerged pontoon were validated against experimental values of them and have been described in detail in Chapter 3 and Chapter 4 respectively.

During this research work, a separate computer code was developed to compute the forces on semi-submersibles and tension leg platforms in cur-



PANEL DISTRIBUTION ON ITTC-SEMI
TOTAL 984 PANELS

Figure 6.1: The panel distribution on the ITTC semi-submersible

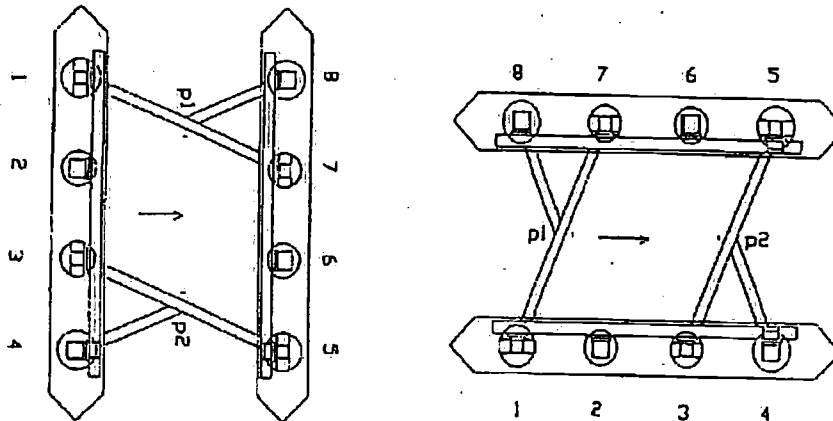


Figure 6.2: Top view of the fixed ITTC semi-submersible model (left) in beam seas and (right) in head seas

rents only and also in winds. This computer program can take account of semi-submersibles and tension leg platforms of different geometry (Dev 1993; Dev 1994). The same program has been used to calculate the forces on the ITTC semi-submersible in currents only.

6.1 Fixed Semi-Submersible

The orientation of the columns and the reference points for relative wave elevation in beam seas and in head seas for the ITTC semi-submersible are shown in Figure 6.2.

6.1.1 In Regular Waves

First Order Forces and Relative Wave Elevation

In Figure 6.3 and Figure 6.4, the first order horizontal and vertical forces for the fixed ITTC semi-submersible in waves only are shown for head sea and beam sea conditions for different wave frequencies associated with different sets of wave amplitudes. The comparison shows some scatter especially in the vertical forces. However no marked non-linearity is observed.

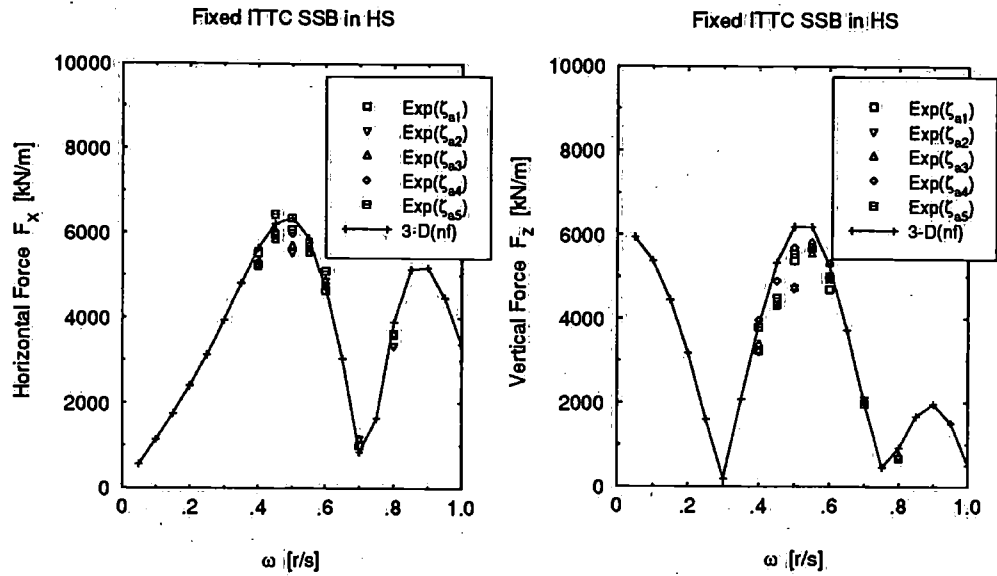


Figure 6.3: Computed and measured (left) horizontal and (right) vertical first order forces on a fixed semi-submersible in waves only in head seas

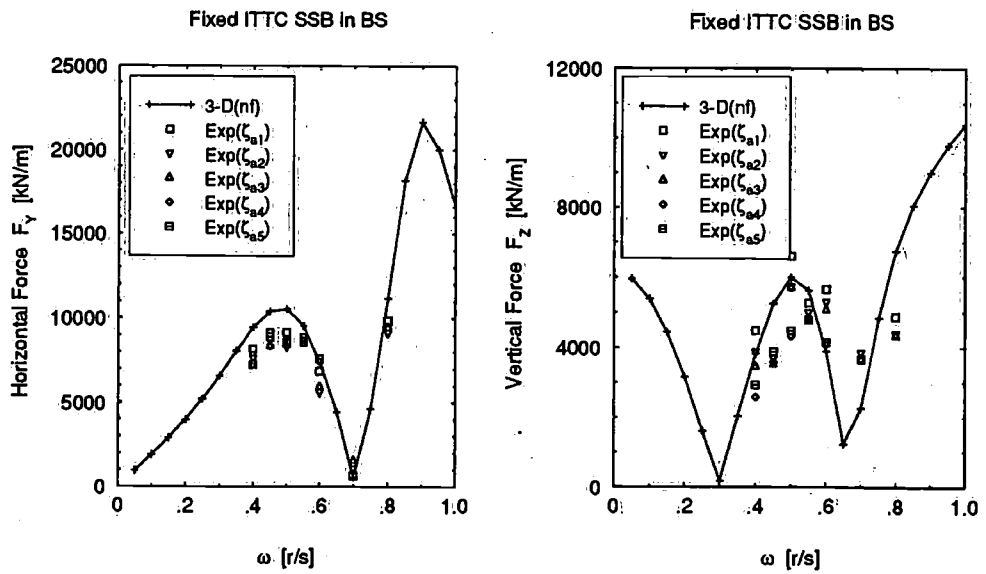


Figure 6.4: Computed and measured (left) horizontal and (right) vertical first order forces on a fixed semi-submersible in waves only in beam seas

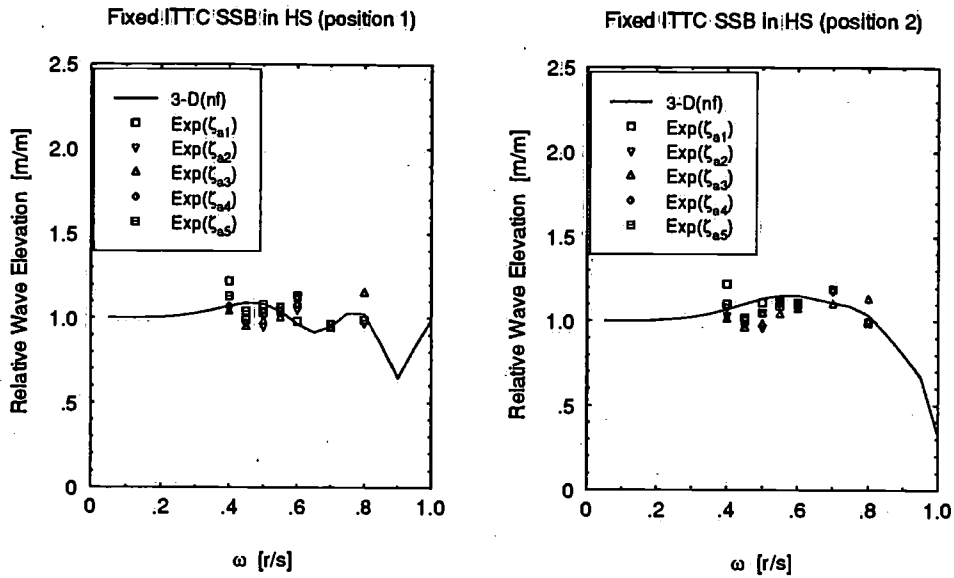


Figure 6.5: Computed and measured relative wave elevation at position 1 and position 2 of a fixed semi-submersible in waves only in head seas

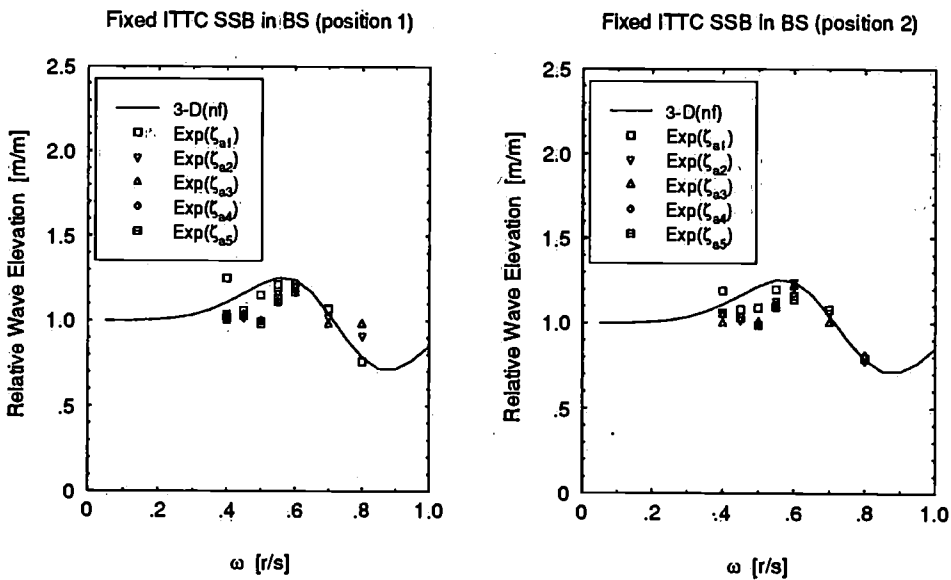


Figure 6.6: Computed and measured relative wave elevation at position 1 and position 2 of a fixed semi-submersible in waves only in beam seas

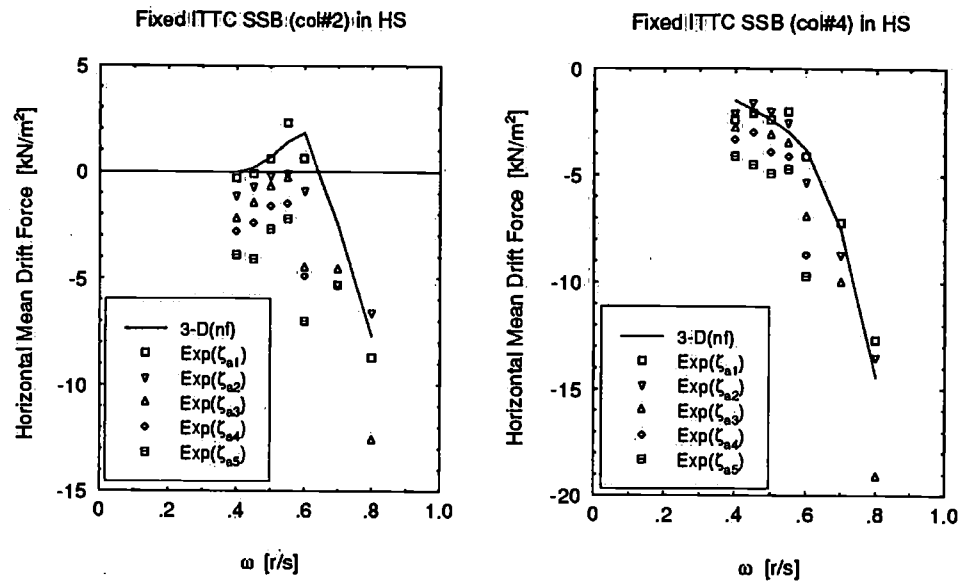


Figure 6.7: Computed and measured horizontal mean drift forces on column no.2 and column no.4 of a fixed semi-submersible in waves only in head seas

The relative wave elevation around the columns is one of the major contributions for the wave drift forces in theoretical computations. It was therefore felt necessary to verify such relative wave elevation within the semi-submersible model by measuring them at two different positions (position 1 and position 2). Comparisons are shown in Figure 6.5 and in Figure 6.6 for both head seas and beam seas. The comparisons are reasonable. This leads to the conclusion that the theoretical calculations of the mean drift force due to potential effects are consistent with the experimental analysis.

Mean Drift Forces

During the experiments, the horizontal mean drift forces were measured for some individual columns of the semi-submersibles. Using the relative wave elevation and second order pressure, the mean wave drift forces on those columns were calculated. The results are shown in Figure 6.7 and in Figure 6.8 for head seas. In Figure 6.9 and in Figure 6.10, the results are shown for beam seas. From the figures, it is clearly seen that there are always differences between the measured forces and the theoretical forces revealing the fact that viscous effects increase the mean drift force on each

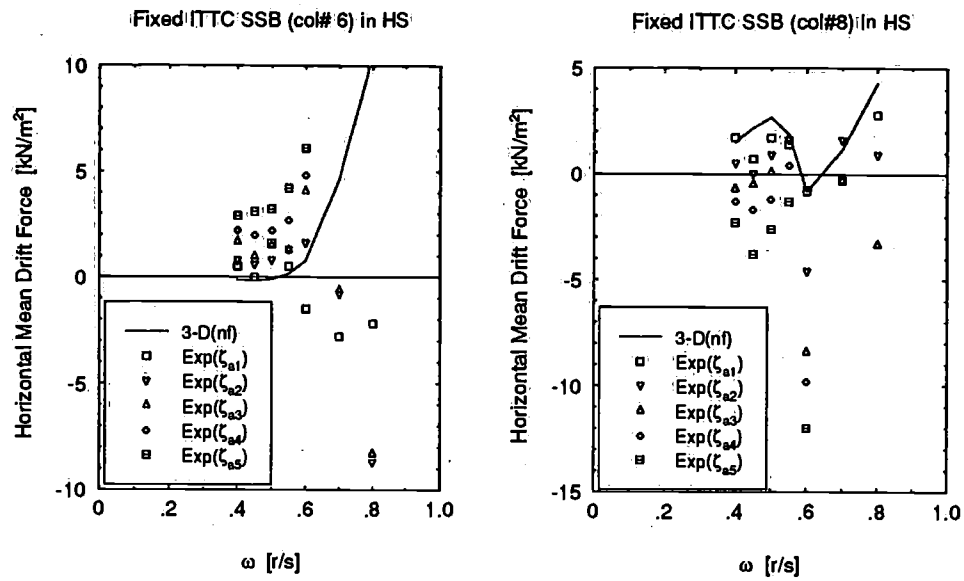


Figure 6.8: Computed and measured horizontal mean drift forces on column no. 6 and column no. 8 of a fixed semi-submersible in waves only in head seas

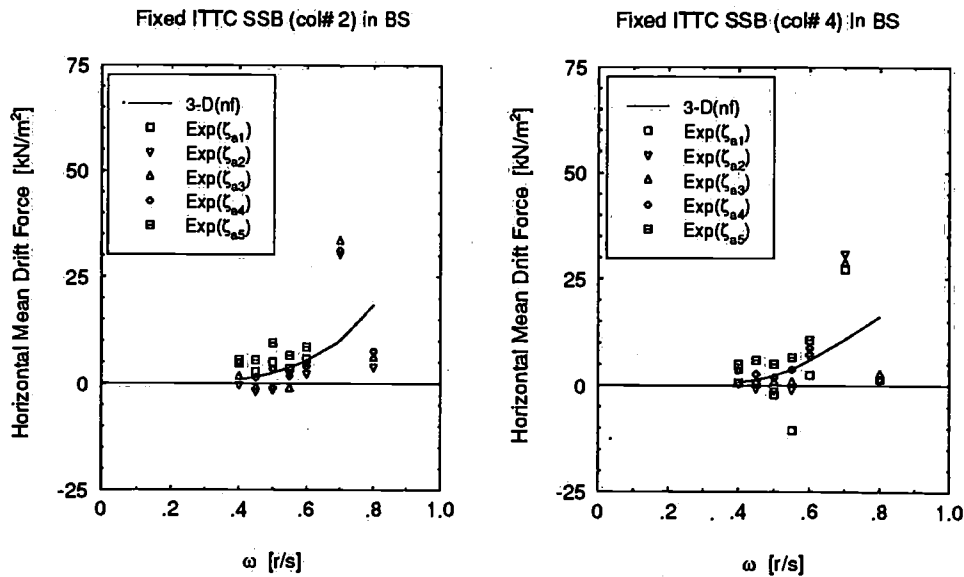


Figure 6.9: Computed and measured horizontal mean drift forces on column no. 2 and column no. 4 of a fixed semi-submersible in waves only in beam seas

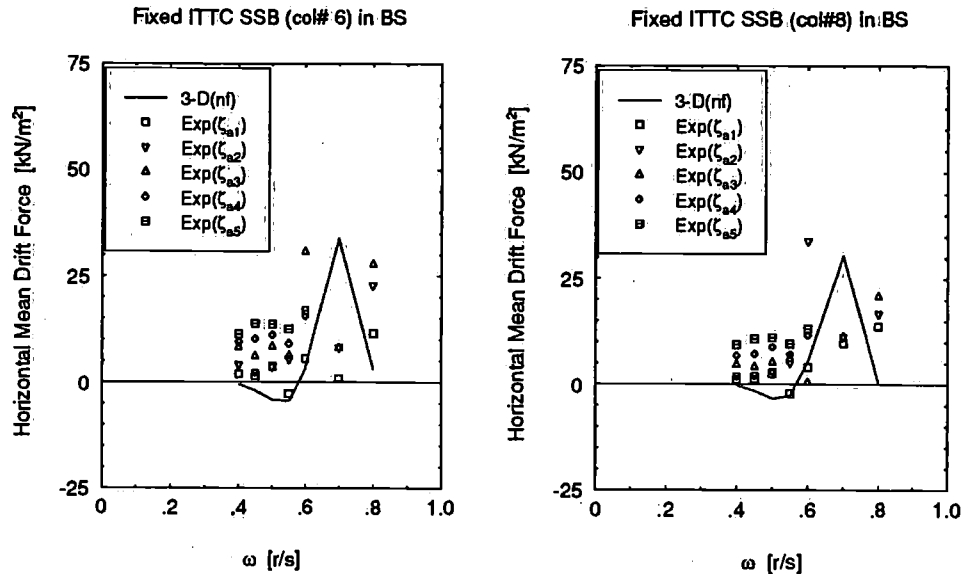


Figure 6.10: Computed and measured horizontal mean drift forces on column no.6 and column no.8 of a fixed semi-submersible in waves only in beam seas

column thus resulting into a overall higher mean drift force for a complete semi-submersible. There is minor scatter and this is more in head seas which may be due to the interference effects because of the close proximity of the columns. But in beam seas, the results are very consistent for column no.2 and column no.4 and also for column no.6 and column no.8 whose layout are symmetric with respect to the coordinate system. The mean drift force on a column based on potential theory is a constant value with the same sign. If the interaction effects due to wave diffraction are neglected, the total wave drift force on a complete semi-submersible consists of the sum of the forces on the individual columns. The mean drift force on a column is a constant for a given wave frequency and also a monotonous function of the wave frequency. This leads to a total drift force which is also a monotonous function of the wave frequency. But the results in the figures for some individual columns show that this is not the case however. Hence it must be concluded that the oscillations in the drift force quadratic transfer functions are due to viscous effects.

Computed and measured horizontal and vertical mean drift forces in waves only for the complete semi-submersible are shown in Figure 6.11 and

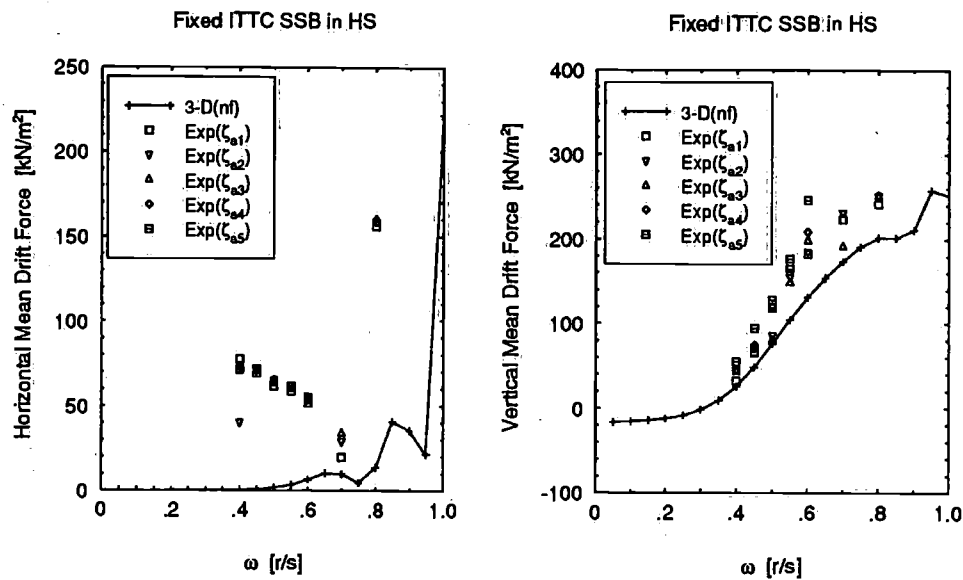


Figure 6.11: Computed and measured (left) horizontal and (right) vertical mean drift forces on a fixed semi-submersible in waves only in head seas

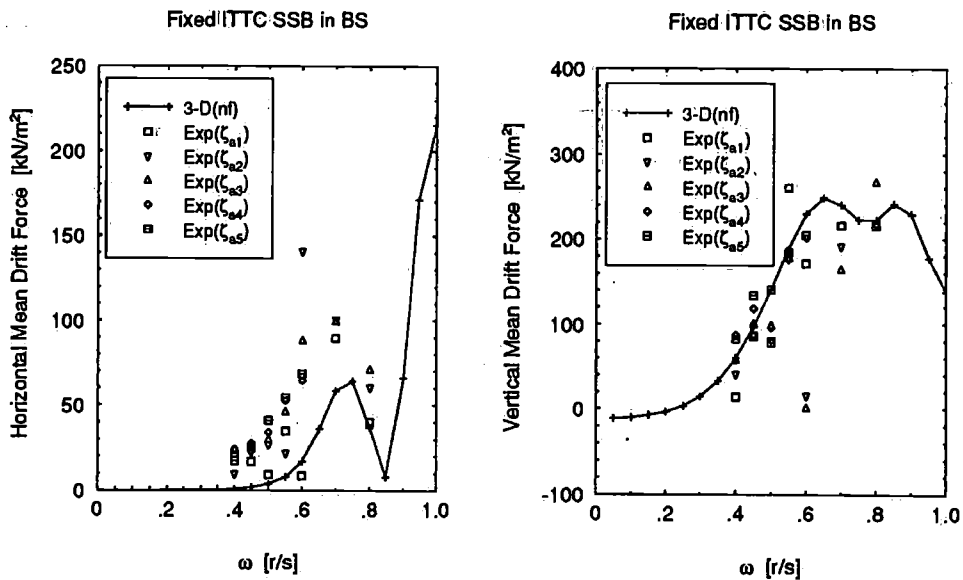


Figure 6.12: Computed and measured (left) horizontal and (right) vertical mean drift forces on a fixed semi-submersible in waves only in beam seas

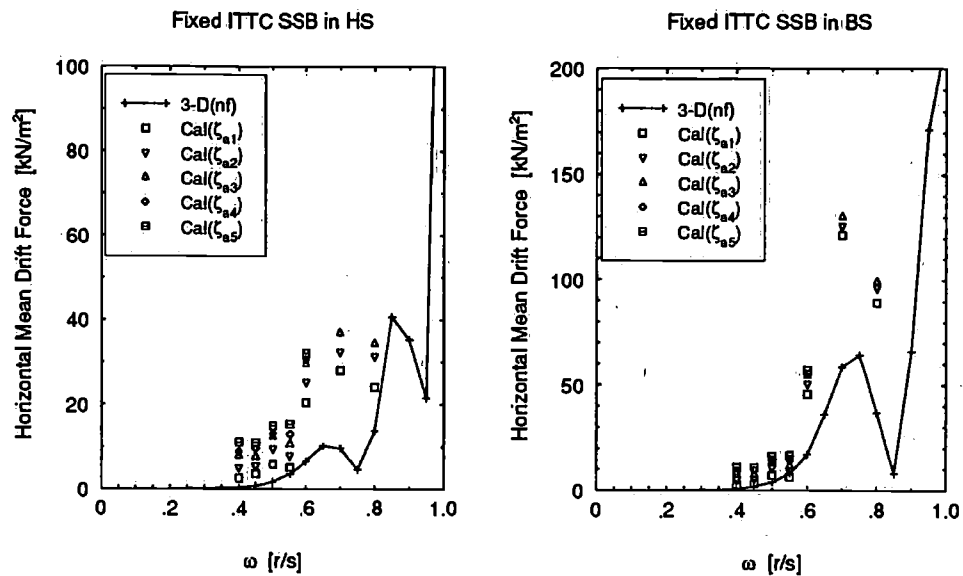


Figure 6.13: *Computed (potential plus viscous) vs. computed (potential only) horizontal mean drift forces on a fixed semi-submersible in waves only in (left) head seas and in (right) beam seas*

in Figure 6.12 for head seas and beam seas. The measured drift mean forces are higher than the potential ones showing the marked viscous effects on the horizontal mean drift forces. Some differences are also observed in the vertical mean drift forces but in magnitude they are small compared to potential contributions.

Finally in Figure 6.13, the computed (potential plus viscous) horizontal mean drift forces for the semi-submersible in waves only are shown for different sets of wave amplitudes. The theory also shows the higher forces when viscous effects are accounted for. These phenomena were also observed in the measured results.

6.1.2 In Regular Waves and Currents

Mean Drift Forces

During the experiments, two different carriage speeds ($\pm U_1 = 1.023\text{m/s}$) and ($\pm U_2 = 1.542\text{m/s}$) were used to simulate positive and negative currents to generate a wave-current coexisting flow field. Two different sets of wave

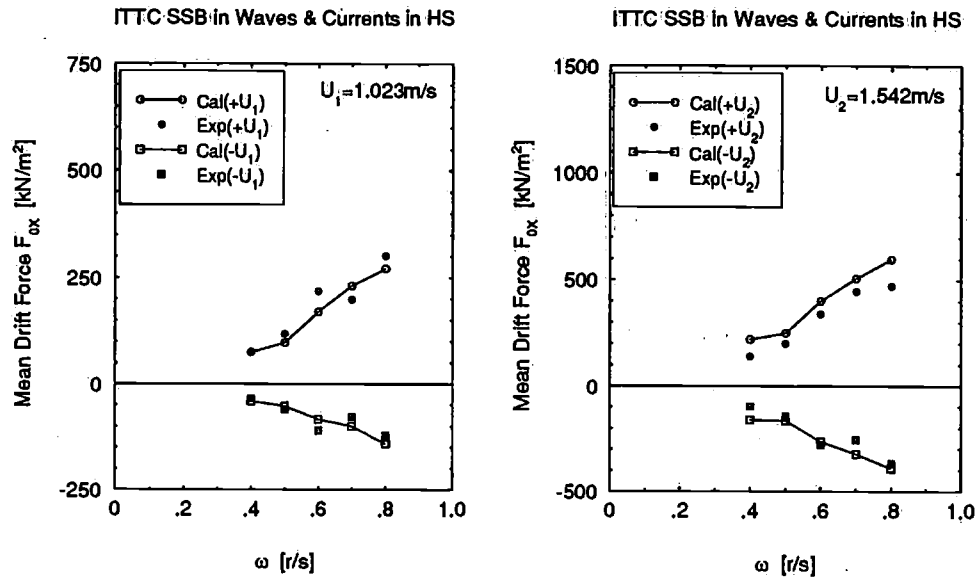


Figure 6.14: *Computed (potential plus viscous) and measured mean drift forces on a fixed semi-submersible in waves and currents in head seas*

amplitudes were used. The results are shown in Figure 6.14 and in Figure 6.15 for head seas and in Figure 6.16 and in Figure 6.17 for beam seas respectively.

In the theoretical computations, experimentally obtained values of the mean drag coefficients were used. The comparison shows satisfactory correlation except for some cases. In spite of some differences, the trend in the predictions is similar to the measured results. The causes of deviations can be due to the values in the mean drag coefficients and also to some extent due to the interference effects.

6.2 Moored Semi-Submersible

6.2.1 In Regular Waves

All signals measured during model tests in regular waves were subjected to a harmonic analysis to determine the mean values of the drift forces and the amplitudes and phase angles of the motion component with wave frequency. The amplitudes of model motions were divided by the amplitude of the undisturbed regular waves, measured at the position of the center of gravity

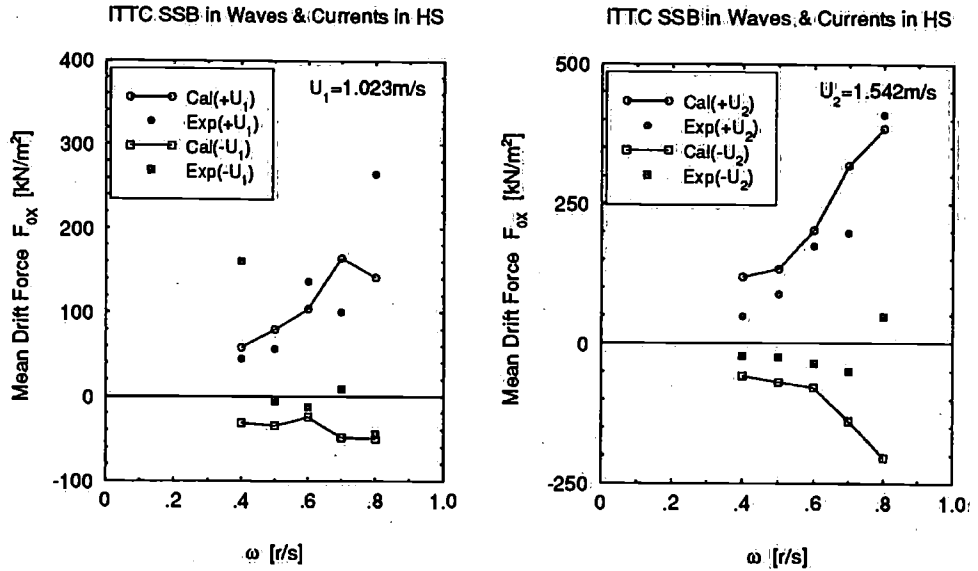


Figure 6.15: Computed (potential plus viscous) and measured mean drift forces on a fixed semi-submersible in waves and currents in head seas

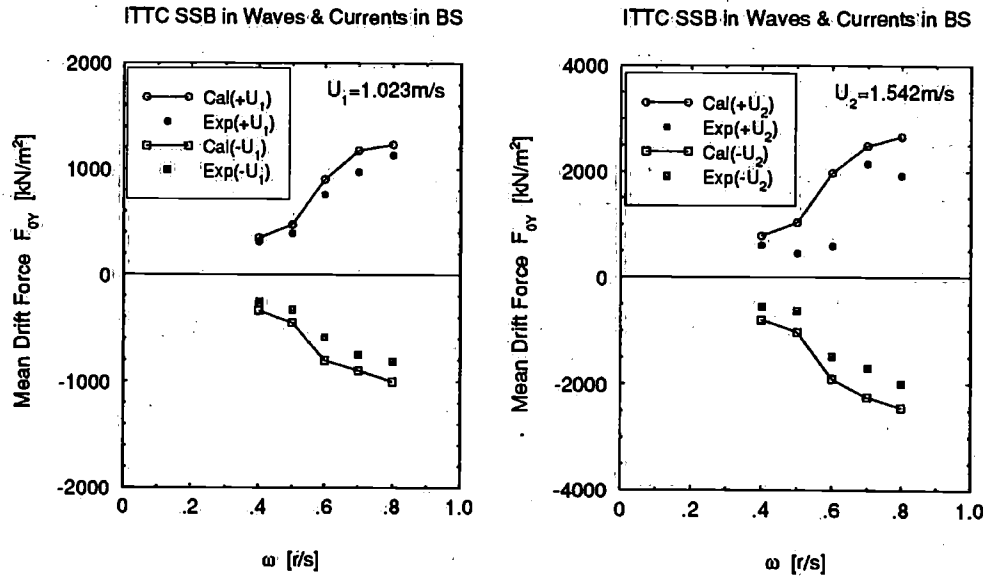


Figure 6.16: Computed (potential plus viscous) and measured mean drift forces on a fixed semi-submersible in waves and currents in beam seas

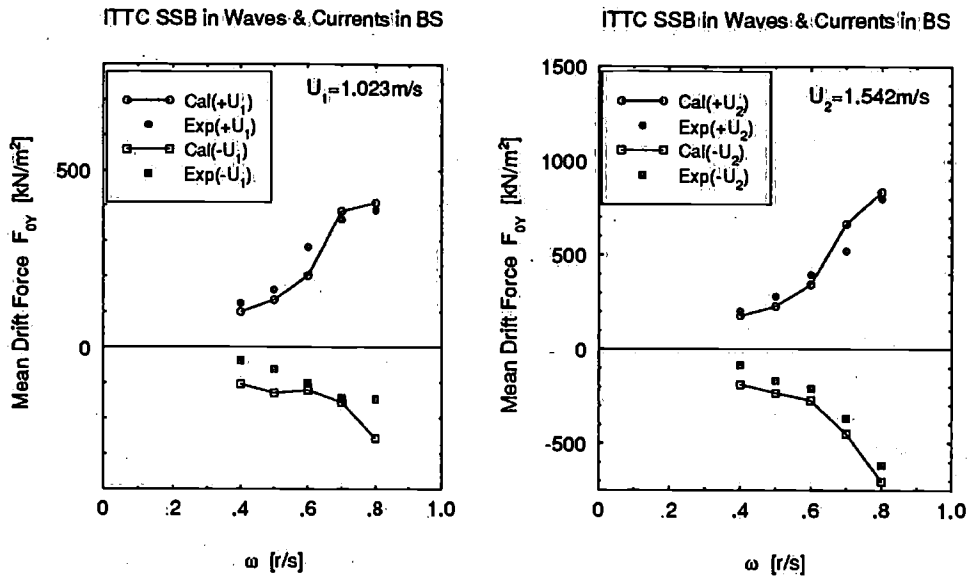


Figure 6.17: *Computed (potential plus viscous) and measured mean drift forces on a fixed semi-submersible in waves and currents in beam seas*

of the model, to supply frequency transfer functions. The phase angles were obtained using the wave elevation measured at a point adjacent to the cog of the model. The mean longitudinal drift force was divided by the square of the amplitude of the undisturbed waves to give the mean wave drift force transfer functions. All experimental data shown were converted to full scale values.

Motion Responses

Figure 6.18 and Figure 6.19 show the computed and the measured results of motion RAOs. Excellent comparison between theory and measurement for vertical, horizontal and angular motion RAOs is observed. The results shown in these figures confirm that the motions at wave frequencies are linear functions of the wave amplitude. Furthermore, it is shown that such motions are accurately predicted by computations based on potential theory. Nonlinearity is observed only in heave motion around heave natural frequency where viscous effects play a dominant role. Horizontal motions were corrected for the deck reference point where the motions had been measured.

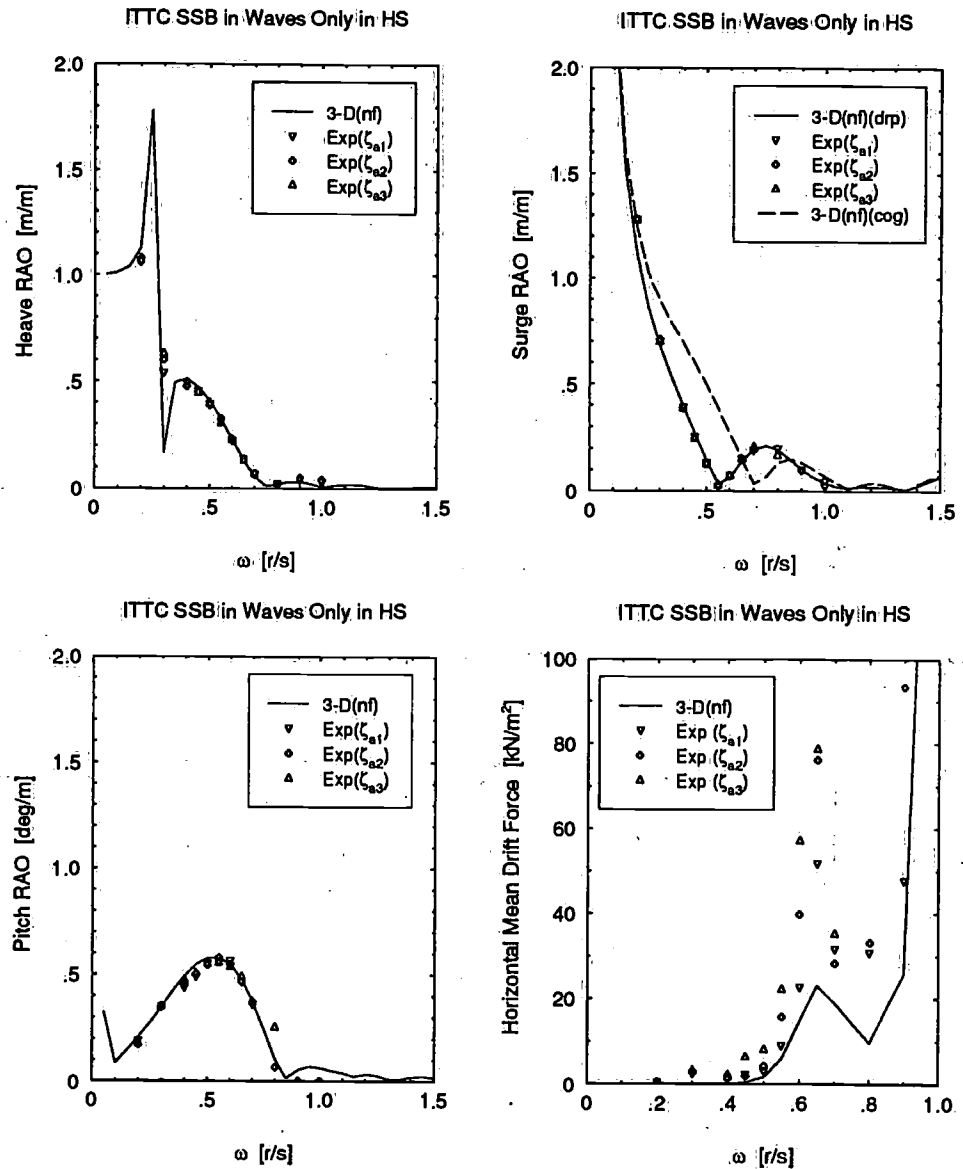


Figure 6.18: Computed and measured motion RAOs (heave: upper left, surge: upper right and pitch: lower left) and horizontal mean drift forces (lower right) on a moored semi-submersible in waves only in head seas

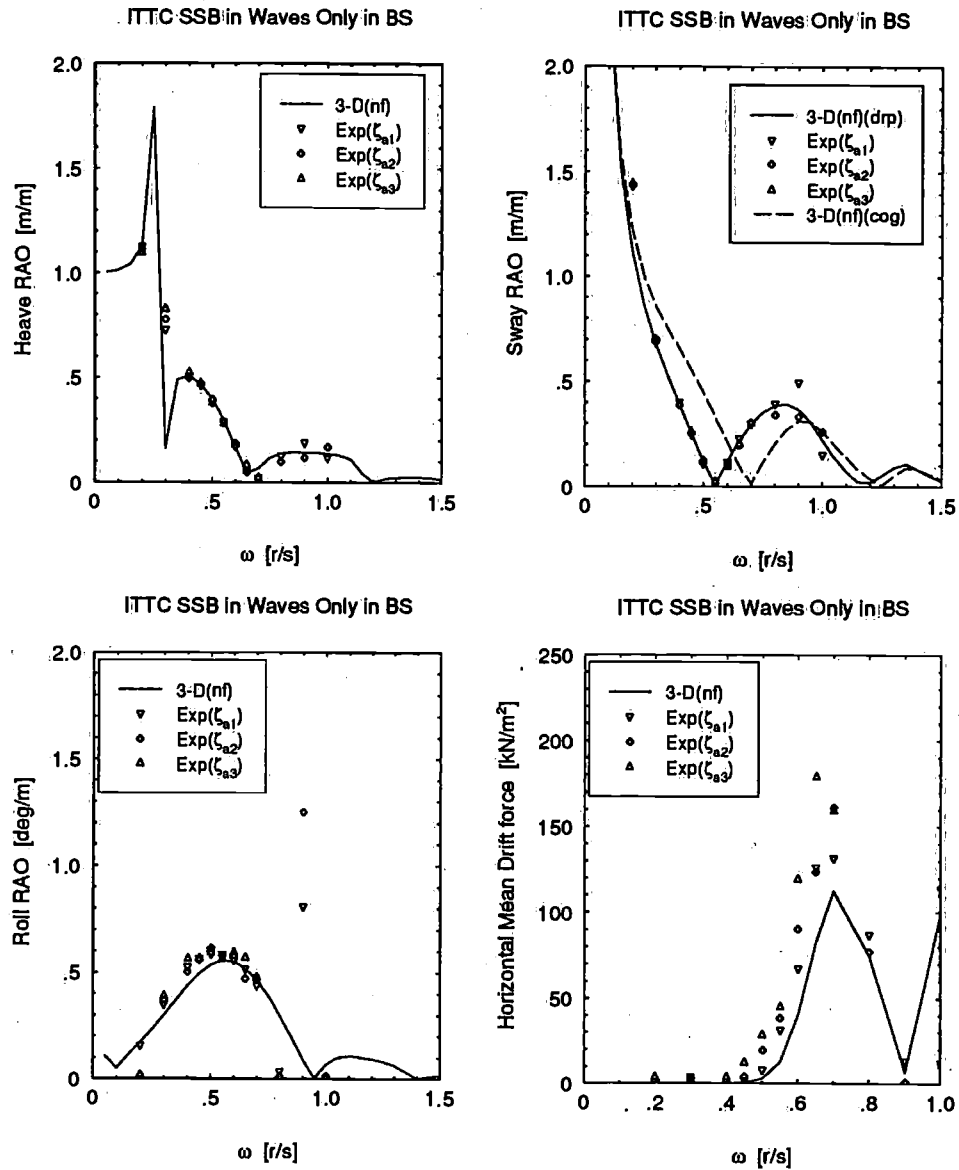


Figure 6.19: Computed and measured motion RAOs (heave:upper left, sway:upper right and roll:lower left) and horizontal mean drift forces (lower right) on a moored semi-submersible in waves only in beam seas

Mean Drift Forces

In the same figures, it is observed that in both head seas and beam seas, the measured drift forces are comparatively higher than those predicted by 3-dimensional predictions. The transfer functions of the mean drift forces show rapid variations to a base of the frequency. The prediction is much improved, when the viscous drift forces, calculated by the computer program using theoretical regular wave motion RAOs and the experimentally obtained values of the mean drag coefficients are added to the wave drift forces. The comparison is shown in Figure 6.20. An anomaly is observed around some frequencies near the peak which may be due to the values of the mean drag coefficients and also to some extent due to the interference effects among the columns.

In this connection, effects of viscous contributions are shown in Figure 6.21 for another moored semi-submersible I in regular waves in head and beam seas. Model test results show discrepancies between 3-dimensional predictions and the measured results. After viscous contributions are added, the overall prediction improves.

6.2.2 In Regular Waves and Currents

Motion Responses

In a wave-current coexisting flow field, the motion RAOs are in fact affected by the forward speed phenomenon. As the present 3-D computations are only valid for zero speed, the use of such RAOs do not sound appropriate even though the speed is of very low magnitude. From the measurements, it is observed that there are no appreciable differences in the measurements and theoretical predictions for the zero speed case except in beam seas where differences are observed in sway motions and thus in roll motions in beam seas. In beam seas, because of the presence of currents, lift forces are generated causing a steady tilt in the model which was not quite high in the case of head seas. In the theoretical computations for the viscous drift forces, zero speed motion RAOs were used.

The comparison of measured motion RAOs in waves and currents are shown against those in waves only in Figure 6.22, Figure 6.23 and in Figure 6.24 for both head and beam seas respectively. Comparison of these results show practically no influence of current speed on the first order motions with and without current.

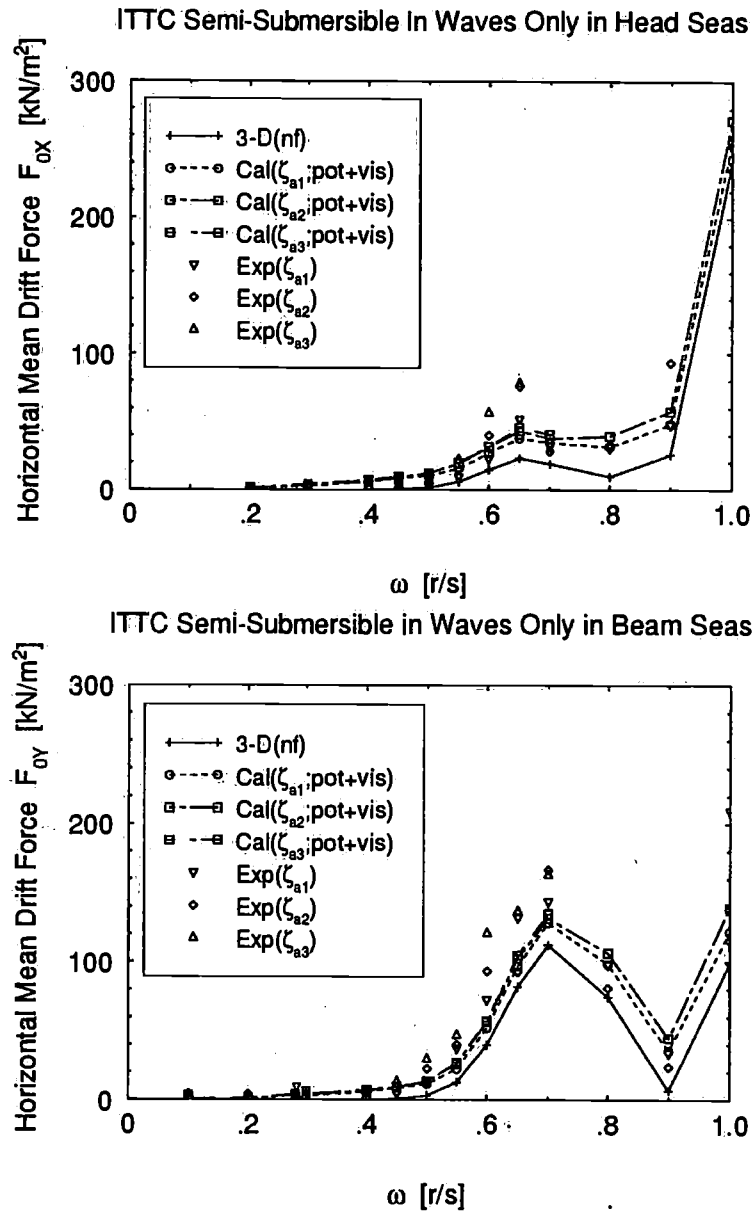


Figure 6.20: Computed (potential only:solid line and potential plus viscous dashed lines) and measured horizontal mean drift forces on a moored semi-submersible in waves only in head seas (upper) and beam seas (lower)

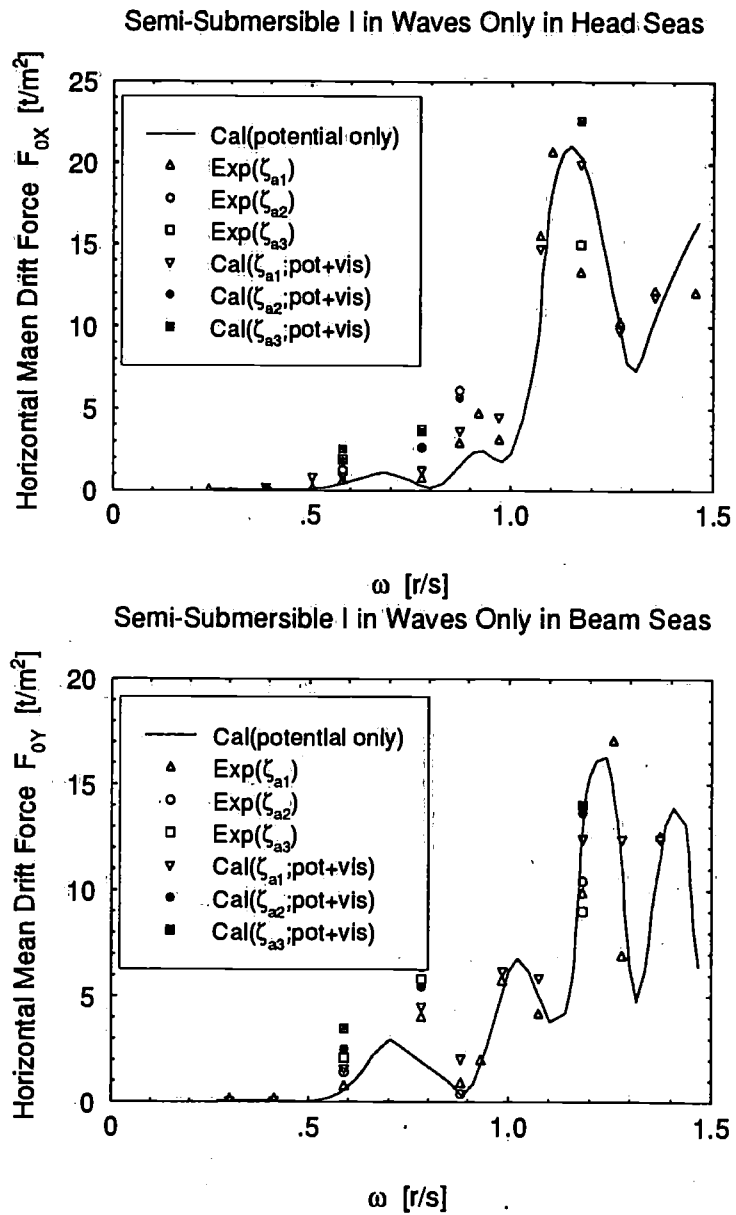


Figure 6.21: Computed (potential only; potential plus viscous) and measured horizontal mean drift forces on a moored semi-submersible in waves only in head seas (upper) and beam seas (lower)

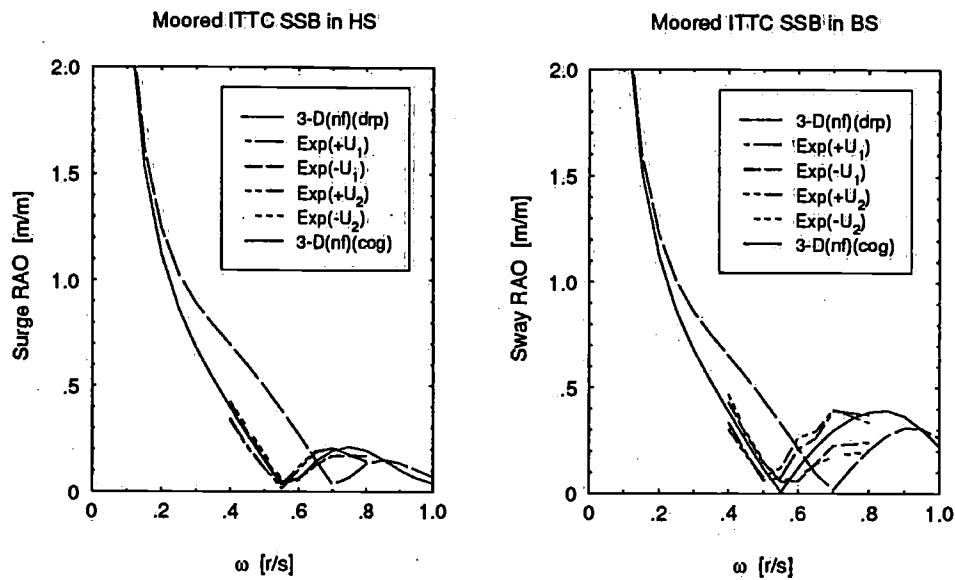


Figure 6.22: *Computed (waves only) and measured (waves and currents) horizontal motion RAOs of a moored semi-submersible in head and beam seas*

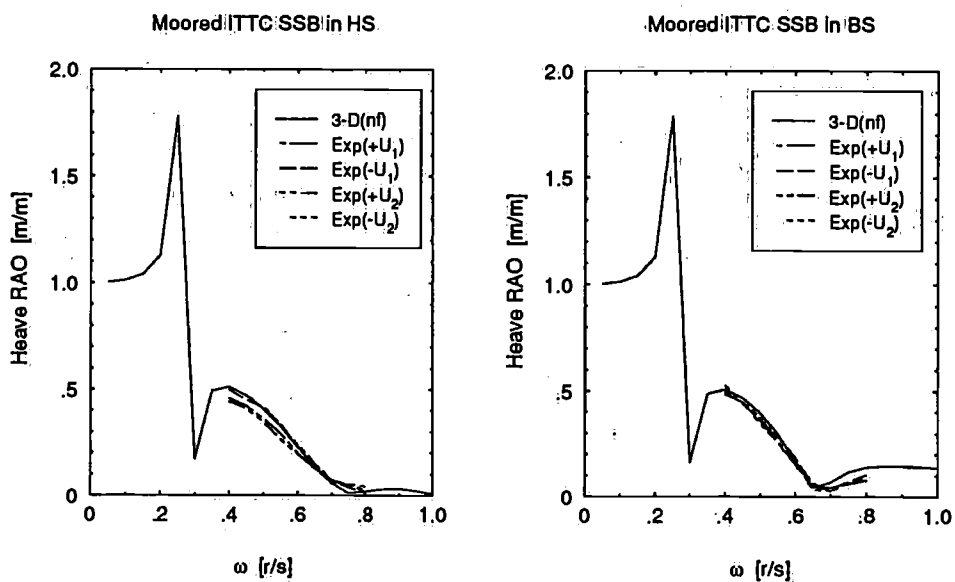


Figure 6.23: *Computed (waves only) and measured (waves and currents) vertical motion RAOs of a moored semi-submersible in head and beam seas*

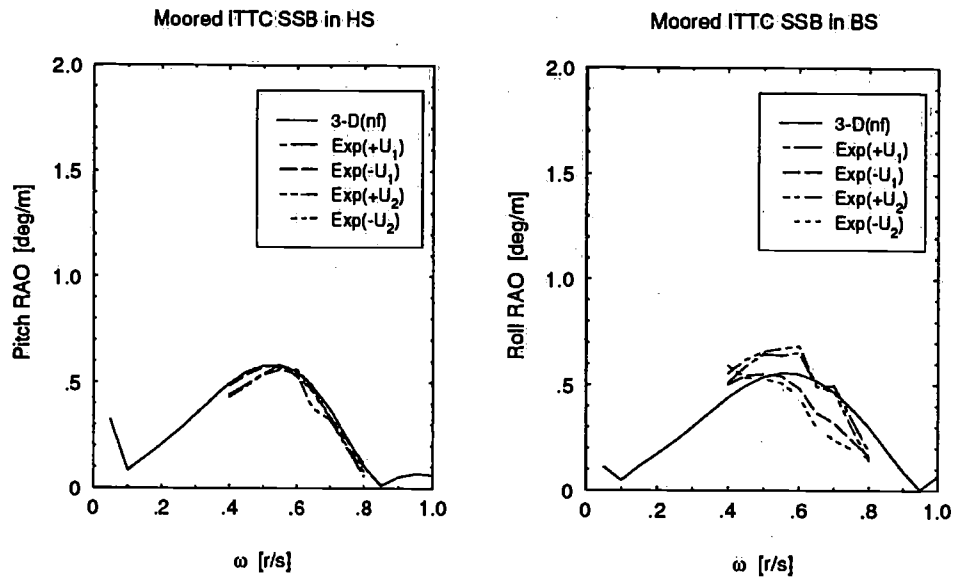


Figure 6.24: Computed (waves only) and measured (waves and currents) angular motion RAOs of a moored semi-submersible in head and beam seas

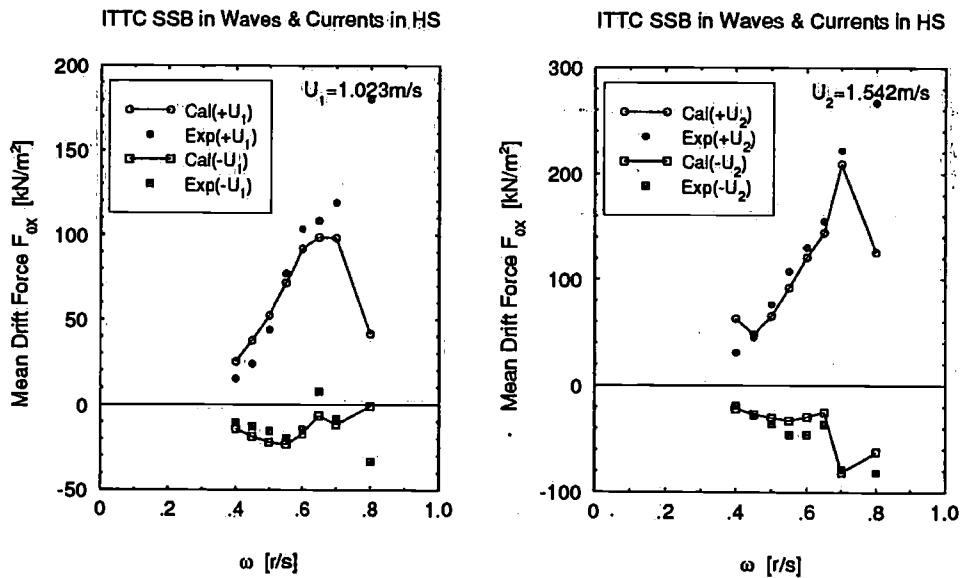


Figure 6.25: Computed (potential plus viscous) and measured mean drift forces on a moored semi-submersible in waves and currents in head seas

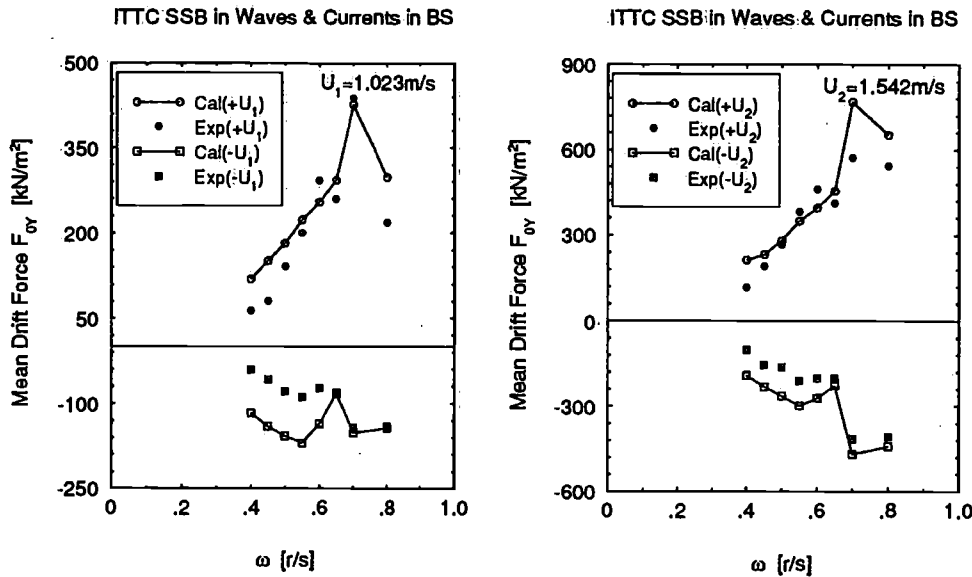


Figure 6.26: Computed (potential plus viscous) and measured mean drift forces on a moored semi-submersible in waves and currents in beam seas

Mean Drift Forces

In Figure 6.25 and in Figure 6.26, the measured mean drift forces in a wave-current coexisting flow field is shown against the theoretical predictions. Similar to a fixed semi-submersible model, the computed results match very well with the measured results. The differences observed in beam seas may be due to the fact that sway and roll RAOs in experiments do not match very well with those predicted for a zero forward speed case. Motion RAOs used in the computations are for a zero forward speed. The other causes may be due to the values in the mean drag coefficient.

6.2.3 In Irregular Waves

The investigations in irregular waves were mainly concerned with the validity of the computational methods for the prediction of first order wave frequency motions and in particular to establish the extent of the viscous effects influencing the low frequency drift forces as such effects have been found to dominate the mean drift forces on a moored semi-submersible in regular waves. The results of motions and the low frequency drift forces will

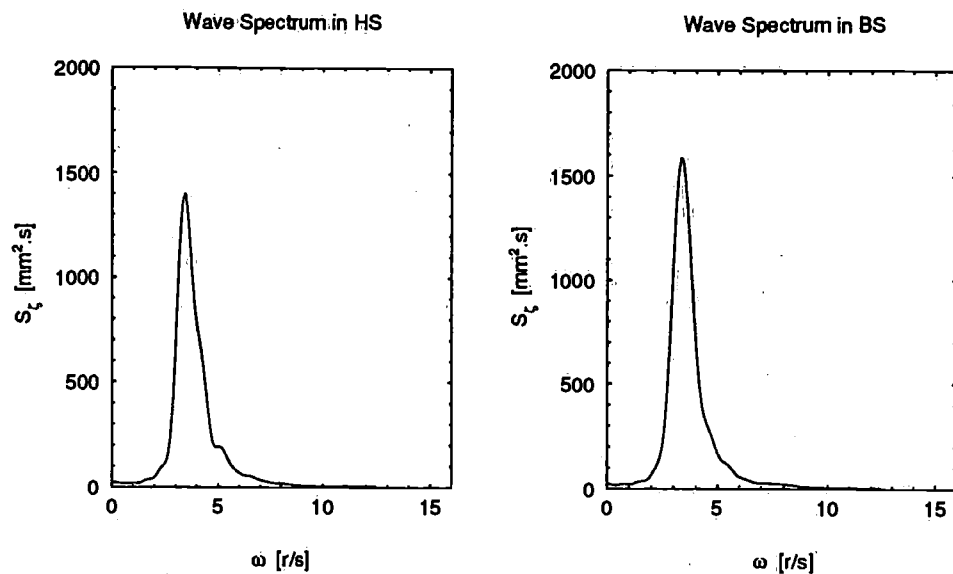


Figure 6.27: Measured wave spectra in head seas and in beam seas

be presented here. The measured spectra of irregular waves used during the experiment for head seas and beam seas are shown in Figure 6.27.

Motion Records

Similar to a moored semi-submersible in regular waves, the measured motions in the time domain are compared first for irregular waves. The reason is that the theoretical motion transfer functions based on regular waves in the frequency domain are used in dealing with the viscous drift forces in the time domain. The calculations were based on measured irregular wave time trace and applying the FFT technique. In dealing with horizontal motions, the measured time traces, which contain low frequency motions as well, was first filtered through a hpf for obtaining high frequency motions only. Additionally, the measured wave trace was also passed through the same hpf to get rid of any low frequency energy present in the spectrum. After these two filters, the correlation between the computed and measured (after filter) is quite satisfactory. Vertical and angular motions show reasonable comparison between the computed and the measured results.

Figure 6.28 and Figure 6.29 show the comparison of horizontal, vertical and angular motions waves only in head seas and beam seas respectively.

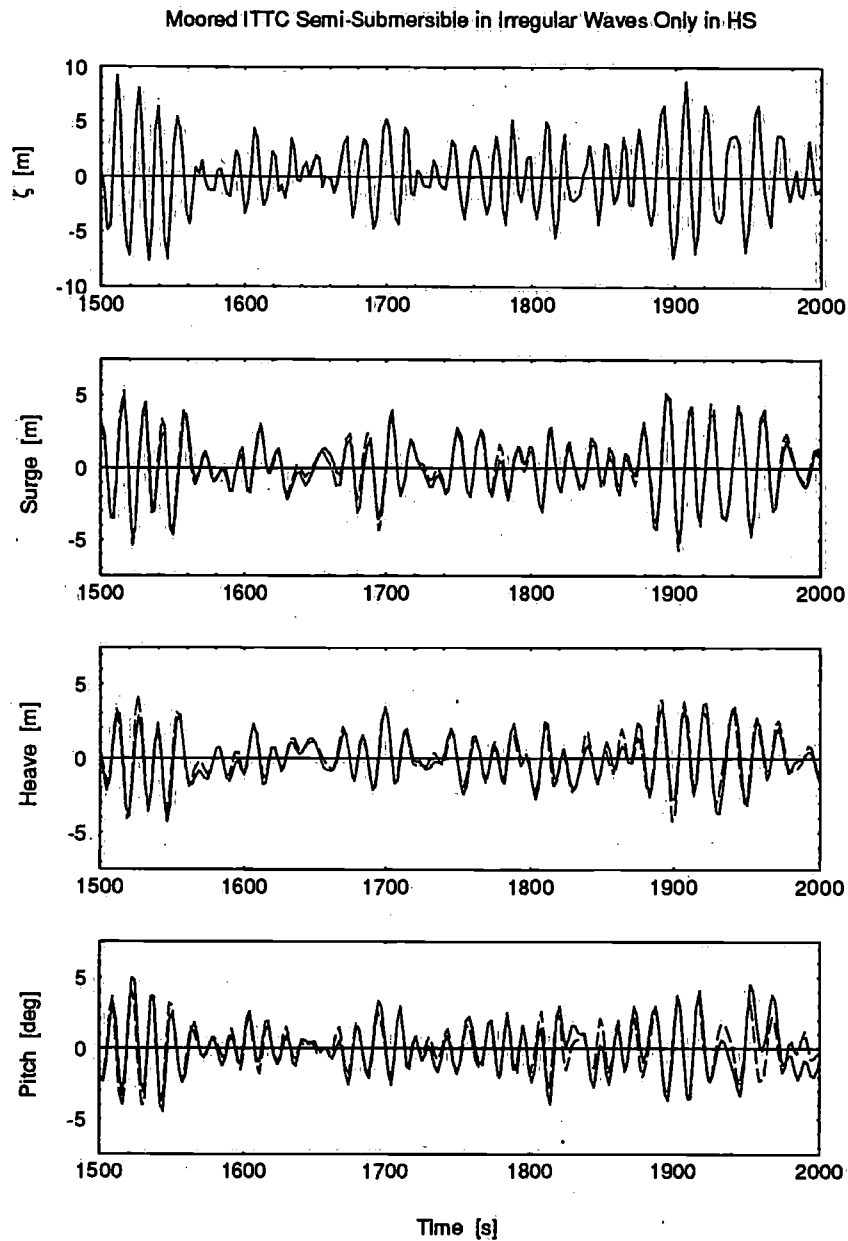


Figure 6.28: *Computed and measured motions (surge, heave and pitch) of a moored semi-submersible in irregular waves only in head seas (calculation:dashed line; experimental:solid line)*

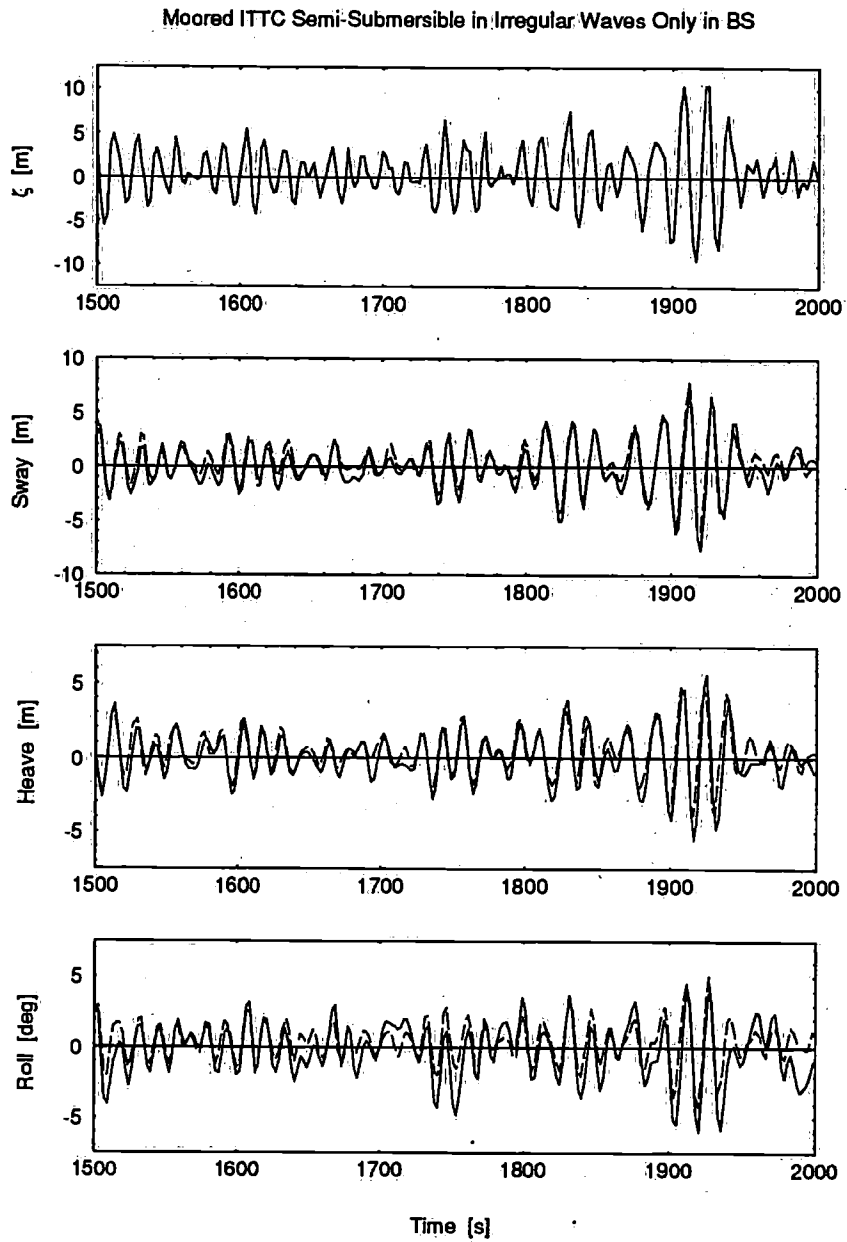


Figure 6.29: Computed and measured motions (sway, heave and roll) of a moored semi-submersible in irregular waves only in beam seas (calculation: dashed line; experimental: solid line)

Measured Uncorrected and Corrected Force Records

Experiments were carried out using a soft-spring restraining or mooring system which consists of horizontal wires incorporating soft linear springs which are connected to the force transducers mounted to the carriage. As a result of the model set-up, the total restraining force is not equal and opposite to the low frequency wave exciting force thus resulting in low frequency residual horizontal motions of the model. In order to obtain the true drift forces on the model from a test, the measured restraining force must be corrected for the effects of low frequency horizontal motions of the model. The basic assumption behind this process is that the instantaneous discrepancy between the true drift force and the measured restraining force results in horizontal motion velocities and accelerations which are described by the following relation:

$$(M + M_A) \ddot{x}(t) + B \dot{x}(t) = F_{drift}(t) - F_{meas}(t) \quad (6.1)$$

in which F_{drift} represents the horizontal drift excitation forces, F_{meas} , the measured spring forces and the acceleration and damping force together on the left hand side of the equation is the correction force F_{corr} . Assuming that at low frequencies both virtual mass and damping coefficients are constant, the acceleration and the damping force together can be determined in the time domain by differentiation of the measured horizontal motions. Having obtained the low frequency force records from the low frequency components of the measured motions, the best estimate of the time record of the horizontal drift force then follows from:

$$F_{drift}(t) = F_{meas}(t) + (M + M_A) \ddot{x}(t) + B \dot{x}(t) \quad (6.2)$$

The method just indicated is based on the assumption of linearity in the hydrodynamic reaction forces and thus fully consistent with potential theory.

In order to measure the mean and slowly varying horizontal wave drift forces in irregular waves, ideally the model should be moored in such a way that all low frequency motion response is suppressed while leaving the model completely free to carry out the motions at wave frequencies. The first requirement ensures that the measured force is not affected by dynamic magnification effects. The second requirement can be deduced from theoretical analysis of the second order wave drift forces which shows that part of the total second order excitation forces are directly dependent on the structural

frequencies (Pinkster 1980). As a consequence, the model restraining system must possess the characteristics of an ideal Dynamic Positioning System. In order to verify the accuracy of this procedure, model tests were repeated using different settings of dynamic restraining systems (Pinkster *et al.* 1993) like the system of restraining being adjusted to representing a spring system (Proportional control), a spring and damper system (Proportional-Differential control) and a Proportional-Differential control including Feed - Forward based on the relative wave elevation measurements. The results shown in (Pinkster *et al.* 1993) indicate that the spectral density of the drift force obtained from tests with significantly different characteristics of the restraining system are reasonably consistent.

Examples of time traces of measured waves, measured horizontal motions, measured restraining forces, correction forces and the slowly varying drift forces for the ITTC semi-submersible are shown in Figure 6.30 and in Figure 6.31 for head seas and beam seas respectively.

The records in Figure 6.32 and in Figure 6.33 for head seas and beam seas respectively show that there are considerable differences between the measured uncorrected and corrected (true) drift force. The differences are not so much in the force magnitude but rather in the phase of the force in relation to the waves. It is further noted that the corrected force records show peak forces which are in phase with groups of higher waves in the wave train, while the peaks in the uncorrected force records tend to lag behind somewhat. Based on such comparisons, it is felt that the corrected drift force records reflect the true drift force sufficiently accurate in order to justify certain general conclusions to be drawn with respect to the magnitude of the drift forces.

Potential vs. Viscous Low Frequency Drift Forces

Results of tests in irregular waves only are given in the form of time records of the measured low frequency drift forces compared with the same of the corresponding predicted low frequency wave drift forces based on 3-dimensional potential theory. For the time domain predictions, use was made of second order impulse response functions combined with measured time traces of the irregular wave records in the tank. The time domain second order impulse response functions for the drift forces are obtained from the complete second order quadratic transfer functions computed in the frequency domain. The quadratic transfer functions were computed based on the pressure integration method (Pinkster 1980).

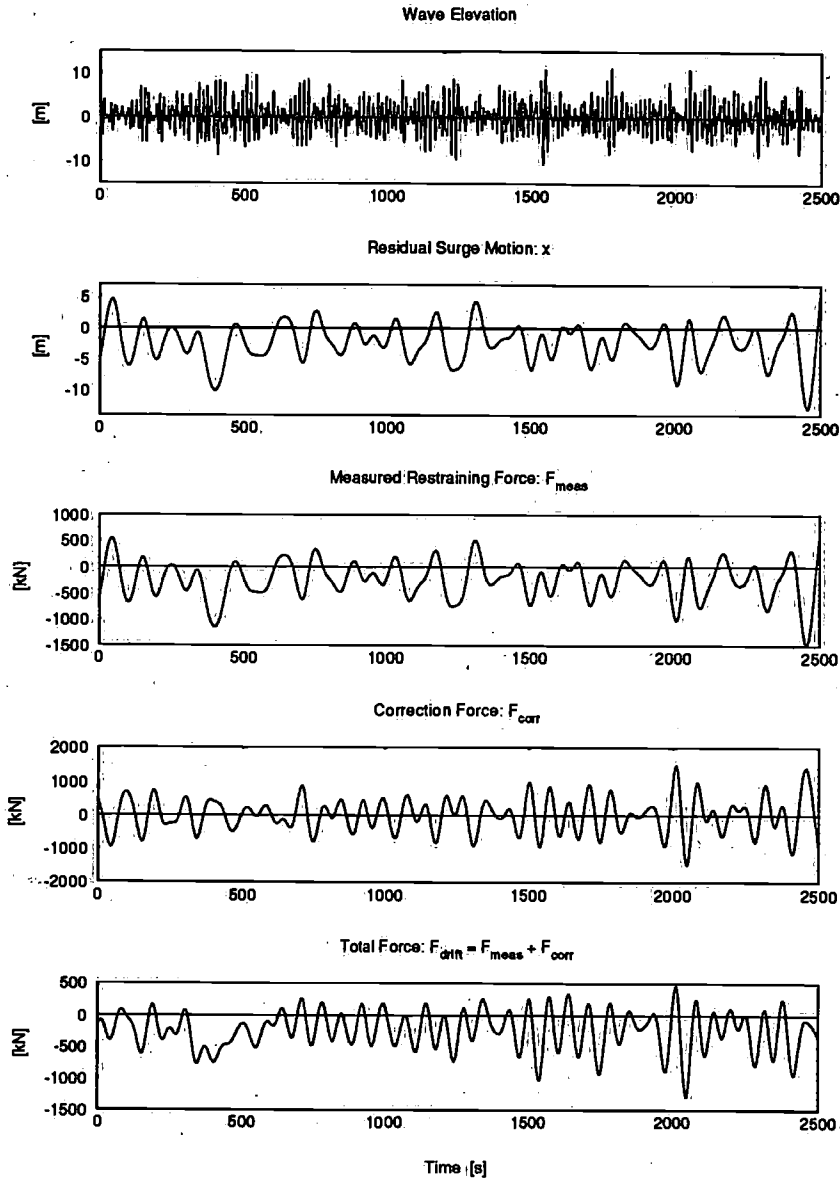


Figure 6.30: *Examples of residual surge motion, measured restraining force, correction force and total drift force on the ITTC moored semi-submersible in irregular waves only in head seas*

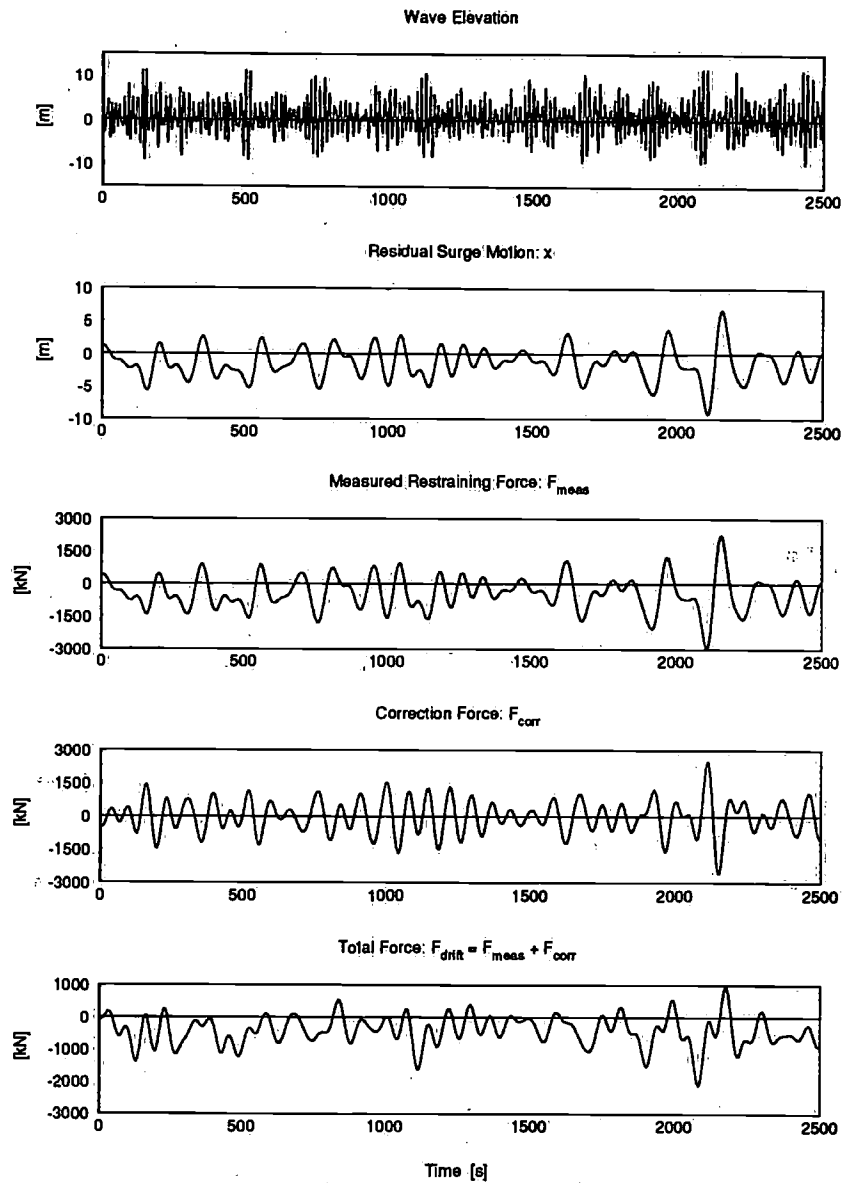


Figure 6.31: Examples of residual surge motion, measured restraining force, correction force and total drift force on the ITTC moored semi-submersible in irregular waves only in beam seas

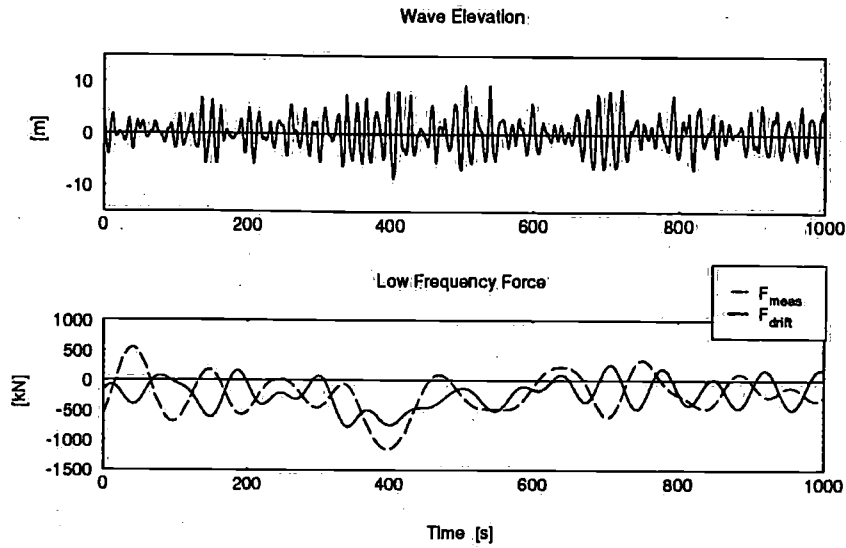


Figure 6.32: Measured uncorrected and corrected drift force on the ITTC moored semi-submersible in irregular waves only in head seas

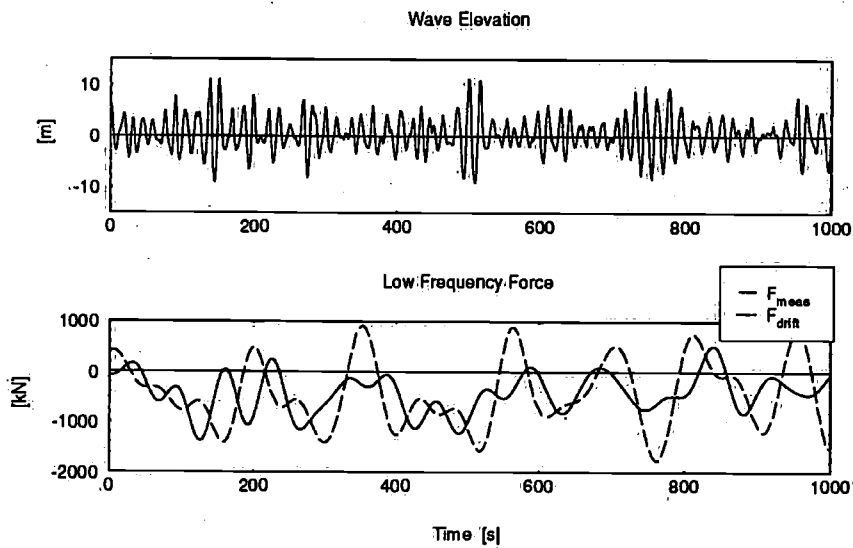


Figure 6.33: Measured uncorrected and corrected drift force on the ITTC moored semi-submersible in irregular waves only in beam seas

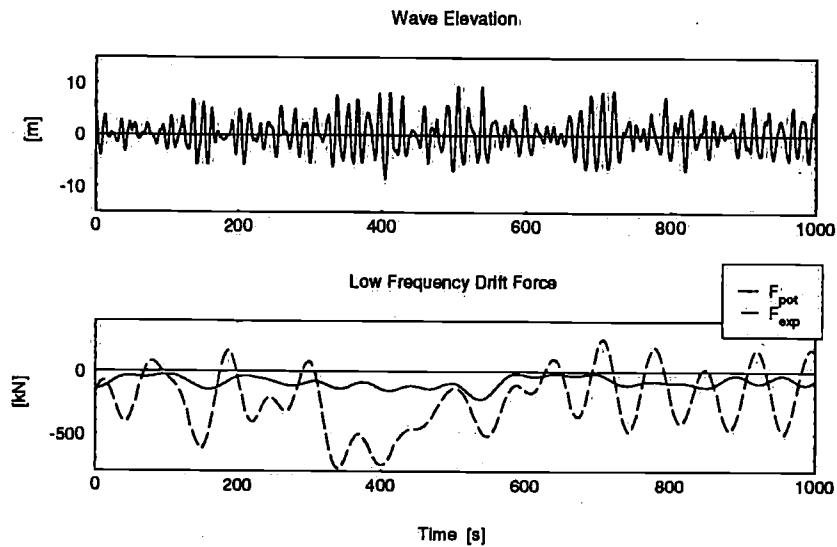


Figure 6.34: *Computed (potential) and experimental (measured corrected) drift force on the ITTC moored semi-submersible in irregular head waves*

Time records of measured and computed drift force records for both irregular head and beam seas are shown in Figure 6.34 and in Figure 6.35 respectively. Significant differences are observed in the force peak values as well as in the phase shift between the peaks in the measured and computed records.

The results found from tests in irregular waves is in a way related to those obtained in regular waves. The correlation between measurements and computations clearly indicates that the drift forces are not a quadratic function of the wave amplitudes. Such differences provide a clear indication that the low frequency drift forces are also well affected by viscous effects. The peaks in the computed drift forces tend to shift relative to the wave groups. This is related to the fact that in longer waves diffraction effects which form the major part of the drift forces in shorter waves are reduced.

In order to investigate the differences, the mathematical model shown in chapter 5 in connection with viscous drift forces in the time domain will now be applied and further comparisons will be made between the measured and the computed drift forces including viscous contributions.

The results of these computations are shown in Figure 6.36 and Figure 6.37 for irregular head seas and beam seas respectively. In these figures,

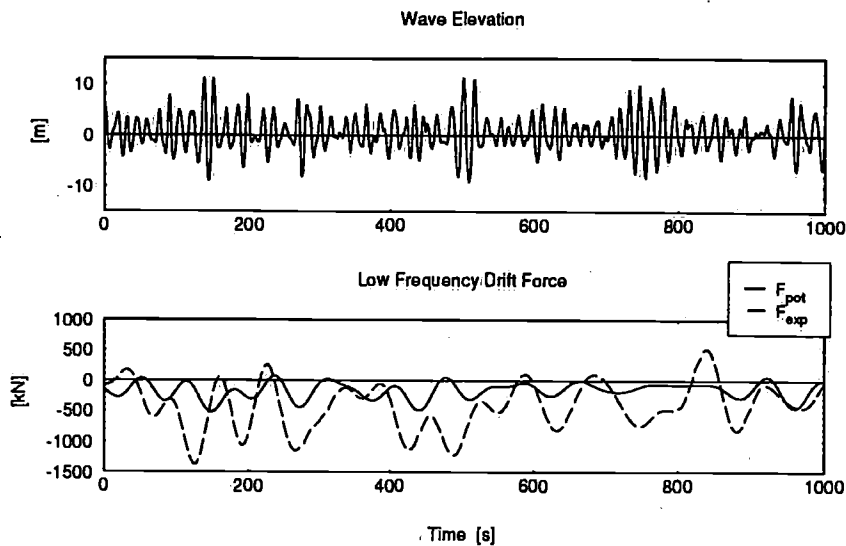


Figure 6.35: Computed (potential) and experimental (measured corrected) drift force on the ITTC moored semi-submersible in irregular beam waves

the wave elevation record, the potential part of the drift force and the viscous part of the drift force are shown in top three traces. The lower trace shows the sum of the viscous force and the potential force compared with the total measured force.

It is clear from the figures that the result of adding the viscous contribution is a clear indication of better correlation with the measured force. Differences still exist but there is no doubt that the force calculated by the 3-dimensional potential theory computation is far less than the measured force and that viscous effects need certainly be taken into consideration for the overall prediction. The differences can be caused by the uncertainties in the choice of the mean drag coefficients though they have been used as a time function rather than a constant value in all the foregoing work related to viscous effects in the drift forces even in irregular waves. One important aspect not accounted for in the mathematical modeling is the interference/shielding effects due to the close proximity of the columns of a semi-submersible. However, the above results give a satisfactory confirmation that there are indeed significant viscous effects in the drift forces on semi-submersible type structures which, in irregular waves without current, is confined to the splash zone (free surface zone) of the columns.

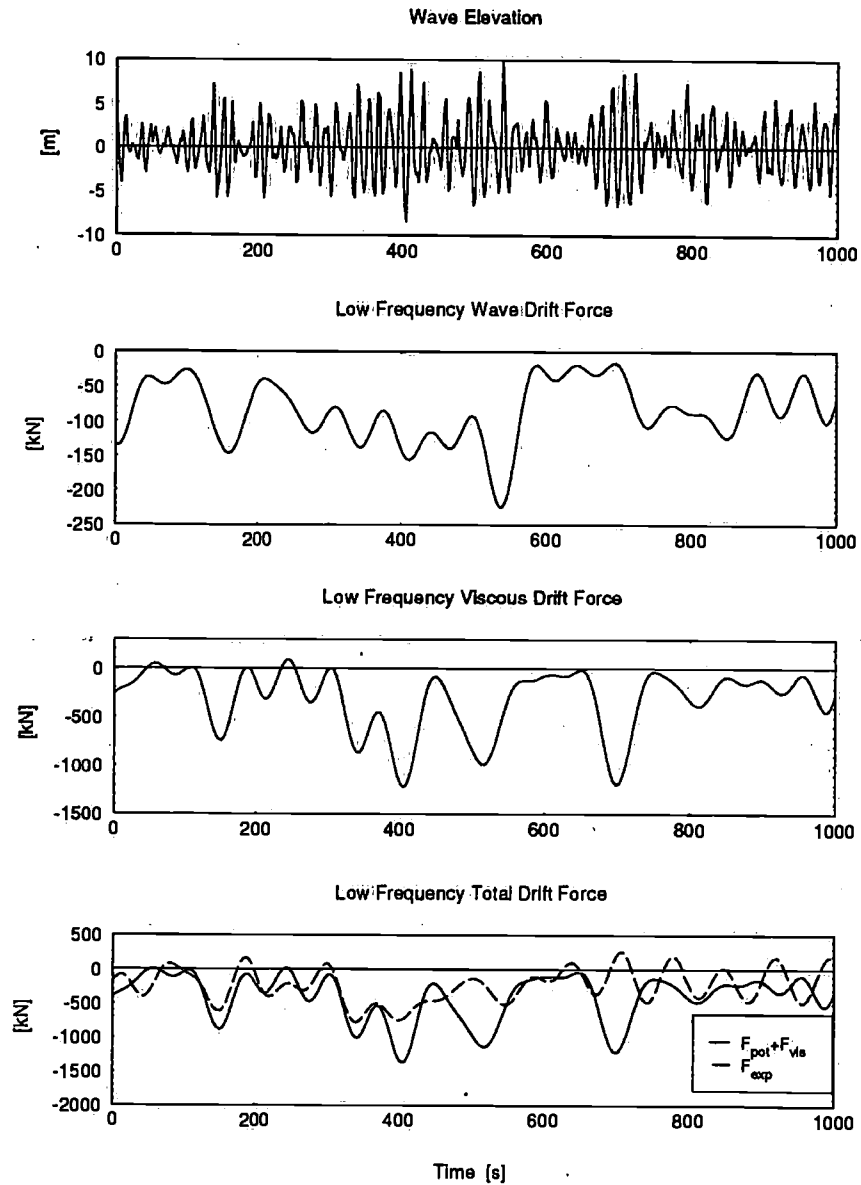


Figure 6.36: Computed (total) and experimental (corrected) drift force on the ITTC moored semi-submersible in irregular waves only in head seas

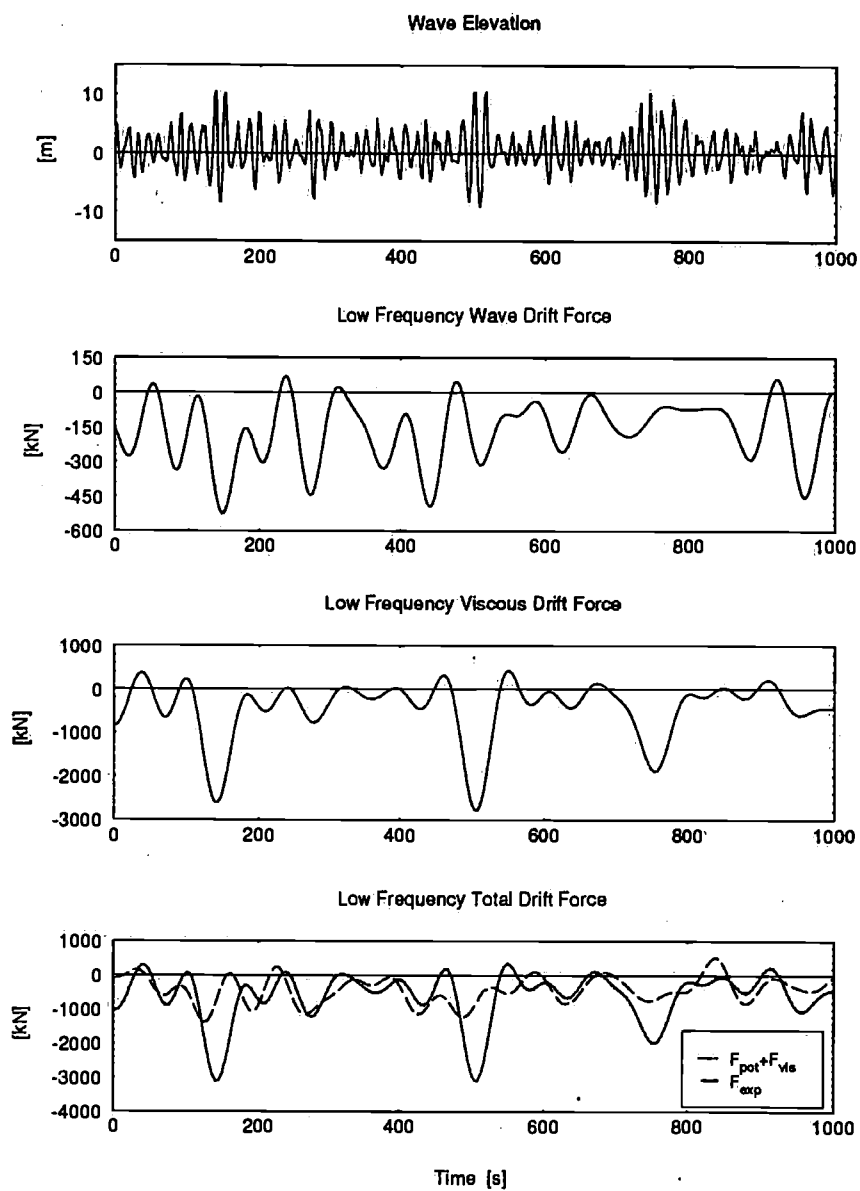


Figure 6.37: Computed (total) and experimental (corrected) drift force on the ITTC moored semi-submersible in irregular waves only in beam seas

References

- DELFRAC (1992). *A 3-D Diffraction Program*. Ship Hydromechanics Laboratory, Delft University of Technology, Delft, The Netherlands.
- Dev, A. K. (1993). Current and wind loads on semi-submersibles (ssbs) and tension leg platforms (tlps). Technical Report 971, Ship Hydromechanics Laboratory, Delft University of Technology, Delft, The Netherlands.
- Dev, A. K. (1994). Hydrodynamic loading on semi-submersibles and tension leg platforms in steady currents. In *Proceedings of the 10th International Offshore South East Asia Conference*, OSEA, Singapore, pp. 855-875.
- Pinkster, J. A. (1980). *Low Frequency Second Order Wave Exciting Forces on Floating Structures*. Ph. D. thesis, Ship Hydromechanics Laboratory, Delft University of Technology, Delft, The Netherlands.
- Pinkster, J. A., A. Dercksen, and A. K. Dev (1993). Hydrodynamic aspects of moored semi-submersibles and tlps. In *Proceedings of the Annual Offshore Technology Conference*, OTC 7190, Houston, Texas, pp. 601-614.

Chapter 7

Conclusions

As a result of both experimental and theoretical investigations carried out in this study, the following conclusions can be drawn in connection with viscous effects in the drift forces on semi-submersibles:

1. Wave (potential) drift force computations based on 3-dimensional potential theory are not adequate for predicting the drift forces on a slender body structure like semi-submersibles in a seastate. The differences in the mean drift force calculations and the experimental results are due to interference effects in which the diffracted waves play a major role. In longer waves diffraction effects are reduced and viscous effects become comparatively important as a result of which the mean drift force is not a quadratic transfer function of the wave amplitude indicating that the drift forces are proportional to the wave amplitude to a power greater than two.
2. Systematic model tests in regular waves with major structural components (vertical columns and submerged pontoons) of a semi-submersible established the fact that the splash zone (free surface zone) of the vertical columns is the main source of viscous contributions in the horizontal mean drift force in waves only. In the case of submerged structures like the constantly submerged zone of a vertical column or a completely submerged pontoon in waves only, the experimental investigations show similar trends in the mean drift forces as predicted by the present 3-dimensional computational techniques. However, in the presence of currents with waves, an additional source is established for further contribution of viscous effects even for the constantly sub-

merged structures.

3. The viscous drag force term of the Morison equation along with the linear (Airy) wave theory up to the instantaneous wave elevation can be taken as a basis in order to develop the mathematical model for a complete semi-submersible when independent model tests with vertical cylinders and a submerged pontoon in waves only and also in waves and currents validate the theory.
4. Uncertainties lie in the choice of the controlling hydrodynamic parameters and subsequently ascertaining the values of mean drag coefficients. In this connection, the values of oscillating drag coefficients in published literature should not be manipulated while dealing with the mean force. In a waves only flow field, the mean drag coefficients are found to be a function of the Keulegan-Carpenter number at very low diffraction values whereas with the increase of the diffraction parameter, they should be evaluated as a combination of both viscous parameter ($\frac{H}{D}$), and the diffraction parameter (kD), i.e. wave steepness (kH). In a wave-current coexisting flow field, instead of using separate hydrodynamic parameters like the Keulegan Carpenter number and the Moe-Verley number, a modified Keulegan-Carpenter number can take care of both with additional effects of crest and trough phases of the interacting waves with either positive currents or negative currents respectively.
5. The present theory can predict the horizontal viscous mean drift force on a vertical column and a submerged pontoon in regular waves in the frequency domain with comparatively better accuracy when experimentally obtained values of the mean drag coefficients are employed. It is expected that the above analogy to behave in a similar fashion for a free floating structure and accordingly they can be applied for a free floating (moored) semi-submersible.
6. The mathematical model when applied to a moored semi-submersible in regular waves with and without currents shows relatively improved predictions of the total drift forces when compared with experimental results. Application of the mean drag coefficients as function of mentioned controlling hydrodynamic parameters seem appropriate.
7. Application of the same mathematical model in the time domain for the viscous effects to the drift forces indicated that in irregular waves

without current, the major source of the viscous contribution is found to be confined at the splash zone of the columns of a semi-submersible. However, additional treatment of the values of the mean drag coefficients for the low frequency viscous drift forces needs to be evaluated as function of the hydrodynamic parameters based on the slowly varying wave kinematics.

8. First order motions which are required in the mathematical model to deal with viscous effects for a semi-submersible can well be predicted by 3-dimensional diffraction theory. Model tests with the floating semi-submersible validates the comparison between the theoretical and experimental results. Even in the presence of small magnitude of currents, the zero speed results of motions and phases can be used.
9. In both regular waves and irregular wave analyses, either the waves-only field or the wave-current coexisting flow field requires to be dealt with separately. Generation of a waves-only flow field from a wave-current coexisting flow field after deducting a currents-only flow field is not appropriate. Similar fact applies in the case of a wave-current coexisting flow field which will not produce the same results when the results of two independent flow fields are simply added neglecting the interaction effects of the coexisting flow field.
10. The actual flow around vertical columns and submerged pontoon in waves and also in waves and currents including viscous effects is in fact an extremely complex phenomenon. Using the drag force term of the Morison equation and overcoming the main uncertainties in the choice of the values of mean drag coefficients from experimental investigations is not a robust technique because of its fragile nature. But at this time, an improved indication can be given with regard to such viscous effects on the horizontal mean drift forces on moored structures like semi-submersibles. The present theory can also be applied for tension leg platforms.

Chapter 8

Recommendations

A rational approach based partly on experimental findings has been developed in this research work to treat viscous effects on the horizontal mean drift forces on semi-submersible type structures in both regular and irregular waves with and without currents. At present, 3-dimensional computational techniques cannot handle the horizontal drift forces on slender body structures like semi-submersibles in low frequencies where diffraction effects are less dominant. The developed computational method for calculating the viscous contributions has certainly been found to be beneficial toward an improved prediction. Anomalies are still present but no doubt the inherent gap between 3-dimensional computations and experiments has been narrowed down to a reasonable magnitude.

While the numerical solution for dealing with viscous effects remains not very attractive from the point of view of mathematical modeling and consequently in terms of computer time, the approach adopted in this work can still be considered as an alternative solution technique provided more experimental back-ups are evaluated and added.

Experiments conducted during this work mainly dealt with a single cylinder and a single pontoon whereas in reality a semi-submersible consists of a number of vertical columns and two pontoons. Because of the orientation of the columns, the interference effects among them are bound to affect the mean drift forces in the viscous regime as well, like what is always taken into account in 3-dimensional diffraction calculations. This important hydrodynamic aspect has not been looked into in this work which has definitely some bearing on the overall viscous predictions.

Apart from uncertainties in viscous effects, some limitations were also

faced in the 3-dimensional computational technique. Motions were used for the zero speed case for a hydrodynamic field where forward speed was present. No robust solution was applied as for the forward speed effects on the mean drift force. Approximate empirical relations were applied without knowing their validity especially for a complete semi-submersible structure.

It will be of great help to reduce uncertainties in the choice of the values of the mean drag coefficient which remain as a highly sensitive parameter in the whole solution domain. In this connection the following experiments can be pursued in future:

1. Model tests with various diameters of fixed vertical cylinders in regular waves with and without currents for obtaining a wide range of the Keulegan-Carpenter number and the Moe-Verley number. If permitted, the Reynolds number dependency can also be looked into though its variations remain not very appreciable. The technique of a segmented model as done in this work should still be followed up for unique additional experimental findings.
2. The above model tests again with cylinders in arrays (resembling the orientation of a semi-submersible in head seas and in beam seas) to investigate the interference effects in the viscous force regime. In this situation, vertical cylinders with a single test section should be used. These tests can be extended to irregular waves also.
3. Model tests with two fixed rectangular submerged pontoons of different aspect ratios need to be conducted in waves without and with positive and negative currents to generate more data on the mean drag coefficients so that they can be applied for a wide range of geometric sections often used in semi-submersible construction. Tests with two pontoons will also enable the investigation of the interference effects though apparently it does not seem much because of the larger distance between them compared to that between columns. Such experiments will also facilitate the understanding of the circulation phenomenon which was strongly observed in the case of a single submerged pontoon. These tests can be extended to irregular waves also.
4. Model tests with a single fixed vertical cylinder in irregular waves with and without positive and negative currents and to make a comparison between the experimental results in the time domain with theoretical computations using the experimentally obtained mean drag coefficients

as functions of appropriate hydrodynamic parameters such as the viscous parameter, diffraction parameter, wave steepness and the newly defined Keulegan-Carpenter number.

5. Model tests with a fixed vertical cylinder with low frequency motions in regular and irregular waves. This type of experiment is necessary to investigate the different aspects of using controlling hydrodynamic parameters to ascertain their suitability in computer coding for a complete semi-submersible.

Apart from the above experimental investigations in connection with viscous effects, the present 3-dimensional computational method certainly requires modifications for the presence of a forward speed. It is expected that changes in the first order forces will occur and so the motions which have not been found so critical in the present work but for the completeness of the solution of the problem, it will remove any doubt. However more important is the change in the drift force due to a forward speed which is required while dealing with the total (potential plus viscous) drift forces in the presence of currents.

In the present study, the validation of the developed computer program has been shown for the head seas and beam seas exclusively as the experiments were done in those two conditions only. But further experimental investigations are necessary to validate the computations against other headings between head and beam waves.

Last but not the least is the "scale effects". Due to the absence of the Reynolds number similarity in model testing, the direct application of the model tests results for the full scale predictions is questionable as long as viscous effects are dominant in the hydrodynamic behavior of structures like semi-submersibles and tension leg platforms. The present investigation presents first line approach toward developing a procedure to deal with viscous effects in the horizontal mean and slowly varying drift forces and the problems of scale effects were kept aside for the time being. The low frequency excitation forces on floating structures like semi-submersibles are well dominated by viscous effects. Equally viscous effects are important for the low frequency damping forces. The presence of currents further enhances viscous effects. However, differences must be established first between model tests and full scale measurements in order to justify the magnitude of such scale effects before any firm conclusion about the importance of such "viscous scale effects" is made.

List of Symbols

Latin symbols:

<i>Symbol</i>	<i>Description</i>
A_P	Projected Area
b	Pontoon breadth
B	Damping coefficient
Cal	Calculation (theoretical/computational results)
C_A	Added mass coefficient
C_D	Oscillating drag coefficient
C_{D0}	Mean drag coefficient
C_{DC}	Drag coefficient due to currents only
C_L	Lift coefficient
C_M	Virtual mass or inertia coefficient ($1 + C_A$)
d	Draft
dl	Length element of the water line
dS	Surface element of S or S_0
D	Cylinder/Column diameter
e	Exponential (=2.718)
Exp	Experiment (measured/experimental results)
f	Wave or oscillating frequency ($\frac{1}{T}$)
F	Force on structure
$g^{(2)}(t_1, t_2)$	Quadratic impulse response function
F_0	Mean Force
F_{DC}	Drag force due to currents only
F_D	Oscillating drag force
F_{D0}	Viscous mean drift force
F_I	Inertia force
F_{P0}	Wave (potential) mean drift force
F_{pot}	Wave (potential) drift force

F_{vis}	Viscous drift force
g	Gravitational acceleration
h	Water depth; Pontoon depth
H	Wave height
H_s	Significant wave height
$\frac{H}{D}$	Viscous Parameter
i	Imaginary quantity ($\sqrt{-1}$)
k	Wave number
kD	Diffraction Parameter
kH	Wave steepness
K	Spring constant
l	Pontoon length
l_e	Pontoon end length
ℓ	A point along the water line
M	Mass; Moment; Mass matrix
M_A	Added mass
M_V	Virtual Mass ($M + M_A$)
N_{K-C}	Keulegan-Carpenter number
N_{M-V}	Moe-Verley number
N_{Re}	Reynolds number
n	Outward pointing normal
p	Pressure
Pub	Publication (published results)
P_{ij}	Component of the qtf dependent on ω_i and ω_j
Q_{ij}	Component of the qtf dependent on ω_i and ω_j
S	Instantaneous wetted hull surface
S_0	Mean wetted hull surface
S_ζ	Wave spectrum
t	Time
t_1, t_2	Time shifts
T	Wave or oscillating period
T_p	Spectral peak period
T_r	Relative wave period in currents
T_{ij}	Amplitude of the qtf
u	Horizontal water particle velocity
U	Current velocity
U_R	Reduced velocity
v	Transverse water particle velocity

V	Volume of structure
w	Vertical water particle velocity
W	Weight
X	First order motion of a surface element dS
x	Longitudinal (horizontal) coordinate or oscillation
y	Transverse (horizontal) coordinate or oscillation
z	Vertical coordinate or oscillation
2-D	Two dimensional
3-D	Three dimensional

Greek symbols:

<i>Symbol</i>	<i>Description</i>
α	Angular motion
β	Frequency parameter (beta parameter)
ϵ	Phase angle
ε	Random phase uniformly distributed over $0 - 2\pi$
γ	Velocity parameter (gamma parameter)
Γ	Circulation
λ	Wave length
μ	Absolute viscosity; Wave heading
μ_C	Current heading
ν	Kinematic viscosity
∇	gradient
ω	Wave or oscillating angular frequency
ω_p	Spectral peak frequency
ω_r	Relative wave frequency in currents
ϕ	Velocity potential (spatial)
$\phi_d^{(2)}$	Second order diffraction potential
$\phi_w^{(2)}$	Second order "undisturbed wave" potential
φ	Roll motion
π	Dimensionless quantity ($=22/7$)
ρ	Mass density of water
θ	Pitch motion
ζ	Wave surface elevation

Systems of axes:

<i>Symbol</i>	<i>Description</i>
$O_0X_0Y_0Z_0$	Righthanded earth-fixed coordinate system with positive Z_0 -axis pointing upward
$OXYZ$	Righthanded body-fixed coordinate system
$O'X'Y'Z'$	Righthanded local body-fixed coordinate system
$O'X_iY_iZ_i$	Coordinates of the center of application of force

Superscripts:

<i>Symbol</i>	<i>Description</i>
—	Nondimensional quantities
*	In the presence of currents with interactions
+	In the presence of currents without interactions
(1)	First order
(2)	Second order
→	Refers to a vector quantity
·	First derivative with respect to time
··	Second derivative with respect to time
N	Total number of components

Subscripts:

<i>Symbol</i>	<i>Description</i>
a	Absolute amplitude
c	Refers to a column
d	Refers to the distance between a point and cog
g	Refers to cog
i	i -th component
j	j -th component
k	k -th component
p	Refers to a pontoon
ra	Relative amplitude
t	Time derivative
x, X	In x -direction or head seas
y, Y	In y -direction or beam seas
z, Z	In z -direction

Acronyms:

<i>Symbol</i>	<i>Description</i>
BS	In the beam sea condition
cog	Center of Gravity
DUT	Delft University of Technology
FFT	Fast Fourier Transformation
FPS	Floating Production System
HS	In the head sea condition
hpf	High Pass Filter
ITTC	International Towing Tank Conference
lpf	Low Pass Filter
mwl	Mean Water Level
MARIN	Maritime Research Institute Netherlands
nf	Near Field DELFRAC
qtf	Quadratic Transfer Function
RAO	Response Amplitude Operator
swl	Still Water Level
sw	Strip Theory SEAWAY
SSB	Semi-Submersible
TLP	Tension Leg Platform
TUD	Technische Universiteit Delft

Acknowledgments

This dissertation is based on the research work carried out at the Ship Hydromechanics Laboratory of Faculty of Mechanical Engineering and Marine Technology of Delft University of Technology, Delft, The Netherlands. Help from many people made this work possible. In this connection, I remember late ing.A.P. de Zwaan as a sincere colleague.

First of all, I wish to thank my promotor Prof.dr.ir.J.A.Pinkster for the help, guidance and encouragement given throughout this work. I also wish to depict my sincere gratitude to Prof.ir.B.Boon for accepting me first as a Research Scientist to work in this University.

For continued assistance and backing with the experimental works, the author is deeply indebted to the colleagues in the Towing Tanks. I am grateful to ir.J.Ooms for his close look in reviewing the English write-up of this thesis and ing.C.P.Poot for producing some excellent model tests' drawings.

I thank dr.ir.J.E.W.Weichers of MARIN for his interest and encouragement for this research work.

Many help and support from ir.J.M.J.Journee, dr.ir.J.A.Keuning and ing.A.Versluis are deeply acknowledged. The cooperation and help in many ways from Ms.P.J.Trijzelaar and Mr.P.W.de Heer are well appreciated. I would always recall the warm hospitality of ing.W.Beukelman family throughout my stay here.

The author expresses gratefulness for close cooperation from his first hand colleagues namely dr.ir.H.J. de Koning-Gans, dr.ir.L.J.M.Adegeest, ing.A.A.M. van Gulik, ir.R. van't Veer and ir.J.Moulijn.

My profound acknowledgment to all other colleagues in the Laboratory whose company I enjoyed very much.

Finally, I credit the patience of my wife Tandra who absorbed quite a lonely time due to my long day and night absence from home during the preparation of this thesis.

Curriculum Vitae

The author was born on 15 January 1954 at Barisal, Bangladesh.

The author had his primary and secondary school education at Brojomohun Institution in Barisal. After passing secondary school certificate (SSC) examination in 1969, he entered Govt. B. M. College also in Barisal to finish his higher secondary education. Due to the liberation war in 1971, the author took an active part as a freedom fighter. After the independence of Bangladesh, he passed his higher secondary certificate (HSC) examination in 1972. The author commenced his engineering education in Bangladesh University of Engineering & Technology (BUET), Dhaka, Bangladesh in 1973 and finished with the degree of Bachelor of Science in Naval Architecture & Marine Engineering in 1977.

After working for sometime as a Naval Architect in a shipyard, he worked as a local counterpart (Naval Architect) to a Dutch Advisory Team in the Design & Inspection Office of Bangladesh Inland Water Transport Authority (BIWTA), Dhaka from 1978 to 1980. The author worked as Projects Engineer in shipyards in Singapore from 1981 to 1983 before entering as a Post-Graduate Research Student under ORS (overseas research students)-awards scheme in the Department of Ship and Marine Technology of University of Strathclyde, Glasgow, Scotland. He obtained the Degree of Master of Science in 1984 on a thesis titled "The Motion Characteristics of a Ring-Hull Semi-Submersible in Regular Waves".

The author worked as a Senior Lecturer in the Department of Marine Technology of Faculty of Mechanical Engineering of University Technology Malaysia (UTM) and then worked as a Structural Engineer in Protek Consultant Engrs Sdn Bhd in Kuala Lumpur, Malaysia from 1985 to 1987. He was engaged as a Marine Consultant to NORAD (Norwegian Agency for Development) and others for various maritime Projects in Bangladesh from 1987 to 1990. Since 1991, he started his work as a Research Scientist in the Ship Hydromechanics Laboratory of Delft University of Technology.